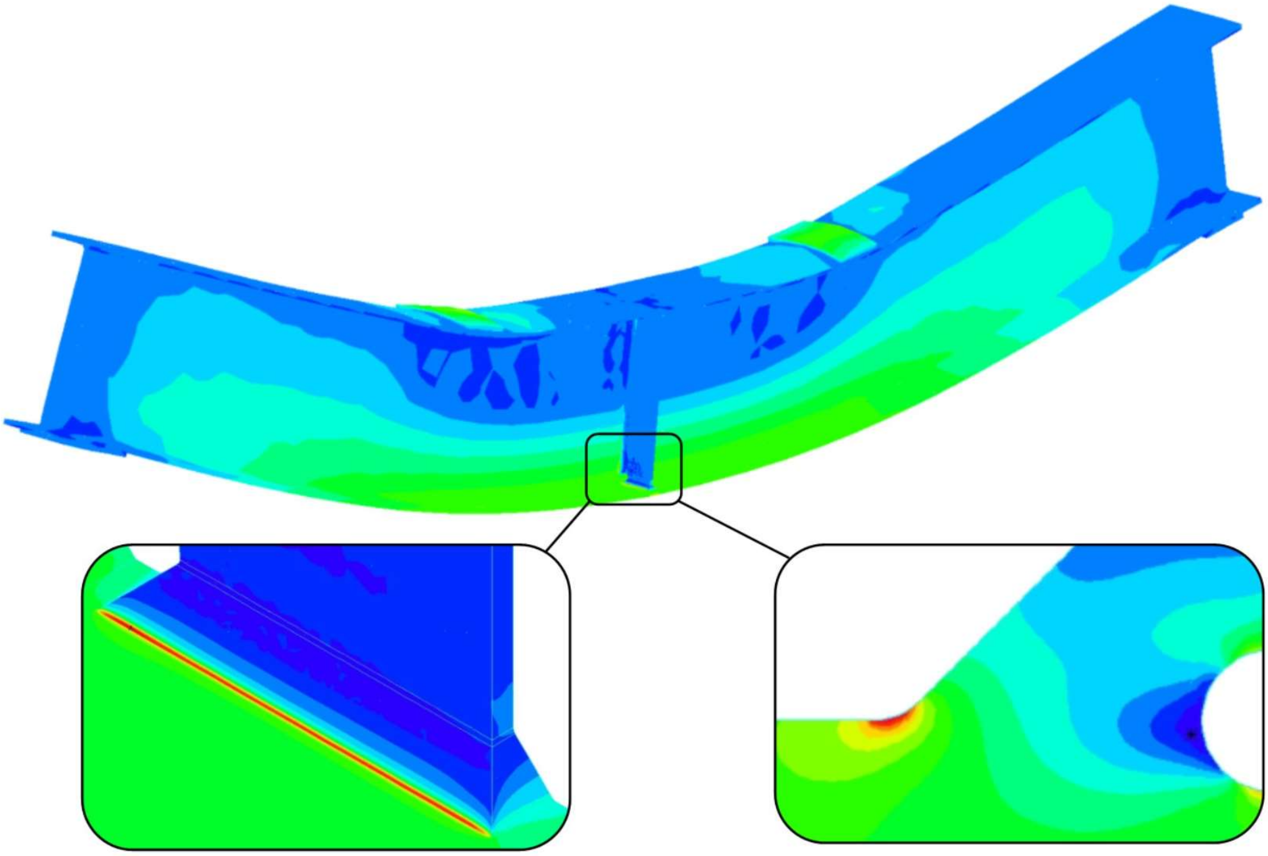

Effective notch stress analysis of transverse attachments in steel bridges

A parametric fatigue life assessment

Master's Thesis in the Master's Programme Structural Engineering and Building Technology

ANTON LINDQVIST
HENRIK NILSSON

Department of Civil and Environmental Engineering
Division of Structural Engineering
Steel and Timber Structures
CHALMERS UNIVERSITY OF TECHNOLOGY
Gothenburg, Sweden 2016
Master's Thesis BOMX02-16-12

MASTER’S THESIS BOMX02-16-12

Effective notch stress analysis of transverse attachments in steel bridges

A parametric fatigue life assessment

Master’s Thesis in the Master’s Programme Structural Engineering and Building Technology

ANTON LINDQVIST

HENRIK NILSSON

Department of Civil and Environmental Engineering

Division of Structural Engineering

Steel and Timber Structures

CHALMERS UNIVERSITY OF TECHNOLOGY

Göteborg, Sweden 2016

Effective notch stress analysis of transverse attachments in steel bridges
A parametric fatigue life assessment

Master's Thesis in the Master's Programme Structural Engineering and Building Technology

ANTON LINDQVIST

HENRIK NILSSON

Examensarbete BOMX02-16-12 / Institutionen för bygg- och miljöteknik,
Chalmers tekniska högskola 2016

Department of Civil and Environmental Engineering
Division of Structural Engineering
Steel and Timber Structures
Chalmers University of Technology
SE-412 96 Göteborg
Sweden
Telephone: + 46 (0)31-772 1000

Cover:
A caption of the full-scale 3D model accompanied by detail views of the sub model and the 2D model.

Chalmers Reproservice
Göteborg, Sweden, 2016

Effective notch stress analysis of transverse attachments in steel bridges

A parametric fatigue life assessment

Master's Thesis in the Master's Programme Structural Engineering and Building Technology

ANTON LINDQVIST
HENRIK NILSSON
Department of Civil and Environmental Engineering
Division of Structural Engineering
Steel and Timber Structures
Chalmers University of Technology

ABSTRACT

The fatigue life of welded steel details is often the governing factor in the bridge design process. In Eurocode 3, the nominal stress method is the most commonly applied approach when designing welded connections. However, due to limitations in this method, some structures are designed according to a lower fatigue strength than the real actual capacity of the detail to compensate for the uncertainties in the method. The effective notch stress method, ENS, can be used to assess the fatigue life of welded connections, which better predicts the actual fatigue life of a structure.

In steel bridges, transverse non load-carrying attachments such as web stiffeners are a very common type of detail, which often govern the design. The fatigue strength of this detail is only defined by the distance L in Eurocode 3, which is the distance between the toes of the fillet welds on each side of the attached plate.

This Master's thesis investigates how the fatigue life of transverse attachments can be assessed with finite element analysis using the effective notch stress method and how the result compares to the fatigue life determined by the nominal stress method. Moreover, a parameter study is performed to examine if other geometric parameters than L has any influence on the fatigue life. The parameter study is also used to see whether a higher fatigue strength class than the one defined in Eurocode 3 can be used for this particular detail.

It is found that the distance L does have the greatest influence on the fatigue strength of transverse attachments, even though the dimension of the weld throat as well as flange thickness does have a small impact. Further, for smaller values of L, a higher fatigue strength compared to the defined fatigue strength classes in Eurocode 3 is obtained. An equation that considers the L-values for transverse stiffeners based on the results from the parameter study is proposed and verified by collected experimental data. The implementation of an equation instead of using FE-analysis in form of the effective notch stress method would also reduce the time-consuming aspect in the design process.

Key words: Steel bridges, Fatigue life assessment, Nominal stress, Effective notch stress, Parameter study, Transverse attachment, Web stiffener

Utmattningsanalys av livavstyvare i stålbroar

En parameterstudie genomförd med "effective notch stress"-metoden

Examensarbete inom masterprogrammet Structural Engineering and Building Technology

ANTON LINDQVIST
HENRIK NILSSON
Institutionen för bygg- och miljöteknik
Avdelningen för Konstruktionsteknik
Stål- och träkonstruktioner
Chalmers tekniska högskola

SAMMANFATTNING

Utmattningshållfastheten i svetsdetaljer är ofta den dimensionerande faktorn i designprocessen för broar. I Eurocode 3 är den nominella spänningsmetoden den vanligaste för att designa svetsdetaljer med avseende på utmattningshållfasthet. Dock är vissa konstruktioner designade med en lägre utmattningshållfasthet än den faktiska för att kompensera för de begränsningar som finns i metoden. "Effective notch stress"-metoden, även kallad ENS, är en noggrannare metod för att utvärdera utmattningshållfastheten i svetsade detaljer.

Transversella anslutningar, så som livavstyvare, är en väldigt vanlig detalj i stålbroar och är ofta dimensionerande. I Eurocode 3 styrs utmattningshållfastheten för denna detalj endast av längden *L*, dvs. avståndet mellan svetstårna på vardera sida av livavstyvaren.

Detta examensarbete undersöker hur utmattningshållfastheten för transversella anslutningar kan utvärderas med finita elementmetoden genom att använda "effective notch stress"-analys och hur dessa resultat står sig mot den nominella spänningsmetoden. Vidare utförs en parameterstudie där andra geometriska parametrars påverkan på utmattningshållfastheten, utöver längden *L*, undersöks. Denna parameterstudie används också för att se om en högre utmattningshållfasthetsklass för den undersökta detaljen än den definierad i Eurocode 3 kan erhållas.

Resultaten visar att längden *L* har den största inverkan på utmattningshållfastheten i transversella anslutningar, trots att dimensionerna på a-måttet och flänsplåttjockleken också har en påverkan. Vidare visar resultaten att en högre utmattningshållfasthet för låga *L*-mått kan uppnås i jämförelse med rekommendationerna från Eurocode 3. En ekvation baserad på parameterstudien som tar hänsyn till längden *L* är framtagen och verifierad med data från tidigare utförda experiment. Implementationen av en sådan ekvation istället för att använda FE-analys i form av "effective notch stress" skulle även reducera tidsåtgången i designprocessen.

Nyckelord: Stålbroar, Utmattningshållfasthet, Nominell spänning, "Effective notch stress"-metoden, Parameterstudie, Transversell anslutning, Livavstyvare

Contents

Preface

This Master's thesis has been carried out as a cooperation between the engineering company ÅF and the department of Civil and Environmental Engineering, Steel and Timber Structures at Chalmers University of Technology between January and June 2016, where the majority of the work was done at ÅF's office in Göteborg.

The examiner for this thesis, Professor Mohammad Al-Emrani, has given us valuable knowledge along the project and we would express our greatest appreciation for his support and enthusiasm.

We would like to thank our supervisor Emanuel Trolin for his guidance and support for our project. Furthermore, we would like to give our appreciations to Mattias Carlsson and Bruno Altona for their support in FE-modelling.

We would also like to thank our opponents Erik Flinck and Martin Olsson for their feedback during the project and to ÅF for letting us carry out our Master's thesis at their office.

Göteborg, June 2016

Anton Lindqvist & Henrik Nilsson

Notations

Roman upper case letters

A	Area of cross section
C_1	Correction factor for flange thickness
C_2	Correction factor for flange thickness
C_3	Correction factor for flange thickness
C_4	Correction factor for flange thickness
C_5	Correction factor for flange thickness
C_6	Correction factor for flange thickness
E	Modulus of elasticity
F	Force
I	Moment of inertia
K_t	Stress concentration factor
L	Distance between weld toes
$L_{max,o}$	Cut-off limit for fatigue strength class of one-sided transverse stiffener
$L_{max,d}$	Cut-off limit for fatigue strength class of double-sided transverse stiffener
M	Moment
N_i	Crack initiation time
N	Fatigue life
N_p	Crack propagation time

Roman lower case letters

a	Weld throat thickness
e	Eccentricity
k_m	Misalignment correction factor
k_s	Thickness correction factor
l	Thickness of transverse attachment plate
l_1	Plate length 1
l_2	Plate length 2
m	Slope of the S-N-curve
n	Exponent
r	Notch radius
s	Stress multi-axiality and strength criterion factor
t	Plate thickness
t_f	Flange thickness
t_{ref}	Reference thickness
t_w	Thickness of transverse attachment

Greek upper case letters

$\Delta\sigma_{ENS}$	Effective notch stress range
$\Delta\sigma_{hss}$	Hot-spot stress range
$\Delta\sigma_{hss,red}$	Reduced hot-spot range
$\Delta\sigma_{NS}$	Nominal stress range
$\Delta\sigma_C$	Detail category, stress range at 2 million cycles
$\Delta\sigma_{C,ENS}$	Fatigue strength class for effective notch stress
$\Delta\sigma_{C,NS}$	Fatigue strength class for nominal stress
$\Delta\sigma_D$	Constant amplitude fatigue limit
$\Delta\sigma_L$	Cut-off limit

Greek lower case letters

α	Angular displacement
γ_{Ff}	Partial factor for fatigue strength
γ_{Mf}	Partial factor for fatigue strength
δ	Distance from hot-spot point
θ	Angle
λ	Restraint coefficient
υ	Poisson's ratio
ρ	Actual notch radius
ρ^*	Micro-structural length
ρ_f	Fictitious radius
ρ_s	Density
$\sigma_{1,2,3}$	Principal stress
σ_e^{vM}	von Mises effective stress
σ_{nom}	Nominal stress
$\sigma_{x,y,z}$	Normal stresses in coordinate system
$\tau_{x,y,z}$	Shear stresses in coordinate system

Abbreviations

CAFL	Constant Amplitude Fatigue Limit
ENS	Effective Notch Stress
FEA	Finite Element Analysis
FEM	Finite Element Method
IIW	International Institute of Welding
NS	Nominal Stress
S-N-curve	Stress-Fatigue life-curve

1 Introduction

1.1 Background

Since steel bridges are sensitive to fatigue loading, it is likely that the dimensions of the structural elements will be governed by the fatigue life of details such as welded connections. Sometimes, the detail categories for the fatigue sensitive steel details are too conservative due to the design recommendations in Eurocode 3. If the details are designed with a more thorough analysis, this might lead to a higher fatigue strength class and hence less material use. Oversized bridges are, of course, a problem for the society concerning economical and environmental aspects, since more material is used which leads to among other things higher carbon dioxide emissions. It is therefore in the interest of the society, constructor and thereby the structural engineer to solve this problem.

The present design recommendations for the fatigue life of steel structures consists of detail categories, which consist of common connections that are presented in tables in Eurocode 3. However, in those cases where the connections are a bit more complex, several simplified connections may have to be combined which could give a lower fatigue strength than in reality. This is due to the fact that stress raisers such as geometrical discontinuities are taken into account on the resistance side using this approach, giving a lower fatigue strength than what would be expected.

In order to reach higher fatigue strength in connections compared to the simplified cases, 2D and 3D FE-analyses can be used in order to better approximate the stresses at the regions sensitive to fatigue. In addition, the fatigue strength of connections that are not covered in Eurocode 3 can be analysed using 3D analyses.

1.2 Aim and objective

This Master's thesis investigates how the effective notch stress method, ENS, can be used to determine the fatigue strength of a specific welded connection. The studied connection is the transverse connection, which appears e.g. at web stiffeners in beams, see Figure 1.1.

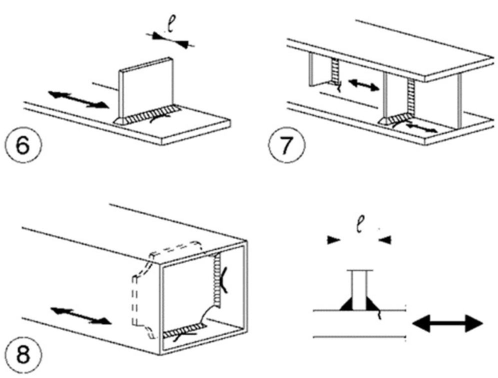

Figure 1.1 The investigated detail category from Eurocode 3 (CEN, 2005).

The fatigue strength of this detail is depending on the thickness, *L*, of the transversally attached plate in Eurocode 3.

The questions that are of interest are:

- How do stresses, using the effective notch stress analysis, compare to the values in the simplified cases in Eurocode 3?
- Do other geometric parameters than that specified in Eurocode 3 affect the fatigue strength of the detail?
- Will a specific set of dimensions result in a higher fatigue strength than specified in Eurocode 3?

1.3 Limitations

The detail category is investigated using the effective notch stress method. Other fatigue assessment methods, such as the nominal stress and the hot-spot stress method are not applied. These methods are however, covered in the theory part of the thesis. The geometrical ranges of the parameter study are in the vicinity of reasonable dimensions for the detail in bridges. Only fillet welds are considered and both the weld root and weld toe stress are analysed in the 2D model. In the 3D model however, only weld toe stress is analysed in order to reduce the size of the model and since the gathered experimental data only had weld toe failure. The dimension of the cope holes, flange width, web height and distance from the edge of the transverse stiffener to the flange end in the 3D model are not included in the parameter study as well as different angles of the welds. Only bending stresses are analysed in the 3D model, therefore the influence of shear stresses is not considered.

1.4 Methodology and structure

The project is divided into four parts where each part is given a specific chapter and reflects the workflow of the project. Chapter 2 consists of a literature study of for example the fatigue life assessment methods, among these methods the effective notch stress method that is to be used on the studied weld detail. Chapter 3 consists of the gathered experimental data that will be compared to the results from the FEA. In Chapter 4 is the weld detail modelling using the FEM-software ADINA explained, where a parameter study is performed to see whether the fatigue life is influenced by other parameters not specified in the Eurocode 3. The results from the FE-analyses are then presented in Chapter 5 and compared both with the specified fatigue strength in Eurocode 3 and to the experimental data collected in the second part. Proposals and conclusions are then stated from these comparisons.

2 Theory

2.1 Introduction to fatigue

Steel bridges are, like any other loadbearing structure, designed in such a way that they can resist the maximum expected load in the ultimate limit state, i.e. the ultimate load. However, if a steel structure is subjected to repeated loading for a certain number of cycles, it is possible that failure will occur even though the stresses are well below the maximum allowed stresses. This process is known as a fatigue failure. The following chapter will cover the basics of fatigue.

2.1.1 Fatigue life of welded bridges

Fatigue is defined as the process where permanent damage occurs locally in a material due to repeated loading. Bridges are one of the most common civil engineering structures exposed to fatigue loading since they are subjected to loads from traffic, pedestrians, wind and more. These loads are not static but vary with time, resulting in fluctuating stresses throughout the bridge, which means that fatigue should be taken into consideration. In general, it is the stress range, $\Delta\sigma$, that governs the fatigue life of a component. A higher stress range leads to a shorter fatigue life (Heshmati, 2012).

The fatigue life of a structure can be divided into crack initiation and crack propagation according to:

$$N = N_i + N_p \tag{2.1}$$

Where the crack initiation time is the time needed for a crack to form in the structure and the crack propagation is the time needed for a crack to grow to a critical length. The crack initiation time for a smooth specimen constitutes about 90% of the fatigue life whereas the crack propagation time is only at around 10% (Al-Emrani & Åkesson, 2013). This is however different for welded details in bridges due to imperfections in the weld itself. Defects such as undercuts, porosity and start-stop points have a great impact of the crack initiation time, reducing it to a fraction of the total fatigue life. These parameters will be discussed more thoroughly in Section 2.1.2.

When handling geometrical stresses, a so-called stress concentration factor, K_t, is often used. The stress concentration factor is the quote of the maximum geometrical stress due to the disturbance of the stress flow and the nominal stress:

$$K_t = \frac{\sigma_{geom}}{\sigma_{nom}} \tag{2.2}$$

The corresponding stresses can be seen in Figure 2.1.

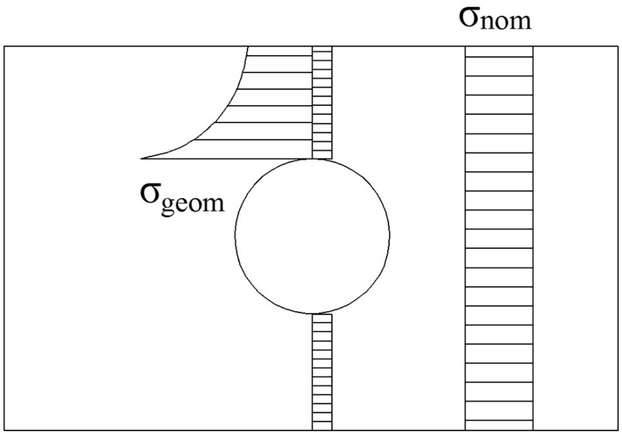

Figure 2.1 The geometrical stress at the stress raiser and the nominal stress, redrawn from (Al-Emrani, 2015).

2.1.2 Parameters affecting fatigue life

A few examples of defects that affect the fatigue life are misalignment, undercuts, porosity, inclusions and crack-like imperfections. Misalignment of welded plates leads to increased stresses in the weld due to an eccentricity of the normal forces, see Figure 2.2. The misalignment can of course be angular as well.

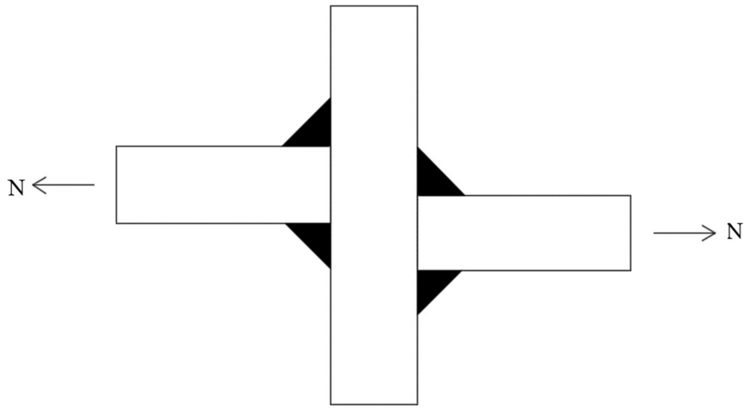

Figure 2.2 An illustration of misalignment in attachments.

An undercut at the weld toe functions as a pre-existing crack where stresses tend to concentrate due to a sudden geometric change of the weld (Heshmati, 2012). Defects such as inclusions and porosity are defects that lower the strength of the weld by trapping slag from the electrodes or gas into the joint respectively. Inclusion is common when you make several runs along the joint, which is why it is important to remove slag between each run in order to prevent this defect, see Figure 2.3. Porosity however is a defect that can occur even though the weld is completed in one run.

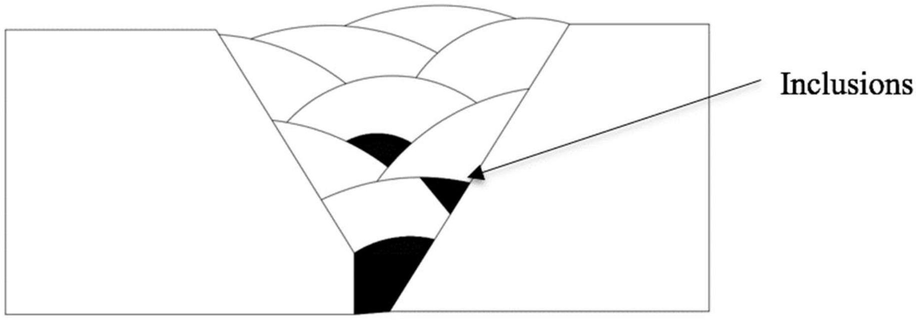

Figure 2.3 Inclusions in a welded butt joint.

As mentioned earlier, the total fatigue life consists of two stages known as crack initiation and crack propagation. Crack initiation is dependent on the strength of the steel, which means that high strength steels require more load cycles to form a crack. However, once a crack is formed the strength of the steel has very little influence on the propagation of the crack. Since welded structures are considered to be cracked from the very beginning of service, the fatigue life of a bridge is not affected considerably by using steel with higher strength (Al-Emrani & Åkesson, 2013).

2.1.3 S-N-curves and detail categories

S-N-curves (stress-life) are used to make a prediction of the fatigue life of a welded detail. These curves are derived from experimental data conducted on welded specimens. Each weld detail is assigned its own detail category, which is defined as the stress range that corresponds to a fatigue life of 2 million cycles. In Eurocode 3 they are denoted, for example, C80 if the detail can survive 2 million load cycles at a stress range of 80 MPa. Figure 2.4 displays a few S-N-curves for different detail categories.

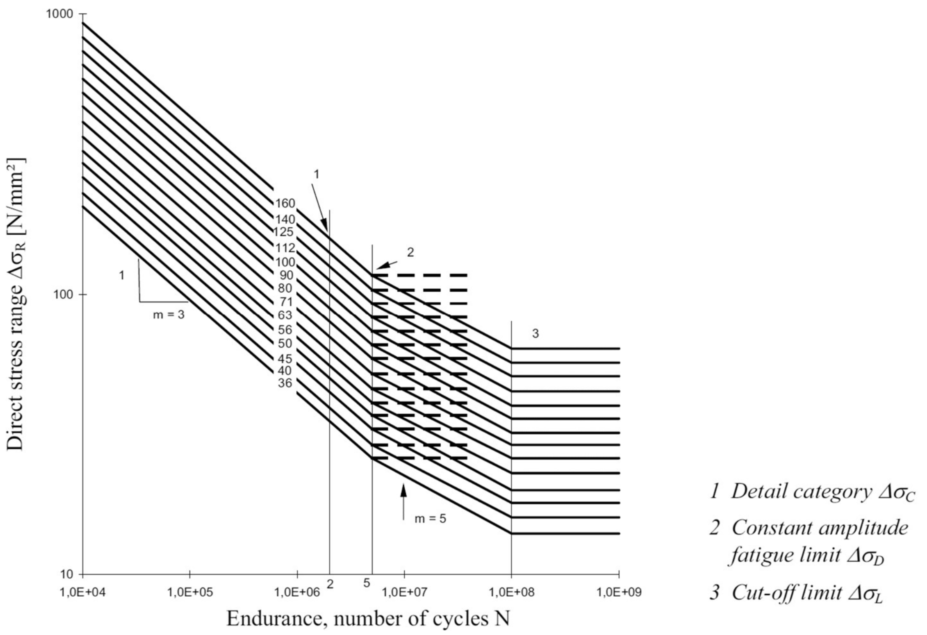

Figure 2.4 Example of S-N-curves for different detail categories exposed to nominal stresses (CEN, 2005).

The constant amplitude fatigue limit (CAFL) is defined at 5 million cycles. It is expected that stress range below that point does not accumulate any fatigue damage to the weld when it is subjected to a load with constant amplitude (Al-Emrani & Åkesson, 2013). At the cut-off limit, which can be found at 100 million cycles, no fatigue damage is assumed to take place at stress ranges below this point.

When the stress ranges and detail categories are known, the number of cycles until failure can be calculated from the S-N-curve using the following expression from Eurocode 3:

$$N = 5 \cdot 10^6 \left[\frac{\frac{\Delta\sigma_D}{\gamma_{Mf}}}{\gamma_{Ff}\Delta\sigma_{NS}} \right]^m \tag{2.3}$$

Where γ_{Ff} and γ_{Mf} are partial factors for fatigue strength and m is the slope of the curve, which is either 3 or 5 depending on the magnitude of the stress range. Where m is equal to 3 when the stress range is higher than $\Delta\sigma_D$ and 5 when the stress range is in between $\Delta\sigma_D$ and $\Delta\sigma_L$. The recommended value from Eurocode 3 for γ_{Ff} is 1 and γ_{Mf} is defined according to Table 2.1. However, the values for these parameters are chosen according to the national annex.

Table 2.1 Values for γ_{Mf} (CEN, 2005).

Assessment method	Consequence of failure	
	Low consequence	High consequence
Damage tolerant	1.00	1.15
Safe life	1.15	1.35

In Eurocode 3, there are a total of 14 detail categories with corresponding S-N-curves for details subjected to normal stresses, which can be seen in Figure 2.4. As mentioned earlier they are based on experimental data. The tested specimens usually have varying dimensions and test configurations which means that they might have different fatigue life for the same stress ranges, leading to a somewhat high scatter of the results.[1] Therefore, a safety margin must be included in the used S-N-curve, which is the reason that some details might become oversized when using the approach defined in Eurocode 3, known as the nominal stress method. This method will be discussed further in Section 2.3.1.

Transverse non load-carrying attachments have two different detail categories, which is either C80 or C71 depending on the distance between the weld toes of the attached plate, L. If L is less than or equal to 50 mm then the detail category is C80. Should L be in the interval 50 mm to 80 mm then the detail category is C71, see Table 2.2.

[1] Mohammad Al-Emrani (Associate Professor, Division of Structural Engineering, Chalmers University of Technology) meeting February 8th 2016.

Table 2.2 Detail categories for transverse non load-carrying attachments (CEN, 2005).

Detail category	Distance L [mm]
C80	$0<L\leq 50$
C71	$50<L\leq 80$

2.2 Stresses

Depending on what method is used to assess the fatigue life of a welded component, different kinds of stresses might be more suitable to study than others. This following section will introduce and discuss the concept of normal, nominal, principal and effective stress.

2.2.1 Normal stress and shear stress

The normal stress is defined as the stress acting perpendicular to the plane where a force has been applied. A common case is a rod subjected to either a tensile or a compressive force, resulting in stresses in the same direction, see Figure 2.5. The stresses are calculated as the force divided by cross sectional area.

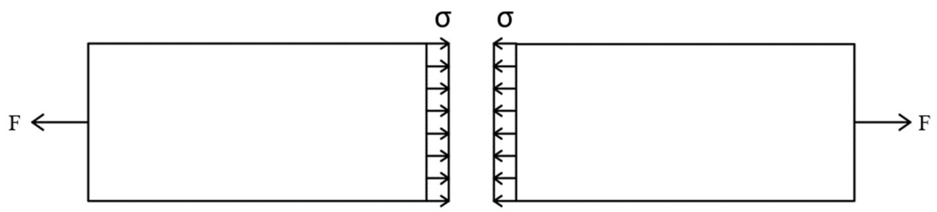

Figure 2.5 Normal stresses in a rod subjected to a tensile force.

However, in this simple case it is assumed that the stresses are evenly distributed over the entire cross section. In reality, the rod may be attached or manufactured in a certain way that the stress distribution is not completely even through the section. Then the calculated stresses may be taken as the average stress, also known as the nominal stress. The nominal stress is used in the nominal stress method when assessing the fatigue life of a welded detail. This will be discussed more thoroughly in Section 2.3.1.

Shear stress is calculated in a similar manner as for the normal stress. The force applied is distributed over the cross section of the structure. However, the force vector component giving rise to shear stresses is not normal to the plane but parallel to it.

2.2.2 Principal stress

In cases where the structure is subjected to a state of stress where both normal stresses and shear stresses are present, it is often useful to calculate the principal stresses. The principle is to rotate the basis of the force vectors such that the shear stresses becomes zero, see Figure 2.6. Hence, the principal stresses can be seen as a resultant of the normal stresses and shear stresses acting in a point.

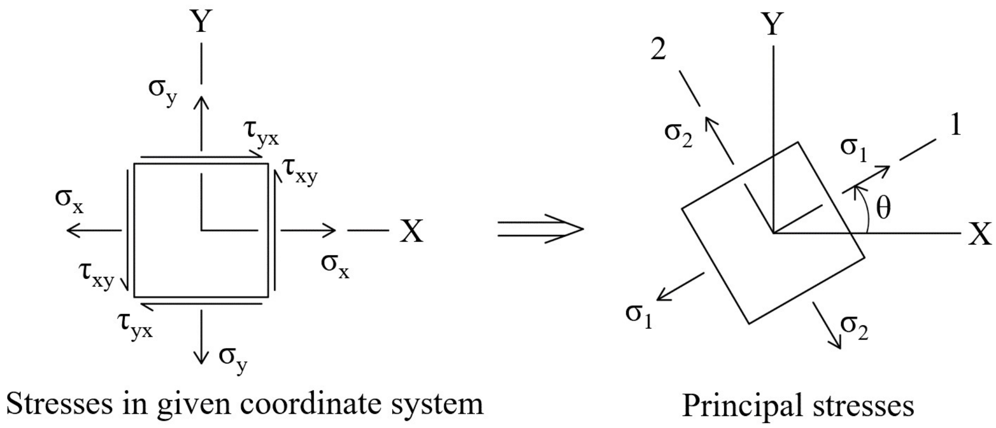

Figure 2.6 The principle of principal stresses illustrated.

In two dimensions, the principal stresses can be calculated according to the following equation derived from Mohr's circle:

$$\sigma_{1,2} = \frac{\sigma_x + \sigma_y}{2} \pm \sqrt{\left(\frac{\sigma_x - \sigma_y}{2}\right)^2 + \tau_{xy}} \tag{2.4}$$

Where the angle, θ, of the principal stresses are calculated as:

$$\theta = \frac{1}{2}\tan^{-1}\left(\frac{2\tau_{xy}}{\sigma_x - \sigma_y}\right) \tag{2.5}$$

2.2.3 Effective stress (von Mises)

As stated earlier, the case of a uni-axially loaded rod is quite simple. It is also a very common setup for testing the characteristics of common engineering materials. In real situations, other loading types such as torsion and shear might also be applied at the same time, resulting in loading configurations, which are more difficult to analyse. To be able to compare a complex loading situation to the strength of a material obtained from a uni-axial tension test, the effective stress as defined by von Mises can be used (Fricke, 2010). For a three dimensional situation, it can be calculated according to the following equation.

$$\sigma_e^{vM} = \sqrt{\sigma_x^2 + \sigma_y^2 + \sigma_z^2 - \sigma_x\sigma_y - \sigma_x\sigma_z - \sigma_y\sigma_z + 3\tau_{xy}^2 + 3\tau_{xz}^2 + 3\tau_{yz}^2} \tag{2.6}$$

This can also be done using the principal stresses:

$$\sigma_e^{vM} = \sqrt{\frac{1}{2}(\sigma_1 - \sigma_2)^2 + \frac{1}{2}(\sigma_2 - \sigma_3)^2 + \frac{1}{2}(\sigma_3 - \sigma_1)^2} \tag{2.7}$$

This means that the stresses in a complex loading situation can be represented by a single scalar, making it more convenient to assess the strength of a structure. The fact that the effective stress is a scalar means that it does not have a direction.

There are also other common methods to evaluate the effective stress, e.g. Tresca. This will however not be covered in this report since only von Mises effective stress is used in the fatigue life assessment methods explained in Section 2.3.

2.3 Fatigue life assessment methods

Fatigue life of welded details can be assessed using different methods. The three most common methods will be covered in the following section to provide basic understanding for assessing fatigue life. The recommendations that are presented in this section are mainly from Eurocode 3 and from the International Institute of Welding, IIW.

2.3.1 Nominal stress method

The nominal stress method is the most commonly applied approach when assessing the fatigue life (Aygül, 2012). It is included in both the recommendations from IIW and Eurocode 3. Nominal stress is calculated as the average stress in the cross section under consideration using Navier's formula, see equation (2.8). The calculated nominal stress is compared to S-N-curves found in design codes such as Eurocode 3 to determine the fatigue life of a welded component.

$$\sigma_{nom} = \frac{F}{A} + \frac{M}{I} \cdot z \qquad (2.8)$$

Since the nominal stress is calculated as the average stress at the cross section, local stress raising effects due to irregularities or geometrical discontinuities are disregarded. This means that the nominal stress does not always correspond to the real stresses in the cross section at notches and similar geometrical changes. Hence, this method might be difficult to apply or perhaps not applicable at all in more complex situations where the geometry is irregular (Hobbacher, 2009). It is however possible in some cases to use finite element modelling to determine the nominal stresses.

As notch effects are not taken into consideration in the stress calculations, they are instead included in the detail categories specified in Eurocode 3. This might result in a design, which is too conservative.

2.3.2 Hot-spot stress method

In structures with complicated geometry, it is sometimes difficult to approximate the correct stresses using the nominal stress method due to apparent stresses from e.g. warping and torsion. In these cases, the structural hot-spot stress method approximates the stresses better.

The structural hot-spot stress method has been used for over 50 years, starting in the offshore industry (Stenberg, Barsoum, & Balawi, 2015). The method estimates the stress at the position where a crack will form, i.e. the hot-spot points. The structural hot-spot method is recommended for cracks at the weld toe, even though there is a solution for root cracking as well (Al-Emrani & Aygül, 2014). The method can be done either analytically, numerically or experimentally, where the numerical solution process is most used due to the high adoption of the well-known Finite element method, FEM. IIW has published a handbook with recommendations for the method, which this report refers to Eurocode 3 also mentions the structural hot-spot stress method without recommendations of the execution.

The fatigue strength of a detail is dependent on three parameters: the geometry of the detail, the effects from the weld geometry and weld defects. The structural hot-spot takes the geometry of the detail into consideration. The stress increase from the weld geometry and defects is however not considered, which is also the disadvantage with the method. This effect is accounted for in the effective notch stress method, see Section 2.3.3. Due to the fact that the detail geometry effect is included in the stress analysis instead of in the S-N-curves, the number of S-N-curves are significantly reduced. There are three different types of stresses in the cross section of the plate: membrane, bending and the stress peak caused by the singularity point at the weld toe. It can be seen in Figure 2.7 that the structural hot-spot stress does not consider the stress peak from the weld, as previously explained.

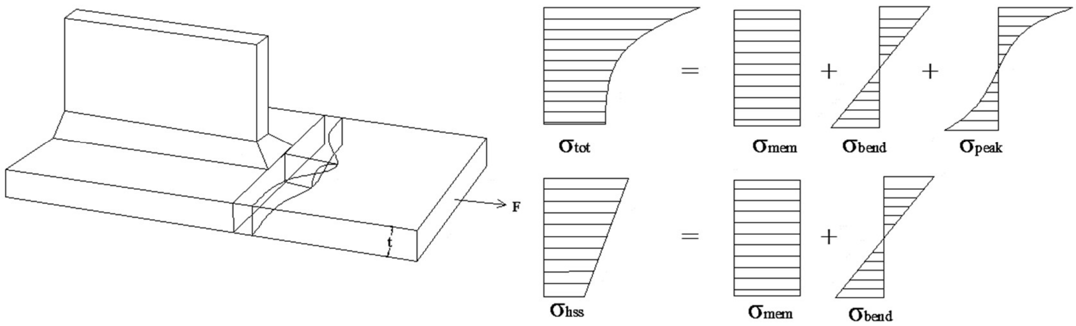

Figure 2.7 Actual stresses at the weld toe compared with the stresses considered in the structural hot-spot stress method, redrawn from (Al-Emrani & Aygül, 2014).

The way the method separates the peak stress from the other stresses is by using stress linearization from predetermined reference points at certain distances from the hot-spot point. This is often done with a surface extrapolation technique of the stress, see Figure 2.8. The stress perpendicular to the crack direction is of interest, which corresponds to the loading direction.

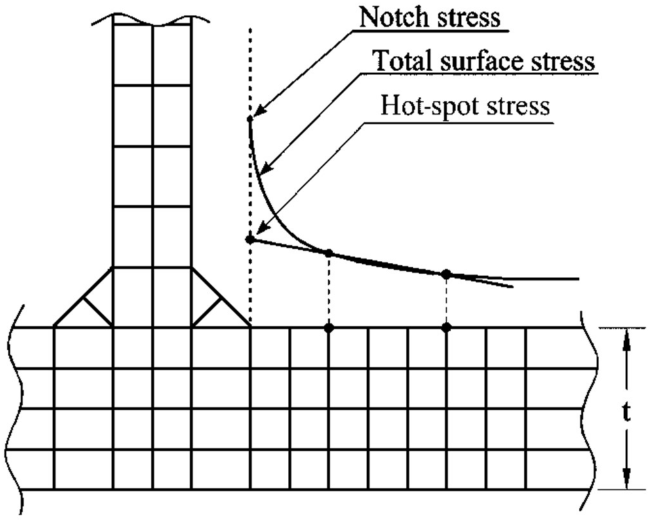

Figure 2.8 Figure demonstrating the principle of stress extrapolation, redrawn from (Al-Emrani & Aygül, 2014).

2.3.2.1.1 FE-modelling

The following recommendations for the FE-modelling of the hot-spot stress method can also be read in (Al-Emrani & Aygül, 2014), where a more thorough modelling guide is presented with modelling recommendations for details other than the detail studied in this report. Since the method is highly mesh sensitive in the FEA due to the high strains at the singularity points, the method requires consistent modelling technique to avoid large stress variations (Al-Emrani & Aygül, 2014).

The structure can, in the structural hot-spot stress method, be modelled with both 2D shell, 2D solid plane strain and 3D solid elements. For the different element types, there are different recommendations and rules due to the mesh size sensitivity as previously explained.

The FE-modelling recommendations for shell elements in transverse attachments can be seen in Table 2.3. These recommendations are given by IIW and can also be seen in (Al-Emrani & Aygül, 2014). It must be pointed out that shell elements should not be used for cruciform joints, plated T-joints and one-side welded butt joints. Shell elements are easier and faster to model compared with solid elements and should therefore be used when it is appropriate (Al-Emrani & Aygül, 2014).

Table 2.3 Recommended FE-modelling technique for shell elements.

Element type	Shell
Material model	Linear elastic
Element order	4-node (fine mesh) / 8-node (coarse mesh)
Element aspect ratio	1:1 or 1:2
Shell orientation	Mid-plane
Welds	Included (Oblique shells or rigid links)
Extrapolation line	Straight

The recommendations for the modelling of solid elements for transverse attachments are presented in Table 2.4.

Table 2.4 Recommended FE-modelling technique for solid elements.

Element type	Solid
Material model	Linear elastic
Element order	8-node (fine mesh) / 20-node (coarse mesh)
Element aspect ratio	1:1 or 1:2
Welds	Included in model
Elements over plate thickness	1 element or more
Extrapolation line	Straight

It should also be noted that the element size for both shell and solid elements is dependent on the locations of the reference points, since the nodal points must coincide with the reference points.

2.3.2.2 Weld modelling techniques

The weld is often not modelled when using the hot-spot stress method. However, some details require the weld geometry, e.g. the transverse attachment. The modelling technique for 3D solid elements is straight forward, using prismatic solid elements for the welds. For 2D shell and solid elements, the procedure is more complicated and the hot-spot stress can be affected by the modelling technique for the welds. The two modelling techniques for transverse attachments recommended by IIW are oblique shell elements and rigid links (Al-Emrani & Aygül, 2014).

When using oblique shell elements for the welds, one connects the weld elements with the elements representing the plates at the section of the weld toe with an angle of 45 degrees to both plates, see Figure 2.9. The thickness of the oblique elements should be the corresponding weld throat thickness.

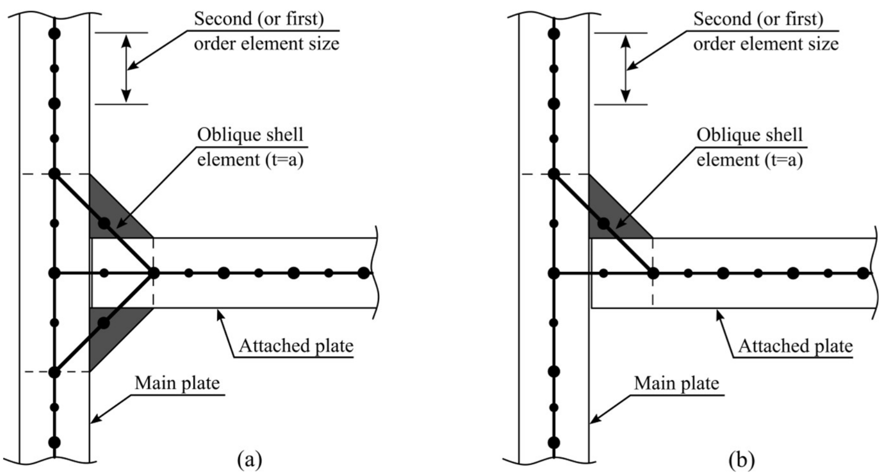

Figure 2.9 Welds modelled with oblique shell elements in the hot-spot stress method (Al-Emrani & Aygül, 2014).

The second weld modelling method is performed by using rigid links between the plates. The distances *E1* and *E2* influence the stiffness of the weld and should therefore be set carefully. It should be noted that the two plates are not connected at the interception point, see Figure 2.10.

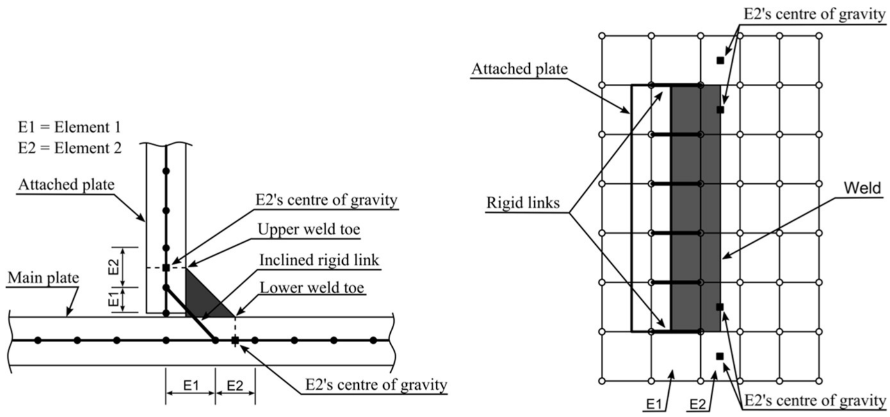

Figure 2.10 Welds modelled with rigid links between the plates in the hot-spot stress (Al-Emrani & Aygül, 2014).

2.3.2.3 Stress extrapolation technique

To obtain the hot-spot stress, one must extrapolate the stress from predefined reference points, which can be seen in Figure 2.12. Depending on mesh size, hot-spot type and extrapolation type, i.e. linear or nonlinear, the distance from the hot-spot, i.e. the weld toe, differs. For the linear and nonlinear extrapolation techniques, two respectively three reference points are needed. The reference point distances can be seen in Figure 2.12, in which t is the thickness of the plate. For the nonlinear extrapolation, it should be noted that only fine mesh should be used.

Table 2.5 Distances from the hot-spot point to the reference points for different extrapolation techniques.

Extrapolation type	Hot-spot type	Mesh size	Distance from hot-spot point		
			1st point	2nd point	3rd point
Linear	Type a	Fine	0.4t	1t	-
Linear	Type a	Course	0.5t	1.5t	-
Linear	Type b	Fine	-	-	-
Linear	Type b	Course	5	15	-
Nonlinear	Type a	Fine	0.4t	0.9t	1.5t
Nonlinear	Type b	Fine	4	8	12

There are two different types of hot-spots, type a and b. Type a has a large variation of the stress distribution over the thickness while b has less variation. This yields that type a needs to consider the thickness for the reference points while b does not. The different type of hot-spots can be seen in Figure 2.11.

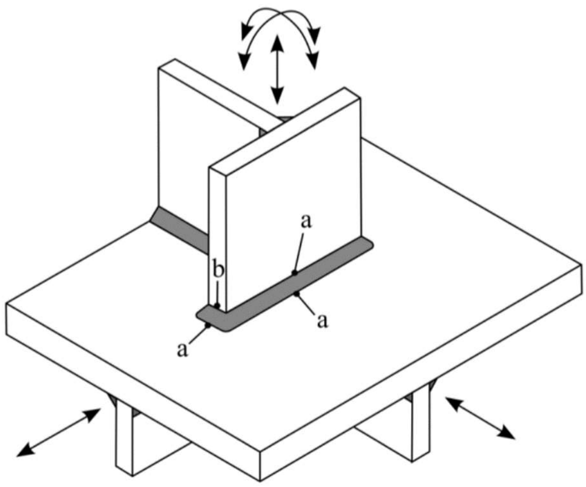

Figure 2.11 The two different types of hot-spot points (Al-Emrani & Aygül, 2014).

In addition to these extrapolation techniques, the one point stress with only one reference point can be used. The stress in this point will then correspond to the hot-spot stress at the weld toe. This point is 0.5t from the hot-spot point. It was found that this stress value must be multiplied with 1.12 to better approximate the hot-spot stress (Fricke, 2001). The one point stress can serve as a verification method for the extrapolation techniques (Al-Emrani & Aygül, 2014).

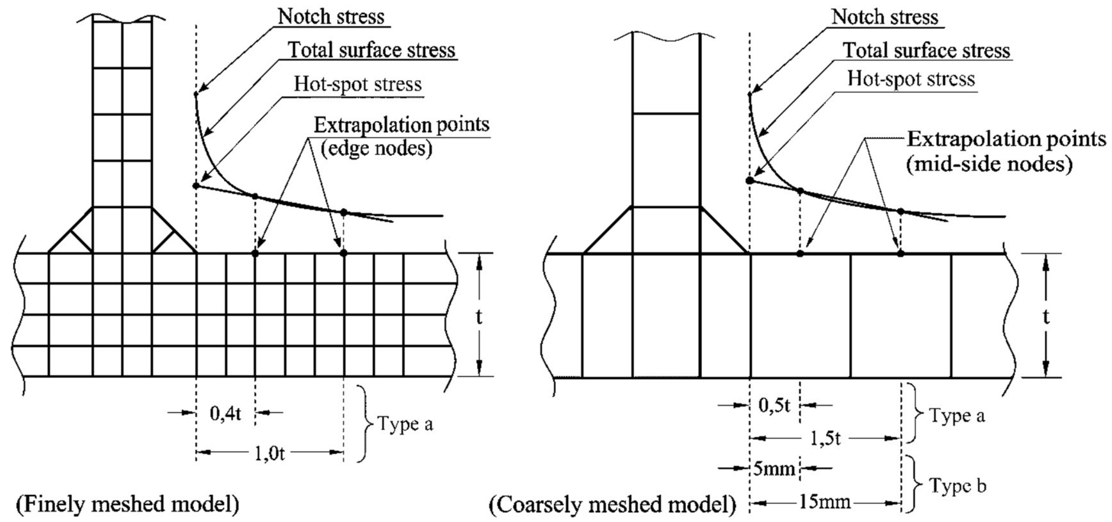

Figure 2.12 The stresses obtained from linear stress extrapolation technique, where a) is used for edge nodes and b) for mid-side nodes, redrawn from (Al-Emrani & Aygül, 2014).

2.3.2.4 Fatigue verification

The hot-spot stress from the FEA is compared with the S-N-curves in Eurocode 3, see Table 2.6.

Table 2.6 S-N-curves for the hot-spot stress method from Eurocode 3.

Detail description	$\Delta\sigma_C$ [MPa]
Full penetration butt joint, ground flushed	112
Full penetration butt joint	100
Cruciform joints, full penetration K-butt welds	100
Non load-carrying fillet welds	100
Bracket ends, ends of longitudinal stiffeners	100
Cover plate ends	100
Cruciform joints, load-carrying fillet welds	90

Equation (2.3) is used in order to obtain the fatigue life of the detail. $\Delta\sigma_{NS}$ is then $\Delta\sigma_{hss}$, i.e. hot-spot stress range, in this case. The stress range is also multiplied with a thickness correction factor:

$$\Delta\sigma_{hss,red} = k_s \Delta\sigma_{hss} \tag{2.9}$$

$$k_s = \left(\frac{t_{ref}}{t}\right)^n \tag{2.10}$$

$$t_{ref} = 25 \text{ mm}$$

$$0.1 \leq n \leq 0.3$$

To account for the misalignment in the detail, one must either multiply the stress range with a correction factor or implement the misalignment in the FE-model. The correction factor can be found in EN 1090-2:2002 and ISO 5817. Two examples are given in (Al-Emrani & Aygül, 2014), see Figure 2.13 and Figure 2.14. One for eccentricity and one for angular displacement:

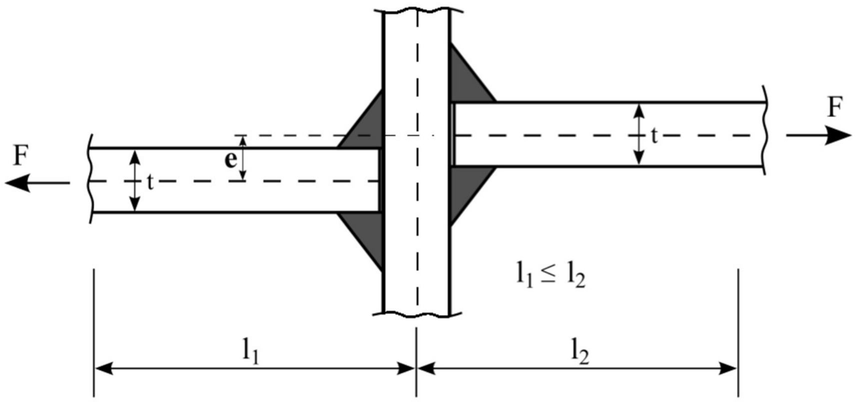

Figure 2.13 An example of misalignment correction factor for eccentricity in cruciform joints with fillet welds (Al-Emrani & Aygül, 2014).

$$k_m = \lambda \frac{e l_1}{t(l_1 + l_2)} \tag{2.11}$$

$\lambda = 3$ (fully restraint)

$\lambda = 6$ (unrestraint)

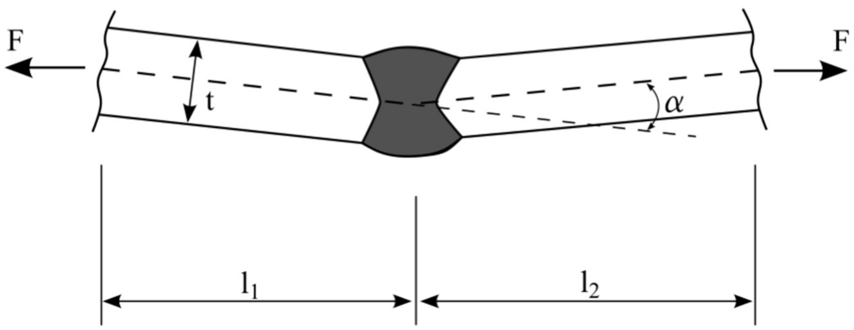

Figure 2.14 An example of misalignment factor for angular displacement in butt joints (Al-Emrani & Aygül, 2014).

$$k_m = 1 + \lambda\alpha \cdot \frac{l_1 l_2}{t(l_1 + l_2)} \tag{2.12}$$

$0.02 \leq \lambda \leq 0.04$ (in-plane displacements of transverse plate restricted)

$3 \leq \lambda \leq 6$ (otherwise)

2.3.2.5 Other structural stress approaches

There are a number of other structural approaches:

- "Through thickness structural stress approach" linearizes the stress distribution at the weld toe through the thickness of the plate. The advantage with this method is that it is mesh insensitive (Fricke, Sonsino, & Radaj D, 2006).
- "Battelle structural stress approach" uses an equilibrium condition between the stress distribution over the thickness at the weld toe and the stress at a distance, δ, from this point. The stress at the second point consists of the membrane and the bending stresses and the stress distribution from the two points must be in equilibrium (Dong, 2001)
- "1 mm structural stress approach" considers the stress at a depth of 1 mm from the surface at the weld toe and this stress is then the stress gradient of the plate thickness, if one does not consider the peak stress (Xiao & Yamada, 2004).

2.3.2.6 Example

To clarify how the workflow and the FE-modelling using the hot-spot stress method for a transverse non load-carrying attachment can be performed, an explanatory example will be studied. For this example, the flange thickness is 20 mm, the transverse attachment thickness 10 mm and the weld throat thickness set to 6 mm, see Figure 2.15. A linear extrapolation technique is chosen together with 3D elements. The hot-spot type for this detail is a, which can also be seen in Figure 2.11.

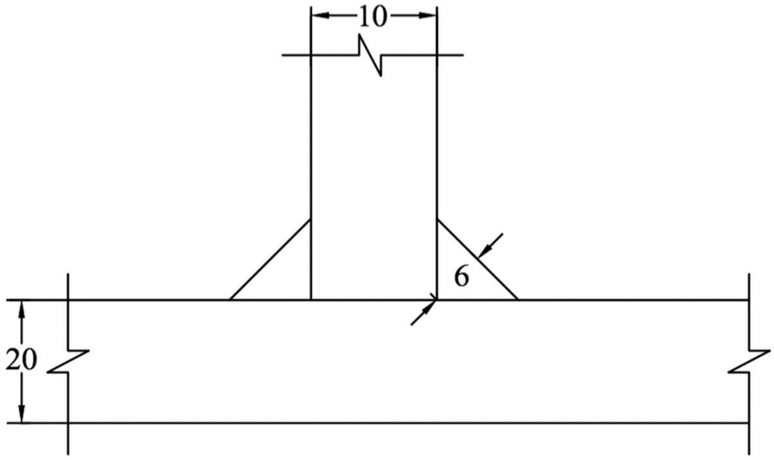

Figure 2.15 Example of a transverse attachment with its dimensions.

The modelling procedure is executed as follows:

1. Table 2.5 states that both coarse and fine mesh can be used with linear extrapolation technique.
2. Weld modelling is required according to Table 2.3. Coarse mesh with 20-node elements are chosen with 1 element over the plate thicknesses.
3. Linear extrapolation for type a hot-spot and course mesh size needs two extrapolation points with distance $0.5t$ respectively $1.5t$ according to Table 2.5.
4. The detail is meshed so that the element nodes and extrapolation points coincide, see Figure 2.12.
5. The static linear elastic analysis is performed.
6. Nodal stress values are extracted at the extrapolation points.
7. The stress is extrapolated to the cross section at the weld toe to obtain the hot-spot stress, see Figure 2.12.
8. The hot-spot stress is multiplied with the thickness correction factor from equation (2.9) and (2.10).
9. The hot-spot stress should also be multiplied with the misalignment correction factor from equation (2.11) if misalignment is present.
10. A non-load-carrying fillet weld gives a detail category of 100 MPa from Table 2.6.
11. The recommended partial factor from Eurocode, γ_{Mf}, is extracted from Table 2.1, if not the recommended value from the national annex is needed.
12. The fatigue life of the detail is calculated according to equation (2.3).

2.3.3 Effective notch stress method

Stress raisers such as porosities, sudden geometrical changes and undercuts are highly difficult to avoid completely in a welded structure. The stresses that occur at these positions are often denoted as “notch stresses” (Al-Emrani & Aygül, 2014). As opposed to the nominal stress method, the effective notch stress method, ENS, includes the effect of stress raisers at the examined notch. If the notch is sharp or even coming close to a notch radius of zero it tends to become a point of singularity, where the stresses goes to infinity.

To avoid this problem, it was proposed in (Radaj, Sonsino, & Fricke, 2006) that the sharp notch is replaced with a reference notch radius. A radius of 1 mm has proven to be consistent in most cases, see Figure 2.16 (Hobbacher, 2009).

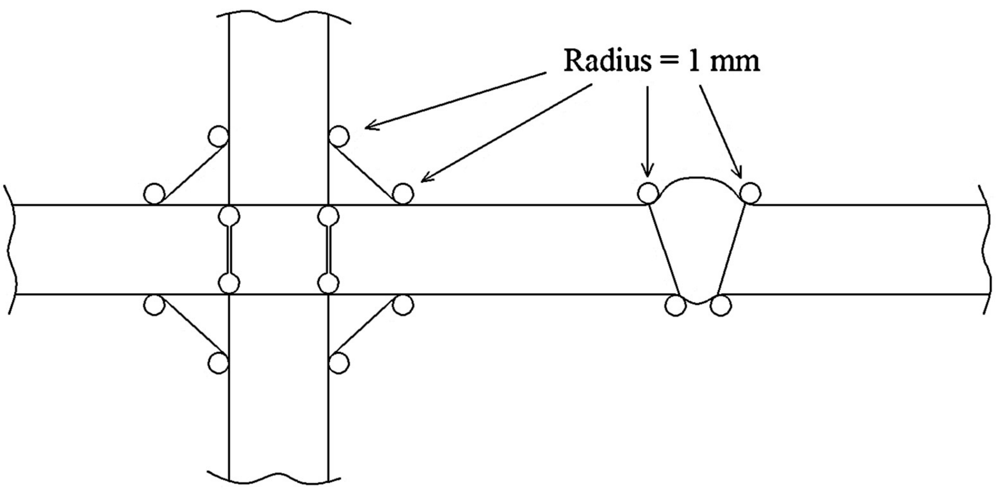

Figure 2.16 Rounding of sharp notches in the effective notch stress method, redrawn from (Sonsino, et al., 2010).

The principle of this method is to determine the fatigue life of a welded detail using the effective notch stress together with a single S-N-curve. This is of course an advantage compared to other methods where several detail categories may have to be combined in order to model the weld properly. The method is executed by means of a linear elastic FE-analysis since the definition of effective notch stress is when the elastic stress reaches its maximum value at the notch (Al-Emrani & Aygül, 2014).

2.3.3.1 Calculation of the effective notch radius

The idea with the effective notch stress method is to replace sharp notches with a fictitious radius to avoid singularity points, as previously stated. In 1968, Neuber invented a formula for this radius:

$$\rho_f = \rho + s\rho^* = 1 \text{ mm} \tag{2.13}$$

(Radaj, 1990) proposed recommendations for the variables in Neuber's formula when using the effective notch stress method:

$\rho = 0$ mm (actual notch radius, worst case) (Radaj, 1990)

$s = 2.5$ (stress multiaxiality and strength criterion) (Radaj, 1990)

$\rho^* = 0.4$ mm (micro – structural length, low strength steel) (Radaj, 1990)

This proposal is only valid for steel plates thicker than 5 mm since it has shown that such large radius for thin plates will change the stress distribution.

Therefore, a radius of 0.05 mm is recommended for plate thicknesses thinner than 5 mm (Richter & Zhang, 2000).

2.3.3.2 FE-modelling

The angle, θ, for the fillet and butt welds are recommended to 30° respectively 45°, see Figure 2.17. There are two different modelling techniques for the weld root, U-shape and keyhole. The type of shape is dependent on the weld. For non-load-carrying welds, the U-shape underestimates the stresses at the weld root and the keyhole overestimates them. However, the U-shape is easier to model and since root cracking is not expected for a non-load-carrying weld, the U-shape is often used.[1] For load-carrying welds, the U-shape is recommended (Fricke, 2010).

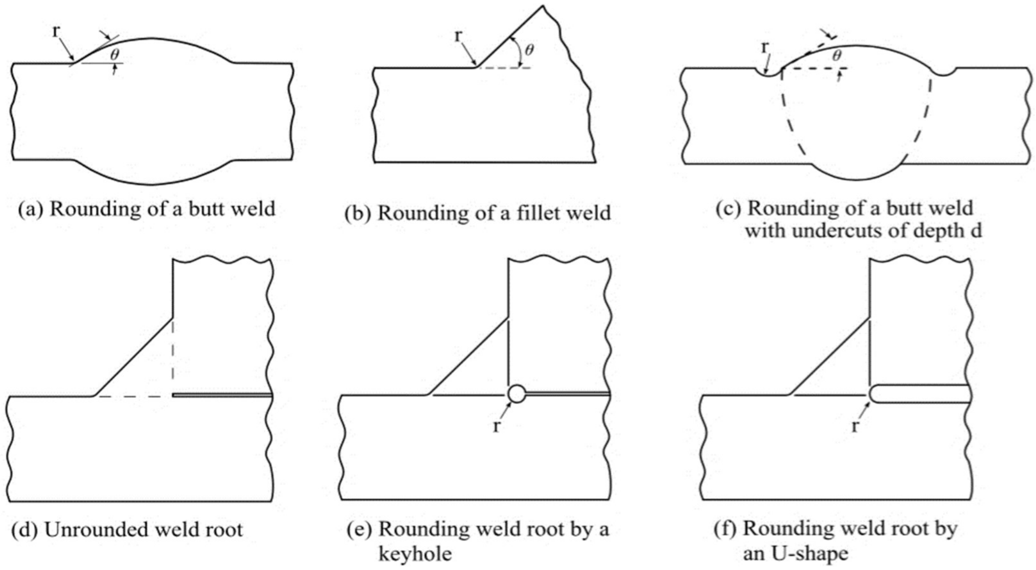

Figure 2.17 Modelling of notch stress radius for fillet and butt welds (Al-Emrani & Aygül, 2014).

Both 2D plane strain solid and 3D solid elements can be used to calculate the notch stress, where the former is easier but often applicable for simpler geometries. This yields that 3D elements can be required. It must be noted that 2D shell elements should not be used with the effective notch stress method. The geometry must be exactly modelled and misalignments not covered in the S-N-curve must be modelled. When using 3D elements, the model can become too large and a sub-modelling technique can be used to overcome this problem (Al-Emrani & Aygül, 2014).

The sub-modelling technique uses higher dense mesh in the areas of interest and a coarser mesh in the other parts of the structure. To achieve this, two finite element analyses are performed. The first FEA considers the whole structure with a coarse mesh. The stresses in the nodes on the cutting edges where the detail start are then

[1] Mohammad Al-Emrani (Associate Professor, Division of Structural Engineering, Chalmers University of Technology) meeting March 10th 2016.

extracted. These nodal stresses are then transferred to the analysis of the detail. It is important that the nodal positions are the same in both analyses. The detail is then modelled with a much denser mesh around the notches according to Table 2.7 and with a gradual transition from coarse to fine mesh.

Table 2.7 Recommended element size for different element types (Fricke, 2010).

Element type		Element size [mm]		
		Relative size	r = 1 mm ($t \geq$ 5 mm)	r = 0.05 mm (t < 5 mm)
Hexahedral	Quadratic	$\leq r$ / 4	0.25	0.012
	Linear	$\leq r$ / 6	0.15	0.008
Tetrahedral	Quadratic	$\leq r$ / 6	0.15	0.008

The different element types, i.e. linear and quadratic, can be seen in Figure 2.18. It should be noted that the quadratic element has mid-side nodes while the linear does not.

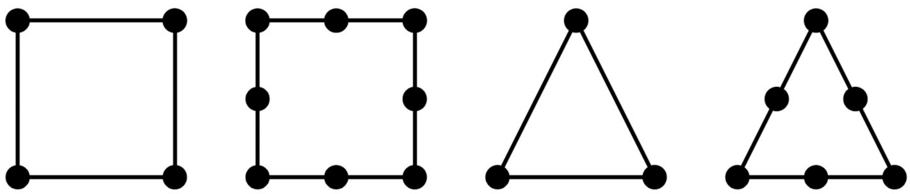

a) b) c) d)

Figure 2.18 a) Hexahedral linear element, i.e. 1st order. b) Hexahedral quadratic element, i.e. 2nd order. c) Tetrahedral linear element, i.e. 1st order. d) Tetrahedral quadratic element, i.e. 2nd order.

2.3.3.3 Fatigue verification

Due to the fact that the effective notch stress method includes the stress raisers from the local geometry, only one S-N-curve is required in respect to detail geometry. However, two different S-N-curves are presented and recommended by IIW for the two different radius sizes. These can be seen in Table 2.8. When the stress state is uni-axial at the notch, the principal stress should be considered.

Should the stress state be multi-axial, e.g. both axial and shear stresses acting at the same time, von Mises effective stress might have to be considered. If the multi-axial stress state is proportional, i.e. the directions of the principal stresses are constant with increasing load, principal stresses can still be considered in the analysis. However, if the stress state is non-proportional so that the directions are not constant then von Mises effective stress should be considered (Fricke, 2010).

Table 2.8 S-N-curves for the effective notch stress method (Fricke, 2010).

Reference radius	$\Delta\sigma_C$ (Principal stress)	$\Delta\sigma_C$ (von Mises stress)
r = 1 mm	FAT225	FAT200
r = 0.05 mm	FAT630	FAT560

The obtained stress value is then inserted in the equation (2.3) to obtain the fatigue life of the detail. $\Delta\sigma_i$ is then $\Delta\sigma_{ENS}$, i.e. effective notch stress range, in this case.

2.3.3.4 Example

To clarify how the workflow and the FE-modelling using the effective notch stress method for a transverse non load-carrying attachment can be performed, an explanatory example is presented. The same detail as in the hot-spot stress example will be studied, see Figure 2.15. 2D plane strain solid quadratic hexahedral elements are chosen and the stress direction is constant in this example.

The modelling procedure is executed as follows:

1. The plate thicknesses are larger than 5 mm, which yields an effective notch radius of 1 mm according to Section 2.3.3.1.
2. For non-load-carrying welds, a U-shape is chosen for the weld root modelling due to practical reasons stated in Section 2.3.3.2.
3. Quadratic hexahedral elements with an effective notch radius of 1 mm yields a recommended element size of 0.25 mm in Table 2.7.
4. The detail is meshed so that elements with a size of 0.25 mm occur at the notches and the gradual transition from coarse to finer mesh is achieved, all according to Section 2.3.3.2.
5. The static linear elastic analysis is executed.
6. For constant stress direction, IIW recommends principal stress as output stress, as stated in Section 2.3.3.3.
7. The maximum principal stress is extracted.
8. A 1 mm reference radius with a principal stress yields a detail category of 225 MPa in Table 2.8.
9. The recommended partial factor from Eurocode, γ_{Mf}, is extracted from Table 2.1, if not the recommended value from the national annex is needed.
10. The fatigue life of the detail is calculated according to equation (2.3).

3 Experimental data

To be able to verify and compare the results from the FE-analyses, data from experiments is gathered and summarised. The experimental data that is of interest comes from fatigue strength tests of non-load-carrying fillet welds, preferably where the dimensions of the specimens have been varied. This is to construct a database that can be compared with the parameter study performed on the detail of interest.

3.1 Experimental procedures

In general, the fatigue tests were conducted with two different setups depending on whether the tested specimen was a beam or a weld detail. Hydraulic fatigue testing machines were used to apply the needed load cycles on the specimen, most often with load frequencies ranging from 3 to 13 Hz. In (Fisher, et al., 1974) several attachments were welded to the beam specimens, see Figure 3.1.

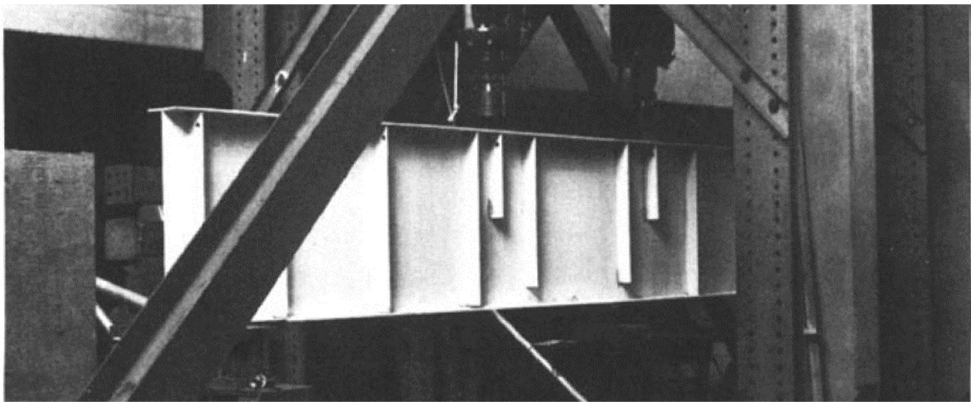

Figure 3.1 Beam test specimen with multiple attachments (Fisher, et al., 1974).

Attachments were placed in certain positions so that when one attachment failed, the experiment could be continued using a smaller span, see Figure 3.2.

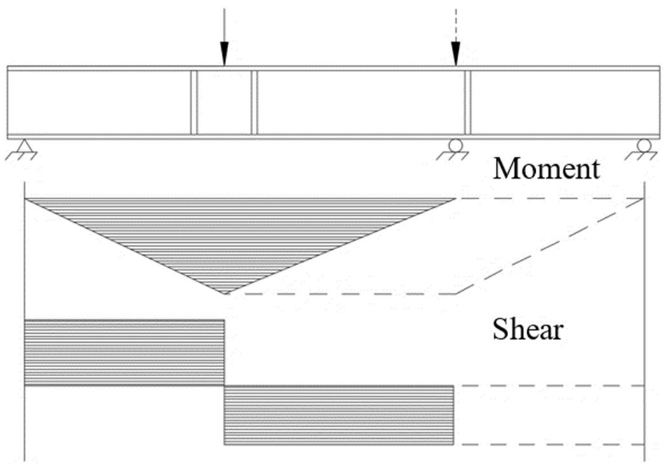

Figure 3.2 Continuation of experiment after cracking at one attachment, redrawn from (Fisher, et al., 1974).

Two point loads were applied on each beam at the beginning of each test series. When cracks appeared at one of the attachments, another support was added and the test was continued with a single point load in the middle of the span.

All double-sided specimens were manufactured as small-scale specimens. The specimens were clamped at each end of the main plate in the hydraulic machine and subjected to loads at a predefined frequency, see Figure 3.3 for an example of a typical configuration.

Figure 3.3 Typical fatigue experimental setup (Spadea & Frank, 2002).

3.2 Gathered experimental data

Table 3.1 lists the references from where the data is gathered as well as the number of tests and whether the test is performed on details or beams subjected to bending respectively.

Table 3.1 Sources from where experimental data is gathered.

Reference	# of tests	Detail/Beam	Single/Double stiffener
(Fisher, et al., 1974)	66	Beam	Single
(Gurney, 1991)	133	Detail	Double
(Albrecht & Friedland, 1979)	80	Detail	Double
(Puthli, Herion, & Bergers, 2006)	19	Detail	Double
(Kuhlmann, et al., 2005)	24	Detail	Double
(Klippstein & Schilling, 1989)	39	Detail	Double
(Gurney, 1995)	29	Detail	Double
(Berge, 1985)	8	Detail	Double
(Xiao & Yamada, 2004)	9	Detail	Double
	Σ 407		

A total of 407 fatigue test results from various sources have been found where the amount of experiments performed on details where only one attachment is welded to the main plate is quite limited. 66 of the total test results are one-sided. However, all of the one-sided tests are performed on beams subjected to bending and therefore not applied on small-scale specimens, which means that effects, such as shear lag, might have to be considered in the FE-model. See Figure 3.4 for diagram over the results. All specimens had a distance *L* smaller than 50 mm, meaning that the detail category is C80 according to Eurocode 3.

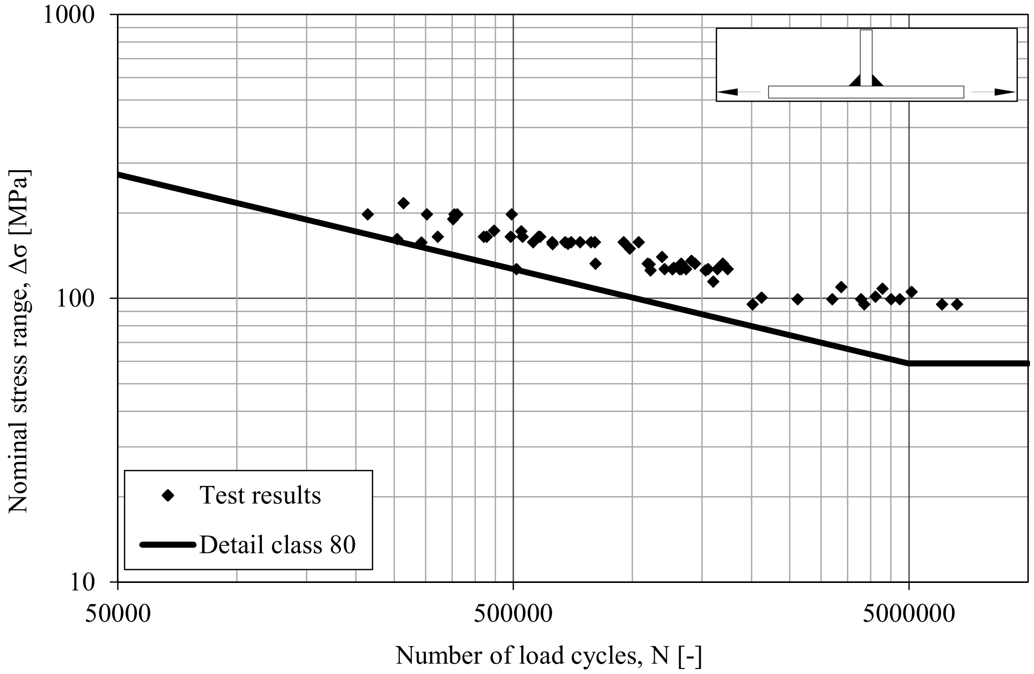

Figure 3.4 Experimental data of one-sided test specimens.

The double-sided test specimens, see Figure 3.5, constitutes over 80% of the constructed database. A great portion of the data comes from (Gurney, 1991) which also provides a good variation of the dimensions of the test specimens.

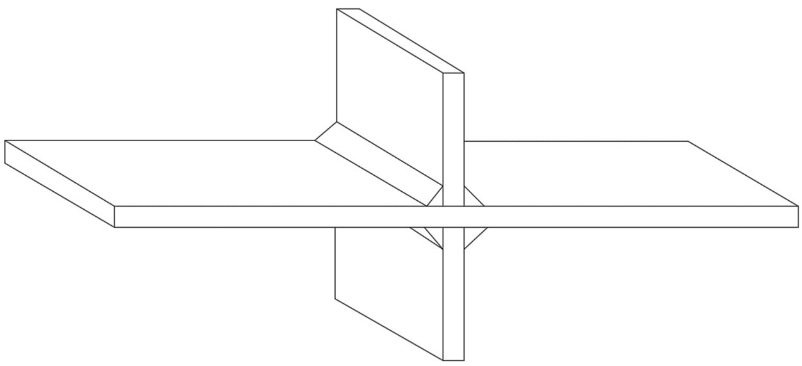

Figure 3.5 Test specimen with transverse stiffeners on both sides.

Some of the specimens in the gathered data are built up by steel plates, which have a very high thickness. The thickest plates used in the experiments are 220 mm thick and are not of interest in this field of application but still used in the verification. Figure 3.6 shows the test result for all specimens with double attachments together with lines representing detail categories C80 and C71 respectively.

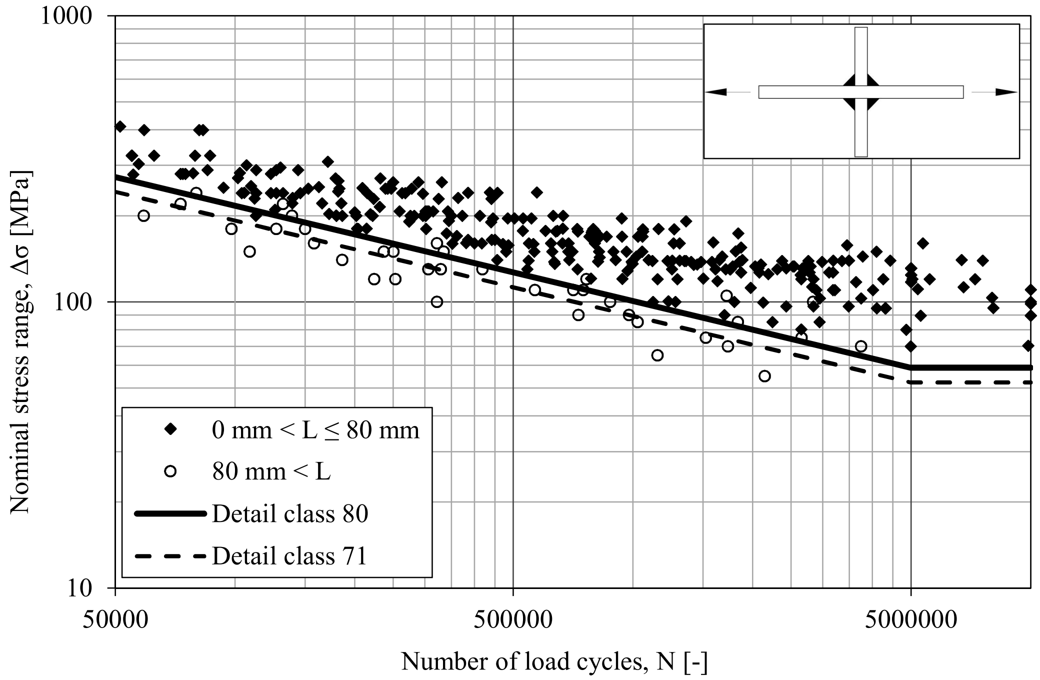

Figure 3.6 All experimental data of double-sided test specimens.

As can be seen in Figure 3.6, some of the points are located under the line for C71. This is simply due to the fact that the dimensions of these specimens are very large. In Eurocode 3, the maximum defined limit of *L*, i.e. the distance between weld toes, is 80 mm and in a few cases, it is up to 250 mm on the test specimens.

3.3 Organisation of experimental data

It is pointed out earlier that the calculated effective notch stress from the FE-analysis is used to calculate the stress concentration factor, K_t. The detail category C225, which is used for the effective notch method, is then divided with the stress concentration factor. This procedure is performed on the parameter study to convert the results into an equivalent detail category according to the nominal stress method.

In order to compare the fatigue test data with the parameter study, all relevant experimental data must be organized in groups based on parameters such as geometry etc., meaning that all data with specimens of the same dimensions are organised in the same group. For each of these groups, a separate detail category is calculated and compared to the FE-results to see how well the results are related. This comparison will be covered more thoroughly in Section 5.5. Tables with details of each group is found in Appendix A.

A detail category for each group is determined using a statistical evaluation of the test result where a linear regression is performed. The 95%-fractile with slope m = 3 is taken as the detail category for the current group.

In a few cases, specimens with similar values of L but different flange thicknesses, t_f, are put in the same group. The reason for this is discussed in Section 5.3.5. Figure 3.7 displays an example where all test data with flange thickness t_f = 25.4 mm and L = 57 mm are plotted. The fatigue strength class, $\Delta\sigma_C$, is in this particular case 80.4 MPa.

A summary of all calculated fatigue strength classes for the groups is found in tables in Appendix A.

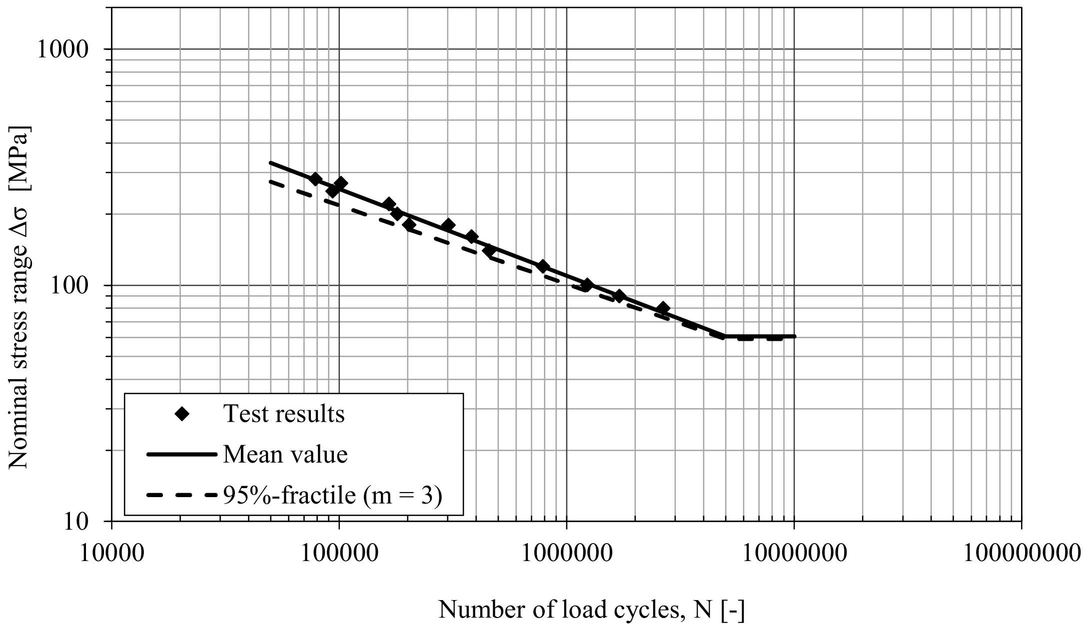

Figure 3.7 An example of the linear regression for the fatigue strength for test series with nominal stress range.

The calculated strength classes for each group are then plotted in the same diagram with respect to the distance *L*, see Figure 3.8. Groups where different flange thicknesses have been combined are written as an interval with the respective dimensions. "Double" and "Single" denotes whether stiffeners were welded to both sides of the main plate or only one respectively.

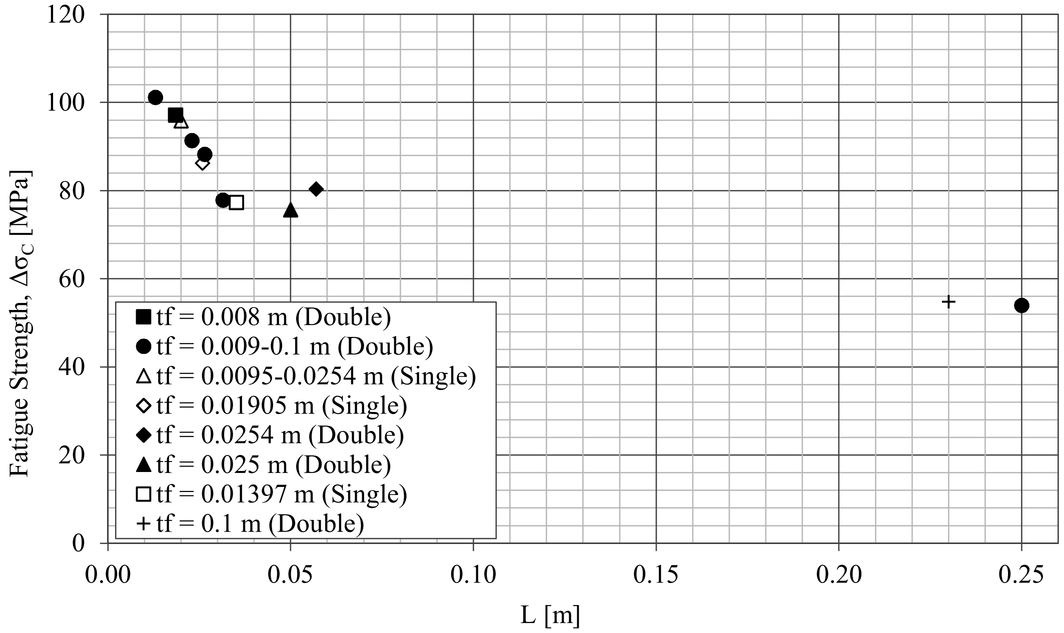

Figure 3.8 All experimental data organised together in groups based on dimensions and whether a single or two attachments are welded to the flange.

4 FE-modelling

The investigated detail for this report is, as previously explained, a transverse attachment, often found at web stiffeners for beams, see Figure 1.1. The following chapter will cover the procedure of the FE-modelling, i.e. how the geometry, material parameters, meshing, loading, boundary conditions and post-processing is executed. In order to make a general parameter study, 468 2D FE-analyses with different measurements are performed for one- and double-sided stiffeners, see Section 4.2.1. 68 of these FE-analyses are performed in order to study the individual effect of parameters, presented in Section 5.2. An additional 35 2D FE-analyses, based on the dimensions of the experimental data, are presented in Section 4.1. This yields a total number of 503 2D FE-analyses. A total of 9 3D FE-analyses are performed, where 5 of them are based on the dimensions from the experimental data in order to capture the 3D effects in the beam tests, see Section 4.3. In total, 512 FE-analyses are performed.

The FE-program used for the analysis is ADINA v.9.1.2 and the operating system is Linux. The software enables the user to create so called .in-files for the analysis, which are practical when performing a parameter study with many similar analyses with varying dimensions.

The .in-files contains all necessary code to run the desired analysis in ADINA. By using Excel, one can easily change different parameters in the code. These files can then be created and saved by an Excel-macro, see Appendix B. The .in-files and the corresponding FE-analyses as well as the extraction of the stresses are performed automatically by writing a script for the Linux terminal window. A flowchart of the process can be seen in Figure 4.1. All files used in the FE-analysis are appended in Appendix B.

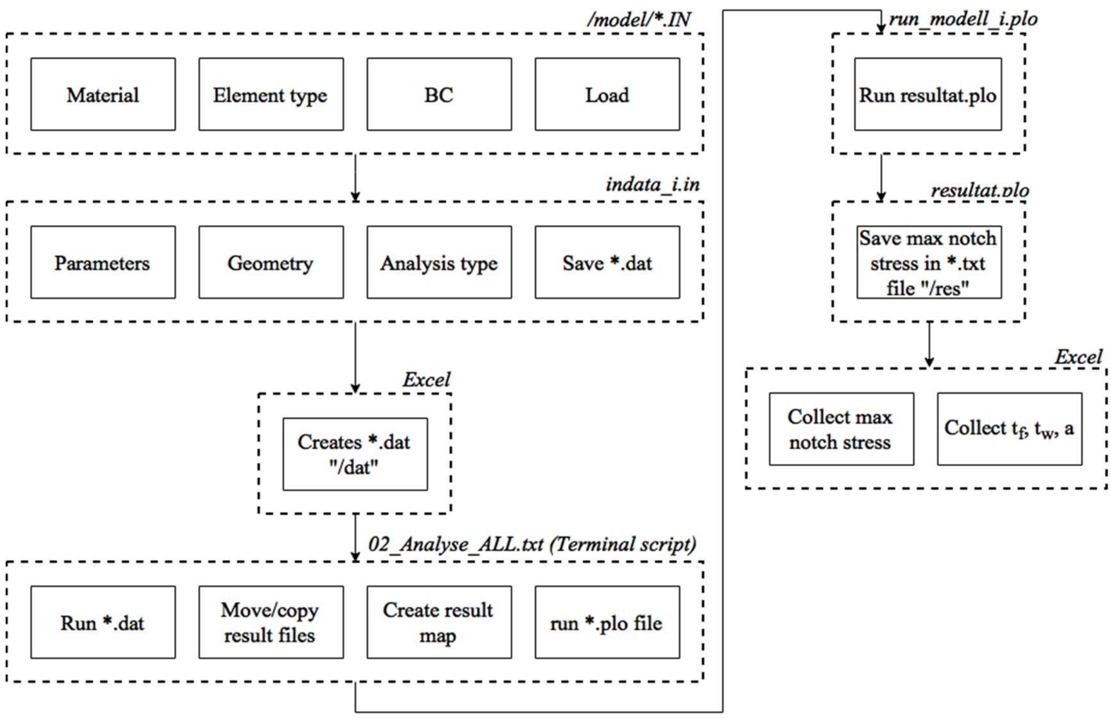

Figure 4.1 Flowchart illustrating the FE-process.

4.1 FE-models from experimental specimens

In order to obtain the fatigue strength class of the experimental data using the effective notch stress method, all dimensional configurations of the experimental data are used as input in the FE-analyses. In Figure 3.6, it can be seen that the data points have a quite high scatter. Similar specimens resist a different number of load cycles even though they were subjected to the same stress range. This is due to the fact the nominal stress does not take the full geometry of the detail into consideration as well as discontinuities, whether the weld is stress-relieved and so forth. As mentioned in Section 2.3.3, the effective notch stress method is able to include the effects of plate thicknesses, weld geometry and discontinuities. This means that the scatter of the results can be reduced significantly by using ENS to determine the fatigue life.

Since many of the tested specimens have similar dimensions, it is not necessary to run a FE-analysis for every data point gathered. Instead, each set of dimensions, i.e. each test series, is used as input for each analysis, resulting in a total of 30 FE-analyses for double-sided stiffeners and 6 for one-sided as stated in Section 5.5.

From the analyses, the stress concentration factor K_t is calculated. The nominal stress for each experimental data point corresponding to the analysed group is then multiplied with the stress concentration factor to get the notch stress of each test. When these notch stresses are plotted together with the number of load cycles until failure, a diagram with less scatter is obtained. See Section 5.2 for the results.

4.2 2D model

Since the experimental data consists of specimens with attachments welded to one side and both sides of the main plate, 2D models are created for both cases. A 2D model with plane strain elements is obviously an idealisation and might not be valid in all cases. In such cases where an idealisation like this is not possible, a more detailed model might be needed such as a 3D model. The following section will cover the work regarding construction of the 2D model.

4.2.1 Geometry

The geometry of the detail consists of a horizontal plate, representing the flange of the beam, a vertical plate, representing the web stiffener, and two equilateral triangles on both sides of the vertical plate, representing the welds. The angle of the welds are 45°. The measurements that will be changed in the analyses are the flange thickness, t_f, the web stiffener thickness, t_w, and the weld throat thickness, a, see Figure 4.2. The same geometry is used for both the one-sided and double-sided case but as will be mentioned in Section 4.2.4, the boundary conditions are slightly different.

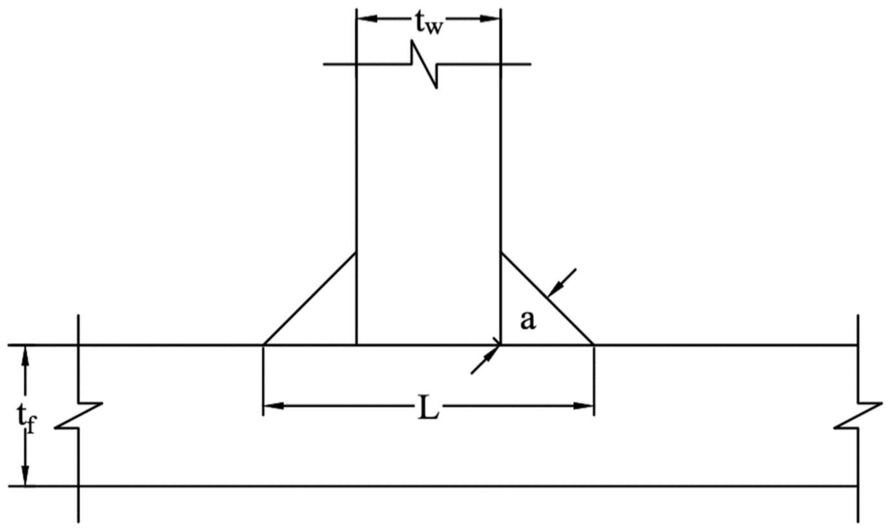

Figure 4.2 Parameters for the investigated detail, transverse attachment.

In this parameter study, the limitations of the measurements are:

$20 \text{ mm} \leq t_f \leq 60 \text{ mm}$ (Step size of 10 mm)

$0.3t_f \leq t_w \leq t_f$ (Step size of $0.1t_f$)

$0.1t_w + 0.0024 \leq a \leq 0.5t_w + 0.0024$ (Step size of $0.1t_w$)

Note that 2.4 mm is added to the weld throat geometry to increase the size of the smallest weld in the study, which otherwise would be 0.6 mm.

The length, L, can be calculated as:

$$L = t_w + 2\sqrt{2}a \quad (4.1)$$

Since the plate thicknesses are not less than 5 mm, an effective notch radius of 1 mm according to equation (2.13) is chosen. This radius complies both with the notches at the weld toes and also to the modelling of the weld root, see Figure 2.16. The weld root is modelled with a U-shape since no root cracking is expected, see Figure 2.17(f). The distance from the weld toes to the end edge of the plates is set to 60 mm.

4.2.2 Material

The investigated material is structural steel and the parameters for the analysis can be seen in Table 4.1. Since the method is performed by a linear elastic analysis, nonlinear material parameters are not needed. Even though the material density is specified, the gravitational force is not considered in the analysis.

Table 4.1 Table of the chosen material parameters.

Modulus of elasticity, E [GPa]	210
Poisson's ratio, υ [-]	0.3
Density, ρ_s [kg/m^3]	7800

4.2.3 Meshing

As presented in Table 2.7, there are recommendations for the maximum allowable mesh size depending on the element type and effective notch radius. In this analysis, 2D-solid plane strain quadratic hexahedral elements are used together with an effective notch radius of 1 mm. This yields a maximum allowable mesh size of 0.25 mm at the area surrounding the notches. The mesh size is then gradually increased from the notches according to the recommendation described in Section 2.3.3, see Figure 4.3 and Figure 4.4.

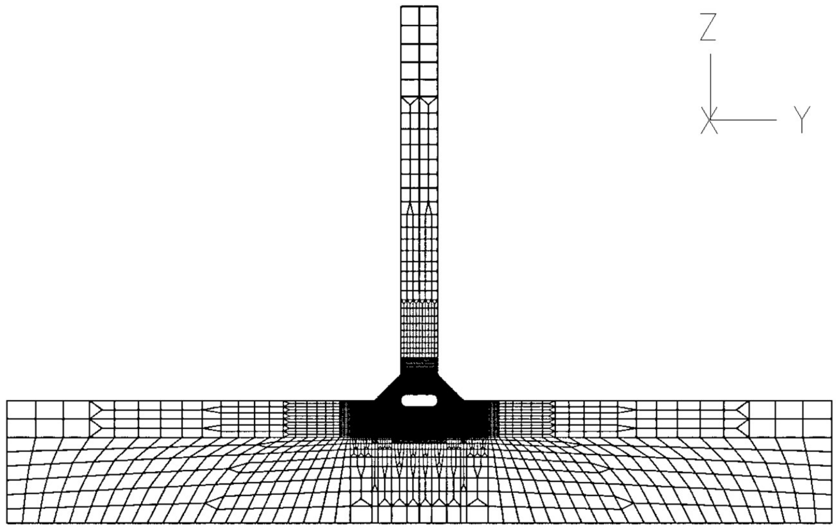

Figure 4.3 Mesh size of the entire geometry.

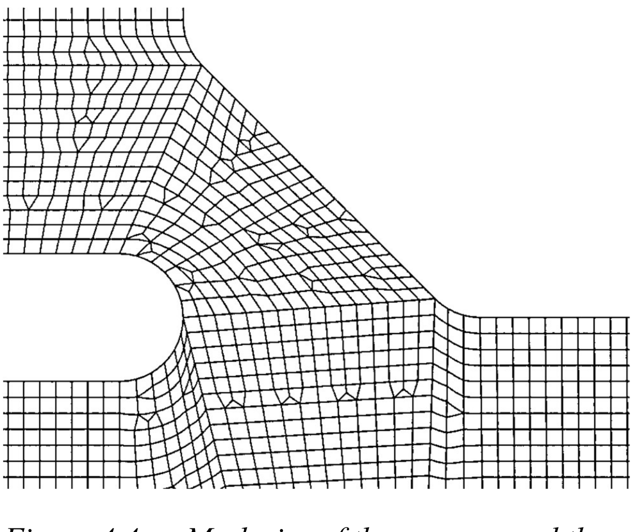

Figure 4.4 Mesh size of the area around the notches.

4.2.4 Loading and boundary conditions

A tensile stress of 1 MPa is applied on the left edge of the horizontal plate, which is meant to simulate the flange stress from the bending moment in a beam, see Figure 4.5. The stress is assumed constant over the height of the plate, while it in reality is varying over the thickness with a linear relationship. This simplification is considered as allowable. By choosing a nominal stress of 1 MPa, one can easily calculate the stress concentration factor, K_t.

In the one-sided case, the horizontal plate is prevented from moving in lateral direction at the bottom corners and prevented from moving in horizontal direction at the right-most edge, see Figure 4.5.

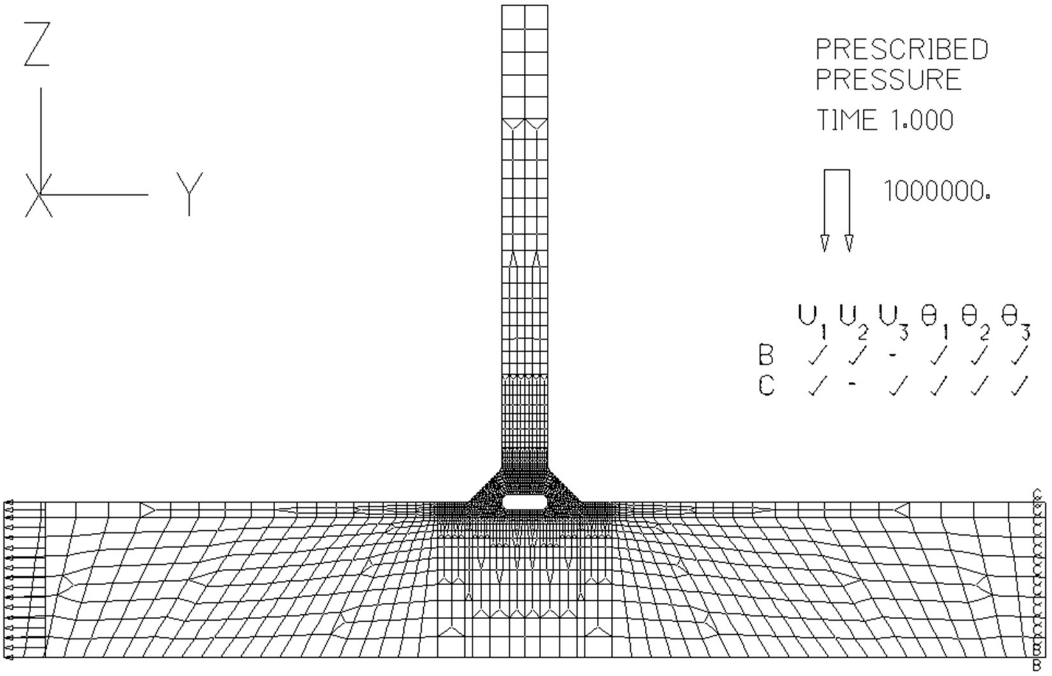

Figure 4.5 Applied load and boundary conditions on one-sided stiffener.

As mentioned earlier, the geometry is similar in the case where attachments are welded to both sides of the main plate. A symmetry line is added to the bottom of the plate to reduce the time needed for solving compared to if the full model would be constructed, see Figure 4.6. Since symmetry is used to construct the model, half of the analysed flange thickness must be used to construct the geometry in order to get correct dimensions of the full model.

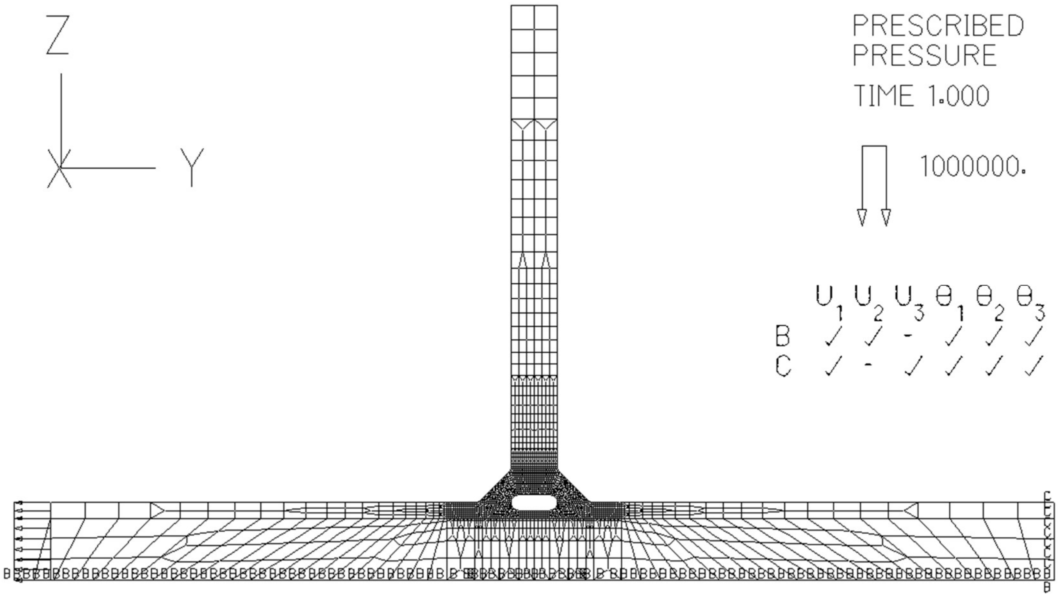

Figure 4.6 Applied load and boundary conditions on double-sided stiffener.

4.2.5 Model verification and mesh convergence

To verify the FE-analyses, one of the FE-models is verified by comparing the applied force and the corresponding reaction forces. The sum of the reaction forces at the boundary, gives a result of 19999.992 N. This value is then compared with the applied force at the opposite side, which has a magnitude of 20000 N. The forces are corresponding well to each other, indicating that the model seems to be correct. A study of the shape of the deflections is also carried out and is considered reasonable. The deformation plots for both one- and double-sided stiffener are seen in Figure 4.7 and Figure 4.8 respectively.

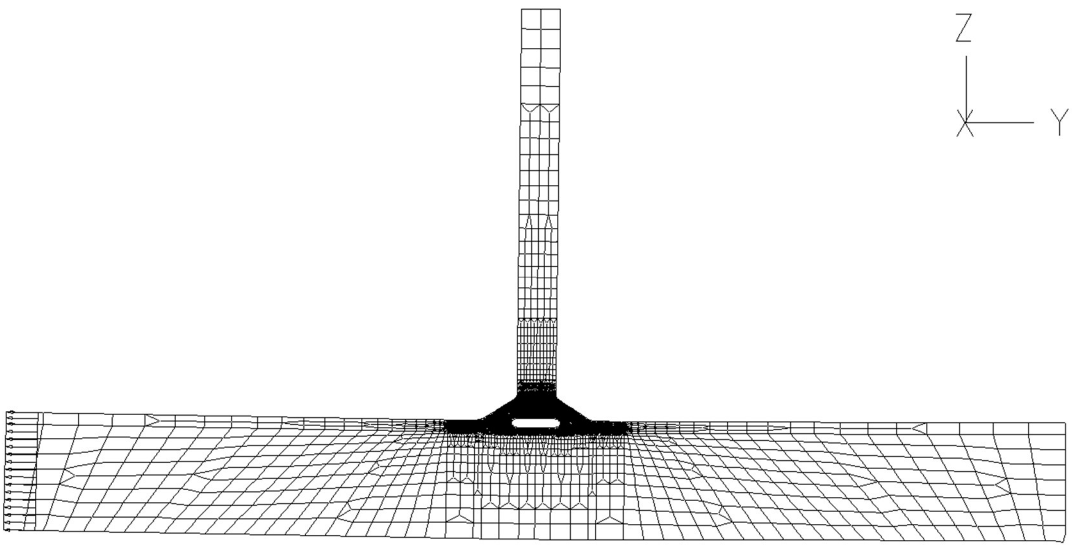

Figure 4.7 Deformation including the small rotation for one-sided stiffener.

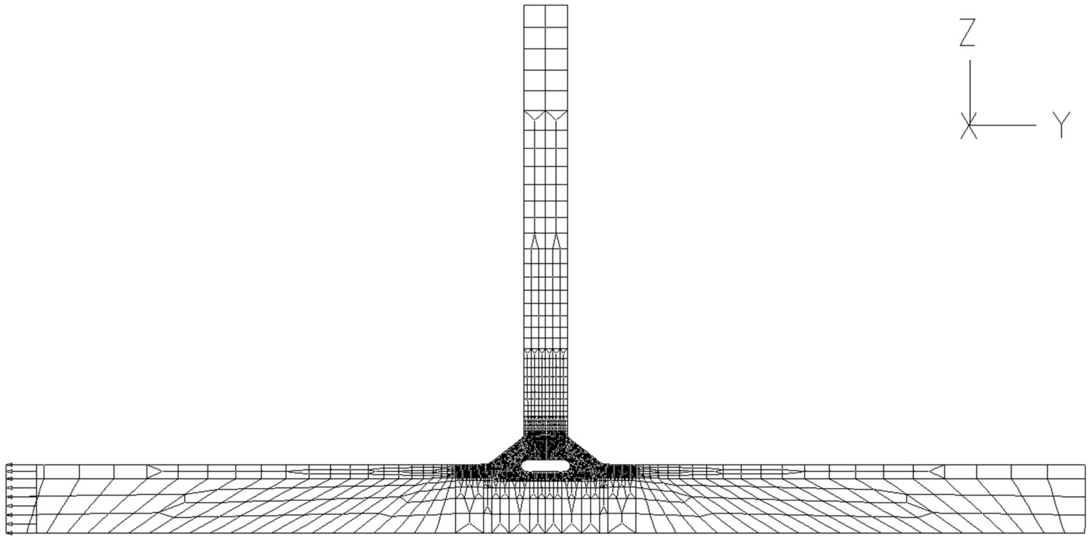

Figure 4.8 Deformation with no rotations for double-sided stiffener.

The chosen mesh size around the notches is 0.25 mm, as described in Section 4.2.3. The value is a recommendation from IIW and the mesh convergence study can be seen in Figure 4.9 and Table 4.2, where it also can be seen that the maximum principal stress is considered to have reached convergence at the chosen element size. The elements further away from the notches are gradually becoming larger and are chosen so that the 1:2 ratio recommendation regarding width and length of the elements is not exceeded.

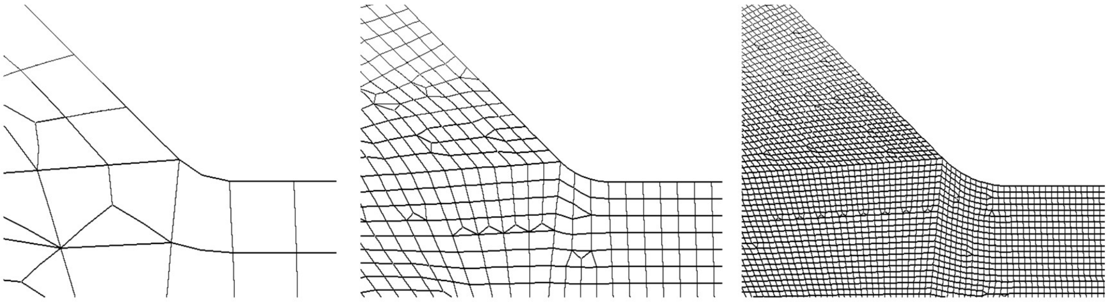

a) b) c)

Figure 4.9 Mesh convergence study for the mesh size around the notches a) 1 mm, b) 0.25 mm and c) 0.0625 mm.

Table 4.2 Mesh convergence study in 2D for the mesh size around the notches.

Mesh size [mm]	1	0.25	0.0625
Maximum principal stress, ENS [MPa]	1.938	2.401	2.396

4.2.6 Post-processing results

Since the stress is uni-axial, the maximum principal stress will represent the effective notch stress according to Table 2.8. When studying the principal stress at the notch region in Figure 4.10, one can see that the maximum principal stress occurs at the notch as predicted. In addition, a smaller stress concentration can be seen at the weld root notch. The major part of the horizontal plate experiences a stress of 1 MPa, which corresponds to the nominal stress. The maximum principal stress is extracted from all FE-models and the data is presented in Appendix C.

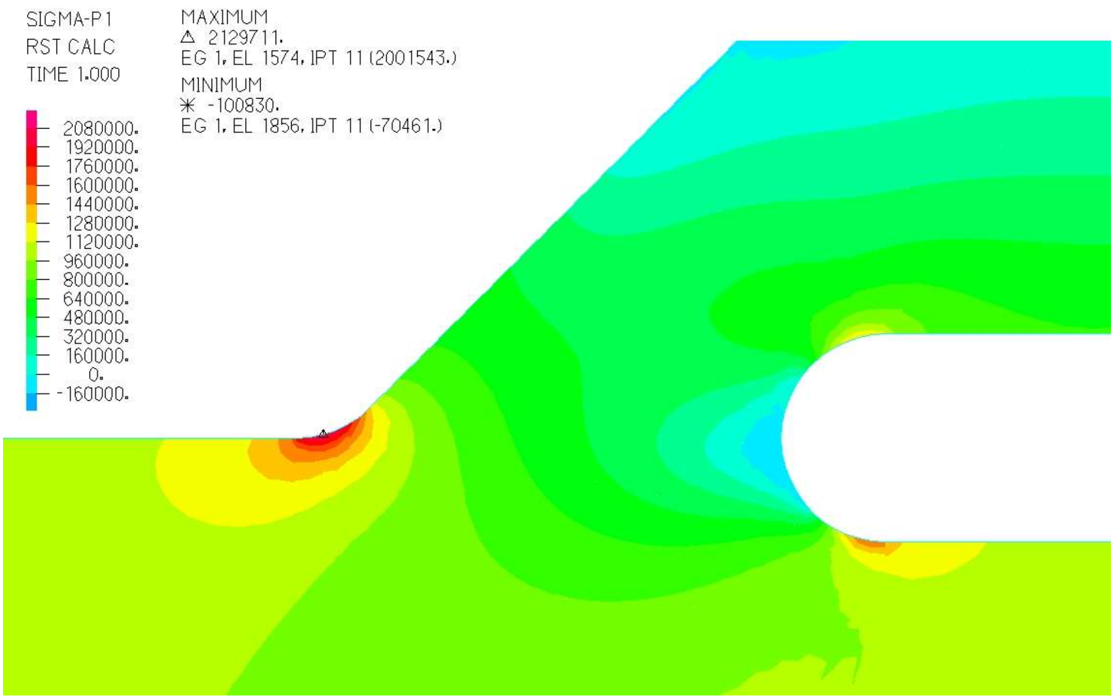

Figure 4.10 Maximum principal stress for one 2D FE-model.

To be able to compare the maximum principal notch stresses, i.e. the effective notch stresses, with the experimental data presented in Section 5.4, the stresses must be converted to corresponding detail category.

From Section 4.2.4:

$$\sigma_{NS} = 1 \text{ MPa}$$

From equation (2.2):

$$K_t = \frac{\sigma_{ENS}}{\sigma_{NS}} \tag{4.2}$$

From Table 2.8:

$$\sigma_{c,ENS} = 225 \text{ MPa}$$

From Eurocode 3:

$$\Delta\sigma_{NS}{}^{m} N = \Delta\sigma_{c,NS}{}^{m} \cdot 2 \cdot 10^6 \tag{4.3}$$

Gives:

$$N = \left(\frac{\Delta\sigma_{c,NS}}{\Delta\sigma_{NS}}\right)^m \cdot 2 \cdot 10^6 \tag{4.4}$$

The corresponding equation for effective notch stress range is:

$$N = \left(\frac{\Delta\sigma_{c,ENS}}{\Delta\sigma_{ENS}}\right)^{m} \cdot 2 \cdot 10^{6} \tag{4.5}$$

The fatigue life, N, should be the same for both approaches and yields:

$$\Delta\sigma_{c,NS} = \frac{\Delta\sigma_{c,ENS}}{\Delta\sigma_{ENS}} \cdot \Delta\sigma_{NS} \tag{4.6}$$

Substitution with K_t yields:

$$\Delta\sigma_{c,NS} = \frac{\Delta\sigma_{c,ENS}}{K_t} \tag{4.7}$$

The obtained detail category from equation (4.7) can then be compared with the detail categories from the experimental data in Chapter 3. This can be seen in Section 5.4.

4.3 3D model

As discussed in Section 5.1.3, 3D-analyses of the one-sided stiffeners from beam tests may be needed in order to capture all effects. A 3D model is more accurate than a 2D model, as previously mentioned in Section 4.2. This section will cover the modelling of these 3D-analyses and the post-processing of the results.

4.3.1 Geometry

The 3D model consists of a beam with transverse stiffeners on both sides of the web located at the midsection of the beam to replicate the one-sided attachment experiments described in Section 3.1. An example of how the experiments are performed can be seen in Figure 3.1. All the geometrical data of the beams and the web stiffeners can be seen in Appendix A.

In order to reduce the size of the analysis, two symmetry planes are used. The first symmetry plane is the x-z-plane, mirroring the geometry at the midsection of the web with y-translation prevented. The second symmetry plane is the y-z-plane, mirroring the geometry at the midsection of the transverse stiffener, see Figure 4.11.

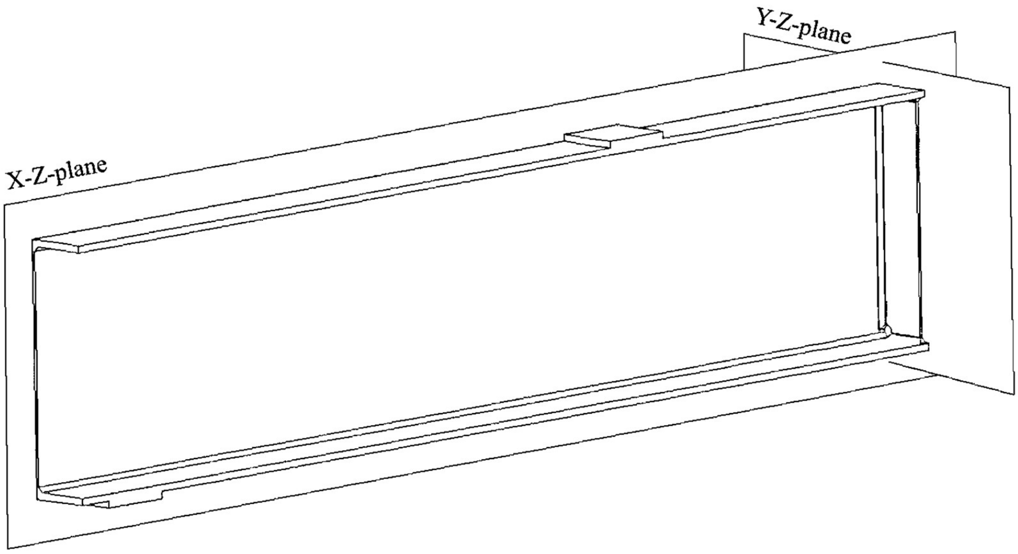

Figure 4.11 The geometry of the 3D models with two symmetry planes.

Two plates are placed at the location of the support and load application respectively. Cope holes at the corners of the transverse stiffener to the web are assumed and their dimension is assumed as well since no information of this is given. The transverse stiffener is welded all around the connecting perimeters with a weld angle of 45° and the notches have a rounding notch of 1 mm, see Figure 4.12.

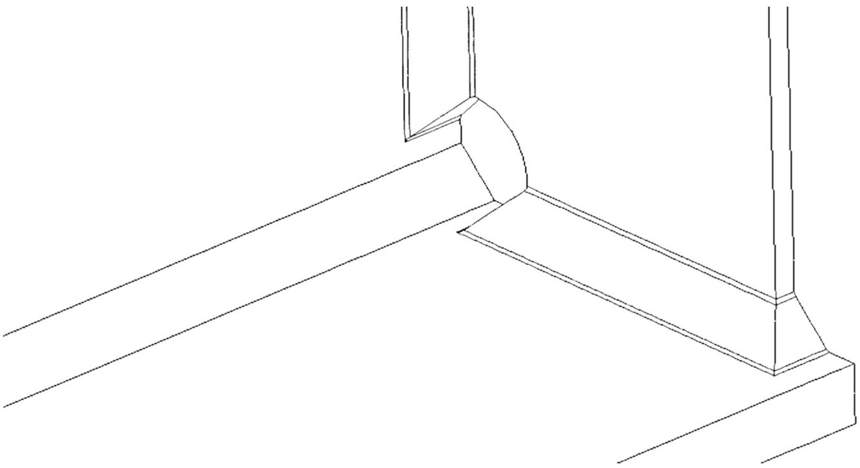

Figure 4.12 The geometry of the welds at the transverse stiffener.

4.3.2 Material

The material is structural steel and the material parameters for the 3D model are the same as for the 2D model described in Section 4.2.2, which can be seen in Table 4.1. As previously stated, the method is performed by a linear elastic analysis and therefore nonlinear material parameters are not needed. The gravitational force is not considered in the 3D-analysis as well.

4.3.3 Meshing

There are recommendations for the maximum allowable mesh size for the 3D analysis as well and the same recommendations, as presented in Table 2.7, for the 2D model applies. The chosen element type for the analyses are quadratic 10-node 3D-solid tetrahedral elements. The same mesh size recommendations as for tetrahedral applies. Since the notches are 1 mm, the maximum recommended mesh size is then 0.15 mm. The mesh size is also gradually increased from the notches, as seen in Figure 4.13 and Figure 4.14.

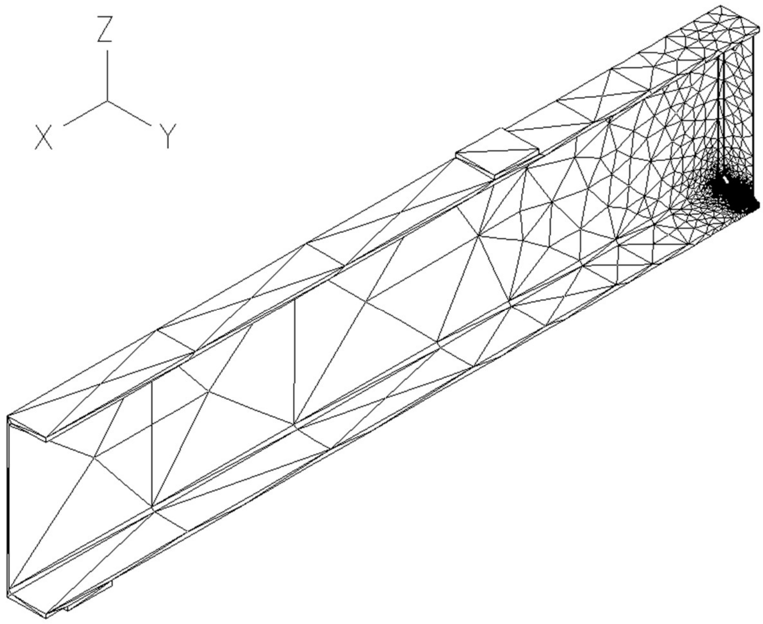

Figure 4.13 Meshing of the entire 3D geometry.

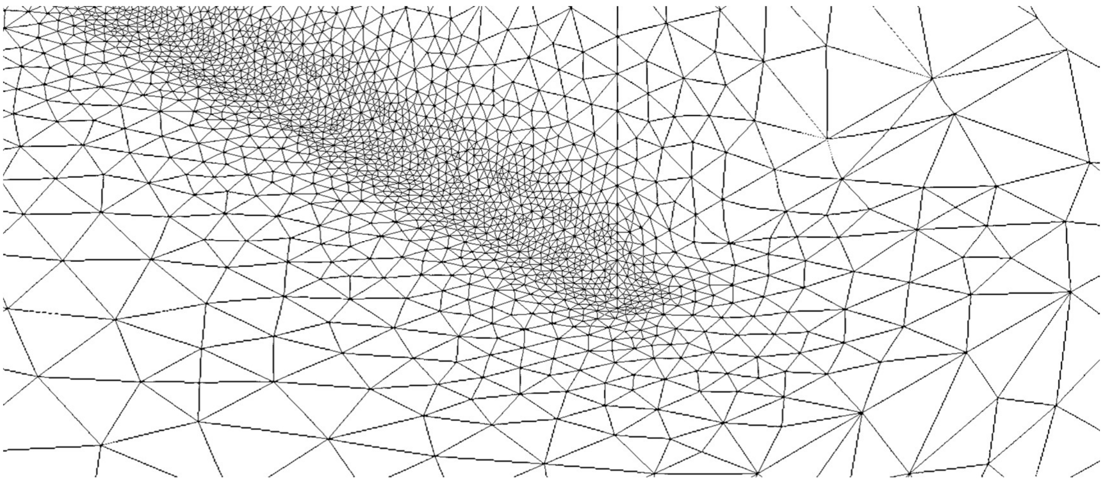

Figure 4.14 Mesh around the notches in the 3D analysis.

4.3.4 Loading and boundary conditions

The beam is subjected to four point bending, i.e. simply supported in both ends and two point loads evenly distributed over the beam length, see Figure 4.15. The loads are of a magnitude of 1 MPa distributed over the loading plates described in Chapter 4.3.1, which yields a maximum moment in the mid-section. The nominal stress in the flange can then be obtained by using Navier's formula from equation (2.8), see Section 4.3.6.

The two symmetry planes in Section 4.3.1 yields additional boundary conditions at those planes. Boundary conditions C and D represents those boundary conditions, see Figure 4.15. The beam is supported at the inner edge of the support plane in order to represent a simply supported beam, represented by boundary conditions B in Figure 4.15.

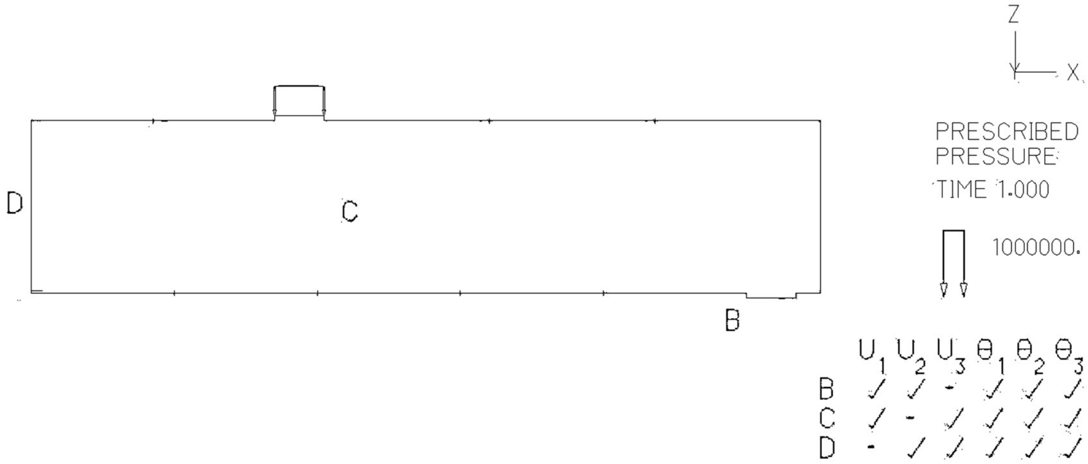

Figure 4.15 Applied load and boundary conditions on the 3D models, view from the backside of the web symmetry plane.

4.3.5 Model verification and mesh convergence

The sum of the reaction forces for the models are compared with the applied load and conforms well. The deflection is also studied and the beam deflects as expected, which is seen in Figure 4.16.

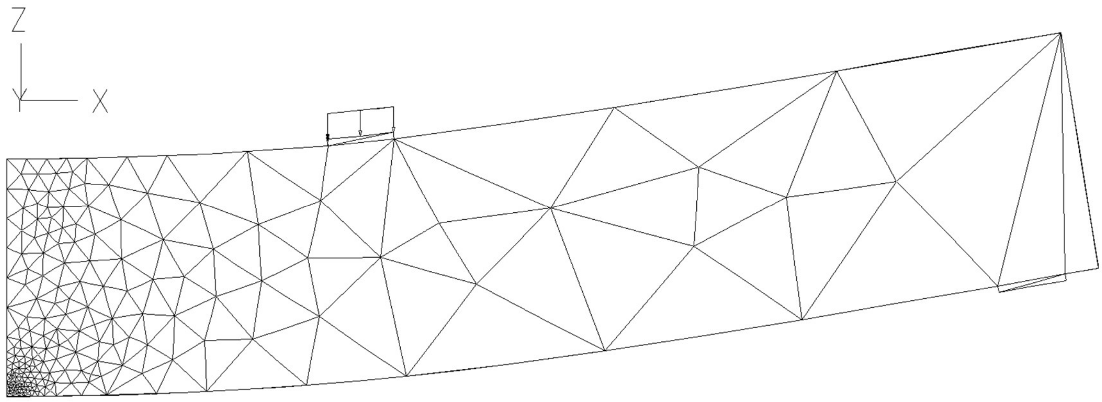

Figure 4.16 Deformation of beam in 3D.

A mesh convergence test is performed on the elements around the notches. It can be seen in Table 4.3 that the maximum principal stress is considered to have reached convergence at 0.15 mm mesh size. Due to computational limitations in the computer program used, smaller element size could not be obtained. Larger element sizes to show the convergence could also not be used, since the size of the notch prevents larger elements as seen in Figure 4.17. The different element sizes used in the convergence test can be seen in Figure 4.17.

Table 4.3 Mesh convergence study in 3D for the mesh size around the notches.

Mesh size [mm]	1	0.5	0.3	0.15
Number of elements [-]	36404	99905	218948	733078
Maximum principal stress, ENS [MPa]	54.57	52.99	51.99	50.98

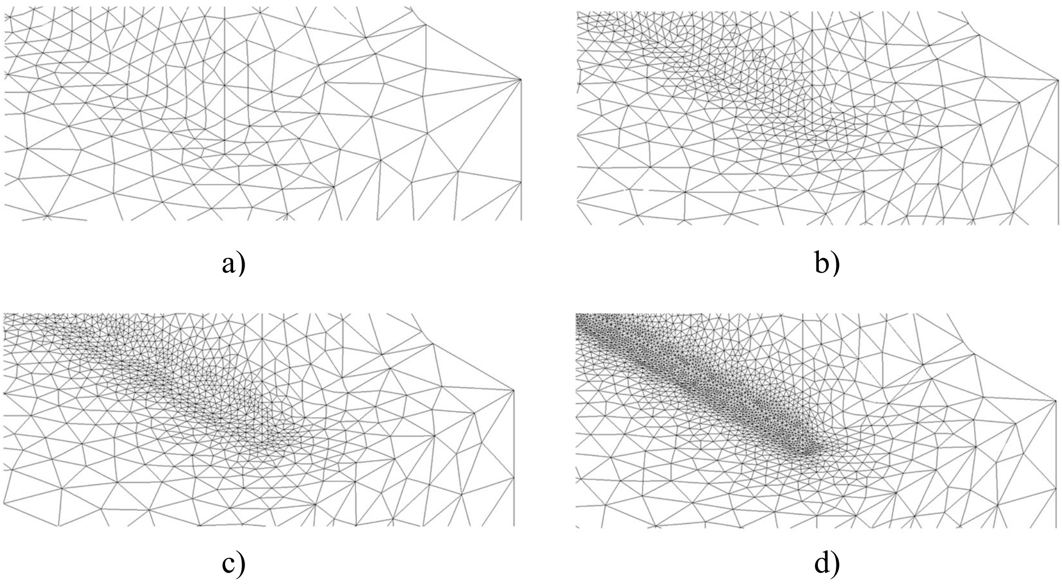

Figure 4.17 Mesh convergence study for the mesh size around the notches a) 1 mm, b) 0.5 mm, c) 0.3 mm and d) 0.15 mm.

4.3.6 Post-processing results

Since the stress at the flange is uni-axial, the maximum principal stress will represent the effective notch stress according to Table 2.8. It can be seen in Figure 4.18 that the maximum principal stress occurs at the weld toe as expected. The weld root stress is not considered in the analysis due to model size and since it can be expected not to exceed the weld toe stress, which the results from the 2D analysis are proving.

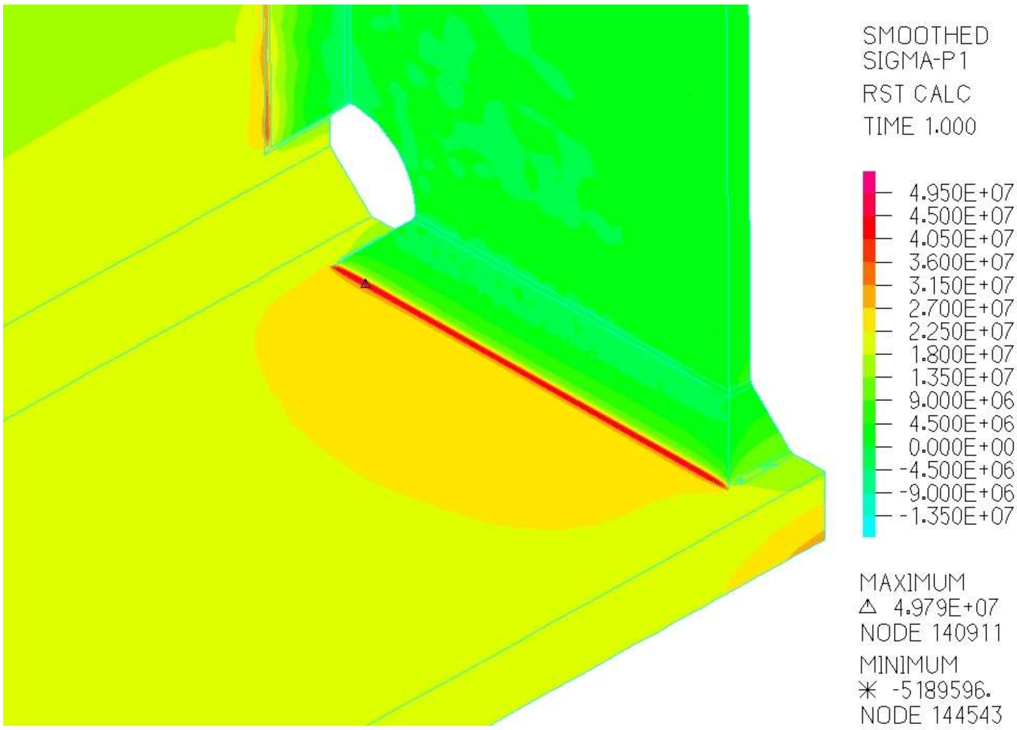

Figure 4.18 Maximum principal stress for one 3D FE-model.

The nominal stress at the upper edge of the flange is calculated by using Navier's formula of the cross section, see equation (2.8). Since the transverse stiffener is located at the mid-section of the beam, the maximum moment over the beam is used in the calculation. Equation (4.2) stated in Section 4.2.6, which converts the effective notch stress to a concentration factor so that the corresponding fatigue strength class can be obtained in equation (4.7), applies to the 3D-results as well.

5 Results

The results from the FE-analyses are divided into three main parts. The first part covers the FE-analyses based on the experimental data whereas the second part consists of the fictitious geometry specifications, i.e. the parameter study. This part investigates the influencing parametrical factors of the detail as well as compares the found results to Eurocode 3. Finally, the experimental data is used to verify the results based on the parametric study.

5.1 Effective notch stress comparisons

The following sections are presented to verify that the effective notch stress method does consider more geometrical parameters compared to e.g. the nominal stress method. Moreover it is also investigated whether the given strength class of $\Delta\sigma_{C,ENS}$ = 225 MPa is reasonable. This is done by applying the effective notch method on the gathered experimental results.

5.1.1 Comparison between nominal and effective notch stress

In this section, the difference between the nominal stress, NS, and the effective notch stress, ENS, will be studied. As discussed in Section 4.1, the nominal stress from the experiment is multiplied with K_t obtained from the FE-analyses, see Appendix C for the K_t-values. One can see that when comparing double-sided stiffeners in Figure 5.1 for nominal stress with Figure 5.2 for effective notch stress, the scatter in the results decreases when effective notch stress is studied. This is because the effective notch stress method takes more effects into account as described in Section 2.3.3.

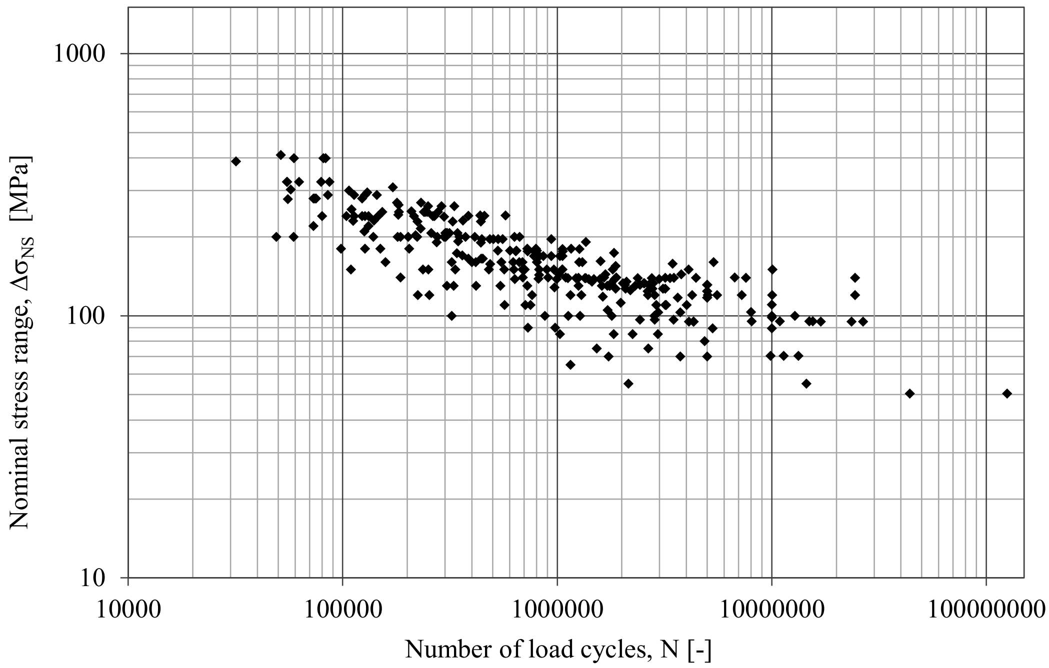

Figure 5.1 S-N-curve for experimental data with nominal stress for double-sided stiffeners.

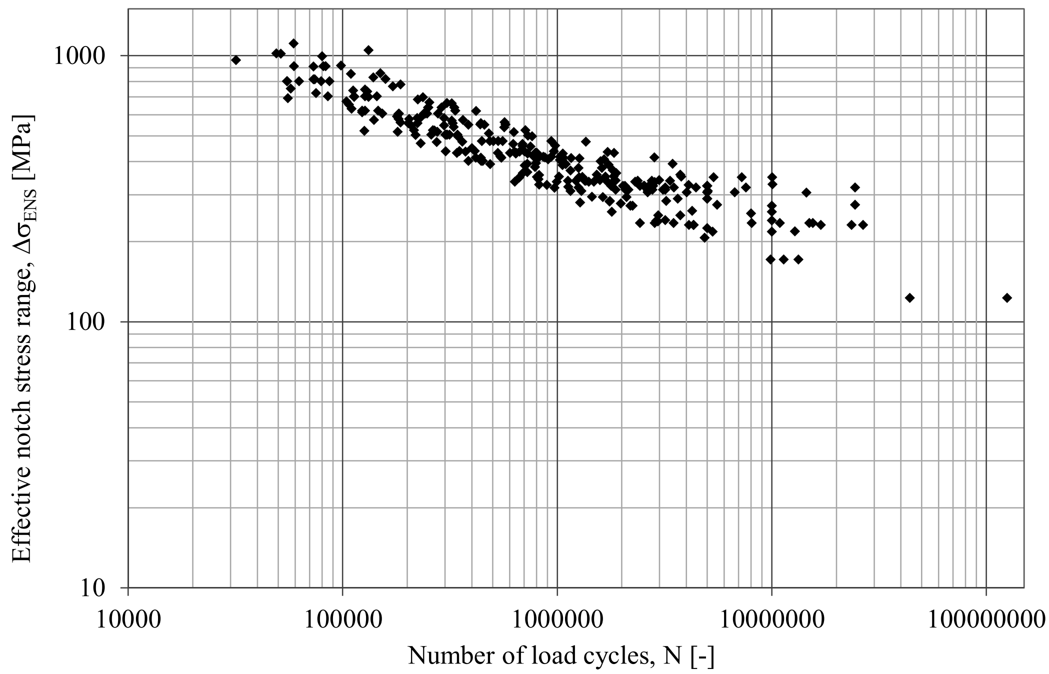

Figure 5.2 S-N-curve for experimental data with effective notch stress from FE-results for double-sided stiffeners.

One can also see that the same phenomenon appears when comparing one-sided stiffeners in Figure 5.3 and Figure 5.4.

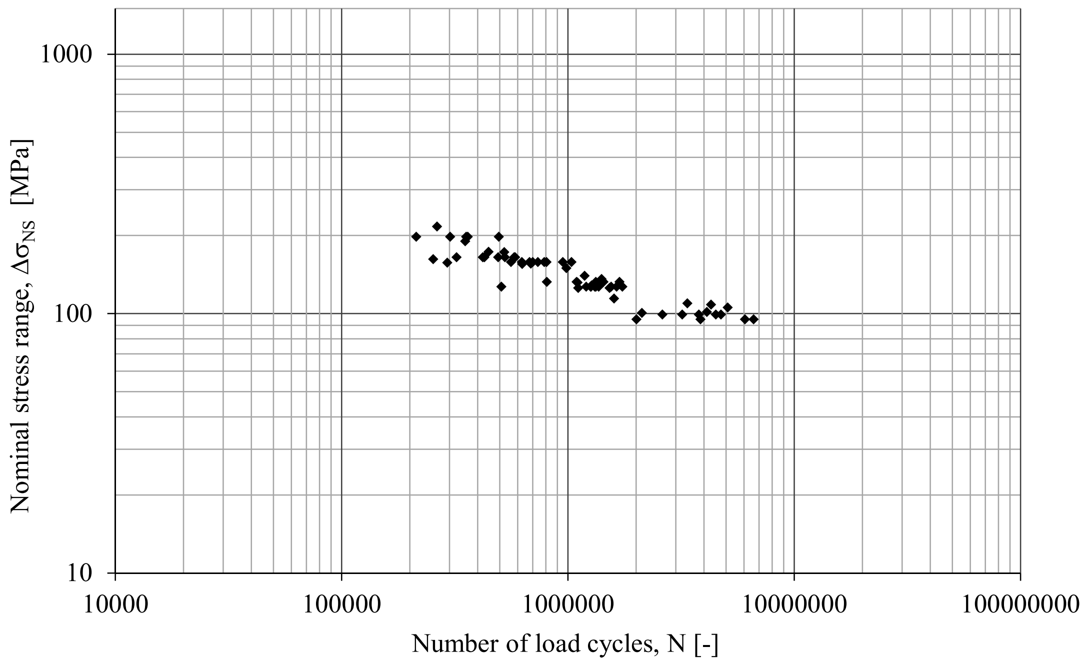

Figure 5.3 S-N-curve for experimental data with nominal stress for one-sided stiffeners.

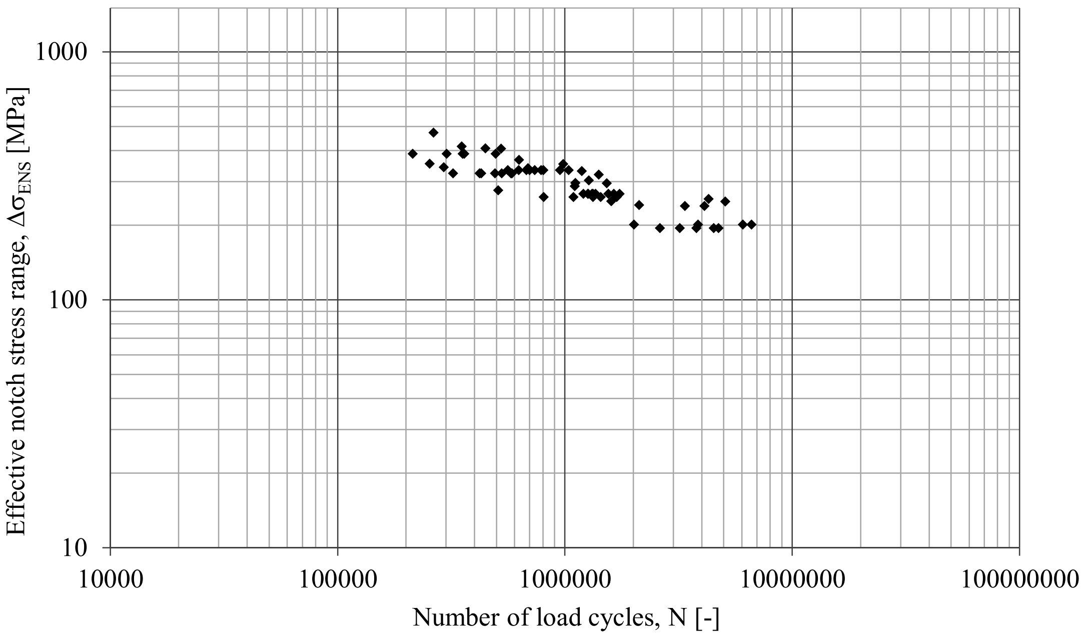

Figure 5.4 *S-N-curve for experimental data with effective notch stress from FE-results for one-sided stiffeners.*

5.1.2 Fatigue strength class for FE-analyses in 2D

In accordance to (CEN, 2002) a linear regression is performed on the results from the notch stress analyses performed on the experimental data to obtain a fatigue strength class. It is taken as the 95%-fractile of the stress range at 2 million load cycles with a slope m = 3. Figure 5.5 shows the linear regression for the double-sided test specimens. The obtained fatigue strength class according to the effective notch stress method with a slope m = 3 is 233 MPa.

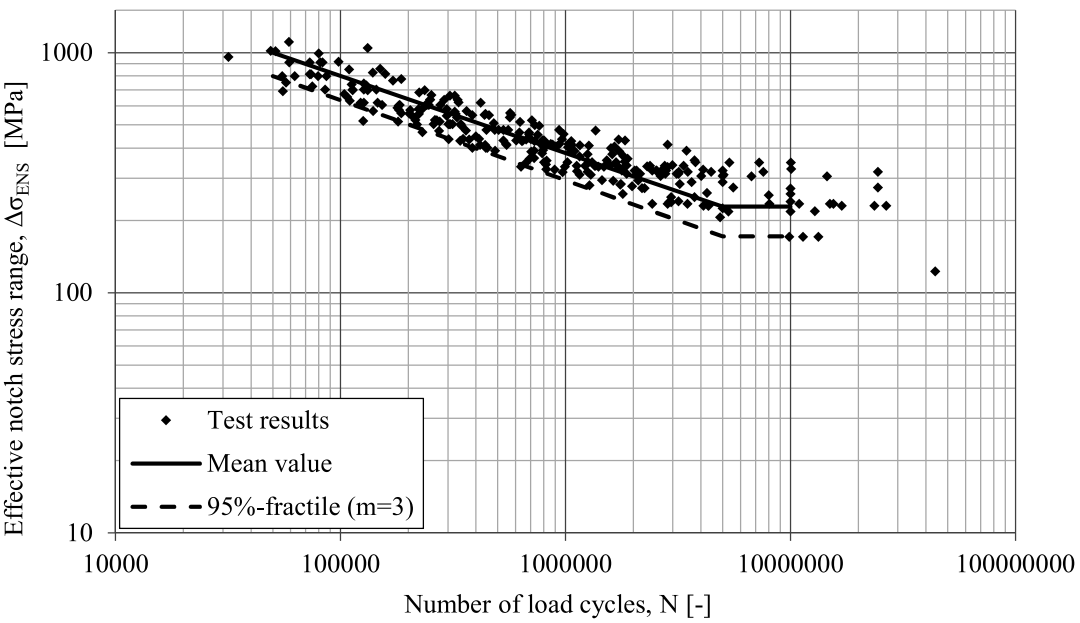

Figure 5.5 *Linear regression of the fatigue strength class for double-sided test series with effective notch stress in 2D.*

In the same manner are the one-sided specimens with corresponding linear regression plotted in Figure 5.6. The fatigue strength class for the one-sided test specimens is 186 MPa.

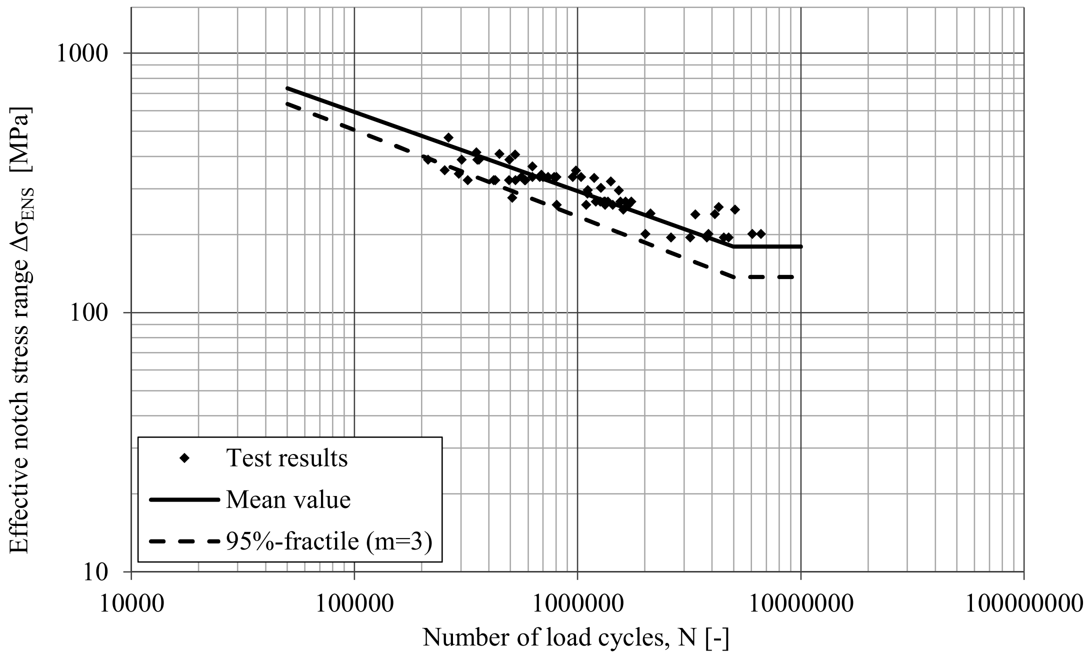

Figure 5.6 Linear regression of the fatigue strength class for one-sided test series with effective notch stress in 2D.

The fatigue strength class for the one- and double-sided stiffeners should be around the same magnitude since the effective notch stress considers stress raising effects from e.g. geometry. It is observed from Table 3.1 that the one-sided test specimens are in fact web stiffeners in a beam that is subjected to four-point-bending. Additional effects, such as shear lag, might influence the results. This yields that a 3D model could be needed in order to capture these effects.

5.1.3 Fatigue strength class for FE-analyses in 3D

As mentioned in Section 5.1.2, shear lag and other effects are not considered in the 2D model, which means that a 3D model may be required. The model is defined according to Section 4.3 where the dimensions, e.g. plate thicknesses, are the same as in the real experiments. The same procedure to calculate the fatigue strength class in Section 5.1.2 is used. Figure 5.7 displays the resulting plot when the nominal stress from the experimental data is multiplied with the stress concentration factor, K_t, from the FE-analyses.

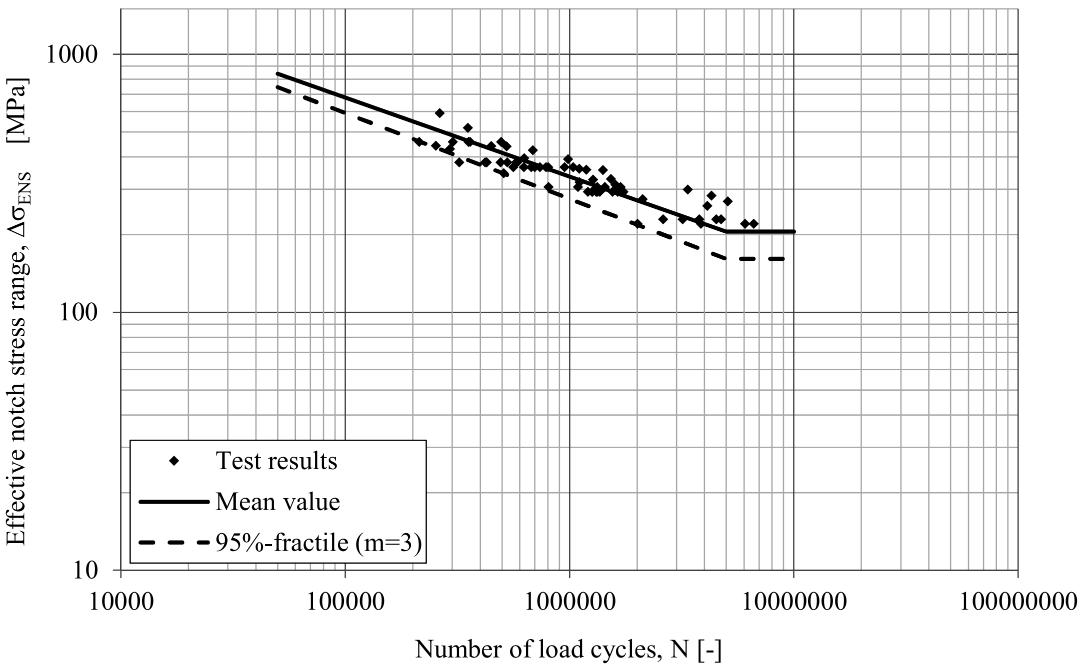

Figure 5.7 Linear regression of the fatigue strength class for one-sided test series with effective notch stress in 3D.

Linear regression results in a fatigue strength class of 219 MPa with a slope m = 3 which is an improvement compared to the previously obtained strength class of 186 MPa.

5.2 FE-analyses

This section presents the results from the FE-analyses in both 2D and 3D, which are explained in Chapter 4.

5.2.1 2D FE-analyses

Figure 5.8 and Figure 5.9 show the results for one- and double-sided transverse stiffeners. The fatigue strength from the FE-analyses is plotted with respect to the length, L, and is obtained by using equation (4.7). These figures are further analysed with regard to both the effect of symmetry as well as other influencing factors in Section 5.3. The curves for the different flange thicknesses in Figure 5.8 are explained by marking the lower and upper bound limits and are decreasing for higher fatigue strength as seen.

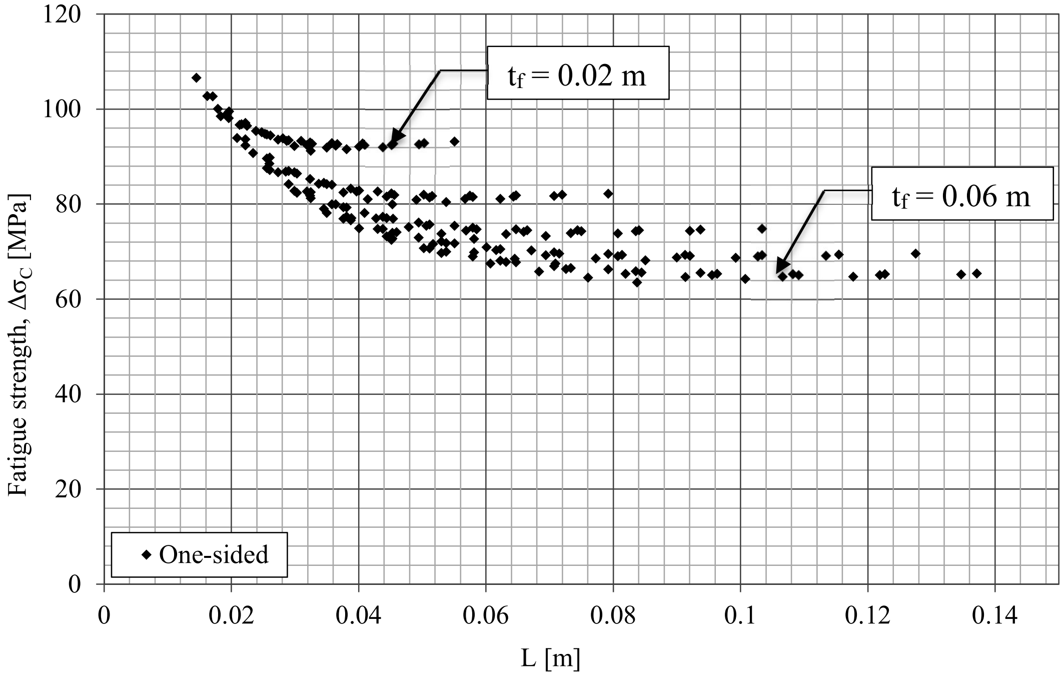

Figure 5.8 One-sided FE-results converted to fatigue strength class.

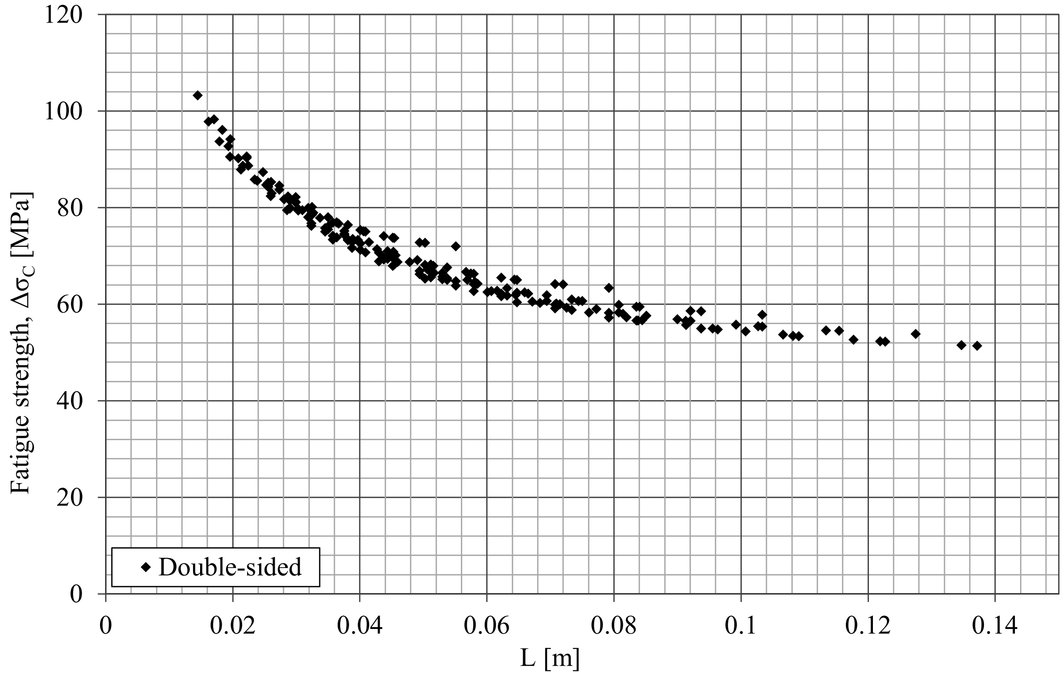

Figure 5.9 Double-sided FE-results converted to fatigue strength class.

5.2.2 3D FE-analyses

The results from the 3D FE-analysis explained in Section 4.3 is presented in Figure 5.10.

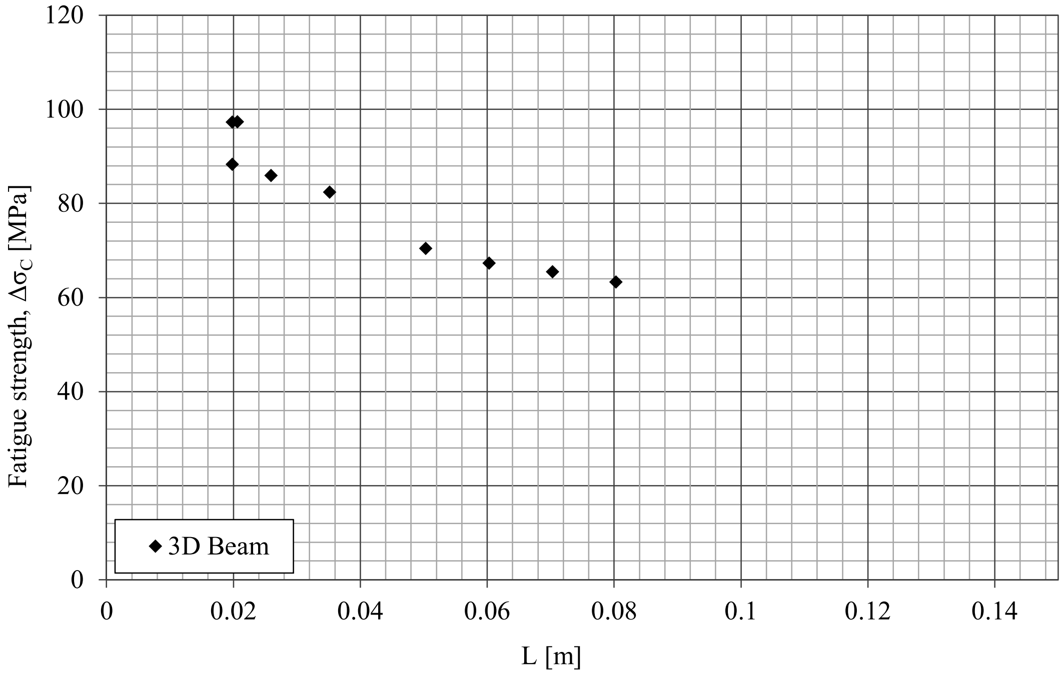

Figure 5.10 3D analyses for beam in 4-point bending.

5.2.3 Comparison between 2D and 3D analyses

The comparison of the FE-results from double-sided transverse stiffeners in 2D by using equation (5.14), that will be presented later in Section 5.3.5, and the 3D-results can be seen in Figure 5.11. The results are coinciding well, indicating that web stiffeners in beams can be modelled as double-sided stiffeners in 2D when using the effective notch stress as fatigue life assessment method. This yields also that equation (5.13) is valid for web stiffeners in beams.

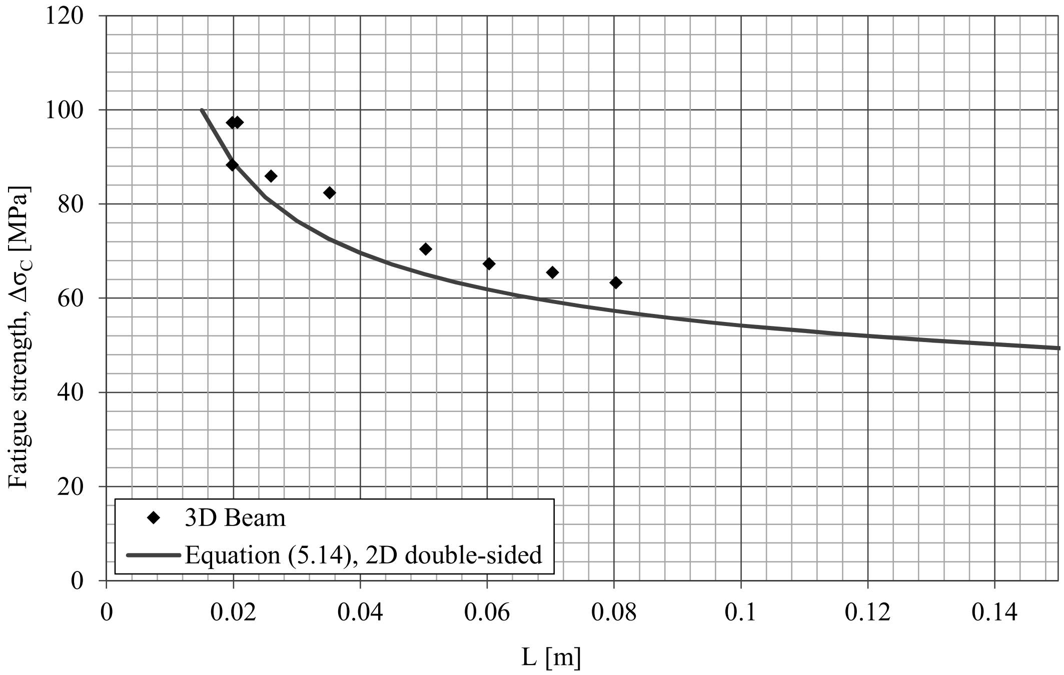

Figure 5.11 Comparison between equation (5.14) and 3D beam analyses.

The gathered experimental data of beams subjected to bending resulted in 5 different dimensional configurations of the 3D model. All of these had value of L below 40 mm. The remaining 4 points in Figure 5.11 are additional analyses performed to see whether the 3D beam is consistent in matching the 2D model even for higher values of L. It can be seen that the 4 points representing the 3D beam with L ranging from 50 mm to 80 mm follows the line representing equation (5.14) well. The reason that the points does not coincide exactly with the line is that the equation is based on the upper-bound values of the stress concentration factor and thus giving the lowest fatigue strength class from the 2D double-sided FE-analyses. However, the results from the 3D-analyses does match the 2D double-sided results well when they are compared directly.

5.3 Influencing factors

In this section, the different geometrical properties for the transverse stiffener are presented and their influence of the fatigue strength are discussed.

5.3.1 Influence of symmetry of stiffeners

The symmetry of the transverse stiffeners influences the results, as the scatter is reduced significantly when symmetry is included. It is observed that the fatigue strength is lower on double-sided stiffener for increasing L-values compared with one-sided stiffener. Another observation is that the flange thickness has higher influence of the fatigue strength class for one-sided stiffeners compared with double-sided and this explains the scatter of the results for the one-sided stiffeners.

5.3.2 Influence of flange thickness, t_f

The stress concentration factor is plotted with respect to the flange thickness, t_f, in order to see how the flange thickness affects the stress concentration factor, see Figure 5.12. First, the double-sided stiffeners are studied. The thickness of the transverse stiffeners and the weld throat are set to constant while the flange thickness is increased. The influence of the flange thickness is higher for lower thicknesses and the stress concentration factor is constant for thicknesses higher than approximately 20 mm. Two different L-values are studied in order to see if the influence of the flange thickness changes with different L-values. It can be seen in Figure 5.12 that the influence from the flange thickness for low thicknesses is decreasing with lower L-values.

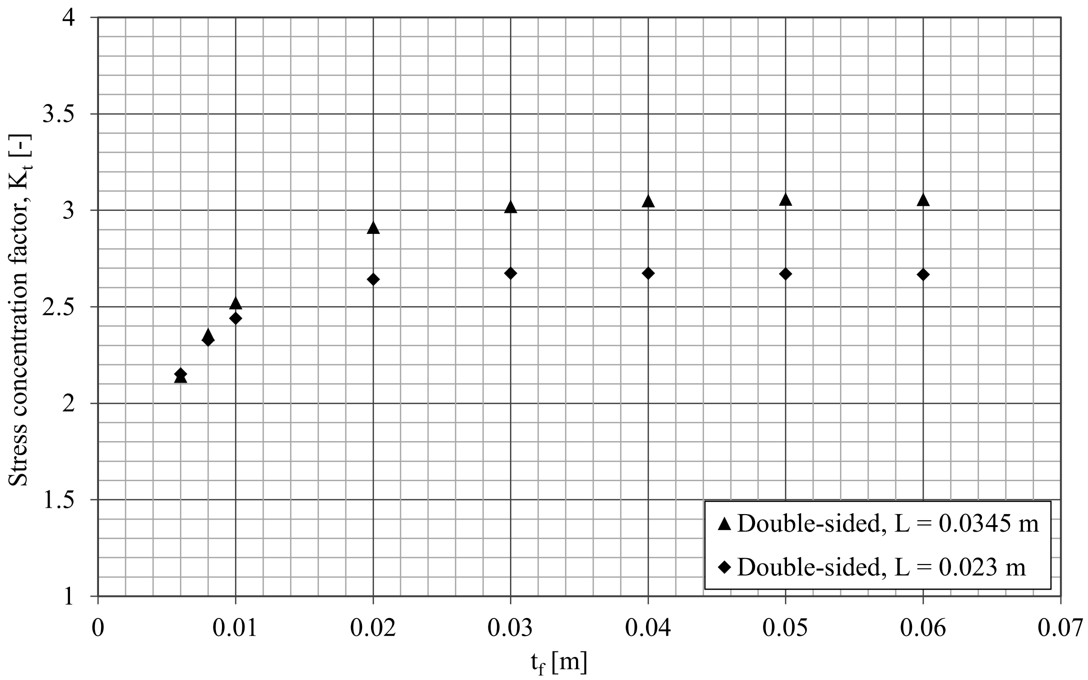

Figure 5.12 Stress concentration factor with respect to flange thickness, t_f for double-sided stiffener.

The same procedure as described above for one-sided stiffener is seen in Figure 5.13.

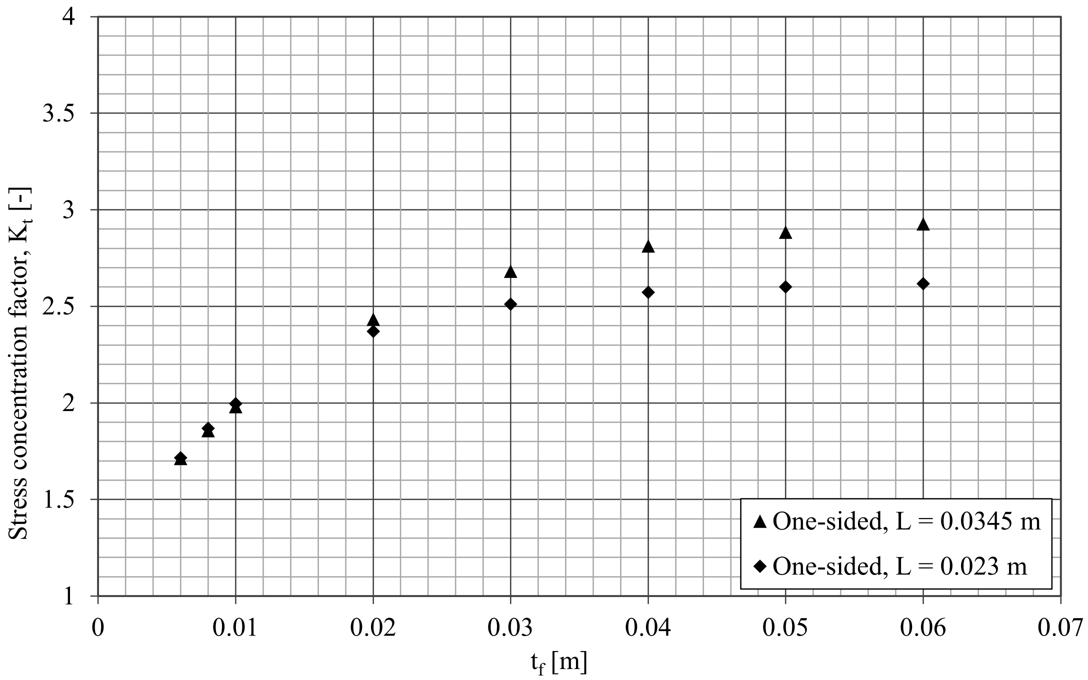

Figure 5.13 Stress concentration factor with respect to flange thickness, tf, for one-sided stiffener.

The difference between these two cases is relatively small. However, the stress concentration factor converges at a later stage for the one-sided stiffener and not as abruptly compared to double-sided stiffeners. Furthermore, the three cases are converging to the same values for smaller flange thicknesses indicating that the *L*-value is not changing the influence from the flange thickness in this span.

5.3.3 Influence of thickness of transverse stiffener, t_w

To see how the thickness of the stiffener affects the stress concentration factor, diagrams are created in the same manner as in Section 5.3.2 where K_t is plotted with respect to flange thickness, t_w, see Figure 5.14 and Figure 5.15 for the double-sided and one-sided case respectively. The flange thickness and the weld throat thickness are both constant.

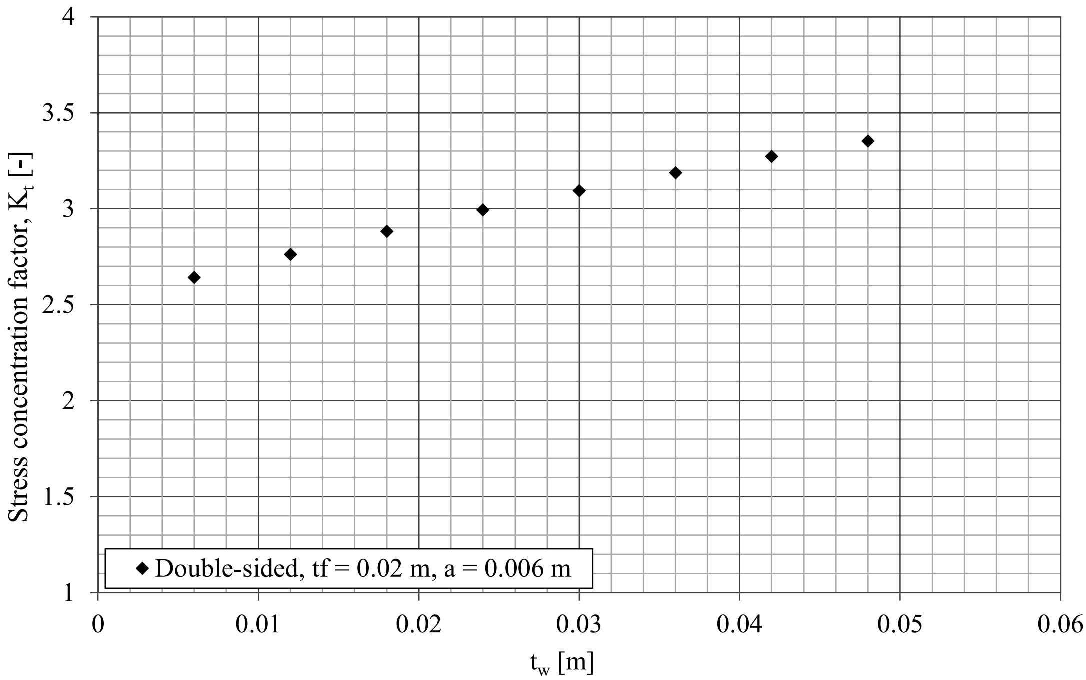

Figure 5.14 Stress concentration factor with respect to the thickness of the transverse stiffener, t_w, for double-sided stiffener.

It can be seen that the stress concentration factor increases almost with a linear relationship when the stiffener thickness increases.

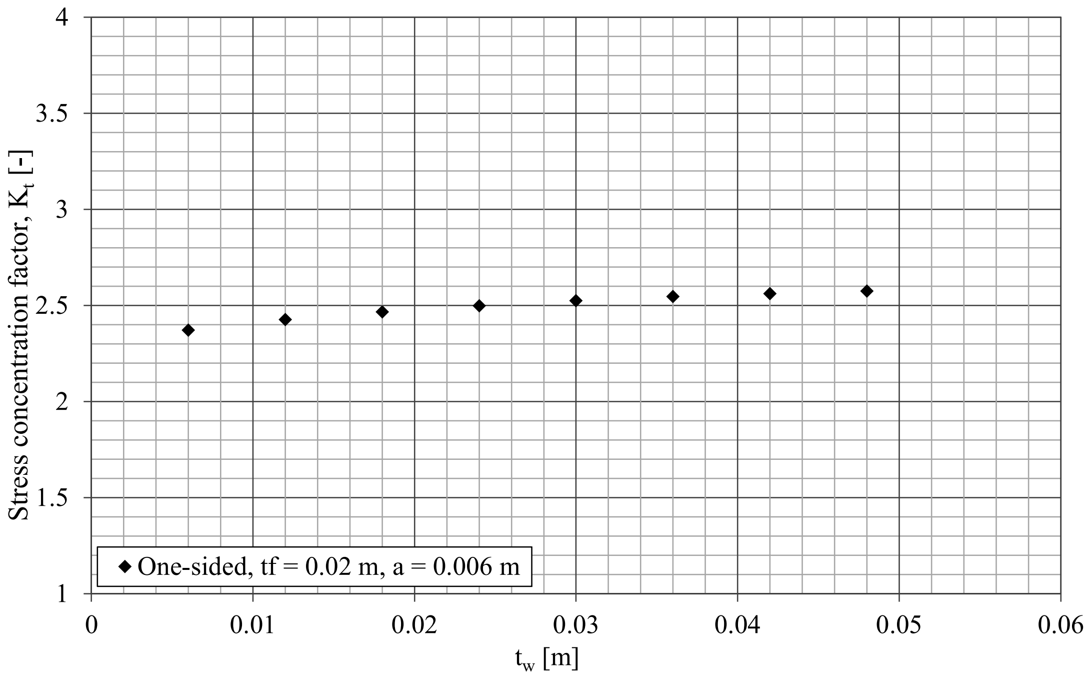

Figure 5.15 Stress concentration factor with respect to the thickness of the transverse stiffener, t_w, for one-sided stiffener.

In both situations, K_t increases with a linear relationship. However, the thickness of the stiffener seems to have a greater influence when stiffeners are welded to both sides due to the greater slope of the line.

5.3.4 Influence of weld throat thickness, *a*

The influence of the weld throat thickness, a, is also studied in a similar manner as earlier where flange thickness, t_f, and stiffener thickness, t_w, are held constant as the weld throat thickness, a, is increasing, see Figure 5.16 and Figure 5.17 for the double-sided and one-sided case respectively.

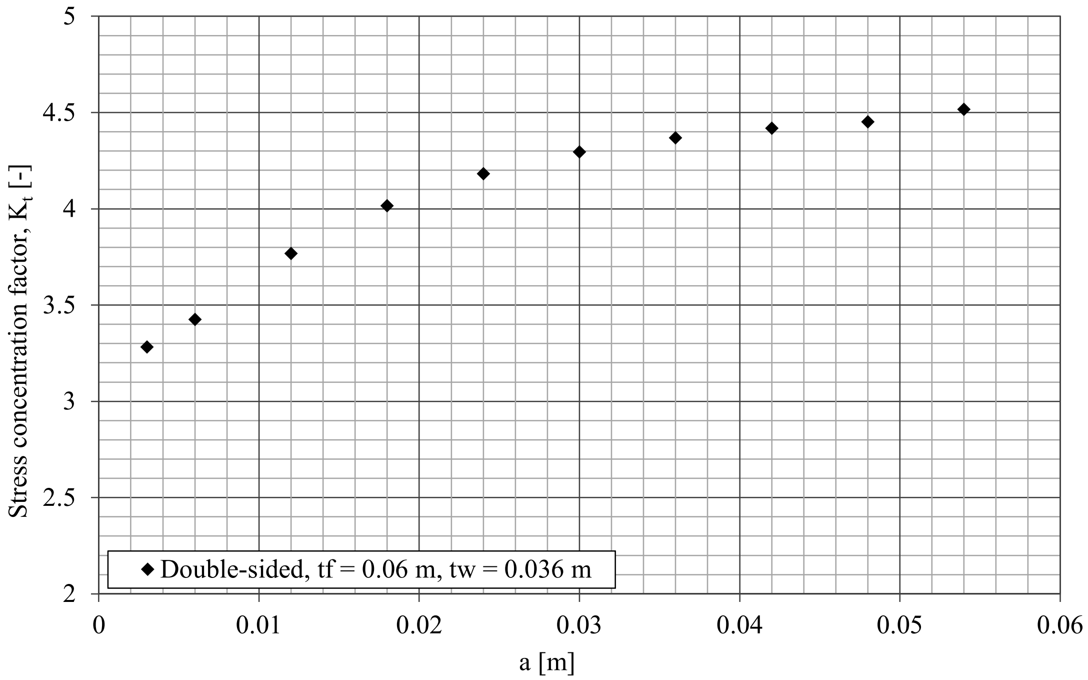

Figure 5.16 Stress concentration factor with respect to the weld throat thickness, a, for double-sided stiffener.

In the case of double-sided stiffeners, K_t increases more rapidly for smaller welds and show signs of converging for greater dimensions of the weld throat.

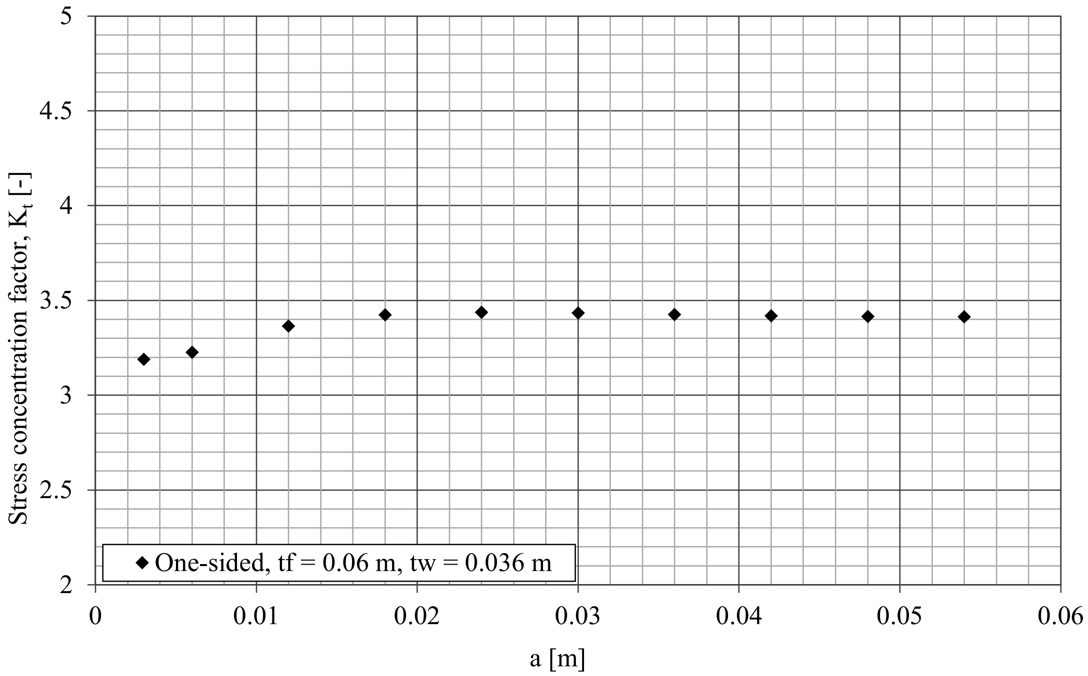

Figure 5.17 Stress concentration factor with respect to the weld throat thickness, a, for one-sided stiffener.

In contrast to the first situation, the weld throat thickness, *a*, appears to have a rather small influence on the stress concentration factor in the one-sided case since it converges at lesser dimensions. In addition, the initial increase of K_t before convergence is small which further indicates that the weld throat thickness is less influencing in this case.

5.3.5 Equation for one- and double-sided transverse stiffener

The one-sided stiffener in 2D has a larger scatter compared to the double-sided stiffener as discussed in Section 5.3.1. This is due to a higher influence of the flange thickness. An upper-bound equation of the stress concentration factor for one-sided stiffener as a function of the flange thickness, t_f, and L, where both are in meter, is therefore obtained and can be seen in Figure 5.18 as well as in Appendix D.

$$K_t = C_1L^2 + C_2L + C_3 \qquad (L < 1.35t_f + 0.008) \qquad (5.1)$$

$$L = L_{max,o} \qquad (L \geq 1.35t_f + 0.008) \qquad (5.2)$$

Where:

$$C_1 = 483.870\ln(t_f) + 43.562 \qquad (5.3)$$

$$C_2 = -92.457t_f^2 + 37.882t_f + 48.476 \qquad (5.4)$$

$$C_3 = 2.168t_f^2 - 1.117t_f + 1.668 \qquad (5.5)$$

$$L_{max,o} = 1.35t_f + 0.008 \qquad (5.6)$$

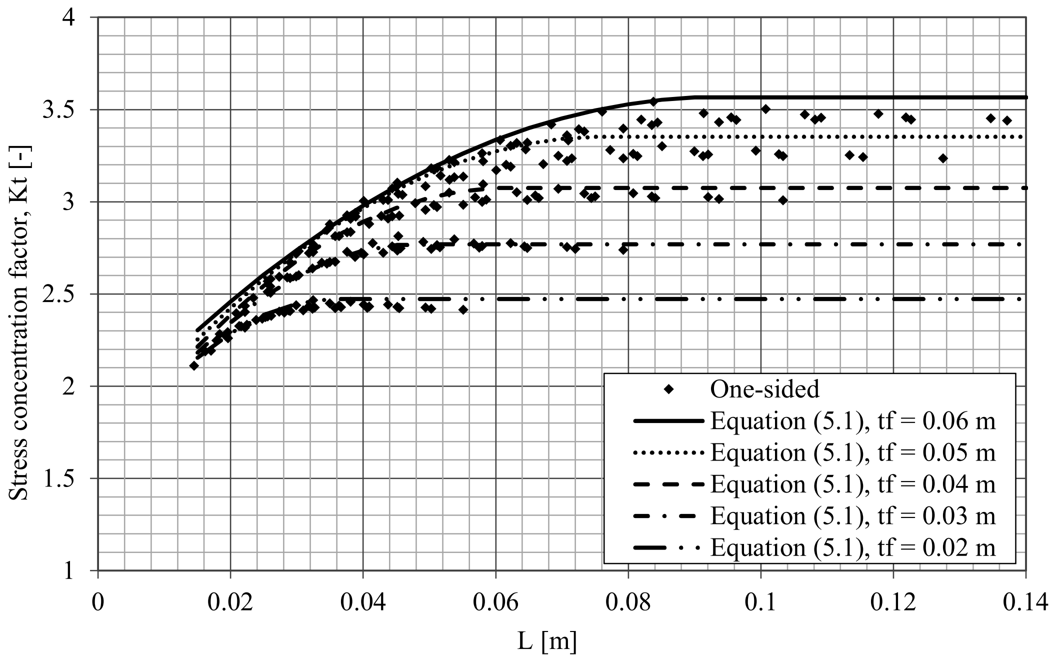

Figure 5.18 Equation for one-sided stiffener.

A similar equation for the double-sided transverse stiffener can be obtained and can be seen in Figure 5.19 and Appendix D.

$$K_t = C_4L^2 + C_5L + C_6 \qquad (L < 2.15t_f + 0.011) \qquad (5.7)$$

$$L = L_{max,d} \qquad (L \geq 2.15t_f + 0.011) \qquad (5.8)$$

Where:

$$C_4 = 7093t_f^3 - 11450t_f^2 + 6571t_f - 1471 \qquad (5.9)$$

$$C_5 = -24.6\ln(t_f) + 21.1 \qquad (5.10)$$

$$C_6 = -13.33t_f^3 + 16.50t_f^2 - 5.12t_f + 2 \qquad (5.11)$$

$$L_{max,d} = 2.15t_f + 0.011 \qquad (5.12)$$

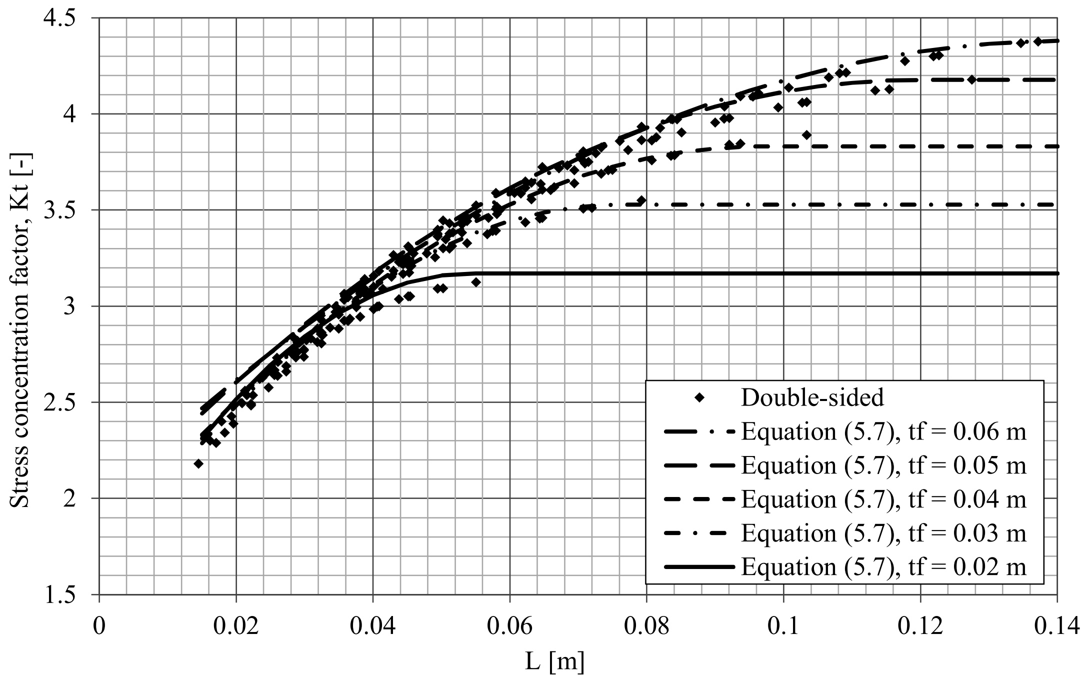

Figure 5.19 Equation for double-sided stiffener, which considers both flange thickness and L.

It can be seen in Section 5.3.2 to 5.3.4 that the parameter that influences the stress concentration factor for double-sided stiffener the most is the *L*-value. Therefore, an upper-bound equation of the stress concentration factor for double-sided stiffener as a function of *L* is obtained and can be seen in Figure 5.20 and Appendix D.

$$K_t = 6.45 + \ln(L) \qquad (5.13)$$

By using equation (5.13) together with equation (4.7), a fatigue strength class according to the nominal stress method can be calculated as:

$$\Delta\sigma_{C,NS} = \frac{\Delta\sigma_{C,ENS}}{6.45 + \ln(L)} \tag{5.14}$$

Where:

$$\Delta\sigma_{C,ENS} = 225\ MPa$$

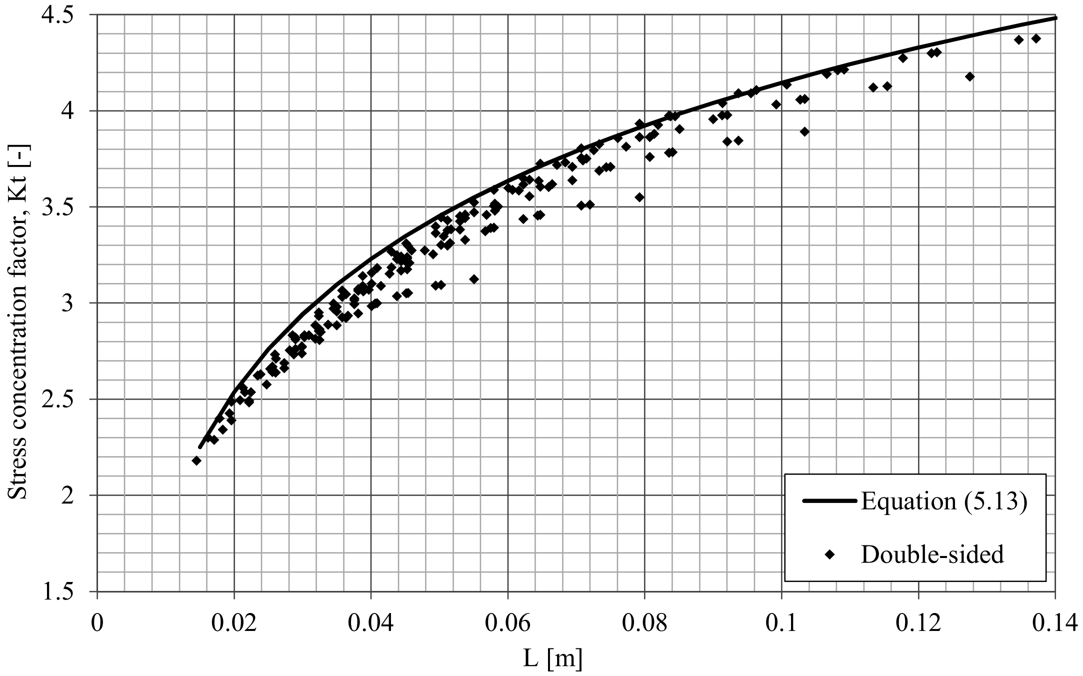

Figure 5.20 Equation for double-sided stiffener, which considers only L.

5.4 Comparison between FE-results and Eurocode

The current design recommendation from Eurocode 3, as described in Section 2.1.3, only gives two fatigue strength classes with respect to the length, *L*. The FE-results are plotted together with this recommendation in Figure 5.21 and Figure 5.22. The recommendation from Eurocode 3 is only valid for *L*-values smaller than 80 mm, which yields that FE-models with larger dimensions are hard to compare with the design recommendations. One can see that for smaller *L*-values, the fatigue strength is increased which indicates that the design recommendations from Eurocode 3 are conservative and can be improved.

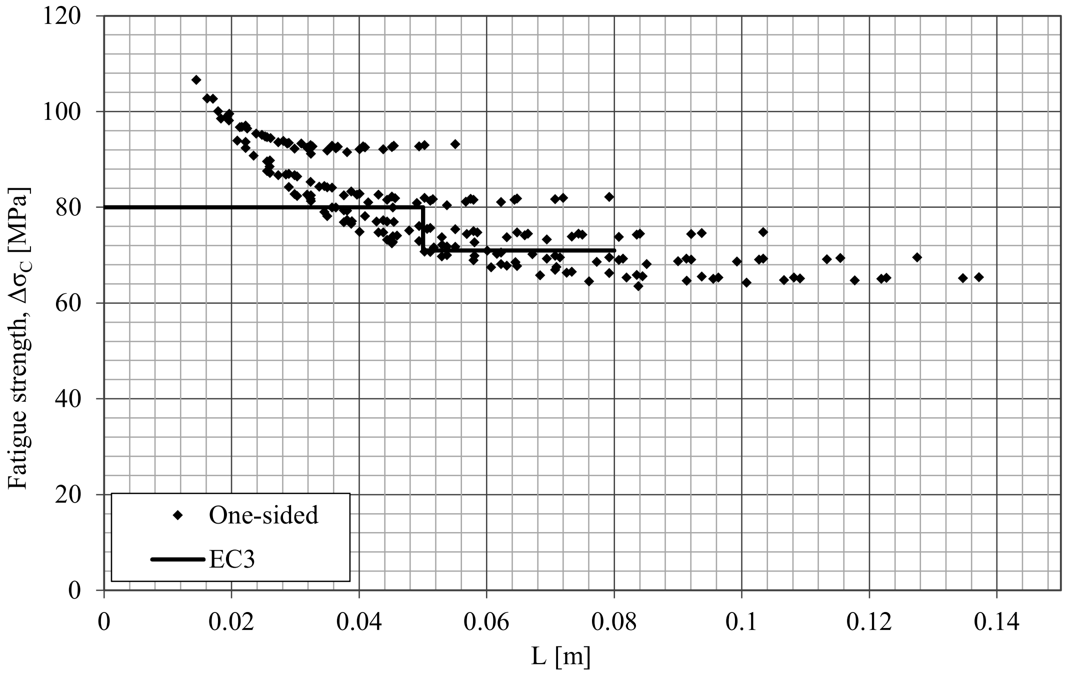

Figure 5.21 FE-results for one-sided compared to Eurocode 3 recommendations.

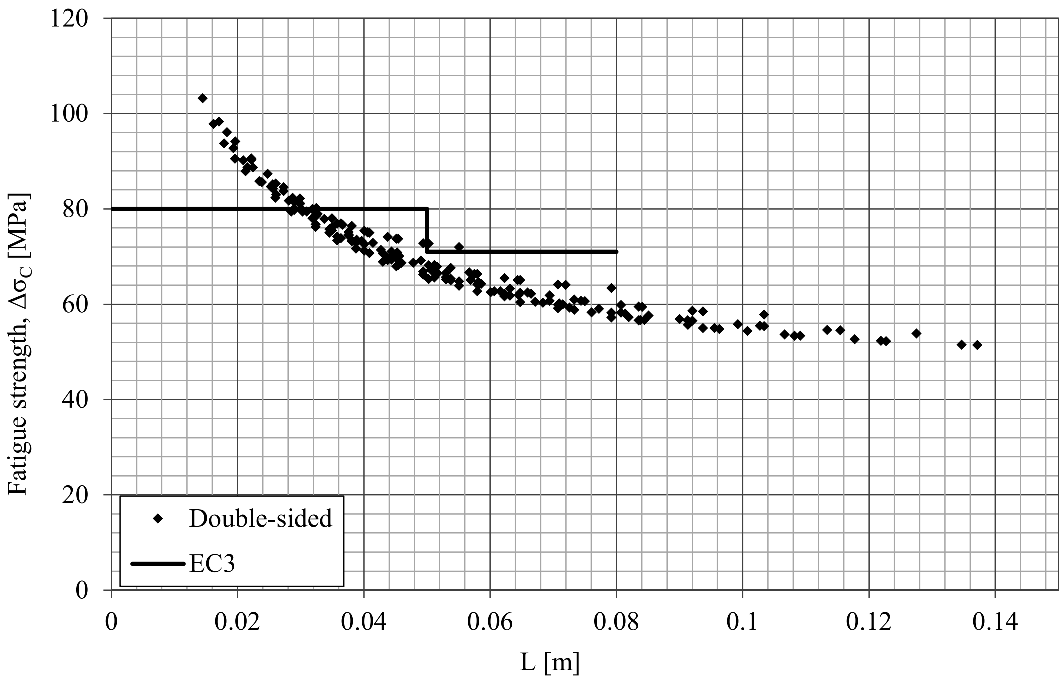

Figure 5.22 FE-results for double-sided compared to Eurocode 3 recommendations.

5.5 Comparison between experimental fatigue strength class and ENS

In order to verify the FE-analyses, the results must be compared with the experimental data. This is done by comparing the fatigue strength from the FE-analyses with the calculated fatigue strength classes from the experimental data described in Section 3.3. This comparison can be seen in Figure 5.23 and Figure 5.24. Only FE-models with a flange thickness of 20 mm are plotted in the one-sided comparison in Figure

5.23. This is because most experimental data are in this range and thus higher flange thicknesses are not of interest in the comparison. When comparing with 2D FE-analyses for one-sided stiffeners, one can see that the experimental data is far away from the FE-results. This can be explained be the asymmetry in the FE-models, which results in additional stresses in form of bending stresses. The rotation from these bending stresses can be seen in Figure 4.7. These bending stresses are dependent on the moment of inertia, which is highly dependent on the flange thickness. This explains the higher dependency of the flange thickness seen in Figure 5.8. Since the one-sided fatigue tests are in fact beam tests, the detail is prevented from rotating and not corresponding to the one-sided FE-model.

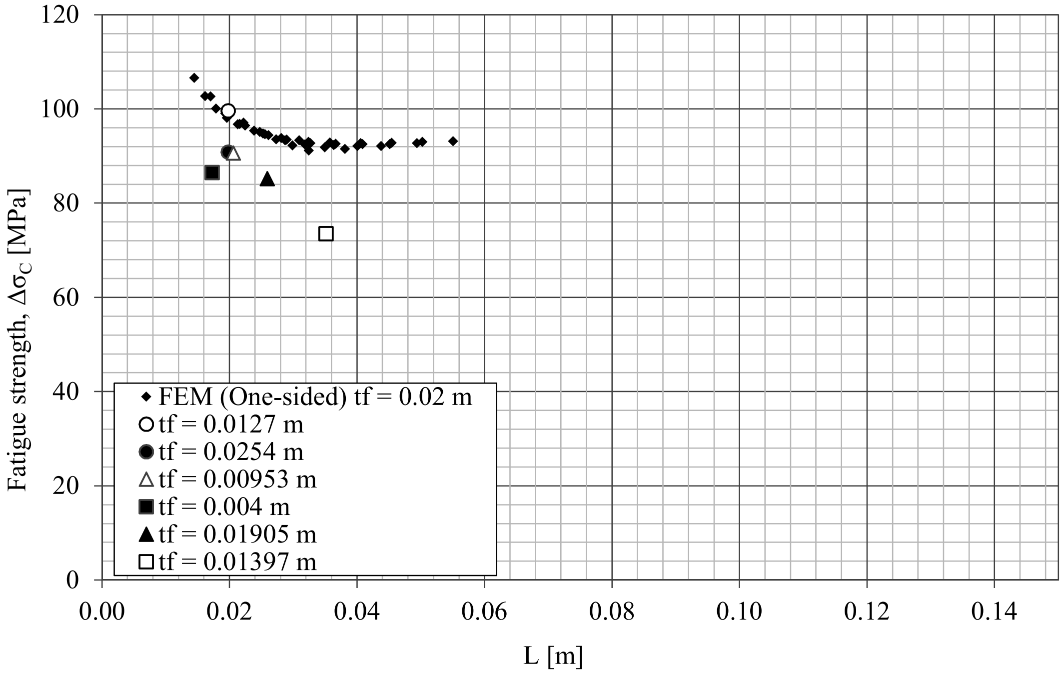

Figure 5.23 Comparison of the fatigue strength between FE in 2D and experimental data for one-sided stiffener.

In Figure 5.24, all calculated experimental fatigue strength classes are displayed for both double- and one-sided attachments. The reason that the one-sided experiments are plotted here as well is to see whether they coincide better with the double-sided 2D model.

It is mentioned in Section 5.3.5 that the parameter that has the greatest influence of the fatigue strength is the distance L. Therefore, test results where the specimens had similar values of L are organised together in groups regardless of the used flange thickness, t_f, and a fatigue strength class is calculated for each of these groups. This increases the number of data points for each group and thus lowers the statistical safety margin, giving a better prediction of the fatigue strength. See Appendix A for all groups, dimensions, number of data points as well as the calculated fatigue strength. In the same figure, a solid line is plotted which represents the calculated fatigue strength by using equation (5.14).

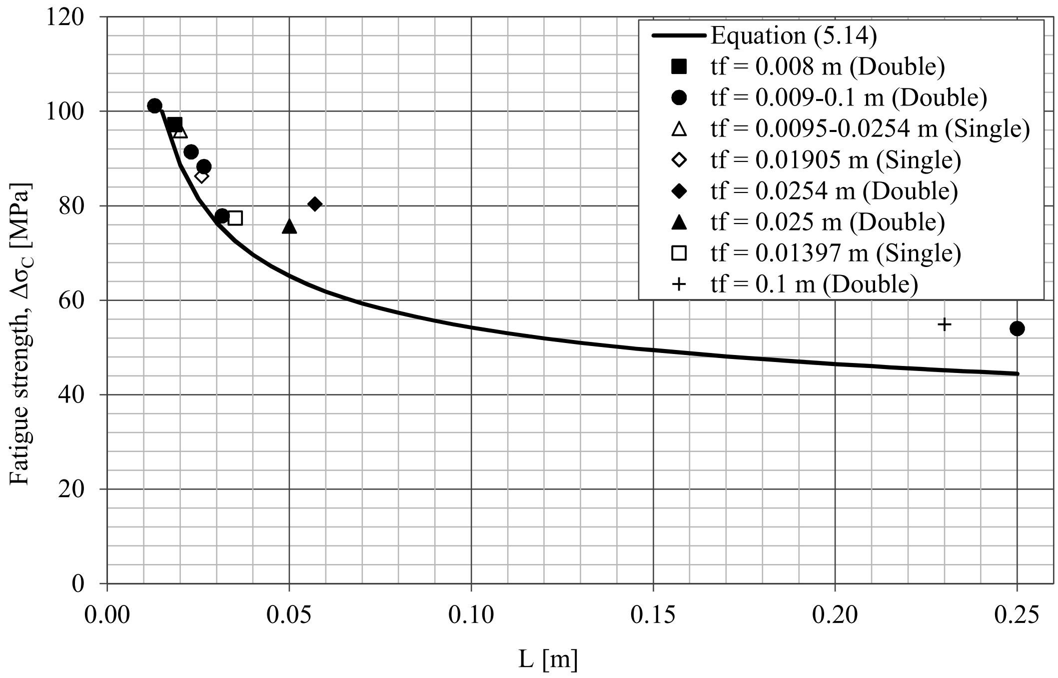

Figure 5.24 Comparison of the fatigue strength between FE in 2D and experimental data for double-sided stiffener.

It can be seen that the experimental data coincides well with equation (5.14) with the exception of a few points. This equation is a lower-bound equation based on the 2D FE-analyses meaning that it gives a fatigue strength on the safe side. However, the points representing fatigue strengths for specimens with a flange thickness t_f of 25 mm and 25.4 mm does coincide better when compared directly to the FE-results.

Also, the difference between equation (5.14) and the calculated fatigue strength of specimens with a distance L of 230 mm and 250 mm could be explained by the fact that the equation is based on FE-analyses where the greatest value of L is not greater than 150 mm.

6 Final remarks

The intention of this report was to investigate the influence of the different dimensions for transverse attachments used in e.g. bridges. The most common fatigue life assessment method at the moment used for this is by applying the nominal stress method with the proposed fatigue strength classes from Eurocode 3 for the studied detail. This report has shown results that do not fully comply with these recommendations. These observations are given in Section 5.4. The conclusions drawn from the results are given in Section 6.1.

6.1 Conclusions

- There is a tendency of a higher fatigue strength class for lower *L*-values and lower fatigue strength class for higher *L*-values that can be seen in Section 5.4. This means that Eurocode 3 tends to be more conservative for lower *L*-values and vice versa.
- Another observation made from Section 5.3.1 is that the flange thickness for one-sided transverse stiffeners has influence on the stress concentration factor but less influence for double-sided. The asymmetry in the one-sided specimens results in additional stresses in form of bending stresses. These bending stresses are highly dependent on the moment of inertia, where the flange thickness has a significant influence. In Section 5.3.2, it can be seen that the influence of the flange thickness decreases with increasing thickness. This can be explained by the fact that the transverse stiffener has less influence of the stress distribution of the cross section when the flange thickness increases. Furthermore, for decreasing *L*-values, the flange thickness has less influence on the stress concentration factor.
- The thickness of the transverse stiffener changes the stress concentration with an almost linear increasing relationship, which is shown in Section 5.3.3, and the stress concentration is increasing logarithmically with the weld throat thickness seen in Section 5.3.4. These two dimensions are influencing the *L*-value and thus influencing the length of the disturbed region of the flange. Increasing length of the disturbed region increases therefore the stress concentration at the notch.
- Transverse stiffeners in beams are behaving as a double-sided stiffener as seen in Section 5.2.3. One explanation to this is that no additional bending stresses due to the asymmetry of the detail occur since the detail is restrained from moving. This yields that a 2D symmetric model can be used when assessing these details instead of a 3D model.
- Shear lag does not seem to have a significant influence when comparing the 2D with the 3D results in Section 5.2.3.
- The experimental data is corresponding well with the 2D double-sided FE-analyses presented in Section 5.4. This yields that the proposed equation (5.14) in Section 5.3.5 seems to be valid for double-sided transverse stiffeners. Since no actual one-sided experimental test specimens were found, equation (5.1) and (5.2) could not be validated.

- Since it is concluded that the double-sided stiffener represents web stiffeners in beams as well as for small L-values, the flange thickness has less influence of the stress concentration factor, equation (5.14) is proposed as a suitable equation to increase the fatigue strength for transverse attachments for L-values below 30 mm compared to the recommendations from Eurocode 3. For higher L-values will the equation yield a lower fatigue strength than Eurocode 3.
- There are no indications that equation (5.14) should not be valid outside the investigated dimensional spans presented in Section 4.2.1 based on the conclusion that the flange thickness has little influence for smaller L-values together with comparisons with experimental data outside the investigated span.
- It is observed in Section 5.4 that the FE-results from both one- and double-sided transverse stiffeners have a lower fatigue strength class for high L-values compared to the recommendations from Eurocode 3. A part of the explanation is that the Eurocode 3 recommendations are only valid to 80 mm. However, this needs to be more investigated in order to fully understand this observation.
- The effective notch stress method is a very time consuming method for assessing the fatigue life of a detail. The hot-spot stress method would probably be more time efficient but it does not take e.g. weld root cracking into consideration. Therefore, it should be of interest for structural engineers if more exact equations for the fatigue life of steel details could be developed, in a similar manner as this investigation, instead of performing these time-consuming fatigue life assessment methods.

6.2 Further studies

- The angle of the welds has in not been studied in this report. Therefore, its influence of the fatigue strength has not been investigated. It may be interesting to investigate this effect.
- Since no detailed information of the cope holes in the experimental tests were given in the literature, their shape and dimensions have been decided by reasonable assumptions. It could be interesting to investigate how the dimension and shape of the cope hole influences the fatigue strength.
- The FE-results showed that for higher L-values, the fatigue strength class is lower than the recommendations from Eurocode 3 and the reason for this observation could be interesting to investigate.

7 References

Albrecht, P., & Friedland, I. (1979). Fatigue-limit effect on variable-amplitude fatigue on stiffeners. *Journal of the structural division*, 2657-2675.

Al-Emrani, M. (2015, 10 06). *Fatigue of steel structures - Lecture 3.* Göteborg.

Al-Emrani, M., & Åkesson, B. (2013). *Steel Structures - Course literature VSM191.* Göteborg: Chalmers.

Al-Emrani, M., & Aygül, M. (2014). *Fatigue design of steel and composite bridges.* Göteborg: Chalmers Reproservice.

Aygül, M. (2012). *Fatigue Analysis of Welded Structures Using the Finite Element Method.* Göteborg: Chalmers Repro Service.

Berge, S. (1985). On the effect of plate thickness in fatigue of welds. *Engineering Fracture Mechanics*, pp. 423-435.

CEN. (2002). *Eurocode SS-EN 1990.* Brussels: European Committee for Standardization.

CEN. (2005). *Eurocode 3.* Brussels: European Committee for Standardization.

Dong, P. (2001). *A structural stress definition and numerical implementation for fatigue analysis of welded joints.* Columbus: Elsevier.

Fisher, J., Albrecht, P., Yen, B., Klingerman, D., & McNamee, B. (1974). *Fatigue strength of steel beams with welded stiffeners and attachments.* Washington D.C.: Transportation Research Board.

Fricke, W. (2001). *Recommended Hot Spot Analysis Procedure for Structural Details of FPSO's and Ships Based on Round-Robin FE Analyses.* Stavanger: International Journal of Offshore and Polar Engineering.

Fricke, W. (2010). *Recommendations for the Fatigue Assessment by Notch Stress Analysis for Welded Structures.* Cambridge: Woodhead Publishing.

Fricke, W., Sonsino, C., & Radaj D. (2006). *Fatigue assessment of welded joints by local approaches.* Cambridge.

Gurney, T. R. (1991). *The fatigue strenght of transverse fillet welded joints.* Abington Publishing.

Gurney, T. R. (1995). *Thickness effect in relatively thin joints.* Norwich: HSE Books.

Heshmati, M. (2012). *Fatigue Life Assessment of Bridge Details Using Finite Element Method.* Göteborg: Chalmers Reproservice.

Hobbacher, A. F. (2009). The new IIW recommendations for fatigue assessment of welded joints and components - A comprehensive code recently updated. *International Journal of Fatigue*, 50-58.

Klippstein, K., & Schilling, C. (1989). Pilot study on the constant and variable behavior of transverse stiffener welds. *J. Construct. Steel Research 12*, pp. 229-252.

Kuhlmann, U., Bergmann, J., Dürr, A., Thumser, R., Günther, H.-P., & Gerth, U. (2005). Erhöhung der Ermüdungsfestigkeit von geschweißten höherfesten Baustählen durch Anwendung von Nachbehandlungsverfahren. *Stahlbau 74*, 358-365.

Puthli, R., Herion, S., & Bergers, J. (2006, 11). Untersuchungen zum Ermüdungsverhalten von hochfesten Stählen im Rahmen von LIFTHIGH. *Stahlbau 75*, pp. 916-924.

Radaj, D. (1990). *Design and Analysis of Fatigue Resistant Welded Structures.* Cambridge: Woodhead Publishing.

Radaj, D., Sonsino, C. M., & Fricke, W. (2006). *Fatigue assessment of welded joints by local approaches.* Cambridge: Woodhead Publishing.

Richter, B., & Zhang, G. (2000). *New approach to the numerical fatigue-life prediction of spot-welded structures.* Wolfsburg: Blackwell Science Ltd.

Sonsino, C., Fricke, W., de Bruyne, F., Hoppe, A., Ahmadi, A., & Zhang, G. (2010). *Notch stress concepts for the fatigue assessment of welded joints – Background and applications.* Hamburg: Elsevier Ltd.

Spadea, J., & Frank, K. (2002). *Fatigue Strength of Fillet-Welded Transverse Stiffeners with Undercuts.* Austin, Texas: Center for transportation research, Bureau of engineering research, The university of Texas at Austin.

Stenberg, T., Barsoum, Z., & Balawi, S. O. (2015). *Comparison of local stress based concepts - Effects of low- and high cycle fatigue and weld quality.* Stockholm: Elsevier Ltd.

Xiao, Z.-G., & Yamada, K. (2004). *A method of determining geometric stress for fatigue strength evaluation of steel welded joints.* Nagoya: Elsevier.

Appendix A

This appendix presents the collected data discussed in Chapter 3 together with the obtained fatigue strength classes for the experimental data discussed in Section 3.3.

A1 Table of experimental data

Database #	LitRef	tf [m]	tw [m]	a [m]	L [m]	FAT EC	ExcelRef	Steel	fy [MPa]	fu [MPa]	Method	Δσ [MPa]	N [-]
1	1	0.025	0.006	0.005	0.020	80	T.1.1	A441			Manual	155.1	628000
2	1	0.025	0.006	0.005	0.020	80	T.1.1	A441			Manual	173.1	447000
3	1	0.025	0.006	0.005	0.020	80	T.1.1	A441			Manual	172.4	524000
4	1	0.025	0.006	0.005	0.020	80	T.1.1	A441			Manual	128.2	1272000
5	1	0.025	0.006	0.005	0.020	80	T.1.1	A441			Manual	125.5	1110000
6	1	0.025	0.006	0.005	0.020	80	T.1.1	A441			Manual	105.5	5078000
7	1	0.025	0.006	0.005	0.020	80	T.1.1	A441			Manual	101.4	4115000
8	1	0.025	0.006	0.005	0.020	80	T.1.1	A441			Manual	140.0	1187000
9	1	0.014	0.013	0.008	0.035	80	T.1.2	A441			Manual	216.5	264000
10	1	0.014	0.013	0.008	0.035	80	T.1.2	A441			Manual	190.3	352000
11	1	0.014	0.013	0.008	0.035	80	T.1.2	A441			Manual	162.0	254000
12	1	0.014	0.013	0.008	0.035	80	T.1.2	A441			Manual	157.2	293000
13	1	0.014	0.013	0.008	0.035	80	T.1.2	A441			Manual	155.8	687000
14	1	0.014	0.013	0.008	0.035	80	T.1.2	A441			Manual	131.7	1105000
15	1	0.014	0.013	0.008	0.035	80	T.1.2	A441			Manual	126.9	509000
16	1	0.014	0.013	0.008	0.035	80	T.1.2	A441			Manual	114.5	1600000
17	1	0.014	0.013	0.008	0.035	80	T.1.2	A441			Manual	109.6	3370000
18	1	0.014	0.013	0.008	0.035	80	T.1.2	A441			Manual	100.7	2121000
19	1	0.019	0.008	0.006	0.026	80	T.1.3	A441			Manual	149.6	984000
20	1	0.019	0.008	0.006	0.026	80	T.1.3	A441			Manual	135.8	1410000
21	1	0.019	0.008	0.006	0.026	80	T.1.3	A441			Manual	125.5	1530000
22	1	0.019	0.008	0.006	0.026	80	T.1.3	A441			Manual	108.2	4290000
23	1	0.010	0.007	0.005	0.021	80	T.1.4	A441			Manual	99.3	2616000
24	1	0.010	0.007	0.005	0.021	80	T.1.4	A441			Manual	99.3	3787000
25	1	0.010	0.007	0.005	0.021	80	T.1.4	A441			Manual	99.3	4512000
26	1	0.010	0.007	0.005	0.021	80	T.1.4	A441			Manual	99.3	4741000
27	1	0.010	0.007	0.005	0.021	80	T.1.4	A441			Manual	99.3	3197000
28	1	0.010	0.007	0.005	0.021	80	T.1.4	A441			Manual	132.4	1691000
29	1	0.010	0.007	0.005	0.021	80	T.1.4	A441			Manual	132.4	1329000
30	1	0.010	0.007	0.005	0.021	80	T.1.4	A441			Manual	132.4	807000
31	1	0.010	0.007	0.005	0.021	80	T.1.4	A441			Manual	132.4	1438000
32	1	0.010	0.007	0.005	0.021	80	T.1.4	A441			Manual	132.4	1092000
33	1	0.010	0.007	0.005	0.021	80	T.1.4	A441			Manual	164.8	584000
34	1	0.010	0.007	0.005	0.021	80	T.1.4	A441			Manual	164.8	579000
35	1	0.010	0.007	0.005	0.021	80	T.1.4	A441			Manual	164.8	492000
36	1	0.010	0.007	0.005	0.021	80	T.1.4	A441			Manual	164.8	527000
37	1	0.010	0.007	0.005	0.021	80	T.1.4	A441			Manual	164.8	421000
38	1	0.010	0.007	0.005	0.021	80	T.1.4	A441			Manual	164.8	322000
39	1	0.010	0.007	0.005	0.021	80	T.1.4	A441			Manual	164.8	428000
40	1	0.010	0.007	0.005	0.021	80	T.1.4	A441			Manual	197.9	355000
41	1	0.010	0.007	0.005	0.021	80	T.1.4	A441			Manual	197.9	302000
42	1	0.010	0.007	0.005	0.021	80	T.1.4	A441			Manual	197.9	214000
43	1	0.010	0.007	0.005	0.021	80	T.1.4	A441			Manual	197.9	361000
44	1	0.010	0.007	0.005	0.021	80	T.1.4	A441			Manual	197.9	495000
45	1	0.013	0.006	0.005	0.020	80	T.1.5	A441			Manual	95.1	6617000
46	1	0.013	0.006	0.005	0.020	80	T.1.5	A514	689	758	Manual	95.1	3854000
47	1	0.013	0.006	0.005	0.020	80	T.1.5	A441			Manual	95.1	6060000
48	1	0.013	0.006	0.005	0.020	80	T.1.5	A441			Manual	95.1	2012000
49	1	0.013	0.006	0.005	0.020	80	T.1.5	A441			Manual	126.9	1742000
50	1	0.013	0.006	0.005	0.020	80	T.1.5	A514	689	758	Manual	126.9	1366000
51	1	0.013	0.006	0.005	0.020	80	T.1.5	A441			Manual	126.9	1316000
52	1	0.013	0.006	0.005	0.020	80	T.1.5	A441			Manual	126.9	1553000
53	1	0.013	0.006	0.005	0.020	80	T.1.5	A441			Manual	126.9	1261000
54	1	0.013	0.006	0.005	0.020	80	T.1.5	A441			Manual	157.9	676000
55	1	0.013	0.006	0.005	0.020	80	T.1.5	A514	689	758	Manual	157.9	737000
56	1	0.013	0.006	0.005	0.020	80	T.1.5	A441			Manual	157.9	786000
57	1	0.013	0.006	0.005	0.020	80	T.1.5	A441			Manual	157.9	700000
58	1	0.013	0.006	0.005	0.020	80	T.1.5	A514	689	758	Manual	157.9	627000
59	1	0.013	0.006	0.005	0.020	80	T.1.6	A441			Manual	126.9	1264000
60	1	0.013	0.006	0.005	0.020	80	T.1.6	A441			Manual	126.9	1641000
61	1	0.013	0.006	0.005	0.020	80	T.1.6	A441			Manual	126.9	1206000
62	1	0.013	0.006	0.005	0.020	80	T.1.6	A441			Manual	126.9	1329000
63	1	0.013	0.006	0.005	0.020	80	T.1.6	A441			Manual	157.9	1037000
64	1	0.013	0.006	0.005	0.020	80	T.1.6	A441			Manual	157.9	561000
65	1	0.013	0.006	0.005	0.020	80	T.1.6	A441			Manual	157.9	804000
66	1	0.013	0.006	0.005	0.020	80	T.1.6	A441			Manual	157.9	950000
67	2	0.013	0.010	0.006	0.026	80	T.2.1	BS 4360 G50	355	470	Stress relieved	280.0	75000
68	2	0.013	0.010	0.006	0.026	80	T.2.1	BS 4360 G50	355	470	Stress relieved	240.0	146000
69	2	0.013	0.010	0.006	0.026	80	T.2.1	BS 4360 G50	355	470	Stress relieved	200.0	276000

Database #	# in series	Axial/Bending	Failure site	1st Author	Specimen type	Width of specimen [m]	Distance to flange edge [m]	Single or double attachment
1	29 B+SB	B	Toe	J. W. Fisher	Beam	0.127	0.010	Single
2	30 B+SB	B	Toe	J. W. Fisher	Beam	0.127	0.010	Single
3	31 B+SB	B	Toe	J. W. Fisher	Beam	0.127	0.010	Single
4	43 B+SB	B	Toe	J. W. Fisher	Beam	0.127	0.010	Single
5	41 B+SB	B	Toe	J. W. Fisher	Beam	0.127	0.010	Single
6	56 B+SB	B		J. W. Fisher	Beam	0.127	0.010	Single
7	55 B+SB	B	Toe	J. W. Fisher	Beam	0.127	0.010	Single
8	44 B+SCX	B	Toe	J. W. Fisher	Beam	0.127	0.010	Single
9	BT 1	B	Toe	J. W. Fisher	Beam	0.178	0.008	Single
10	BT 2	B	Toe	J. W. Fisher	Beam	0.178	0.008	Single
11	BT 3	B	Toe (Rough weld)	J. W. Fisher	Beam	0.178	0.008	Single
12	BT 4	B	Toe (Rough weld)	J. W. Fisher	Beam	0.178	0.008	Single
13	BT 5	B	Toe	J. W. Fisher	Beam	0.178	0.008	Single
14	BT 6	B	Toe	J. W. Fisher	Beam	0.178	0.008	Single
15	BT 7	B	Toe	J. W. Fisher	Beam	0.178	0.008	Single
16	BT 8	B	Toe	J. W. Fisher	Beam	0.178	0.008	Single
17	BT 9	B		J. W. Fisher	Beam	0.178	0.008	Single
18	BT 10	B		J. W. Fisher	Beam	0.178	0.008	Single
19	2 B	B	Toe	J. W. Fisher	Beam	0.305	0.008	Single
20	2 C	B	Toe	J. W. Fisher	Beam	0.305	0.008	Single
21	2 D	B	Toe	J. W. Fisher	Beam	0.305	0.008	Single
22	2 A	B	Toe	J. W. Fisher	Beam	0.305	0.008	Single
23	SCB 211	B	Toe	J. W. Fisher	Beam	0.172	0.012	Single
24	SCB 212	B	Toe	J. W. Fisher	Beam	0.172	0.012	Single
25	SCB 213	B	Toe	J. W. Fisher	Beam	0.172	0.012	Single
26	SCB 311	B	Toe	J. W. Fisher	Beam	0.172	0.012	Single
27	SCB 312	B	Toe	J. W. Fisher	Beam	0.172	0.012	Single
28	SCB 221	B	Toe	J. W. Fisher	Beam	0.172	0.012	Single
29	SCB 222	B	Toe	J. W. Fisher	Beam	0.172	0.012	Single
30	SCB 223	B	Toe	J. W. Fisher	Beam	0.172	0.012	Single
31	SCB 321	B	Toe	J. W. Fisher	Beam	0.172	0.012	Single
32	SCB 322	B	Toe	J. W. Fisher	Beam	0.172	0.012	Single
33	SCB 131	B	Toe	J. W. Fisher	Beam	0.172	0.012	Single
34	SCB 132	B	Toe	J. W. Fisher	Beam	0.172	0.012	Single
35	SCB 231	B	Toe	J. W. Fisher	Beam	0.172	0.012	Single
36	SCB 232	B	Toe	J. W. Fisher	Beam	0.172	0.012	Single
37	SCB 233	B	Toe	J. W. Fisher	Beam	0.172	0.012	Single
38	SCB 331	B	Toe	J. W. Fisher	Beam	0.172	0.012	Single
39	SCB 332	B	Toe	J. W. Fisher	Beam	0.172	0.012	Single
40	SCB 141	B	Toe	J. W. Fisher	Beam	0.172	0.012	Single
41	SCB 142	B	Toe	J. W. Fisher	Beam	0.172	0.012	Single
42	SCB 241	B	Toe	J. W. Fisher	Beam	0.172	0.012	Single
43	SCB 242	B	Toe	J. W. Fisher	Beam	0.172	0.012	Single
44	SCB 243	B	Toe	J. W. Fisher	Beam	0.172	0.012	Single
45	SGB 211	B	No visible crack	J. W. Fisher	Beam	0.197	0.006	Single
46	SGC 212	B	No visible crack	J. W. Fisher	Beam	0.197	0.006	Single
47	SGB 311	B	No visible crack	J. W. Fisher	Beam	0.197	0.006	Single
48	SGB 312	B	Toe	J. W. Fisher	Beam	0.197	0.006	Single
49	SGB 211	B	Toe	J. W. Fisher	Beam	0.197	0.006	Single
50	SGC 222	B	Toe	J. W. Fisher	Beam	0.197	0.006	Single
51	SGB 321	B	Toe	J. W. Fisher	Beam	0.197	0.006	Single
52	SGB 322	B	Toe	J. W. Fisher	Beam	0.197	0.006	Single
53	SGB 323	B	Toe	J. W. Fisher	Beam	0.197	0.006	Single
54	SGB 231	B	Toe	J. W. Fisher	Beam	0.197	0.006	Single
55	SGC 232	B	Toe	J. W. Fisher	Beam	0.197	0.006	Single
56	SGB 331	B	Toe	J. W. Fisher	Beam	0.197	0.006	Single
57	SGB 332	B	Toe	J. W. Fisher	Beam	0.197	0.006	Single
58	SGC 333	B	Toe	J. W. Fisher	Beam	0.197	0.006	Single
59	SBB 221	B	Toe	J. W. Fisher	Beam	0.197	0.006	Single
60	SBB 222	B	Toe	J. W. Fisher	Beam	0.197	0.006	Single
61	SBB 321	B	Toe	J. W. Fisher	Beam	0.197	0.006	Single
62	SBB 322	B	Toe	J. W. Fisher	Beam	0.197	0.006	Single
63	SBB 231	B	Toe	J. W. Fisher	Beam	0.197	0.006	Single
64	SBB 232	B	Toe	J. W. Fisher	Beam	0.197	0.006	Single
65	SBB 331	B	Toe	J. W. Fisher	Beam	0.197	0.006	Single
66	SBB 332	B	Toe	J. W. Fisher	Beam	0.197	0.006	Single
67	1	A	Toe	T. Gurney	Detail	0.150	0.015	Double
68	2	A	Toe	T. Gurney	Detail	0.150	0.015	Double
69	3	A	Toe	T. Gurney	Detail	0.150	0.015	Double

Database #	LitRef	tf [m]	tw [m]	a [m]	L [m]	FAT EC	ExcelRef	Steel	fy [MPa]	fu [MPa]	Method	Δσ [MPa]	N [-]
70	2	0.013	0.010	0.006	0.026	80	T.2.1	BS 4360 G50	355	470	Stress relieved	160.0	548000
71	2	0.013	0.010	0.006	0.026	80	T.2.1	BS 4360 G50	355	470	Stress relieved	140.0	1885000
72	2	0.013	0.010	0.006	0.026	80	T.2.1	BS 4360 G50	355	470	Stress relieved	130.0	1713000
73	2	0.013	0.010	0.006	0.026	80	T.2.1	BS 4360 G50	355	470	Stress relieved	120.0	5037000
74	2	0.013	0.010	0.006	0.026	80	T.2.2	BS 4360 G50	355	470	Stress relieved	240.0	123000
75	2	0.013	0.010	0.006	0.026	80	T.2.2	BS 4360 G50	355	470	Stress relieved	192.0	345000
76	2	0.013	0.010	0.006	0.026	80	T.2.2	BS 4360 G50	355	470	Stress relieved	150.0	1056000
77	2	0.013	0.010	0.006	0.026	80	T.2.2	BS 4360 G50	355	470	Stress relieved	130.0	2306000
78	2	0.013	0.010	0.006	0.026	80	T.2.2	BS 4360 G50	355	470	Stress relieved	120.0	1294000
79	2	0.013	0.010	0.006	0.026	80	T.2.2	BS 4360 G50	355	470	Stress relieved	120.0	2648000
80	2	0.013	0.010	0.006	0.026	80	T.2.2	BS 4360 G50	355	470	Stress relieved	110.0	3219000
81	2	0.013	0.010	0.006	0.026	80	T.2.2	BS 4360 G50	355	470	Stress relieved	100.0	10000000
82	2	0.025	0.003	0.004	0.013	80	T.2.3	BS 4360 G50	355	470	Stress relieved	280.0	123000
83	2	0.025	0.003	0.004	0.013	80	T.2.3	BS 4360 G50	355	470	Stress relieved	240.0	263000
84	2	0.025	0.003	0.004	0.013	80	T.2.3	BS 4360 G50	355	470	Stress relieved	200.0	413000
85	2	0.025	0.003	0.004	0.013	80	T.2.3	BS 4360 G50	355	470	Stress relieved	180.0	795000
86	2	0.025	0.003	0.004	0.013	80	T.2.3	BS 4360 G50	355	470	Stress relieved	160.0	1311000
87	2	0.025	0.003	0.004	0.013	80	T.2.3	BS 4360 G50	355	470	Stress relieved	155.0	1871000
88	2	0.025	0.003	0.004	0.013	80	T.2.3	BS 4360 G50	355	470	Stress relieved	150.0	10080000
89	2	0.025	0.003	0.004	0.013	80	T.2.3	BS 4360 G50	355	470	Stress relieved	140.0	6710000
90	2	0.025	0.013	0.007	0.033	80	T.2.4	BS 4360 G50	355	470	Stress relieved	280.0	74000
91	2	0.025	0.013	0.007	0.033	80	T.2.4	BS 4360 G50	355	470	Stress relieved	240.0	132000
92	2	0.025	0.013	0.007	0.033	80	T.2.4	BS 4360 G50	355	470	Stress relieved	200.0	297000
93	2	0.025	0.013	0.007	0.033	80	T.2.4	BS 4360 G50	355	470	Stress relieved	160.0	689000
94	2	0.025	0.013	0.007	0.033	80	T.2.4	BS 4360 G50	355	470	Stress relieved	150.0	702000
95	2	0.025	0.013	0.007	0.033	80	T.2.4	BS 4360 G50	355	470	Stress relieved	140.0	1653000
96	2	0.025	0.013	0.007	0.033	80	T.2.4	BS 4360 G50	355	470	Stress relieved	130.0	1614000
97	2	0.025	0.013	0.007	0.033	80	T.2.4	BS 4360 G50	355	470	Stress relieved	120.0	10030000
98	2	0.025	0.013	0.007	0.033	80	T.2.5	BS 4360 G50	355	470	Stress relieved	280.0	73000
99	2	0.025	0.013	0.007	0.033	80	T.2.5	BS 4360 G50	355	470	Stress relieved	240.0	113000
100	2	0.025	0.013	0.007	0.033	80	T.2.5	BS 4360 G50	355	470	Stress relieved	200.0	222000
101	2	0.025	0.013	0.007	0.033	80	T.2.5	BS 4360 G50	355	470	Stress relieved	160.0	623000
102	2	0.025	0.013	0.007	0.033	80	T.2.5	BS 4360 G50	355	470	Stress relieved	150.0	964000
103	2	0.025	0.013	0.007	0.033	80	T.2.5	BS 4360 G50	355	470	Stress relieved	140.0	905000
104	2	0.025	0.013	0.007	0.033	80	T.2.5	BS 4360 G50	355	470	Stress relieved	130.0	1255000
105	2	0.025	0.013	0.007	0.033	80	T.2.5	BS 4360 G50	355	470	Stress relieved	120.0	7250000
106	2	0.025	0.220	0.011	0.250	71	T.2.6	BS 4360 G50	355	470	Stress relieved	240.0	80000
107	2	0.025	0.220	0.011	0.250	71	T.2.6	BS 4360 G50	355	470	Stress relieved	200.0	139000
108	2	0.025	0.220	0.011	0.250	71	T.2.6	BS 4360 G50	355	470	Stress relieved	160.0	322000
109	2	0.025	0.220	0.011	0.250	71	T.2.6	BS 4360 G50	355	470	Stress relieved	150.0	335000
110	2	0.025	0.220	0.011	0.250	71	T.2.6	BS 4360 G50	355	470	Stress relieved	120.0	764000
111	2	0.025	0.220	0.011	0.250	71	T.2.6	BS 4360 G50	355	470	Stress relieved	105.0	1720000
112	2	0.025	0.220	0.011	0.250	71	T.2.6	BS 4360 G50	355	470	Stress relieved	100.0	2839000
113	2	0.050	0.003	0.004	0.013	80	T.2.7	BS 4360 G50	355	470	Stress relieved	265.0	182000
114	2	0.050	0.003	0.004	0.013	80	T.2.7	BS 4360 G50	355	470	Stress relieved	240.0	268000
115	2	0.050	0.003	0.004	0.013	80	T.2.7	BS 4360 G50	355	470	Stress relieved	200.0	668000
116	2	0.050	0.003	0.004	0.013	80	T.2.7	BS 4360 G50	355	470	Stress relieved	200.0	631000
117	2	0.050	0.003	0.004	0.013	80	T.2.7	BS 4360 G50	355	470	Stress relieved	175.0	788000
118	2	0.050	0.003	0.004	0.013	80	T.2.7	BS 4360 G50	355	470	Stress relieved	160.0	1265000
119	2	0.050	0.003	0.004	0.013	80	T.2.7	BS 4360 G50	355	470	Stress relieved	160.0	5357000
120	2	0.050	0.220	0.011	0.250	71	T.2.8	BS 4360 G50	355	470	Stress relieved	200.0	49000
121	2	0.050	0.220	0.011	0.250	71	T.2.8	BS 4360 G50	355	470	Stress relieved	180.0	98000
122	2	0.050	0.220	0.011	0.250	71	T.2.8	BS 4360 G50	355	470	Stress relieved	160.0	158000
123	2	0.050	0.220	0.011	0.250	71	T.2.8	BS 4360 G50	355	470	Stress relieved	130.0	306000
124	2	0.050	0.220	0.011	0.250	71	T.2.8	BS 4360 G50	355	470	Stress relieved	110.0	567000
125	2	0.050	0.220	0.011	0.250	71	T.2.8	BS 4360 G50	355	470	Stress relieved	90.0	979000
126	2	0.050	0.220	0.011	0.250	71	T.2.8	BS 4360 G50	355	470	Stress relieved	70.0	3745000
127	2	0.100	0.003	0.004	0.013	80	T.2.9	BS 4360 G50	355	470	Stress relieved	270.0	232000
128	2	0.100	0.003	0.004	0.013	80	T.2.9	BS 4360 G50	355	470	Stress relieved	200.0	373000
129	2	0.100	0.003	0.004	0.013	80	T.2.9	BS 4360 G50	355	470	Stress relieved	160.0	665000
130	2	0.100	0.003	0.004	0.013	80	T.2.9	BS 4360 G50	355	470	Stress relieved	150.0	4094000
131	2	0.100	0.003	0.004	0.013	80	T.2.9	BS 4360 G50	355	470	Stress relieved	135.0	2100000
132	2	0.100	0.003	0.004	0.013	80	T.2.9	BS 4360 G50	355	470	Stress relieved	120.0	4258000
133	2	0.100	0.013	0.006	0.029	80	T.2.10	BS 4360 G50	355	470	Stress relieved	200.0	202000
134	2	0.100	0.013	0.006	0.029	80	T.2.10	BS 4360 G50	355	470	Stress relieved	170.0	361000
135	2	0.100	0.013	0.006	0.029	80	T.2.10	BS 4360 G50	355	470	Stress relieved	140.0	1096000
136	2	0.100	0.013	0.006	0.029	80	T.2.10	BS 4360 G50	355	470	Stress relieved	120.0	2841000
137	2	0.100	0.013	0.006	0.029	80	T.2.10	BS 4360 G50	355	470	Stress relieved	110.0	4016000
138	2	0.100	0.200	0.011	0.230	71	T.2.11	BS 4360 G50	355	470	Stress relieved	200.0	59000
139	2	0.100	0.200	0.011	0.230	71	T.2.11	BS 4360 G50	355	470	Stress relieved	140.0	186000
140	2	0.100	0.200	0.011	0.230	71	T.2.11	BS 4360 G50	355	470	Stress relieved	120.0	253000
141	2	0.100	0.200	0.011	0.230	71	T.2.11	BS 4360 G50	355	470	Stress relieved	90.0	730000
142	2	0.100	0.200	0.011	0.230	71	T.2.11	BS 4360 G50	355	470	Stress relieved	70.0	1734000
143	2	0.100	0.200	0.011	0.230	71	T.2.11	BS 4360 G50	355	470	Stress relieved	55.0	14520000
144	2	0.013	0.003	0.004	0.013	80	T.2.12	BS 4360 G50	355	470	As-welded	300.0	107000
145	2	0.013	0.003	0.004	0.013	80	T.2.12	BS 4360 G50	355	470	As-welded	250.0	209000
146	2	0.013	0.003	0.004	0.013	80	T.2.12	BS 4360 G50	355	470	As-welded	200.0	302000
147	2	0.013	0.003	0.004	0.013	80	T.2.12	BS 4360 G50	355	470	As-welded	150.0	822000
148	2	0.013	0.003	0.004	0.013	80	T.2.12	BS 4360 G50	355	470	As-welded	135.0	1452000
149	2	0.013	0.003	0.004	0.013	80	T.2.12	BS 4360 G50	355	470	As-welded	125.0	2189000

Database #	# in series	Axial/Bending	Failure site	1st Author	Specimen type	Width of specimen [m]	Distance to flange edge [m]	Single or double attachment
70	4	A	Toe	T. Gurney	Detail	0.150	0.015	Double
71	5	A	Toe	T. Gurney	Detail	0.150	0.015	Double
72	6	A	Toe	T. Gurney	Detail	0.150	0.015	Double
73	7	A	Toe	T. Gurney	Detail	0.150	0.015	Double
74	1	A	Toe	T. Gurney	Detail	0.150	0.015	Double
75	2	A	Toe	T. Gurney	Detail	0.150	0.015	Double
76	3	A	Toe	T. Gurney	Detail	0.150	0.015	Double
77	4	A	Toe	T. Gurney	Detail	0.150	0.015	Double
78	5	A	Toe	T. Gurney	Detail	0.150	0.015	Double
79	6	A	Toe	T. Gurney	Detail	0.150	0.015	Double
80	7	A	Toe	T. Gurney	Detail	0.150	0.015	Double
81	8	A	Toe	T. Gurney	Detail	0.150	0.015	Double
82	1	A	Toe	T. Gurney	Detail	0.150	0.015	Double
83	2	A	Toe	T. Gurney	Detail	0.150	0.015	Double
84	3	A	Toe	T. Gurney	Detail	0.150	0.015	Double
85	4	A	Toe	T. Gurney	Detail	0.150	0.015	Double
86	5	A	Toe	T. Gurney	Detail	0.150	0.015	Double
87	6	A	Toe	T. Gurney	Detail	0.150	0.015	Double
88	7	A	Toe	T. Gurney	Detail	0.150	0.015	Double
89	8	A	Toe	T. Gurney	Detail	0.150	0.015	Double
90	1	A	Toe	T. Gurney	Detail	0.150	0.015	Double
91	2	A	Toe	T. Gurney	Detail	0.150	0.015	Double
92	3	A	Toe	T. Gurney	Detail	0.150	0.015	Double
93	4	A	Toe	T. Gurney	Detail	0.150	0.015	Double
94	5	A	Toe	T. Gurney	Detail	0.150	0.015	Double
95	6	A	Toe	T. Gurney	Detail	0.150	0.015	Double
96	7	A	Toe	T. Gurney	Detail	0.150	0.015	Double
97	8	A	Toe	T. Gurney	Detail	0.150	0.015	Double
98	1	A	Toe	T. Gurney	Detail	0.150	0.015	Double
99	2	A	Toe	T. Gurney	Detail	0.150	0.015	Double
100	3	A	Toe	T. Gurney	Detail	0.150	0.015	Double
101	4	A	Toe	T. Gurney	Detail	0.150	0.015	Double
102	5	A	Toe	T. Gurney	Detail	0.150	0.015	Double
103	6	A	Toe	T. Gurney	Detail	0.150	0.015	Double
104	7	A	Toe	T. Gurney	Detail	0.150	0.015	Double
105	8	A	Toe	T. Gurney	Detail	0.150	0.015	Double
106	1	A	Toe	T. Gurney	Detail	0.150	0.015	Double
107	2	A	Toe	T. Gurney	Detail	0.150	0.015	Double
108	3	A	Toe	T. Gurney	Detail	0.150	0.015	Double
109	4	A	Toe	T. Gurney	Detail	0.150	0.015	Double
110	5	A	Toe	T. Gurney	Detail	0.150	0.015	Double
111	6	A	Toe	T. Gurney	Detail	0.150	0.015	Double
112	7	A	Toe	T. Gurney	Detail	0.150	0.015	Double
113	1	A	Toe	T. Gurney	Detail	0.076	0.013	Double
114	2	A	Toe	T. Gurney	Detail	0.076	0.013	Double
115	3	A	Toe	T. Gurney	Detail	0.076	0.013	Double
116	4	A	Toe	T. Gurney	Detail	0.076	0.013	Double
117	5	A	Toe	T. Gurney	Detail	0.076	0.013	Double
118	6	A	Toe	T. Gurney	Detail	0.076	0.013	Double
119	7	A	Toe	T. Gurney	Detail	0.076	0.013	Double
120	1	A	Toe	T. Gurney	Detail	0.076	0.013	Double
121	2	A	Toe	T. Gurney	Detail	0.076	0.013	Double
122	3	A	Toe	T. Gurney	Detail	0.076	0.013	Double
123	4	A	Toe	T. Gurney	Detail	0.076	0.013	Double
124	5	A	Toe	T. Gurney	Detail	0.076	0.013	Double
125	6	A	Toe	T. Gurney	Detail	0.076	0.013	Double
126	7	A	Toe	T. Gurney	Detail	0.076	0.013	Double
127	1	A	Toe	T. Gurney	Detail	0.046	0	Double
128	2	A	Toe	T. Gurney	Detail	0.046	0	Double
129	3	A	Toe	T. Gurney	Detail	0.046	0	Double
130	4	A	Toe	T. Gurney	Detail	0.046	0	Double
131	5	A	Toe	T. Gurney	Detail	0.046	0	Double
132	6	A	Toe	T. Gurney	Detail	0.046	0	Double
133	1	A	Toe	T. Gurney	Detail	0.046	0	Double
134	2	A	Toe	T. Gurney	Detail	0.046	0	Double
135	3	A	Toe	T. Gurney	Detail	0.046	0	Double
136	4	A	Toe	T. Gurney	Detail	0.046	0	Double
137	5	A	Toe	T. Gurney	Detail	0.046	0	Double
138	1	A	Toe	T. Gurney	Detail	0.046	0	Double
139	2	A	Toe	T. Gurney	Detail	0.046	0	Double
140	3	A	Toe	T. Gurney	Detail	0.046	0	Double
141	4	A	Toe	T. Gurney	Detail	0.046	0	Double
142	5	A	Toe	T. Gurney	Detail	0.046	0	Double
143	6	A	Toe	T. Gurney	Detail	0.046	0	Double
144	1	A	Toe	T. Gurney	Detail	0.150	0.015	Double
145	2	A	Toe	T. Gurney	Detail	0.150	0.015	Double
146	3	A	Toe	T. Gurney	Detail	0.150	0.015	Double
147	4	A	Toe	T. Gurney	Detail	0.150	0.015	Double
148	5	A	Toe	T. Gurney	Detail	0.150	0.015	Double
149	6	A	Toe	T. Gurney	Detail	0.150	0.015	Double

Database #	LitRef	tf [m]	tw [m]	a [m]	L [m]	FAT EC	ExcelRef	Steel	fy [MPa]	fu [MPa]	Method	Δσ [MPa]	N [-]
150	2	0.013	0.010	0.006	0.026	80	T.2.13	BS 4360 G50	355	470	As-welded	240.0	127000
151	2	0.013	0.010	0.006	0.026	80	T.2.13	BS 4360 G50	355	470	As-welded	200.0	180000
152	2	0.013	0.010	0.006	0.026	80	T.2.13	BS 4360 G50	355	470	As-welded	160.0	417000
153	2	0.013	0.010	0.006	0.026	80	T.2.13	BS 4360 G50	355	470	As-welded	140.0	692000
154	2	0.013	0.010	0.006	0.026	80	T.2.13	BS 4360 G50	355	470	As-welded	120.0	1154000
155	2	0.013	0.010	0.006	0.026	80	T.2.13	BS 4360 G50	355	470	As-welded	100.0	1798000
156	2	0.013	0.010	0.006	0.026	80	T.2.13	BS 4360 G50	355	470	As-welded	80.0	4865000
157	2	0.025	0.003	0.004	0.013	80	T.2.14	BS 4360 G50	355	470	As-welded	270.0	179000
158	2	0.025	0.003	0.004	0.013	80	T.2.14	BS 4360 G50	355	470	As-welded	240.0	215000
159	2	0.025	0.003	0.004	0.013	80	T.2.14	BS 4360 G50	355	470	As-welded	200.0	350000
160	2	0.025	0.003	0.004	0.013	80	T.2.14	BS 4360 G50	355	470	As-welded	160.0	803000
161	2	0.025	0.003	0.004	0.013	80	T.2.14	BS 4360 G50	355	470	As-welded	130.0	1761000
162	2	0.025	0.003	0.004	0.013	80	T.2.14	BS 4360 G50	355	470	As-welded	110.0	3183000
163	2	0.025	0.003	0.004	0.013	80	T.2.14	BS 4360 G50	355	470	As-welded	100.0	12830000
164	2	0.025	0.032	0.006	0.050	80	T.2.15	BS 4360 G50	355	470	As-welded	230.0	112000
165	2	0.025	0.032	0.006	0.050	80	T.2.15	BS 4360 G50	355	470	As-welded	180.0	204000
166	2	0.025	0.032	0.006	0.050	80	T.2.15	BS 4360 G50	355	470	As-welded	130.0	543000
167	2	0.025	0.032	0.006	0.050	80	T.2.15	BS 4360 G50	355	470	As-welded	100.0	1124000
168	2	0.025	0.032	0.006	0.050	80	T.2.15	BS 4360 G50	355	470	As-welded	85.0	2242000
169	2	0.025	0.032	0.006	0.050	80	T.2.15	BS 4360 G50	355	470	As-welded	70.0	4996000
170	2	0.025	0.220	0.011	0.250	71	T.2.16	BS 4360 G50	355	470	As-welded	220.0	73000
171	2	0.025	0.220	0.011	0.250	71	T.2.16	BS 4360 G50	355	470	As-welded	180.0	127000
172	2	0.025	0.220	0.011	0.250	71	T.2.16	BS 4360 G50	355	470	As-welded	130.0	329000
173	2	0.025	0.220	0.011	0.250	71	T.2.16	BS 4360 G50	355	470	As-welded	110.0	751000
174	2	0.025	0.220	0.011	0.250	71	T.2.16	BS 4360 G50	355	470	As-welded	100.0	877000
175	2	0.025	0.220	0.011	0.250	71	T.2.16	BS 4360 G50	355	470	As-welded	85.0	1835000
176	2	0.025	0.220	0.011	0.250	71	T.2.16	BS 4360 G50	355	470	As-welded	75.0	2656000
177	2	0.038	0.013	0.006	0.029	80	T.2.17	BS 4360 G50	355	470	As-welded	240.0	104000
178	2	0.038	0.013	0.006	0.029	80	T.2.17	BS 4360 G50	355	470	As-welded	200.0	186000
179	2	0.038	0.013	0.006	0.029	80	T.2.17	BS 4360 G50	355	470	As-welded	160.0	400000
180	2	0.038	0.013	0.006	0.029	80	T.2.17	BS 4360 G50	355	470	As-welded	130.0	726000
181	2	0.038	0.013	0.006	0.029	80	T.2.17	BS 4360 G50	355	470	As-welded	100.0	1279000
182	2	0.038	0.013	0.006	0.029	80	T.2.17	BS 4360 G50	355	470	As-welded	85.0	2947000
183	2	0.038	0.220	0.011	0.250	71	T.2.18	BS 4360 G50	355	470	As-welded	220.0	132000
184	2	0.038	0.220	0.011	0.250	71	T.2.18	BS 4360 G50	355	470	As-welded	180.0	150000
185	2	0.038	0.220	0.011	0.250	71	T.2.18	BS 4360 G50	355	470	As-welded	130.0	419000
186	2	0.038	0.220	0.011	0.250	71	T.2.18	BS 4360 G50	355	470	As-welded	110.0	709000
187	2	0.038	0.220	0.011	0.250	71	T.2.18	BS 4360 G50	355	470	As-welded	85.0	1028000
188	2	0.038	0.220	0.011	0.250	71	T.2.18	BS 4360 G50	355	470	As-welded	75.0	1526000
189	2	0.100	0.003	0.004	0.013	80	T.2.19	BS 4360 G50	355	470	As-welded	215.0	231000
190	2	0.100	0.003	0.004	0.013	80	T.2.19	BS 4360 G50	355	470	As-welded	190.0	440000
191	2	0.100	0.003	0.004	0.013	80	T.2.19	BS 4360 G50	355	470	As-welded	180.0	725000
192	2	0.100	0.003	0.004	0.013	80	T.2.19	BS 4360 G50	355	470	As-welded	150.0	894000
193	2	0.100	0.003	0.004	0.013	80	T.2.19	BS 4360 G50	355	470	As-welded	130.0	1753000
194	2	0.100	0.003	0.004	0.013	80	T.2.19	BS 4360 G50	355	470	As-welded	110.0	2893000
195	2	0.100	0.220	0.011	0.250	71	T.2.20	BS 4360 G50	355	470	As-welded	150.0	109000
196	2	0.100	0.220	0.011	0.250	71	T.2.20	BS 4360 G50	355	470	As-welded	120.0	224000
197	2	0.100	0.220	0.011	0.250	71	T.2.20	BS 4360 G50	355	470	As-welded	100.0	322000
198	2	0.100	0.220	0.011	0.250	71	T.2.20	BS 4360 G50	355	470	As-welded	65.0	1153000
199	2	0.100	0.220	0.011	0.250	71	T.2.20	BS 4360 G50	355	470	As-welded	55.0	2147000
200	3	0.010	0.006	0.006	0.023	80	T.3.1	A588	345		Automatic subm.	98.5	10000000
201	3	0.010	0.006	0.006	0.023	80	T.3.1	A588	345		Automatic subm.	144.0	1676000
202	3	0.010	0.006	0.006	0.023	80	T.3.1	A588	345		Automatic subm.	144.0	1020000
203	3	0.010	0.006	0.006	0.023	80	T.3.1	A588	345		Automatic subm.	144.0	3780000
204	3	0.010	0.006	0.006	0.023	80	T.3.1	A588	345		Automatic subm.	176.0	727000
205	3	0.010	0.006	0.006	0.023	80	T.3.1	A588	345		Automatic subm.	176.0	1062000
206	3	0.010	0.006	0.006	0.023	80	T.3.1	A588	345		Automatic subm.	176.0	640000
207	3	0.010	0.006	0.006	0.023	80	T.3.1	A588	345		Automatic subm.	229.0	223000
208	3	0.010	0.006	0.006	0.023	80	T.3.1	A588	345		Automatic subm.	229.0	441000
209	3	0.010	0.006	0.006	0.023	80	T.3.1	A588	345		Automatic subm.	229.0	325000
210	3	0.010	0.006	0.006	0.023	80	T.3.1	A588	345		Automatic subm.	262.0	289000
211	3	0.010	0.006	0.006	0.023	80	T.3.1	A588	345		Automatic subm.	262.0	331000
212	3	0.010	0.006	0.006	0.023	80	T.3.1	A588	345		Automatic subm.	262.0	250000
213	3	0.010	0.006	0.006	0.023	80	T.3.2	A588	345		Automatic subm.	94.9	16912000
214	3	0.010	0.006	0.006	0.023	80	T.3.2	A588	345		Automatic subm.	94.9	26657000
215	3	0.010	0.006	0.006	0.023	80	T.3.2	A588	345		Automatic subm.	94.9	23569000
216	3	0.010	0.006	0.006	0.023	80	T.3.2	A588	345		Automatic subm.	139.0	3353000
217	3	0.010	0.006	0.006	0.023	80	T.3.2	A588	345		Automatic subm.	139.0	2373000
218	3	0.010	0.006	0.006	0.023	80	T.3.2	A588	345		Automatic subm.	139.0	2760000
219	3	0.010	0.006	0.006	0.023	80	T.3.2	A588	345		Automatic subm.	139.0	1347000
220	3	0.010	0.006	0.006	0.023	80	T.3.2	A588	345		Automatic subm.	177.0	529000
221	3	0.010	0.006	0.006	0.023	80	T.3.2	A588	345		Automatic subm.	177.0	794000
222	3	0.010	0.006	0.006	0.023	80	T.3.2	A588	345		Automatic subm.	177.0	790000
223	3	0.010	0.006	0.006	0.023	80	T.3.3	A588	345		Automatic subm.	133.0	2028000
224	3	0.010	0.006	0.006	0.023	80	T.3.3	A588	345		Automatic subm.	133.0	2798000
225	3	0.010	0.006	0.006	0.023	80	T.3.3	A588	345		Automatic subm.	133.0	1782000
226	3	0.010	0.006	0.006	0.023	80	T.3.3	A588	345		Automatic subm.	133.0	2717000
227	3	0.010	0.006	0.006	0.023	80	T.3.3	A588	345		Automatic subm.	133.0	2528000
228	3	0.010	0.006	0.006	0.023	80	T.3.3	A588	345		Automatic subm.	133.0	2545000
229	3	0.010	0.006	0.006	0.023	80	T.3.3	A588	345		Automatic subm.	196.0	937000

Database #	# in series	Axial/Bending	Failure site	1st Author	Specimen type	Width of specimen [m]	Distance to flange edge [m]	Single or double attachment
150	1	A	Toe	T. Gurney	Detail	0.150	0.015	Double
151	2	A	Toe	T. Gurney	Detail	0.150	0.015	Double
152	3	A	Toe	T. Gurney	Detail	0.150	0.015	Double
153	4	A	Toe	T. Gurney	Detail	0.150	0.015	Double
154	5	A	Toe	T. Gurney	Detail	0.150	0.015	Double
155	6	A	Toe	T. Gurney	Detail	0.150	0.015	Double
156	7	A	Toe	T. Gurney	Detail	0.150	0.015	Double
157	1	A	Toe	T. Gurney	Detail	0.150	0.015	Double
158	2	A	Toe	T. Gurney	Detail	0.150	0.015	Double
159	3	A	Toe	T. Gurney	Detail	0.150	0.015	Double
160	4	A	Toe	T. Gurney	Detail	0.150	0.015	Double
161	5	A	Toe	T. Gurney	Detail	0.150	0.015	Double
162	6	A	Toe	T. Gurney	Detail	0.150	0.015	Double
163	7	A	Toe	T. Gurney	Detail	0.150	0.015	Double
164	1	A	Toe	T. Gurney	Detail	0.150	0.015	Double
165	2	A	Toe	T. Gurney	Detail	0.150	0.015	Double
166	3	A	Toe	T. Gurney	Detail	0.150	0.015	Double
167	4	A	Toe	T. Gurney	Detail	0.150	0.015	Double
168	5	A	Toe	T. Gurney	Detail	0.150	0.015	Double
169	6	A	Toe	T. Gurney	Detail	0.150	0.015	Double
170	1	A	Toe	T. Gurney	Detail	0.150	0.015	Double
171	2	A	Toe	T. Gurney	Detail	0.150	0.015	Double
172	3	A	Toe	T. Gurney	Detail	0.150	0.015	Double
173	4	A	Toe	T. Gurney	Detail	0.150	0.015	Double
174	5	A	Toe	T. Gurney	Detail	0.150	0.015	Double
175	6	A	Toe	T. Gurney	Detail	0.150	0.015	Double
176	7	A	Toe	T. Gurney	Detail	0.150	0.015	Double
177	1	A	Toe	T. Gurney	Detail	0.100	0.015	Double
178	2	A	Toe	T. Gurney	Detail	0.100	0.015	Double
179	3	A	Toe	T. Gurney	Detail	0.100	0.015	Double
180	4	A	Toe	T. Gurney	Detail	0.100	0.015	Double
181	5	A	Toe	T. Gurney	Detail	0.100	0.015	Double
182	6	A	Toe	T. Gurney	Detail	0.100	0.015	Double
183	1	A	Toe	T. Gurney	Detail	0.100	0.015	Double
184	2	A	Toe	T. Gurney	Detail	0.100	0.015	Double
185	3	A	Toe	T. Gurney	Detail	0.100	0.015	Double
186	4	A	Toe	T. Gurney	Detail	0.100	0.015	Double
187	5	A	Toe	T. Gurney	Detail	0.100	0.015	Double
188	6	A	Toe	T. Gurney	Detail	0.100	0.015	Double
189	1	A	Toe	T. Gurney	Detail	0.046	0	Double
190	2	A	Toe	T. Gurney	Detail	0.046	0	Double
191	3	A	Toe	T. Gurney	Detail	0.046	0	Double
192	4	A	Toe	T. Gurney	Detail	0.046	0	Double
193	5	A	Toe	T. Gurney	Detail	0.046	0	Double
194	6	A	Toe	T. Gurney	Detail	0.046	0	Double
195	1	A	Toe	T. Gurney	Detail	0.046	0	Double
196	2	A	Toe	T. Gurney	Detail	0.046	0	Double
197	3	A	Toe	T. Gurney	Detail	0.046	0	Double
198	4	A	Toe	T. Gurney	Detail	0.046	0	Double
199	5	A	Toe	T. Gurney	Detail	0.046	0	Double
200	AX1	A	Runout	P. Albrecht	Detail	0.026	0	Double
201	A101	A	Toe	P. Albrecht	Detail	0.026	0	Double
202	A102	A	Toe	P. Albrecht	Detail	0.026	0	Double
203	A103	A	Toe	P. Albrecht	Detail	0.026	0	Double
204	A201	A	Toe	P. Albrecht	Detail	0.026	0	Double
205	A202	A	Toe	P. Albrecht	Detail	0.026	0	Double
206	A203	A	Toe	P. Albrecht	Detail	0.026	0	Double
207	A301	A	Toe	P. Albrecht	Detail	0.026	0	Double
208	A302	A	Toe	P. Albrecht	Detail	0.026	0	Double
209	A303	A	Toe	P. Albrecht	Detail	0.026	0	Double
210	AX2	A	Toe	P. Albrecht	Detail	0.026	0	Double
211	AX3	A	Toe	P. Albrecht	Detail	0.026	0	Double
212	AX4	A	Toe	P. Albrecht	Detail	0.026	0	Double
213	D311	A	Toe	P. Albrecht	Detail	0.026	0	Double
214	D312	A	Toe	P. Albrecht	Detail	0.026	0	Double
215	D313	A	Toe	P. Albrecht	Detail	0.026	0	Double
216	D314	A	Toe	P. Albrecht	Detail	0.026	0	Double
217	D411	A	Toe	P. Albrecht	Detail	0.026	0	Double
218	D412	A	Toe	P. Albrecht	Detail	0.026	0	Double
219	D413	A	Toe	P. Albrecht	Detail	0.026	0	Double
220	D511	A	Toe	P. Albrecht	Detail	0.026	0	Double
221	D512	A	Toe	P. Albrecht	Detail	0.026	0	Double
222	D513	A	Toe	P. Albrecht	Detail	0.026	0	Double
223	C101	A	Toe	P. Albrecht	Detail	0.026	0	Double
224	C102	A	Toe	P. Albrecht	Detail	0.026	0	Double
225	C103	A	Toe	P. Albrecht	Detail	0.026	0	Double
226	C111	A	Toe	P. Albrecht	Detail	0.026	0	Double
227	C112	A	Toe	P. Albrecht	Detail	0.026	0	Double
228	C113	A	Toe	P. Albrecht	Detail	0.026	0	Double
229	C201	A	Toe	P. Albrecht	Detail	0.026	0	Double

Database #	LitRef	tf [m]	tw [m]	a [m]	L [m]	FAT EC	ExcelRef	Steel	fy [MPa]	fu [MPa]	Method	Δσ [MPa]	N [-]
230	3	0.010	0.006	0.006	0.023	80	T.3.3	A588	345		Automatic subm.	196.0	504000
231	3	0.010	0.006	0.006	0.023	80	T.3.3	A588	345		Automatic subm.	196.0	485000
232	3	0.010	0.006	0.006	0.023	80	T.3.3	A588	345		Automatic subm.	196.0	445000
233	3	0.010	0.006	0.006	0.023	80	T.3.3	A588	345		Automatic subm.	196.0	556000
234	3	0.010	0.006	0.006	0.023	80	T.3.3	A588	345		Automatic subm.	196.0	530000
235	3	0.010	0.006	0.006	0.023	80	T.3.3	A588	345		Automatic subm.	249.0	153000
236	3	0.010	0.006	0.006	0.023	80	T.3.3	A588	345		Automatic subm.	249.0	183000
237	3	0.010	0.006	0.006	0.023	80	T.3.3	A588	345		Automatic subm.	249.0	242000
238	3	0.010	0.006	0.006	0.023	80	T.3.3	A588	345		Automatic subm.	249.0	239000
239	3	0.010	0.006	0.006	0.023	80	T.3.3	A588	345		Automatic subm.	249.0	247000
240	3	0.010	0.006	0.006	0.023	80	T.3.3	A588	345		Automatic subm.	249.0	278000
241	3	0.010	0.006	0.006	0.023	80	T.3.4	A588	345		Manual	89.6	10000000
242	3	0.010	0.006	0.006	0.023	80	T.3.4	A588	345		Manual	89.6	10000000
243	3	0.010	0.006	0.006	0.023	80	T.3.4	A588	345		Manual	89.6	5293000
244	3	0.010	0.006	0.006	0.023	80	T.3.4	A588	345		Manual	96.5	2843000
245	3	0.010	0.006	0.006	0.023	80	T.3.4	A588	345		Manual	96.5	2430000
246	3	0.010	0.006	0.006	0.023	80	T.3.4	A588	345		Manual	96.5	3487000
247	3	0.010	0.006	0.006	0.023	80	T.3.4	A588	345		Manual	103.0	3747000
248	3	0.010	0.006	0.006	0.023	80	T.3.4	A588	345		Manual	103.0	2952000
249	3	0.010	0.006	0.006	0.023	80	T.3.4	A588	345		Manual	138.0	634000
250	3	0.010	0.006	0.006	0.023	80	T.3.4	A588	345		Manual	138.0	993000
251	3	0.010	0.006	0.006	0.023	80	T.3.4	A588	345		Manual	138.0	1483000
252	3	0.010	0.006	0.006	0.023	80	T.3.4	A588	345		Manual	138.0	1401000
253	3	0.010	0.006	0.006	0.023	80	T.3.4	A588	345		Manual	165.0	442000
254	3	0.010	0.006	0.006	0.023	80	T.3.4	A588	345		Manual	165.0	385000
255	3	0.010	0.006	0.006	0.023	80	T.3.4	A588	345		Manual	165.0	450000
256	3	0.010	0.006	0.006	0.023	80	T.3.4	A588	345		Manual	207.0	259000
257	3	0.010	0.006	0.006	0.023	80	T.3.4	A588	345		Manual	207.0	315000
258	3	0.010	0.006	0.006	0.023	80	T.3.4	A588	345		Manual	207.0	304000
259	3	0.010	0.006	0.006	0.023	80	T.3.4	A588	345		Manual	207.0	307000
260	3	0.010	0.006	0.006	0.023	80	T.3.4	A588	345		Manual	207.0	301000
261	3	0.010	0.006	0.006	0.023	80	T.3.4	A588	345		Manual	207.0	343000
262	3	0.010	0.006	0.006	0.023	80	T.3.4	A588	345		Manual	289.0	127000
263	3	0.010	0.006	0.006	0.023	80	T.3.4	A588	345		Manual	289.0	113000
264	3	0.010	0.006	0.006	0.023	80	T.3.4	A588	345		Manual	289.0	144000
265	3	0.010	0.006	0.006	0.023	80	T.3.4	A588	345		Manual	289.0	85300
266	3	0.010	0.006	0.006	0.023	80	T.3.5	A588	345		Manual	50.5	43925000
267	3	0.010	0.006	0.006	0.023	80	T.3.5	A588	345		Manual	50.5	125000000
268	3	0.010	0.006	0.006	0.023	80	T.3.5	A588	345		Manual	70.3	9863000
269	3	0.010	0.006	0.006	0.023	80	T.3.5	A588	345		Manual	70.3	11355000
270	3	0.010	0.006	0.006	0.023	80	T.3.5	A588	345		Manual	70.3	13313000
271	3	0.010	0.006	0.006	0.023	80	T.3.5	A588	345		Manual	94.9	4104000
272	3	0.010	0.006	0.006	0.023	80	T.3.5	A588	345		Manual	94.9	4325000
273	3	0.010	0.006	0.006	0.023	80	T.3.5	A588	345		Manual	94.9	4308000
274	3	0.010	0.006	0.006	0.023	80	T.3.5	A588	345		Manual	139.0	1121000
275	3	0.010	0.006	0.006	0.023	80	T.3.5	A588	345		Manual	139.0	1361000
276	3	0.010	0.006	0.006	0.023	80	T.3.5	A588	345		Manual	139.0	1221000
277	3	0.010	0.006	0.006	0.023	80	T.3.5	A588	345		Manual	177.0	646000
278	3	0.010	0.006	0.006	0.023	80	T.3.5	A588	345		Manual	177.0	803000
279	3	0.010	0.006	0.006	0.023	80	T.3.5	A588	345		Manual	177.0	603000
280	4	0.008	0.008	0.004	0.019	80	T.4.1	S1100				399.0	59129
281	4	0.008	0.008	0.004	0.019	80	T.4.1	S1100				399.0	81308
282	4	0.008	0.008	0.004	0.019	80	T.4.1	S1100				399.0	83179
283	4	0.008	0.008	0.004	0.019	80	T.4.1	S1100				238.9	296709
284	4	0.008	0.008	0.004	0.019	80	T.4.1	S1100				240.3	385453
285	4	0.008	0.008	0.004	0.019	80	T.4.1	S1100				241.1	436839
286	4	0.008	0.008	0.004	0.019	80	T.4.1	S1100				240.3	457170
287	4	0.008	0.008	0.004	0.019	80	T.4.1	S1100				241.1	573972
288	4	0.008	0.008	0.004	0.019	80	T.4.1	S1100				179.5	1059484
289	4	0.008	0.008	0.004	0.019	80	T.4.1	S1100				180.0	1160442
290	4	0.008	0.008	0.004	0.019	80	T.4.1	S1100				139.5	1255184
291	4	0.008	0.008	0.004	0.019	80	T.4.1	S1100				179.5	1270986
292	4	0.008	0.008	0.004	0.019	80	T.4.1	S1100				139.5	3190206
293	4	0.008	0.008	0.004	0.019	80	T.4.1	S1100				139.5	3494152
294	4	0.008	0.008	0.004	0.019	80	T.4.1	S1100				139.5	4437004
295	4	0.008	0.008	0.004	0.019	80	T.4.1	S1100				120.0	5566766
296	4	0.008	0.008	0.004	0.019	80	T.4.1	S1100				139.5	7573346
297	4	0.008	0.008	0.004	0.019	80	T.4.1	S1100				120.0	24426020
298	4	0.008	0.008	0.004	0.019	80	T.4.1	S1100				139.5	24442590
299	5	0.012	0.012	0.004	0.023	80	T.5.1	S355				118.3	1631160
300	5	0.012	0.012	0.004	0.023	80	T.5.1	S355				128.2	970001
301	5	0.012	0.012	0.004	0.023	80	T.5.1	S355				143.2	824418
302	5	0.012	0.012	0.004	0.023	80	T.5.1	S355				157.6	486490
303	5	0.012	0.012	0.004	0.023	80	T.5.1	S355				173.4	340532
304	5	0.012	0.012	0.004	0.023	80	T.5.1	S355				190.8	274104
305	5	0.012	0.012	0.004	0.023	80	T.5.1	S355				231.0	139617
306	5	0.012	0.012	0.004	0.023	80	T.5.1	S355				209.9	126176
307	5	0.012	0.012	0.004	0.023	80	T.5.1	S355				254.2	109795
308	5	0.012	0.012	0.004	0.023	80	T.5.1	S355				303.2	57239
309	5	0.012	0.012	0.004	0.023	80	T.5.1	S355				278.6	55474

Database #	# in series	Axial/Bending	Failure site	1st Author	Specimen type	Width of specimen [m]	Distance to flange edge [m]	Single or double attachment
230	C202	A	Toe	P. Albrecht	Detail	0.026	0	Double
231	C203	A	Toe	P. Albrecht	Detail	0.026	0	Double
232	C211	A	Toe	P. Albrecht	Detail	0.026	0	Double
233	C212	A	Toe	P. Albrecht	Detail	0.026	0	Double
234	C213	A	Toe	P. Albrecht	Detail	0.026	0	Double
235	C301	A	Toe	P. Albrecht	Detail	0.026	0	Double
236	C302	A	Toe	P. Albrecht	Detail	0.026	0	Double
237	C303	A	Toe	P. Albrecht	Detail	0.026	0	Double
238	C311	A	Toe	P. Albrecht	Detail	0.026	0	Double
239	C312	A	Toe	P. Albrecht	Detail	0.026	0	Double
240	C313	A	Toe	P. Albrecht	Detail	0.026	0	Double
241	E111	A	Toe	P. Albrecht	Detail	0.026	0	Double
242	E112	A	Toe	P. Albrecht	Detail	0.026	0	Double
243	E113	A	Toe	P. Albrecht	Detail	0.026	0	Double
244	E114	A	Toe	P. Albrecht	Detail	0.026	0	Double
245	EX3	A	Toe	P. Albrecht	Detail	0.026	0	Double
246	EX4	A	Toe	P. Albrecht	Detail	0.026	0	Double
247	EX5	A	Toe	P. Albrecht	Detail	0.026	0	Double
248	EX2	A	Toe	P. Albrecht	Detail	0.026	0	Double
249	E211	A	Toe	P. Albrecht	Detail	0.026	0	Double
250	E212	A	Toe	P. Albrecht	Detail	0.026	0	Double
251	E213	A	Toe	P. Albrecht	Detail	0.026	0	Double
252	E214	A	Toe	P. Albrecht	Detail	0.026	0	Double
253	EX6	A	Toe	P. Albrecht	Detail	0.026	0	Double
254	EX7	A	Toe	P. Albrecht	Detail	0.026	0	Double
255	EX8	A	Toe	P. Albrecht	Detail	0.026	0	Double
256	E311	A	Toe	P. Albrecht	Detail	0.026	0	Double
257	E312	A	Toe	P. Albrecht	Detail	0.026	0	Double
258	E313	A	Toe	P. Albrecht	Detail	0.026	0	Double
259	E314	A	Toe	P. Albrecht	Detail	0.026	0	Double
260	EX1	A	Toe	P. Albrecht	Detail	0.026	0	Double
261	EX9	A	Toe	P. Albrecht	Detail	0.026	0	Double
262	E411	A	Toe	P. Albrecht	Detail	0.026	0	Double
263	E412	A	Toe	P. Albrecht	Detail	0.026	0	Double
264	E413	A	Toe	P. Albrecht	Detail	0.026	0	Double
265	E414	A	Toe	P. Albrecht	Detail	0.026	0	Double
266	D121	A	Toe	P. Albrecht	Detail	0.026	0	Double
267	D122	A	Toe	P. Albrecht	Detail	0.026	0	Double
268	D221	A	Toe	P. Albrecht	Detail	0.026	0	Double
269	D222	A	Toe	P. Albrecht	Detail	0.026	0	Double
270	D223	A	Toe	P. Albrecht	Detail	0.026	0	Double
271	D321	A	Toe	P. Albrecht	Detail	0.026	0	Double
272	D322	A	Toe	P. Albrecht	Detail	0.026	0	Double
273	D323	A	Toe	P. Albrecht	Detail	0.026	0	Double
274	D421	A	Toe	P. Albrecht	Detail	0.026	0	Double
275	D422	A	Toe	P. Albrecht	Detail	0.026	0	Double
276	D423	A	Toe	P. Albrecht	Detail	0.026	0	Double
277	D521	A	Toe	P. Albrecht	Detail	0.026	0	Double
278	D522	A	Toe	P. Albrecht	Detail	0.026	0	Double
279	D523	A	Toe	P. Albrecht	Detail	0.026	0	Double
280		A		R. Puthli	Detail	0.050	0	Double
281		A		R. Puthli	Detail	0.050	0	Double
282		A		R. Puthli	Detail	0.050	0	Double
283		A		R. Puthli	Detail	0.050	0	Double
284		A		R. Puthli	Detail	0.050	0	Double
285		A		R. Puthli	Detail	0.050	0	Double
286		A		R. Puthli	Detail	0.050	0	Double
287		A		R. Puthli	Detail	0.050	0	Double
288		A		R. Puthli	Detail	0.050	0	Double
289		A		R. Puthli	Detail	0.050	0	Double
290		A		R. Puthli	Detail	0.050	0	Double
291		A		R. Puthli	Detail	0.050	0	Double
292		A		R. Puthli	Detail	0.050	0	Double
293		A		R. Puthli	Detail	0.050	0	Double
294		A		R. Puthli	Detail	0.050	0	Double
295		A		R. Puthli	Detail	0.050	0	Double
296		A		R. Puthli	Detail	0.050	0	Double
297		A		R. Puthli	Detail	0.050	0	Double
298		A		R. Puthli	Detail	0.050	0	Double
299		A		U. Kuhlmann	Detail	0.040	0	Double
300		A		U. Kuhlmann	Detail	0.040	0	Double
301		A		U. Kuhlmann	Detail	0.040	0	Double
302		A		U. Kuhlmann	Detail	0.040	0	Double
303		A		U. Kuhlmann	Detail	0.040	0	Double
304		A		U. Kuhlmann	Detail	0.040	0	Double
305		A		U. Kuhlmann	Detail	0.040	0	Double
306		A		U. Kuhlmann	Detail	0.040	0	Double
307		A		U. Kuhlmann	Detail	0.040	0	Double
308		A		U. Kuhlmann	Detail	0.040	0	Double
309		A		U. Kuhlmann	Detail	0.040	0	Double

Database #	LitRef	tf [m]	tw [m]	a [m]	L [m]	FAT EC	ExcelRef	Steel	fy [MPa]	fu [MPa]	Method	Δσ [MPa]	N [-]
310	5	0.012	0.012	0.004	0.023	80	T.5.2	S460				112.0	1978319
311	5	0.012	0.012	0.004	0.023	80	T.5.2	S460				161.4	1592283
312	5	0.012	0.012	0.004	0.023	80	T.5.2	S460				138.2	817444
313	5	0.012	0.012	0.004	0.023	80	T.5.2	S460				202.8	218810
314	5	0.012	0.012	0.004	0.023	80	T.5.2	S460				242.9	181660
315	5	0.012	0.012	0.004	0.023	80	T.5.2	S460				295.2	130160
316	5	0.012	0.012	0.004	0.023	80	T.5.2	S460				387.8	31746
317	5	0.012	0.012	0.004	0.023	80	T.5.3	S690				409.8	51432
318	5	0.012	0.012	0.004	0.023	80	T.5.3	S690				308.6	171281
319	5	0.012	0.012	0.004	0.023	80	T.5.3	S690				230.7	363642
320	5	0.012	0.012	0.004	0.023	80	T.5.3	S690				191.1	1360529
321	5	0.012	0.012	0.004	0.023	80	T.5.3	S690				173.7	1841486
322	5	0.012	0.012	0.004	0.023	80	T.5.3	S690				157.8	3453045
323	6	0.010	0.010	0.006	0.027	80	T.6.1	ASTK A572 Grade 50				131.0	2067000
324	6	0.010	0.010	0.006	0.027	80	T.6.1	ASTK A572 Grade 50				117.2	3638830
325	6	0.010	0.010	0.006	0.027	80	T.6.1	ASTK A572 Grade 50				103.4	8000000
326	6	0.010	0.010	0.006	0.027	80	T.6.1	ASTK A572 Grade 50				110.3	10000000
327	6	0.010	0.010	0.006	0.027	80	T.6.1	ASTK A572 Grade 50				117.2	5000000
328	6	0.010	0.010	0.006	0.027	80	T.6.1	ASTK A572 Grade 50				124.1	5000000
329	6	0.010	0.010	0.006	0.027	80	T.6.1	ASTK A572 Grade 50				131.0	2429080
330	6	0.010	0.010	0.006	0.027	80	T.6.1	ASTK A572 Grade 50				124.1	5000000
331	6	0.010	0.010	0.006	0.027	80	T.6.1	ASTK A572 Grade 50				131.0	5000000
332	6	0.010	0.010	0.006	0.027	80	T.6.1	ASTK A572 Grade 50				137.9	1853930
333	6	0.010	0.010	0.006	0.027	80	T.6.1	ASTK A572 Grade 50				131.0	5000000
334	6	0.010	0.010	0.006	0.027	80	T.6.1	ASTK A572 Grade 50				137.9	2986710
335	6	0.010	0.010	0.006	0.027	80	T.6.1	ASTK A572 Grade 50				131.0	5000000
336	6	0.010	0.010	0.006	0.027	80	T.6.1	ASTK A572 Grade 50				137.9	1581290
337	6	0.010	0.010	0.006	0.027	80	T.6.1	ASTK A572 Grade 50				131.0	2670370
338	6	0.010	0.010	0.006	0.027	80	T.6.1	ASTK A572 Grade 50				124.1	2640940
339	6	0.010	0.010	0.006	0.027	80	T.6.1	ASTK A572 Grade 50				117.2	5000000
340	6	0.010	0.010	0.006	0.027	80	T.6.2	ASTK A572 Grade 50				168.9	1056520
341	6	0.010	0.010	0.006	0.027	80	T.6.2	ASTK A572 Grade 50				168.9	938770
342	6	0.010	0.010	0.006	0.027	80	T.6.2	ASTK A572 Grade 50				168.9	826580
343	6	0.010	0.010	0.006	0.027	80	T.6.2	ASTK A572 Grade 50				168.9	1030760
344	6	0.010	0.010	0.006	0.027	80	T.6.2	ASTK A572 Grade 50				168.9	859460
345	6	0.010	0.010	0.006	0.027	80	T.6.2	ASTK A572 Grade 50				168.9	777940
346	6	0.010	0.010	0.006	0.027	80	T.6.2	ASTK A572 Grade 50				324.1	55120
347	6	0.010	0.010	0.006	0.027	80	T.6.2	ASTK A572 Grade 50				324.1	55140
348	6	0.010	0.010	0.006	0.027	80	T.6.2	ASTK A572 Grade 50				324.1	54990
349	6	0.010	0.010	0.006	0.027	80	T.6.2	ASTK A572 Grade 50				324.1	79350
350	6	0.010	0.010	0.006	0.027	80	T.6.2	ASTK A572 Grade 50				324.1	62560
351	6	0.010	0.010	0.006	0.027	80	T.6.2	ASTK A572 Grade 50				324.1	86630
352	6	0.010	0.010	0.006	0.027	80	T.6.3	ASTK A572 Grade 50				150.3	1811550
353	6	0.010	0.010	0.006	0.027	80	T.6.3	ASTK A572 Grade 50				126.9	3115150
354	6	0.010	0.010	0.006	0.027	80	T.6.3	ASTK A572 Grade 50				126.9	2078200
355	6	0.010	0.010	0.006	0.027	80	T.6.3	ASTK A572 Grade 50				126.9	2781900
356	6	0.010	0.010	0.006	0.027	80	T.6.3	ASTK A572 Grade 50				126.9	1870600
357	6	0.010	0.010	0.006	0.027	80	T.6.3	ASTK A572 Grade 50				126.9	3182250
358	6	0.010	0.010	0.006	0.027	80	T.6.3	ASTK A572 Grade 50				95.1	14979550
359	6	0.010	0.010	0.006	0.027	80	T.6.3	ASTK A572 Grade 50				95.1	8060700
360	6	0.010	0.010	0.006	0.027	80	T.6.3	ASTK A572 Grade 50				95.1	15523200
361	6	0.010	0.010	0.006	0.027	80	T.6.3	ASTK A572 Grade 50				95.1	10914450
362	7	0.008			0.018	80	T.7.1					282.3	102758
363	7	0.008			0.018	80	T.7.1					251.9	162646
364	7	0.008			0.018	80	T.7.1					221.2	184994
365	7	0.008			0.018	80	T.7.1					199.9	282155
366	7	0.008			0.018	80	T.7.1					180.5	666365
367	7	0.008			0.018	80	T.7.1					139.5	1310296
368	7	0.008			0.018	80	T.7.1					120.6	1503979
369	7	0.008			0.018	80	T.7.1					110.9	5202536
370	7	0.025			0.057	71	T.7.2					281.6	78457
371	7	0.025			0.057	71	T.7.2					250.6	93501
372	7	0.025			0.057	71	T.7.2					271.0	101759
373	7	0.025			0.057	71	T.7.2					220.9	165450
374	7	0.025			0.057	71	T.7.2					200.5	179698
375	7	0.025			0.057	71	T.7.2					180.5	202554
376	7	0.025			0.057	71	T.7.2					180.0	302179
377	7	0.025			0.057	71	T.7.2					160.7	380806
378	7	0.025			0.057	71	T.7.2					140.2	455834
379	7	0.025			0.057	71	T.7.2					120.6	784178
380	7	0.025			0.057	71	T.7.2					100.4	1228726
381	7	0.025			0.057	71	T.7.2					90.1	1699504
382	7	0.025			0.057	71	T.7.2					80.1	2652599
383	7	0.013			0.029	80	T.7.3					240.9	105473
384	7	0.013			0.029	80	T.7.3					199.8	112851
385	7	0.013			0.029	80	T.7.3					221.0	139290
386	7	0.013			0.029	80	T.7.3					180.2	214178
387	7	0.013			0.029	80	T.7.3					159.9	351833
388	7	0.013			0.029	80	T.7.3					139.4	546471
389	7	0.013			0.029	80	T.7.3					120.3	940138

Database #	# in series	Axial/Bending	Failure site	1st Author	Specimen type	Width of specimen [m]	Distance to flange edge [m]	Single or double attachment
310		A		U. Kuhlmann	Detail	0.040	0	Double
311		A		U. Kuhlmann	Detail	0.040	0	Double
312		A		U. Kuhlmann	Detail	0.040	0	Double
313		A		U. Kuhlmann	Detail	0.040	0	Double
314		A		U. Kuhlmann	Detail	0.040	0	Double
315		A		U. Kuhlmann	Detail	0.040	0	Double
316		A		U. Kuhlmann	Detail	0.040	0	Double
317		A		U. Kuhlmann	Detail	0.040	0	Double
318		A		U. Kuhlmann	Detail	0.040	0	Double
319		A		U. Kuhlmann	Detail	0.040	0	Double
320		A		U. Kuhlmann	Detail	0.040	0	Double
321		A		U. Kuhlmann	Detail	0.040	0	Double
322		A		U. Kuhlmann	Detail	0.040	0	Double
323	62	A	Not recorded	K. Klippstein	Detail	0.064	0	Double
324	68	A	Front, 0-4	K. Klippstein	Detail	0.064	0	Double
325	101	A	No visible crack	K. Klippstein	Detail	0.064	0	Double
326	75	A	No visible crack	K. Klippstein	Detail	0.064	0	Double
327	109	A	No visible crack	K. Klippstein	Detail	0.064	0	Double
328	65	A	No visible crack	K. Klippstein	Detail	0.064	0	Double
329	72	A	Front, 2-4	K. Klippstein	Detail	0.064	0	Double
330	66	A	No visible crack	K. Klippstein	Detail	0.064	0	Double
331	73	A	No visible crack	K. Klippstein	Detail	0.064	0	Double
332	124	A	Not recorded	K. Klippstein	Detail	0.064	0	Double
333	115	A	No visible crack	K. Klippstein	Detail	0.064	0	Double
334	94	A	Front, 4	K. Klippstein	Detail	0.064	0	Double
335	100	A	1/4 in at 4	K. Klippstein	Detail	0.064	0	Double
336	89	A	Rear, 0-4	K. Klippstein	Detail	0.064	0	Double
337	112	A	Rear, 0-2	K. Klippstein	Detail	0.064	0	Double
338	120	A	Rear, 2-4	K. Klippstein	Detail	0.064	0	Double
339	79	A	No visible crack	K. Klippstein	Detail	0.064	0	Double
340	90	A	Rear, 0-4	K. Klippstein	Detail	0.064	0	Double
341	97	A	RT, 0-3; FB, 4	K. Klippstein	Detail	0.064	0	Double
342	92	A	Rear, 1	K. Klippstein	Detail	0.064	0	Double
343	70	A	Front, 4	K. Klippstein	Detail	0.064	0	Double
344	84	A	Front	K. Klippstein	Detail	0.064	0	Double
345	122	A	Front & Back	K. Klippstein	Detail	0.064	0	Double
346	114	A	Front, 0-4	K. Klippstein	Detail	0.064	0	Double
347	108	A	Front, 0-4	K. Klippstein	Detail	0.064	0	Double
348	64	A	Front, 2-3	K. Klippstein	Detail	0.064	0	Double
349	106	A	Front, 0-4	K. Klippstein	Detail	0.064	0	Double
350	111	A	Rear, 0-1	K. Klippstein	Detail	0.064	0	Double
351	123	A	Rear	K. Klippstein	Detail	0.064	0	Double
352	104	A	Front, 0-4	K. Klippstein	Detail	0.064	0	Double
353	93	A	Front, 0-4	K. Klippstein	Detail	0.064	0	Double
354	99	A	Front, 0-3	K. Klippstein	Detail	0.064	0	Double
355	96	A	Rear, 0-4	K. Klippstein	Detail	0.064	0	Double
356	81	A	Front/rear	K. Klippstein	Detail	0.064	0	Double
357	98	A	Rear, 0-4	K. Klippstein	Detail	0.064	0	Double
358	77	A	Rear, 0-3	K. Klippstein	Detail	0.064	0	Double
359	105	A	Front, 0-3	K. Klippstein	Detail	0.064	0	Double
360	125	A	Top, 0-1	K. Klippstein	Detail	0.064	0	Double
361	117	A	Bottom, 0-4	K. Klippstein	Detail	0.064	0	Double
362		A		T. Gurney	Detail			Double
363		A		T. Gurney	Detail			Double
364		A		T. Gurney	Detail			Double
365		A		T. Gurney	Detail			Double
366		A		T. Gurney	Detail			Double
367		A		T. Gurney	Detail			Double
368		A		T. Gurney	Detail			Double
369		A		T. Gurney	Detail			Double
370		A		T. Gurney	Detail			Double
371		A		T. Gurney	Detail			Double
372		A		T. Gurney	Detail			Double
373		A		T. Gurney	Detail			Double
374		A		T. Gurney	Detail			Double
375		A		T. Gurney	Detail			Double
376		A		T. Gurney	Detail			Double
377		A		T. Gurney	Detail			Double
378		A		T. Gurney	Detail			Double
379		A		T. Gurney	Detail			Double
380		A		T. Gurney	Detail			Double
381		A		T. Gurney	Detail			Double
382		A		T. Gurney	Detail			Double
383		A		T. Gurney	Detail			Double
384		A		T. Gurney	Detail			Double
385		A		T. Gurney	Detail			Double
386		A		T. Gurney	Detail			Double
387		A		T. Gurney	Detail			Double
388		A		T. Gurney	Detail			Double
389		A		T. Gurney	Detail			Double

Database #	LitRef	tf [m]	tw [m]	a [m]	L [m]	FAT EC	ExcelRef	Steel	fy [MPa]	fu [MPa]	Method	Δσ [MPa]	N [-]
390	7	0.013			0.029	80	T.7.3					99.6	2127151
391	8	0.013	0.013	0.005	0.027	80	T.8.1	C-Mn DnV standard				150.0	705000
392	8	0.032	0.032	0.010	0.060	71	T.8.2	C-Mn DnV standard				150.0	627300
393	8	0.060	0.060	0.020	0.117	71	T.8.3	C-Mn DnV standard				150.0	250300
394	8	0.080	0.080	0.025	0.151	71	T.8.4	C-Mn DnV standard				150.0	236800
395	8	0.031	0.012	0.005	0.026	80	T.8.5	C-Mn DnV standard				150.0	1054600
396	8	0.031	0.012	0.009	0.037	80	T.8.6	C-Mn DnV standard				150.0	687700
397	8	0.031	0.031	0.010	0.059	71	T.8.7	C-Mn DnV standard				150.0	480200
398	8	0.031	0.031	0.020	0.087	71	T.8.8	C-Mn DnV standard				150.0	565700
399	9	0.009	0.009	0.006	0.026	80	T.9.1	SM490YA	440	550		203.0	172467
400	9	0.009	0.009	0.006	0.026	80	T.9.1	SM490YA	440	550		205.7	200062
401	9	0.009	0.009	0.006	0.026	80	T.9.1	SM490YA	440	550		159.5	471098
402	9	0.009	0.009	0.006	0.026	80	T.9.1	SM490YA	440	550		159.5	562386
403	9	0.009	0.009	0.006	0.026	80	T.9.1	SM490YA	440	550		136.0	636746
404	9	0.009	0.009	0.006	0.026	80	T.9.1	SM490YA	440	550		136.0	998602
405	9	0.009	0.009	0.006	0.026	80	T.9.1	SM490YA	440	550		134.7	1423087
406	9	0.009	0.009	0.006	0.026	80	T.9.1	SM490YA	440	550		113.0	2820940
407	9	0.009	0.009	0.006	0.026	80	T.9.1	SM490YA	440	550		112.6	6774055

Database #	# in series	Axial/Bending	Failure site	1st Author	Specimen type	Width of specimen [m]	Distance to flange edge [m]	Single or double attachment
390		A		T. Gurney	Detail			Double
391	T1	A		S. Berge	Detail	0.075	0	Double
392	T2	A		S. Berge	Detail	0.100	0	Double
393	T3	A		S. Berge	Detail	0.100	0	Double
394	T4	A		S. Berge	Detail	0.130	0	Double
395	T5	A		S. Berge	Detail	0.100	0	Double
396	T6	A		S. Berge	Detail	0.100	0	Double
397	T7	A		S. Berge	Detail	0.100	0	Double
398	T8	A		S. Berge	Detail	0.100	0	Double
399		A		Z. Xiao	Detail		0	Double
400		A		Z. Xiao	Detail		0	Double
401		A		Z. Xiao	Detail		0	Double
402		A		Z. Xiao	Detail		0	Double
403		A		Z. Xiao	Detail		0	Double
404		A		Z. Xiao	Detail		0	Double
405		A		Z. Xiao	Detail		0	Double
406		A		Z. Xiao	Detail		0	Double
407		A		Z. Xiao	Detail		0	Double

References							
LitRef	Year	1st Author	2nd Author	3rd Author	4th Author	5th Author	6th Author
1	1974	J. W. Fisher	P. A. Albrecht	B. T. Yen	D. J. Klingerman	B. M. McNamee	
2	1991	T. Gurney					
3	1979	P. Albrecht	Ian M. Friedland				
4	2006	R. Puthli	S. Herion	J. Bergers			
5	2005	U. Kuhlmann	J. Bergmann	A. Dürr	R. Thumser	H.P Günther	U. Gerth
6	1989	K. Klippstein	C. Schilling				
7	1995	T. Gurney					
8	1985	S. Berge					
9	2005	Z. Xiao	K. Yamada				

LitRef	Title	Info
1	Fatigue strengh of steel beams with welded stiffeners and attachments	Beams
2	The fatigue strength of transverse fillet welded joints	Details
3	Fatigue - Limit effect on variable-amplitude fatigue of stiffeners	Details
4	Untersuchungen zum Ermüdungsverhelten von hochfesten Stählen im Rahmen von LIFTHIGH	Details
5	Erhöhung der Ermüdungsfestigkeit von geschweissten höherfesten Baustählen durch Anwendung von Nachbehandlungsverfahren	Details
6	Pilot study on the constant and variable behaviour of transverse stiffener welds	Details
7	Thickness effect in relatively thin joints	Details
8	On the effect of plate thickness in fatigue of welds	Details
9	Fatigue strength of intersecting attachments	Details

A2 Experimental fatigue strength classes

Double-sided stiffener					
Calculated values of $\Delta\sigma_C$ for various dimensional configurations					
Group #	**t_f [m]**	**L [m]**	**$\Delta\sigma_C$ [MPa]**	**Std. dev.**	**# of data points**
1	t_f = 0.008 m (Double)	0.019	97.2	0.225	27
2	t_f = 0.025 m (Double)	0.050	75.7	0.074	6
3	t_f = 0.0254 m (Double)	0.057	80.4	0.077	13
4	t_f = 0.1 m (Double)	0.230	54.9	0.059	6

Double-sided stiffener, combined					
Calculated values of $\Delta\sigma_C$ for various dimensional configurations					
Group #	**t_f [m]**	**L [m]**	**$\Delta\sigma_C$ [MPa]**	**Std. dev.**	**# of data points**
5	t_f = 0.013-0.1 m (Double)	0.013	101.2	0.155	40
6	t_f = 0.01-0.012 m (Double)	0.023	91.4	0.210	104
7	t_f = 0.009-0.0305 m (Double)	0.027	88.3	0.209	72
8	t_f = 0.0127-0.1 m (Double)	0.032	77.9	0.184	35
9	t_f = 0.025-0.1 m (Double)	0.250	54	0.231	32

One-sided stiffener					
Calculated values of $\Delta\sigma_C$ for various dimensional configurations					
Group #	**t_f [m]**	**L [m]**	**$\Delta\sigma_C$ [MPa]**	**Std. dev.**	**# of data points**
10	t_f = 0.01397 m (Single)	0.0352	77.4	0.187	8
11	t_f = 0.01905 m (Single)	0.0259	86.3	0.139	4

One-sided stiffener, combined					
Calculated values of $\Delta\sigma_C$ for various dimensional configurations					
Group #	**t_f [m]**	**L [m]**	**$\Delta\sigma_C$ [MPa]**	**Std. dev.**	**# of data points**
12	t_f = 0.0095-0.0254 m (Single)	0.020	95.9	0.113	52

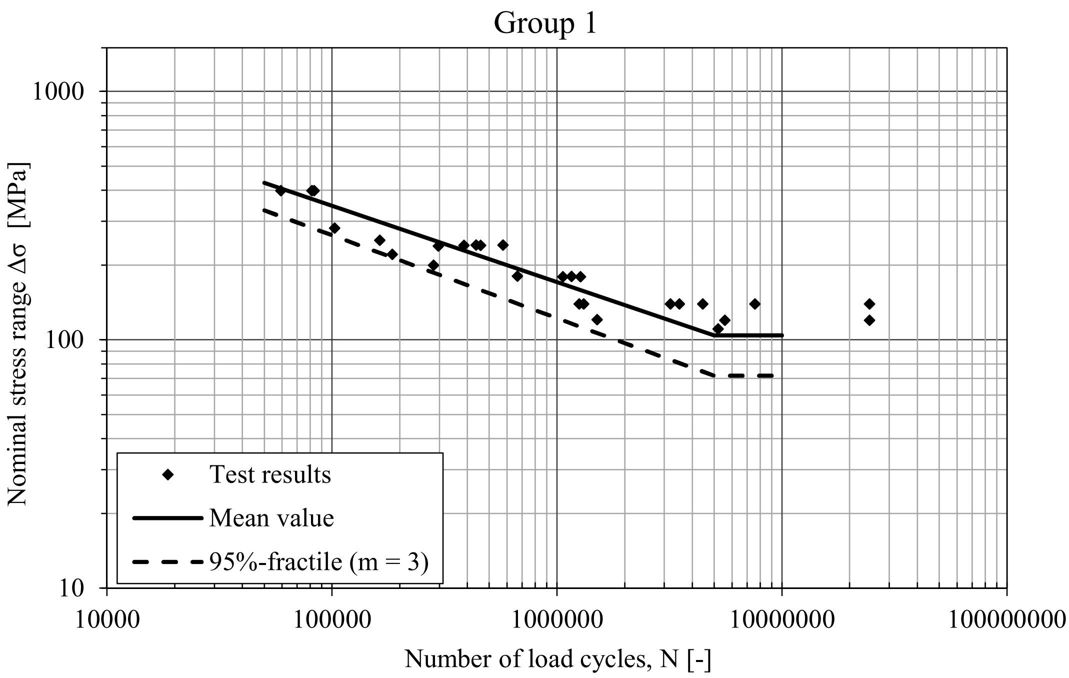
Group 1
1000
100
10
Nominal stress range Δσ [MPa]
Test results
Mean value
95%-fractile (m = 3)
10000
100000
1000000
10000000
100000000
Number of load cycles, N [-]

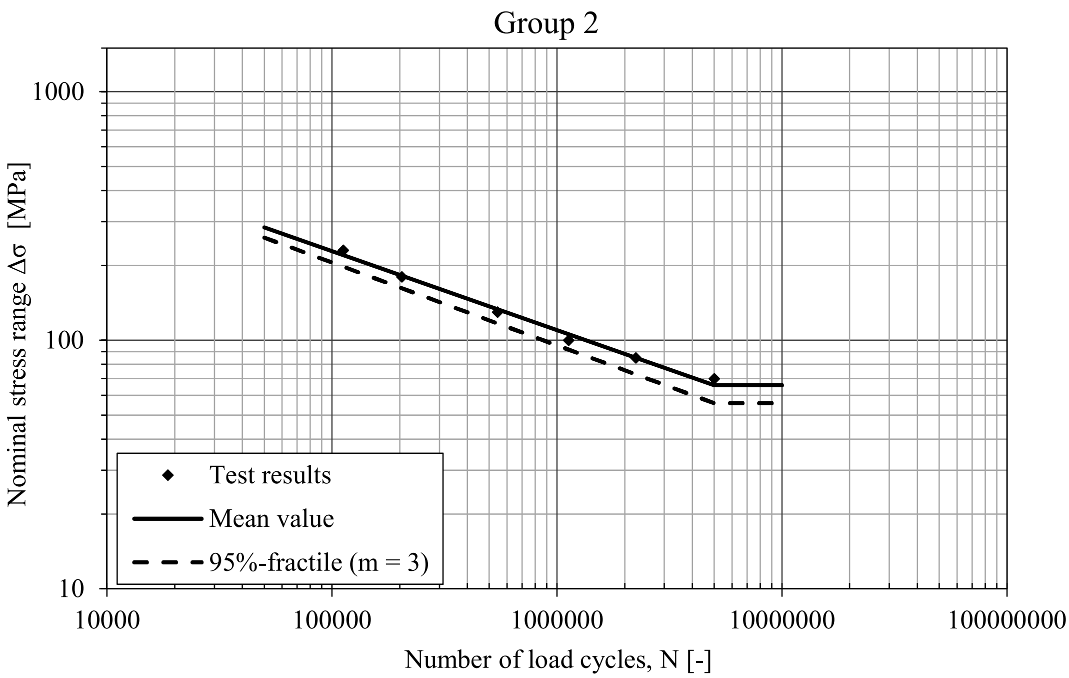
Group 2
1000
100
10
Nominal stress range Δσ [MPa]
Test results
Mean value
95%-fractile (m = 3)
10000
100000
1000000
10000000
100000000
Number of load cycles, N [-]

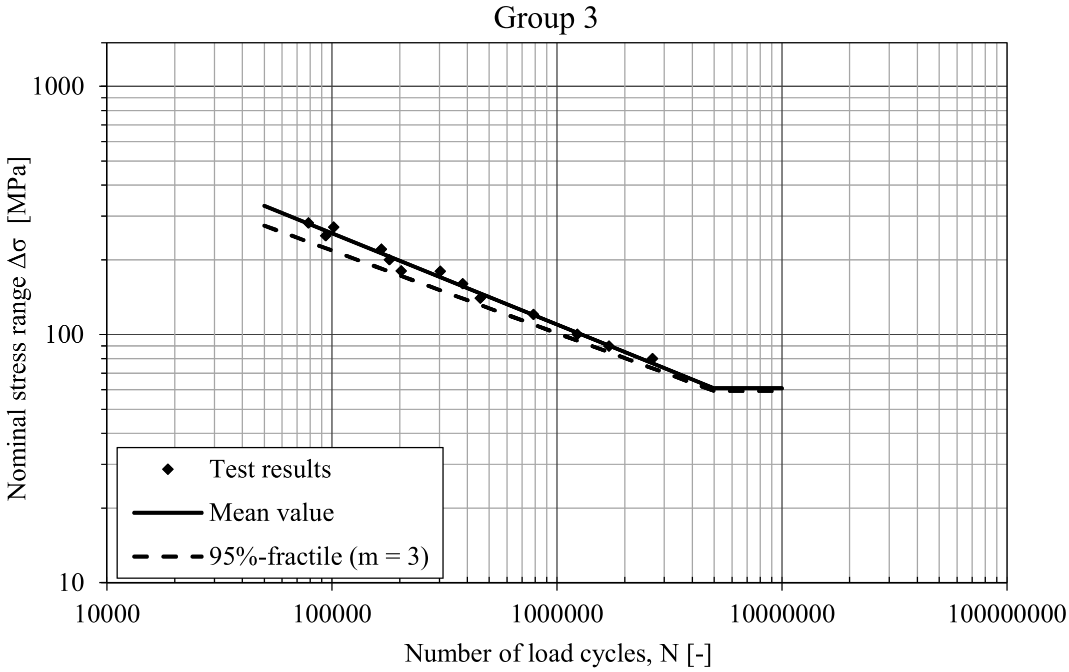
Group 3
1000
100
10
Nominal stress range Δσ [MPa]
10000
100000
1000000
10000000
100000000
Number of load cycles, N [-]
Test results
Mean value
95%-fractile (m = 3)

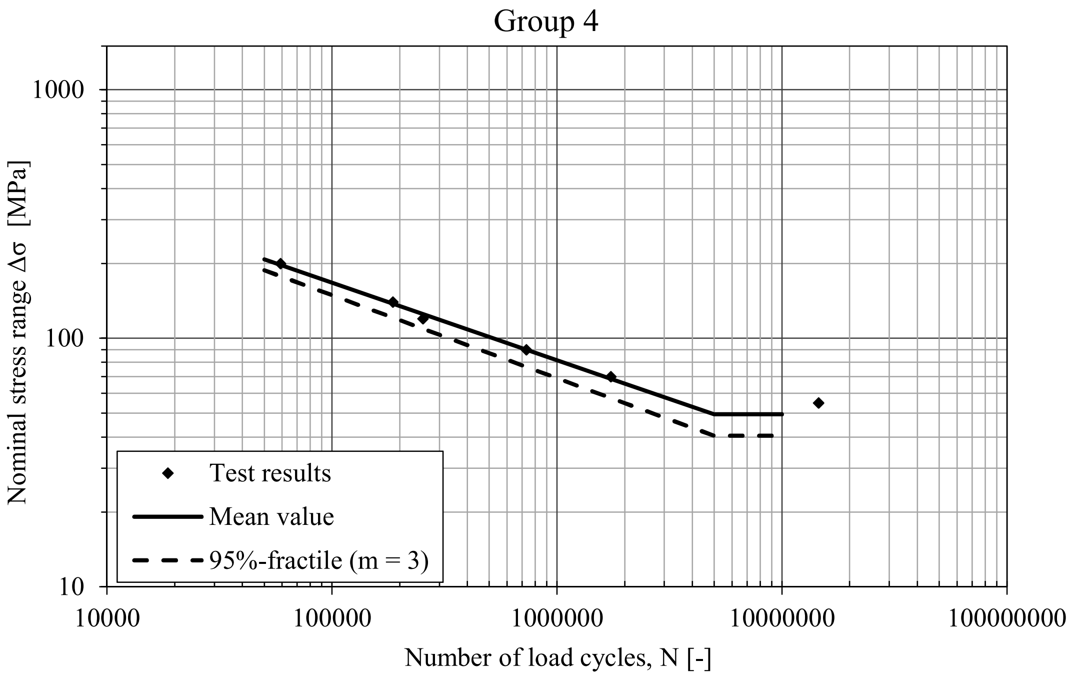
Group 4
1000
100
10
Nominal stress range Δσ [MPa]
10000
100000
1000000
10000000
100000000
Number of load cycles, N [-]
Test results
Mean value
95%-fractile (m = 3)

Group 5

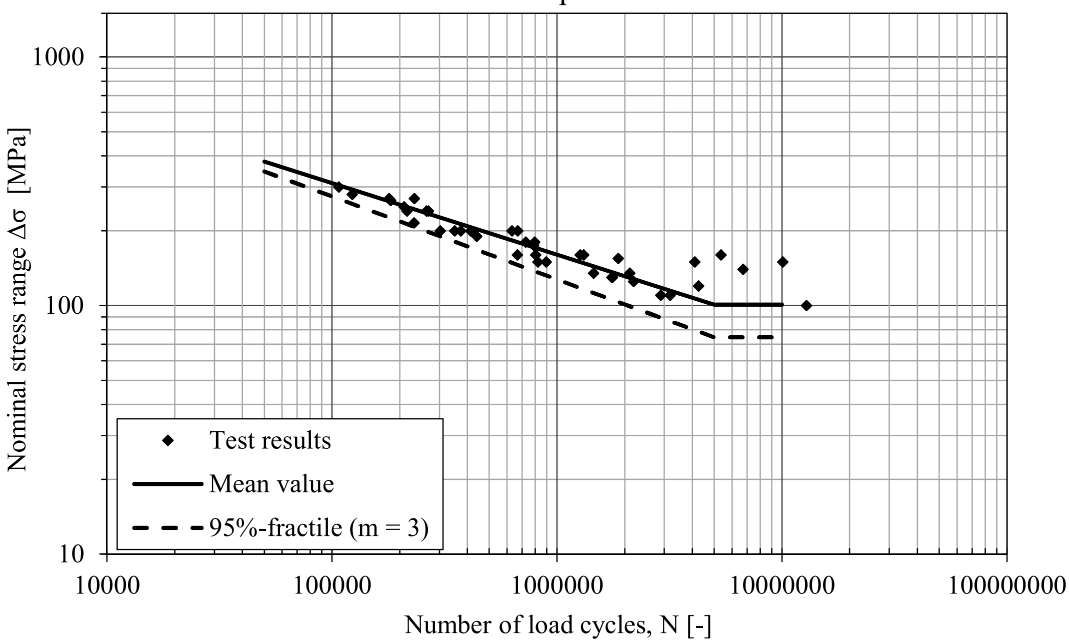

Group 6

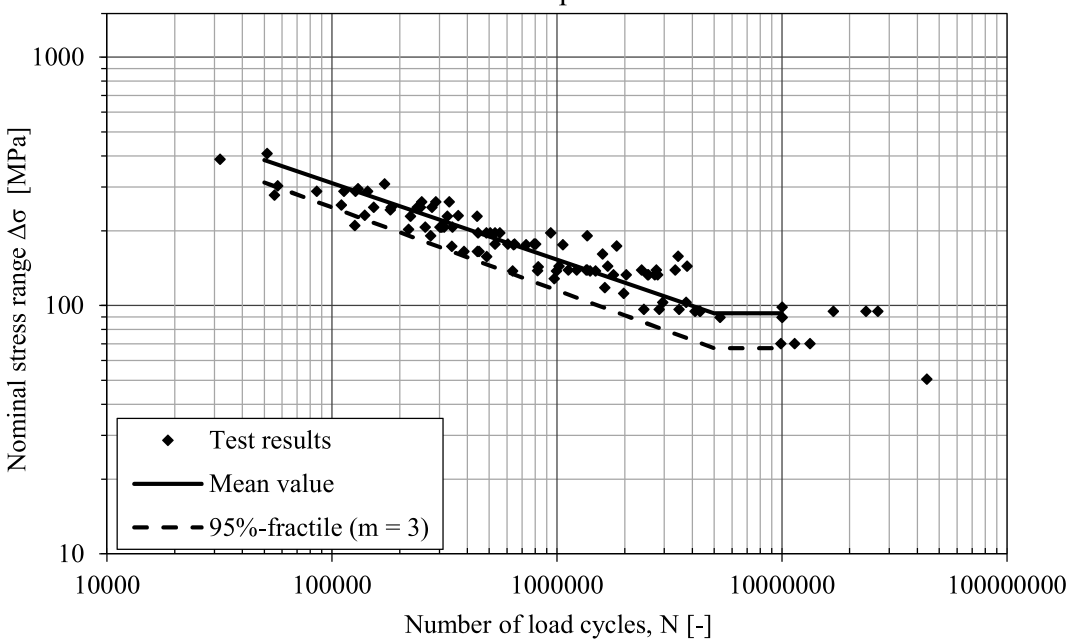

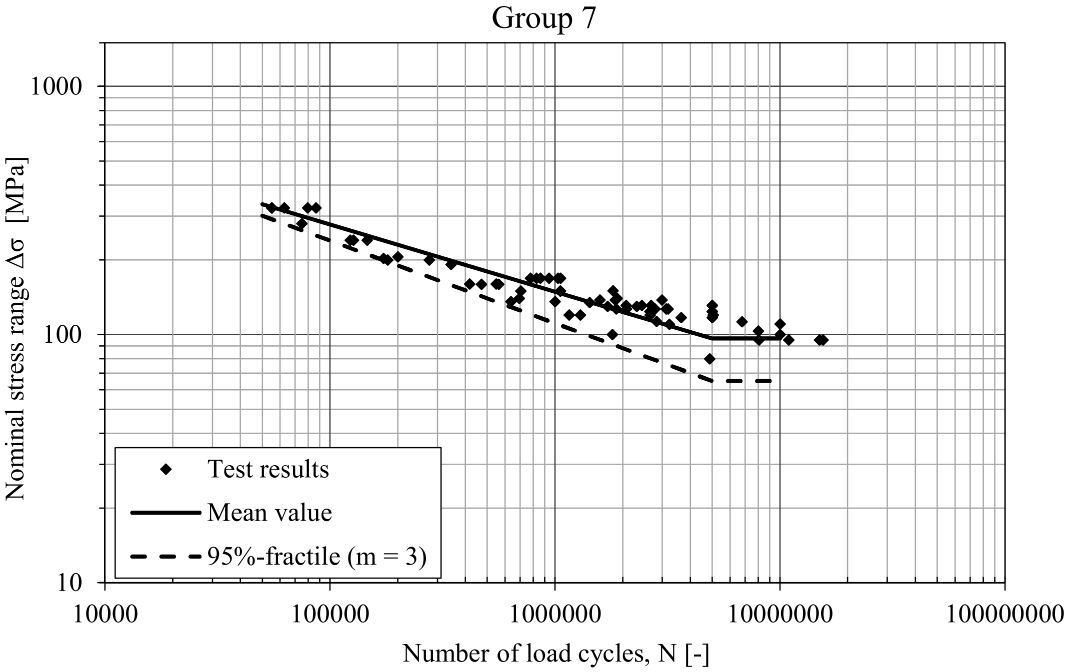
Group 7
Nominal stress range Δσ [MPa]
1000
100
10
10000
100000
1000000
10000000
100000000
Number of load cycles, N [-]
Test results
Mean value
95%-fractile (m = 3)

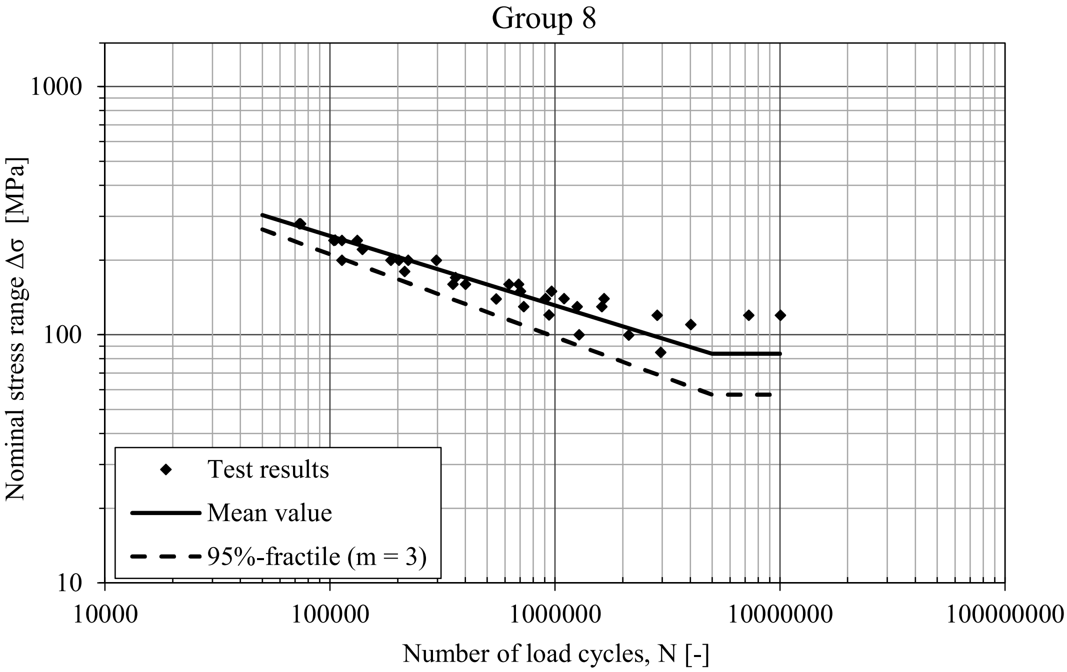
Group 8
Nominal stress range Δσ [MPa]
1000
100
10
10000
100000
1000000
10000000
100000000
Number of load cycles, N [-]
Test results
Mean value
95%-fractile (m = 3)

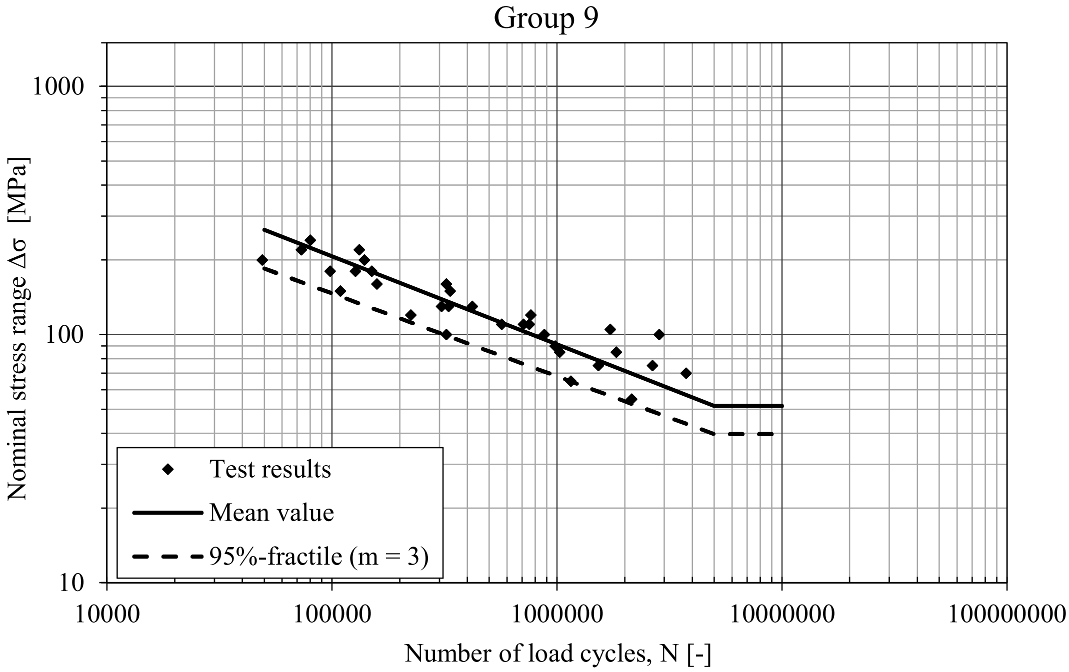

Group 9
1000
100
10
Nominal stress range Δσ [MPa]
10000
100000
1000000
10000000
100000000
Number of load cycles, N [-]
Test results
Mean value
95%-fractile (m = 3)

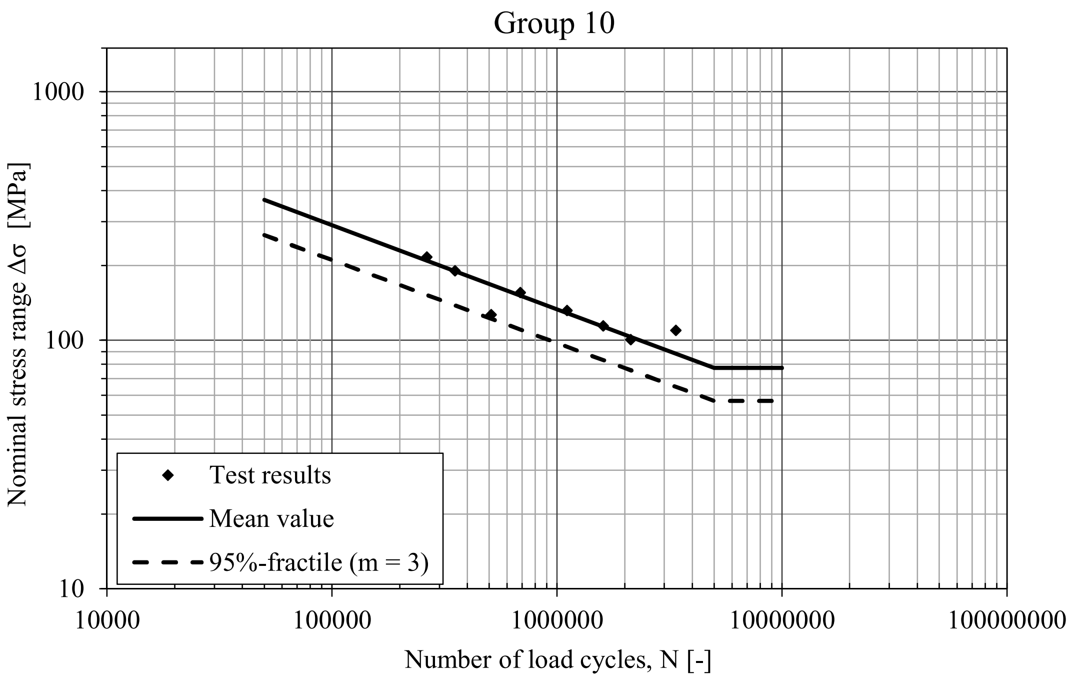

Group 10
1000
100
10
Nominal stress range Δσ [MPa]
10000
100000
1000000
10000000
100000000
Number of load cycles, N [-]
Test results
Mean value
95%-fractile (m = 3)

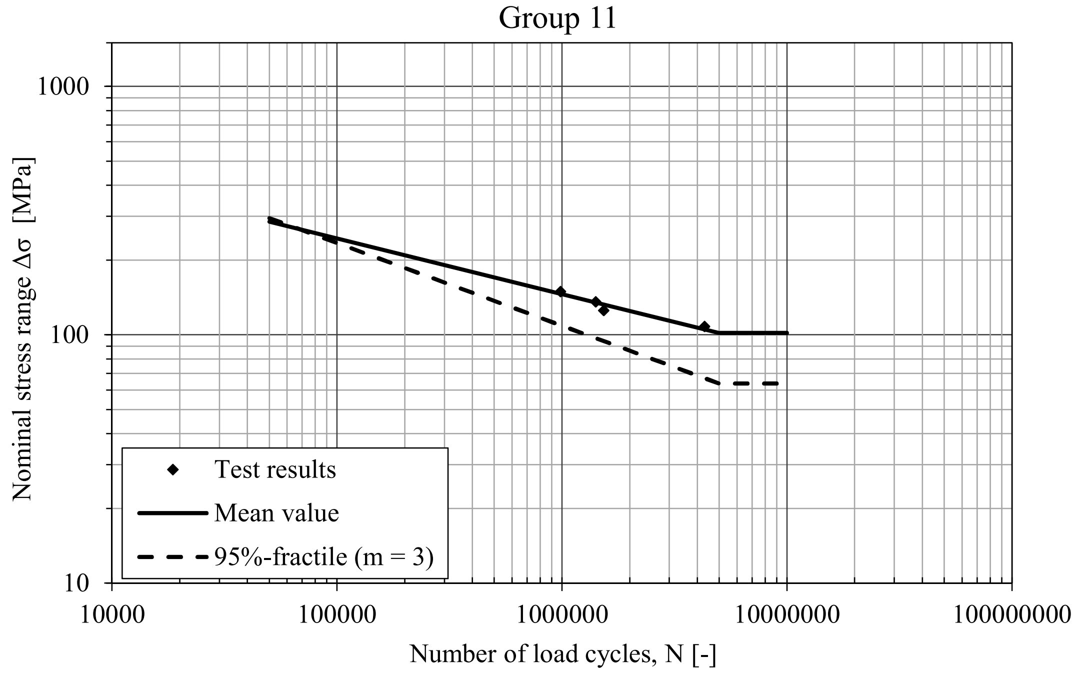

Group 11
Nominal stress range Δσ [MPa]
1000
100
10
10000
100000
1000000
10000000
100000000
Number of load cycles, N [-]
Test results
Mean value
95%-fractile (m = 3)

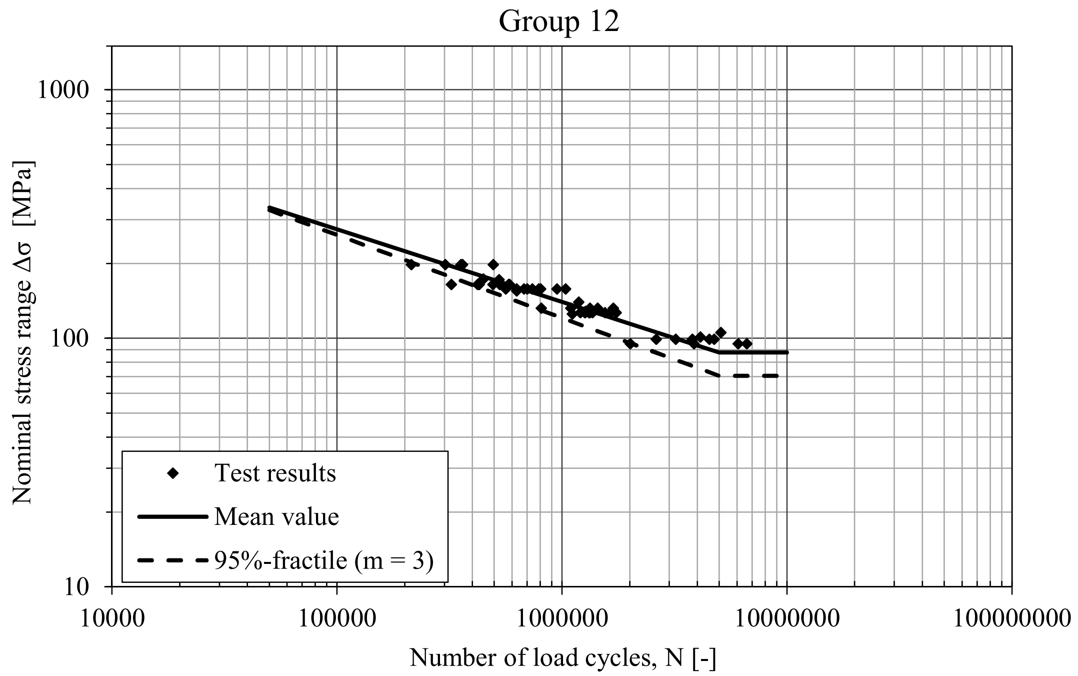

Group 12
Nominal stress range Δσ [MPa]
1000
100
10
10000
100000
1000000
10000000
100000000
Number of load cycles, N [-]
Test results
Mean value
95%-fractile (m = 3)

Appendix B

This appendix contains all code used to run the FE-analyses in both 2D and 3D. The .in-files are used to define the geometry, loads, BC etc. as well as define the analysis type in ADINA. The Linux script is pasted into a terminal window to run the analyses in batch mode. The .plo-files are used to extract the maximum principal stress from each analysis. Note that the code given in the .in-files is for one model only, which means that separate files must be created for each model in the parameter study. In this thesis, it is done by using Excel. The same goes for the Linux-code and .plo-files. A flowchart of the analysis process can be seen in Figure 4.1.

B1 2D FE-modelling

B1.1 .in-file, one-sided model

```
DATABASE    NEW   SAVE=NO     PROMPT=NO
FEPROGRAM   ADINA
CONTROL     FILEVERSION=V84

FEPROGRAM   PROGRAM=ADINA

CONTROL     UNDO=-1     AUTOMREBUILD=YES
FILEECHO    OPTION=FILE F=loggfil.ut
FILELOG     OPTION=FILE F=loggfil.ut

*     Indata

PARAMETER   tf    0.02
PARAMETER   tw    0.006
PARAMETER   a     0.003
PARAMETER   r     0.001

*     Y-direction

PARAMETER   L1    0.06
PARAMETER   L2    $L1+sqrt(2)*$a
PARAMETER   L3    $L2+$tw
PARAMETER   L4    $L3+sqrt(2)*$a
PARAMETER   L5    $L4+$L1
PARAMETER   L6    $L2+$r
PARAMETER   L7    $L3-$r
PARAMETER   L8    $L1-2*$r
PARAMETER   L9    $L4+2*$r
PARAMETER   L10   $L1-0.5*$r
PARAMETER   L11   $L1+0.5*$r
PARAMETER   L18   $L8-2*$r
PARAMETER   L19   $L9+2*$r
PARAMETER   L20   $L4-0.5*$r
PARAMETER   L21   $L4+0.5*$r
PARAMETER   L23   $L2-1.5*$r
PARAMETER   L24   $L3+1.5*$r

*     Z-direction

PARAMETER   L12   $tf+sqrt(2)*$a
PARAMETER   L13   $L12+$L1
```

```
PARAMETER   L14   $tf-$r
PARAMETER   L15   $tf+$r
PARAMETER   L16   $tf-2*$r
PARAMETER   L17   $tf+2*$r
PARAMETER   L22   $tf-2*$r

*     Scale factor

PARAMETER   s     anint($L22*666)

*     Coordinate system

COORDINATE  POINTS      SYSTEM=0
1     0     0     0
2     0     0     $tf
3     0     $L1   $tf
4     0     $L2   $tf
5     0     $L2   $L12
6     0     $L2   $L13
7     0     $L3   $L13
8     0     $L3   $L12
9     0     $L3   $tf
10    0     $L4   $tf
11    0     $L5   $tf
12    0     $L5   0
13    0     $L6   $L15
14    0     $L6   $L14
15    0     $L7   $L15
16    0     $L7   $L14
17    0     $L18  $0
18    0     $L10  $0
19    0     $L11  $0
20    0     $L23  $0
21    0     $L6   $0
22    0     $L7   $0
23    0     $L24  $0
24    0     $L20  $0
25    0     $L21  $0
26    0     $L19  $0
27    0     $L18  $L22
28    0     $L10  $L22
29    0     $L11  $L22
30    0     $L23  $L22
31    0     $L6   $L22
32    0     $L7   $L22
33    0     $L24  $L22
34    0     $L20  $L22
35    0     $L21  $L22
36    0     $L19  $L22
37    0     0     $L22
38    0     $L5   $L22
39    0     $L18  $tf
40    0     $L19  $tf
41    0     $L6   $tf
42    0     $L7   $tf

*     Lines
```

```
LINE  STRAIGHT   NAME=1      P1=1  P2=37
LINE  STRAIGHT   NAME=2      P1=37 P2=2
LINE  STRAIGHT   NAME=3      P1=39 P2=2
LINE  STRAIGHT   NAME=4      P1=39 P2=3
LINE  STRAIGHT   NAME=5      P1=3  P2=5
LINE  STRAIGHT   NAME=6      P1=5  P2=6
LINE  STRAIGHT   NAME=7      P1=6  P2=7
LINE  STRAIGHT   NAME=8      P1=8  P2=7
LINE  STRAIGHT   NAME=9      P1=8  P2=10
LINE  STRAIGHT   NAME=10     P1=10 P2=40
LINE  STRAIGHT   NAME=11     P1=40 P2=11
LINE  STRAIGHT   NAME=12     P1=11 P2=38
LINE  STRAIGHT   NAME=13     P1=38 P2=12
LINE  STRAIGHT   NAME=14     P1=12 P2=26
LINE  STRAIGHT   NAME=15     P1=26 P2=25
LINE  STRAIGHT   NAME=16     P1=25 P2=24
LINE  STRAIGHT   NAME=17     P1=24 P2=23
LINE  STRAIGHT   NAME=18     P1=23 P2=22
LINE  STRAIGHT   NAME=19     P1=22 P2=21
LINE  STRAIGHT   NAME=20     P1=21 P2=20
LINE  STRAIGHT   NAME=21     P1=20 P2=19
LINE  STRAIGHT   NAME=22     P1=19 P2=18
LINE  STRAIGHT   NAME=23     P1=18 P2=17
LINE  STRAIGHT   NAME=24     P1=17 P2=1
LINE  STRAIGHT   NAME=25     P1=27 P2=37
LINE  STRAIGHT   NAME=26     P1=27 P2=28
LINE  STRAIGHT   NAME=27     P1=28 P2=29
LINE  STRAIGHT   NAME=28     P1=29 P2=30
LINE  STRAIGHT   NAME=29     P1=30 P2=31
LINE  STRAIGHT   NAME=30     P1=31 P2=32
LINE  STRAIGHT   NAME=31     P1=32 P2=33
LINE  STRAIGHT   NAME=32     P1=33 P2=34
LINE  STRAIGHT   NAME=33     P1=34 P2=35
LINE  STRAIGHT   NAME=34     P1=35 P2=36
LINE  STRAIGHT   NAME=35     P1=36 P2=38
LINE  STRAIGHT   NAME=36     P1=13 P2=15
LINE  STRAIGHT   NAME=37     P1=14 P2=16
LINE  ARC   NAME=38     MODE=1      P1=13 P2=4  CENTER=41
LINE  ARC   NAME=39     MODE=1      P1=4  P2=14 CENTER=41
LINE  ARC   NAME=40     MODE=7      P3=0  CENTER=17   RADIUS=0.001
@CLEAR
4
5
@
LINE  ARC   NAME=41     MODE=7      P3=0  CENTER=17   RADIUS=0.001
@CLEAR
5
6
@
LINE  ARC   NAME=42     MODE=7      P3=0  CENTER=17   RADIUS=0.001
@CLEAR
8
9
@
LINE  ARC   NAME=43     MODE=7      P3=0  CENTER=17   RADIUS=0.001
@CLEAR
9
10
```

```
@
LINE  STRAIGHT   NAME=44     P1=39 P2=27
LINE  STRAIGHT   NAME=45     P1=27 P2=17
LINE  STRAIGHT   NAME=46     P1=43 P2=28
LINE  STRAIGHT   NAME=47     P1=28 P2=18
LINE  STRAIGHT   NAME=48     P1=44 P2=29
LINE  STRAIGHT   NAME=49     P1=29 P2=19
LINE  STRAIGHT   NAME=50     P1=4  P2=30
LINE  STRAIGHT   NAME=51     P1=30 P2=20
LINE  STRAIGHT   NAME=52     P1=14 P2=31
LINE  STRAIGHT   NAME=53     P1=31 P2=21
LINE  STRAIGHT   NAME=54     P1=16 P2=32
LINE  STRAIGHT   NAME=55     P1=32 P2=22
LINE  STRAIGHT   NAME=56     P1=9  P2=33
LINE  STRAIGHT   NAME=57     P1=33 P2=23
LINE  STRAIGHT   NAME=58     P1=52 P2=34
LINE  STRAIGHT   NAME=59     P1=34 P2=24
LINE  STRAIGHT   NAME=60     P1=53 P2=35
LINE  STRAIGHT   NAME=61     P1=35 P2=25
LINE  STRAIGHT   NAME=62     P1=40 P2=36
LINE  STRAIGHT   NAME=63     P1=36 P2=26
LINE  STRAIGHT   NAME=64     P1=44 P2=4
LINE  STRAIGHT   NAME=65     P1=9  P2=52
LINE  STRAIGHT   NAME=66     P1=46 P2=13
LINE  STRAIGHT   NAME=67     P1=50 P2=15
LINE  STRAIGHT   NAME=68     P1=46 P2=50
LINE  STRAIGHT   NAME=69     P1=47 P2=49
LINE  ARC   NAME=70     MODE=1      P1=15 P2=9  CENTER=42
LINE  ARC   NAME=71     MODE=1      P1=9  P2=16 CENTER=42

SURFACE     PATCH NAME=1 EDGE1=1    EDGE2=25 EDGE3=45 EDGE4=24
SURFACE     PATCH NAME=2 EDGE1=2    EDGE2=25 EDGE3=44 EDGE4=3
SURFACE     PATCH NAME=3 EDGE1=45   EDGE2=26    EDGE3=47    EDGE4=23
SURFACE     PATCH NAME=4 EDGE1=47   EDGE2=27    EDGE3=49    EDGE4=22
SURFACE     PATCH NAME=5 EDGE1=49   EDGE2=28    EDGE3=51    EDGE4=21
SURFACE     PATCH NAME=6 EDGE1=51   EDGE2=29    EDGE3=53    EDGE4=20
SURFACE     PATCH NAME=7 EDGE1=53   EDGE2=30    EDGE3=55    EDGE4=19
SURFACE     PATCH NAME=8 EDGE1=55   EDGE2=31    EDGE3=57    EDGE4=18
SURFACE     PATCH NAME=9 EDGE1=57   EDGE2=32    EDGE3=59    EDGE4=17
SURFACE     PATCH NAME=10 EDGE1=59 EDGE2=33    EDGE3=61    EDGE4=16
SURFACE     PATCH NAME=11 EDGE1=61 EDGE2=34    EDGE3=63    EDGE4=15
SURFACE     PATCH NAME=12 EDGE1=63 EDGE2=35    EDGE3=13    EDGE4=14
SURFACE     PATCH NAME=13 EDGE1=62 EDGE2=11    EDGE3=12    EDGE4=35
SURFACE     PATCH NAME=14 EDGE1=6  EDGE2=7     EDGE3=8     EDGE4=69
SURFACE     PATCH NAME=15 EDGE1=44 EDGE2=4     EDGE3=46    EDGE4=26
SURFACE     PATCH NAME=16 EDGE1=46 EDGE2=40    EDGE3=48    EDGE4=27
SURFACE     PATCH NAME=17 EDGE1=48 EDGE2=64    EDGE3=50    EDGE4=28
SURFACE     PATCH NAME=18 EDGE1=50 EDGE2=39    EDGE3=52    EDGE4=29
SURFACE     PATCH NAME=19 EDGE1=52 EDGE2=37    EDGE3=54    EDGE4=30
SURFACE     PATCH NAME=20 EDGE1=54 EDGE2=71    EDGE3=56    EDGE4=31
SURFACE     PATCH NAME=21 EDGE1=56 EDGE2=65    EDGE3=58    EDGE4=32
SURFACE     PATCH NAME=22 EDGE1=58 EDGE2=43    EDGE3=60    EDGE4=33
SURFACE     PATCH NAME=23 EDGE1=60 EDGE2=10    EDGE3=62    EDGE4=34
SURFACE     PATCH NAME=24 EDGE1=64 EDGE2=5     EDGE3=66    EDGE4=38
SURFACE     PATCH NAME=25 EDGE1=66 EDGE2=68    EDGE3=67    EDGE4=36
SURFACE     PATCH NAME=26 EDGE1=67 EDGE2=9     EDGE3=65    EDGE4=70
SURFACE     PATCH NAME=27 EDGE1=41 EDGE2=69    EDGE3=42    EDGE4=68
```

```
READ  F='model/material.in'

SUBDIVIDE   SURFACE     NAME=15     MODE=LENGTH SIZE=0.00025
@CLEAR
16
to
27
@
SUBDIVIDE   LINE  NAME=3     MODE=DIVISIONS   NDIV=22     RATIO=12
      PROGRESS=ARITHMETIC
@CLEAR
25
11
35
@
SUBDIVIDE   LINE  NAME=6     MODE=DIVISIONS   NDIV=35     RATIO=10
      PROGRESS=ARITHMETIC
@CLEAR
8
@

SUBDIVIDE   LINE  NAME=45    MODE=DIVISIONS   NDIV=$s     RATIO=8
      PROGRESS=ARITHMETIC
@CLEAR
47
49
51
53
55
57
59
61
63
@

SUBDIVIDE   LINE  NAME=1     MODE=LENGTH SIZE=0.0025
@CLEAR
2
7
12
to
24
@

READ  F='model/shell_element.in'
READ  F='model/boundary.in'
READ  F='model/load.in'

      MASTER ANALYSIS=STATIC MODEX=EXECUTE TSTART=0.00
      IDOF=100111 OVALIZAT=NONE FLUIDPOT=AUTOMATIC CYCLICPA=1
      IPOSIT=STOP REACTION=YES INITIALS=NO FSINTERA=NO
      IRINT=DEFAULT CMASS=NO SHELLNDO=AUTOMATIC AUTOMATI=OFF
      SOLVER=SPARSE CONTACT-=CONSTRAINT-FUNCTION TRELEASE=0.00
      RESTART-=NO FRACTURE=NO LOAD-CAS=NO LOAD-PEN=NO SINGULAR=YES
      STIFFNES=0.0001  MAP-OUTP=NONE MAP-FORM=NO
      NODAL-DE='' POROUS-C=NO ADAPTIVE=0  ZOOM-LAB=1  AXIS-CYC=0
      PERIODIC=NO VECTOR-S=GEOMETRY EPSI-FIR=NO STABILIZ=NO
      STABFACT=1.00E-10 RESULTS=PORTHOLE FEFCORR=NO
```

```
      BOLTSTEP=1  EXTEND-S=YES CONVERT-=NO DEGEN=YES
      TMC-MODE=NO ENSIGHT-=NO IRSTEPS=1 INITIALT=NO TEMP-INT=NO
      ESINTERA=NO OP2GEOM=NO INSITU-D=NO OP2ERCS=ELEMENT
      2DPL-AX=YZ-Z

ADINA OPTIMIZE=SOLVER  FILE='dat/modell_1.dat' FIXBOUND=YES MID=NO
OVERWRIT=YES
```

B1.2 .in-file, double-sided model

```
DATABASE    NEW   SAVE=NO     PROMPT=NO
FEPROGRAM   ADINA
CONTROL     FILEVERSION=V84

FEPROGRAM   PROGRAM=ADINA

CONTROL     UNDO=-1    AUTOMREBUILD=YES
FILEECHO    OPTION=FILE F=loggfil.ut
FILELOG     OPTION=FILE F=loggfil.ut

*     Indata

PARAMETER   tf    0.02
PARAMETER   tw    0.006
PARAMETER   a     0.003
PARAMETER   r     0.001

*     Y-direction

PARAMETER   L1    0.06
PARAMETER   L2    $L1+sqrt(2)*$a
PARAMETER   L3    $L2+$tw
PARAMETER   L4    $L3+sqrt(2)*$a
PARAMETER   L5    $L4+$L1
PARAMETER   L6    $L2+$r
PARAMETER   L7    $L3-$r
PARAMETER   L8    $L1-2*$r
PARAMETER   L9    $L4+2*$r
PARAMETER   L10   $L1-0.5*$r
PARAMETER   L11   $L1+0.5*$r
PARAMETER   L18   $L8-2*$r
PARAMETER   L19   $L9+2*$r
PARAMETER   L20   $L4-0.5*$r
PARAMETER   L21   $L4+0.5*$r
PARAMETER   L23   $L2-1.5*$r
PARAMETER   L24   $L3+1.5*$r

*     Z-direction

PARAMETER   L12   $tf+sqrt(2)*$a
PARAMETER   L13   $L12+$L1
PARAMETER   L14   $tf-$r
PARAMETER   L15   $tf+$r
PARAMETER   L16   $tf-2*$r
PARAMETER   L17   $tf+2*$r
PARAMETER   L22   $tf-2*$r
```

```
*     Scale factor

PARAMETER   s     anint($L22*666)

*     Coordinate system

COORDINATE  POINTS      SYSTEM=0
1     0     0     0
2     0     0     $tf
3     0     $L1   $tf
4     0     $L2   $tf
5     0     $L2   $L12
6     0     $L2   $L13
7     0     $L3   $L13
8     0     $L3   $L12
9     0     $L3   $tf
10    0     $L4   $tf
11    0     $L5   $tf
12    0     $L5   0
13    0     $L6   $L15
14    0     $L6   $L14
15    0     $L7   $L15
16    0     $L7   $L14
17    0     $L18  $0
18    0     $L10  $0
19    0     $L11  $0
20    0     $L23  $0
21    0     $L6   $0
22    0     $L7   $0
23    0     $L24  $0
24    0     $L20  $0
25    0     $L21  $0
26    0     $L19  $0
27    0     $L18  $L22
28    0     $L10  $L22
29    0     $L11  $L22
30    0     $L23  $L22
31    0     $L6   $L22
32    0     $L7   $L22
33    0     $L24  $L22
34    0     $L20  $L22
35    0     $L21  $L22
36    0     $L19  $L22
37    0     0     $L22
38    0     $L5   $L22
39    0     $L18  $tf
40    0     $L19  $tf
41    0     $L6   $tf
42    0     $L7   $tf

*     Lines

LINE  STRAIGHT    NAME=1      P1=1  P2=37
LINE  STRAIGHT    NAME=2      P1=37 P2=2
LINE  STRAIGHT    NAME=3      P1=39 P2=2
LINE  STRAIGHT    NAME=4      P1=39 P2=3
LINE  STRAIGHT    NAME=5      P1=3  P2=5
LINE  STRAIGHT    NAME=6      P1=5  P2=6
```

```
LINE  STRAIGHT   NAME=7     P1=6  P2=7
LINE  STRAIGHT   NAME=8     P1=8  P2=7
LINE  STRAIGHT   NAME=9     P1=8  P2=10
LINE  STRAIGHT   NAME=10    P1=10 P2=40
LINE  STRAIGHT   NAME=11    P1=40 P2=11
LINE  STRAIGHT   NAME=12    P1=11 P2=38
LINE  STRAIGHT   NAME=13    P1=38 P2=12
LINE  STRAIGHT   NAME=14    P1=12 P2=26
LINE  STRAIGHT   NAME=15    P1=26 P2=25
LINE  STRAIGHT   NAME=16    P1=25 P2=24
LINE  STRAIGHT   NAME=17    P1=24 P2=23
LINE  STRAIGHT   NAME=18    P1=23 P2=22
LINE  STRAIGHT   NAME=19    P1=22 P2=21
LINE  STRAIGHT   NAME=20    P1=21 P2=20
LINE  STRAIGHT   NAME=21    P1=20 P2=19
LINE  STRAIGHT   NAME=22    P1=19 P2=18
LINE  STRAIGHT   NAME=23    P1=18 P2=17
LINE  STRAIGHT   NAME=24    P1=17 P2=1
LINE  STRAIGHT   NAME=25    P1=27 P2=37
LINE  STRAIGHT   NAME=26    P1=27 P2=28
LINE  STRAIGHT   NAME=27    P1=28 P2=29
LINE  STRAIGHT   NAME=28    P1=29 P2=30
LINE  STRAIGHT   NAME=29    P1=30 P2=31
LINE  STRAIGHT   NAME=30    P1=31 P2=32
LINE  STRAIGHT   NAME=31    P1=32 P2=33
LINE  STRAIGHT   NAME=32    P1=33 P2=34
LINE  STRAIGHT   NAME=33    P1=34 P2=35
LINE  STRAIGHT   NAME=34    P1=35 P2=36
LINE  STRAIGHT   NAME=35    P1=36 P2=38
LINE  STRAIGHT   NAME=36    P1=13 P2=15
LINE  STRAIGHT   NAME=37    P1=14 P2=16
LINE  ARC   NAME=38    MODE=1     P1=13 P2=4  CENTER=41
LINE  ARC   NAME=39    MODE=1     P1=4  P2=14 CENTER=41
LINE  ARC   NAME=40    MODE=7     P3=0  CENTER=17   RADIUS=0.001
@CLEAR
4
5
@
LINE  ARC   NAME=41    MODE=7     P3=0  CENTER=17   RADIUS=0.001
@CLEAR
5
6
@
LINE  ARC   NAME=42    MODE=7     P3=0  CENTER=17   RADIUS=0.001
@CLEAR
8
9
@
LINE  ARC   NAME=43    MODE=7     P3=0  CENTER=17   RADIUS=0.001
@CLEAR
9
10
@
LINE  STRAIGHT   NAME=44    P1=39 P2=27
LINE  STRAIGHT   NAME=45    P1=27 P2=17
LINE  STRAIGHT   NAME=46    P1=43 P2=28
LINE  STRAIGHT   NAME=47    P1=28 P2=18
LINE  STRAIGHT   NAME=48    P1=44 P2=29
```

```
LINE  STRAIGHT   NAME=49    P1=29 P2=19
LINE  STRAIGHT   NAME=50    P1=4  P2=30
LINE  STRAIGHT   NAME=51    P1=30 P2=20
LINE  STRAIGHT   NAME=52    P1=14 P2=31
LINE  STRAIGHT   NAME=53    P1=31 P2=21
LINE  STRAIGHT   NAME=54    P1=16 P2=32
LINE  STRAIGHT   NAME=55    P1=32 P2=22
LINE  STRAIGHT   NAME=56    P1=9  P2=33
LINE  STRAIGHT   NAME=57    P1=33 P2=23
LINE  STRAIGHT   NAME=58    P1=52 P2=34
LINE  STRAIGHT   NAME=59    P1=34 P2=24
LINE  STRAIGHT   NAME=60    P1=53 P2=35
LINE  STRAIGHT   NAME=61    P1=35 P2=25
LINE  STRAIGHT   NAME=62    P1=40 P2=36
LINE  STRAIGHT   NAME=63    P1=36 P2=26
LINE  STRAIGHT   NAME=64    P1=44 P2=4
LINE  STRAIGHT   NAME=65    P1=9  P2=52
LINE  STRAIGHT   NAME=66    P1=46 P2=13
LINE  STRAIGHT   NAME=67    P1=50 P2=15
LINE  STRAIGHT   NAME=68    P1=46 P2=50
LINE  STRAIGHT   NAME=69    P1=47 P2=49
LINE  ARC   NAME=70    MODE=1     P1=15 P2=9  CENTER=42
LINE  ARC   NAME=71    MODE=1     P1=9  P2=16 CENTER=42

SURFACE    PATCH NAME=1 EDGE1=1   EDGE2=25 EDGE3=45 EDGE4=24
SURFACE    PATCH NAME=2 EDGE1=2   EDGE2=25 EDGE3=44 EDGE4=3
SURFACE    PATCH NAME=3 EDGE1=45  EDGE2=26   EDGE3=47   EDGE4=23
SURFACE    PATCH NAME=4 EDGE1=47  EDGE2=27   EDGE3=49   EDGE4=22
SURFACE    PATCH NAME=5 EDGE1=49  EDGE2=28   EDGE3=51   EDGE4=21
SURFACE    PATCH NAME=6 EDGE1=51  EDGE2=29   EDGE3=53   EDGE4=20
SURFACE    PATCH NAME=7 EDGE1=53  EDGE2=30   EDGE3=55   EDGE4=19
SURFACE    PATCH NAME=8 EDGE1=55  EDGE2=31   EDGE3=57   EDGE4=18
SURFACE    PATCH NAME=9 EDGE1=57  EDGE2=32   EDGE3=59   EDGE4=17
SURFACE    PATCH NAME=10 EDGE1=59 EDGE2=33   EDGE3=61   EDGE4=16
SURFACE    PATCH NAME=11 EDGE1=61 EDGE2=34   EDGE3=63   EDGE4=15
SURFACE    PATCH NAME=12 EDGE1=63 EDGE2=35   EDGE3=13   EDGE4=14
SURFACE    PATCH NAME=13 EDGE1=62 EDGE2=11   EDGE3=12   EDGE4=35
SURFACE    PATCH NAME=14 EDGE1=6  EDGE2=7    EDGE3=8    EDGE4=69
SURFACE    PATCH NAME=15 EDGE1=44 EDGE2=4    EDGE3=46   EDGE4=26
SURFACE    PATCH NAME=16 EDGE1=46 EDGE2=40   EDGE3=48   EDGE4=27
SURFACE    PATCH NAME=17 EDGE1=48 EDGE2=64   EDGE3=50   EDGE4=28
SURFACE    PATCH NAME=18 EDGE1=50 EDGE2=39   EDGE3=52   EDGE4=29
SURFACE    PATCH NAME=19 EDGE1=52 EDGE2=37   EDGE3=54   EDGE4=30
SURFACE    PATCH NAME=20 EDGE1=54 EDGE2=71   EDGE3=56   EDGE4=31
SURFACE    PATCH NAME=21 EDGE1=56 EDGE2=65   EDGE3=58   EDGE4=32
SURFACE    PATCH NAME=22 EDGE1=58 EDGE2=43   EDGE3=60   EDGE4=33
SURFACE    PATCH NAME=23 EDGE1=60 EDGE2=10   EDGE3=62   EDGE4=34
SURFACE    PATCH NAME=24 EDGE1=64 EDGE2=5    EDGE3=66   EDGE4=38
SURFACE    PATCH NAME=25 EDGE1=66 EDGE2=68   EDGE3=67   EDGE4=36
SURFACE    PATCH NAME=26 EDGE1=67 EDGE2=9    EDGE3=65   EDGE4=70
SURFACE    PATCH NAME=27 EDGE1=41 EDGE2=69   EDGE3=42   EDGE4=68

READ  F='model/material.in'

SUBDIVIDE  SURFACE    NAME=15    MODE=LENGTH SIZE=0.00025
@CLEAR
16
to
```

```
27
@
SUBDIVIDE   LINE  NAME=3      MODE=DIVISIONS   NDIV=22     RATIO=12
      PROGRESS=ARITHMETIC
@CLEAR
25
11
35
@
SUBDIVIDE   LINE  NAME=6      MODE=DIVISIONS   NDIV=35     RATIO=10
      PROGRESS=ARITHMETIC
@CLEAR
8
@

SUBDIVIDE   LINE  NAME=45     MODE=DIVISIONS   NDIV=$s     RATIO=8
      PROGRESS=ARITHMETIC
@CLEAR
47
49
51
53
55
57
59
61
63
@

SUBDIVIDE   LINE  NAME=1      MODE=LENGTH SIZE=0.0025
@CLEAR
2
7
12
to
24
@

READ  F='model/shell_element.in'
READ  F='model/boundary.in'
READ  F='model/load.in'

FIXBOUNDARY LINES FIXITY=BOUNDARYZ
14     'BOUNDARYZ'
15     'BOUNDARYZ'
16     'BOUNDARYZ'
17     'BOUNDARYZ'
18     'BOUNDARYZ'
19     'BOUNDARYZ'
20     'BOUNDARYZ'
21     'BOUNDARYZ'
22     'BOUNDARYZ'
23     'BOUNDARYZ'
24     'BOUNDARYZ'
@

      MASTER ANALYSIS=STATIC MODEX=EXECUTE TSTART=0.00
```

```
      IDOF=100111 OVALIZAT=NONE FLUIDPOT=AUTOMATIC CYCLICPA=1
      IPOSIT=STOP REACTION=YES INITIALS=NO FSINTERA=NO
      IRINT=DEFAULT CMASS=NO SHELLNDO=AUTOMATIC AUTOMATI=OFF
      SOLVER=SPARSE CONTACT-=CONSTRAINT-FUNCTION TRELEASE=0.00
      RESTART-=NO FRACTURE=NO LOAD-CAS=NO LOAD-PEN=NO SINGULAR=YES
      STIFFNES=0.0001  MAP-OUTP=NONE MAP-FORM=NO
      NODAL-DE='' POROUS-C=NO ADAPTIVE=0  ZOOM-LAB=1  AXIS-CYC=0
      PERIODIC=NO VECTOR-S=GEOMETRY EPSI-FIR=NO STABILIZ=NO
      STABFACT=1.00E-10 RESULTS=PORTHOLE FEFCORR=NO
      BOLTSTEP=1  EXTEND-S=YES CONVERT-=NO DEGEN=YES
      TMC-MODE=NO ENSIGHT-=NO IRSTEPS=1  INITIALT=NO TEMP-INT=NO
      ESINTERA=NO OP2GEOM=NO  INSITU-D=NO  OP2ERCS=ELEMENT
      2DPL-AX=YZ-Z

ADINA OPTIMIZE=SOLVER  FILE='dat/modell_1.dat' FIXBOUND=YES MID=NO
OVERWRIT=YES
```

B1.3 .in-files for material, BC etc.

Material

```
* Steel
MATERIAL ELASTIC NAME=1 E=210E+9 NU=0.3 DENSITY=7800
```

Elements

```
EGROUP TWODSOLID NAME=1 SUBTYPE=STRAIN MATERIAL=1
RESULTS=STRESSES

GSURFACE NODES=8 PATTERN=AUTOMATIC NCOINCID=ALL NCEDGE=1234,
     NCVERTEX=1234 NCTOLERA=1.00E-05 SUBSTRUC=0 GROUP=1,
     PREFSHAP=QUADRILATERAL MESHING=MAPPED SMOOTHIN=NO
DEGENERA=NO,
     COLLAPSE=NO MIDNODES=CURVED METHOD=ADVFRONT FLIP=NO
@CLEAR
1
to
27
@
```

Boundary conditions

```
FIXITY NAME=BOUNDARYY
@CLEAR
 'Y-TRANSLATION'
 'OVALIZATION'
@

FIXITY NAME=BOUNDARYZ
@CLEAR
 'Z-TRANSLATION'
 'OVALIZATION'
@

FIXBOUNDARY LINES FIXITY=BOUNDARYY
12   'BOUNDARYY'
13         'BOUNDARYY'
@

FIXBOUNDARY POINTS FIXITY=BOUNDARYZ
```

```
12  'BOUNDARYZ'
@
```

Load

```
LOAD PRESSURE NAME=1 MAGNITUD=1000000

APPLY-LOAD BODY=0
@CLEAR
1  'PRESSURE' 1 'LINE' 1 0 1 0.0 0 -1 0 0 0  'NO',
     0.0 0.0 1 0  'MID'
2  'PRESSURE' 1 'LINE' 2 0 1 0.0 0 -1 0 0 0  'NO',
     0.0 0.0 1 0  'MID'
@
```

B2 3D FE-modelling

B2.1 .in-file

```
DATABASE NEW SAVE=NO PROMPT=NO
FEPROGRAM ADINA
CONTROL FILEVERSION=V91

*       Indata
PARAMETER       tf      0.00953
PARAMETER       tw1     0.00714
PARAMETER       tw2     0.00714
PARAMETER       a       0.0048
PARAMETER       r       0.001
PARAMETER       d       0.0123
PARAMETER       rat     0.01
PARAMETER       liv     0.332
PARAMETER       hliv    $liv*0.5
PARAMETER       nmesh   0.00015
PARAMETER       fmesh   0.03
PARAMETER       cmesh   0.3
* Rext must be greater than Lext
PARAMETER       Lext    1.5252
PARAMETER       Rext    1.5252

PARAMETER       L1      0.15
PARAMETER       L2      0.172
PARAMETER       L3      $tf*0.5+0.25*$liv
PARAMETER       L4      $L2*0.5-$tw1*0.5-$d
PARAMETER       L5      $L4*0.5+$tw1*0.5
PARAMETER       L6      $rat+sqrt(2)*$a+0.001
PARAMETER       L7      $L6*0.5+$tw1*0.5
PARAMETER       L8      $L6*0.5+$tf*0.5
PARAMETER       L9      sqrt(2)*$a
PARAMETER       L10     2*$r
PARAMETER       L11     $L4*0.5-$L6*0.5+$L6+$tw1*0.5
PARAMETER       L12     0.5*$tf
PARAMETER       L13     $L4-$L6
PARAMETER       L14     0.5*$tw2
PARAMETER       L15     $L3+0.5*$L6
PARAMETER       L16     $hliv-$L6
PARAMETER       L17     $tw2*0.5+sqrt(2)*$a+$r*0.3
```

```
PARAMETER       L35     $tw2*0.5+sqrt(2)*$a-$r*0.3
PARAMETER       L18     $L11-0.5*$L13-sqrt(2)*$a-$r*0.3
PARAMETER       L19     $L11+0.5*$L13+sqrt(2)*$a+$r*0.3
PARAMETER       L20     $tf*0.5-$r
PARAMETER       L21     $tf*0.5+$r
PARAMETER       L22     $tw2*0.5+$L10+0.004
PARAMETER       L23     $tw1*0.5+0.004
PARAMETER       L24     $L2+0.5*$tf
PARAMETER       L25     0.5*$tf+$L6-sqrt(2)*$a-$r-0.004

PARAMETER       L26     0.1
PARAMETER       L27     $Rext-$L26*0.5-0.05+$L1*0.5
PARAMETER       L28     $Lext-$L26*0.5-0.05+$L1*0.5
PARAMETER       L29     $Rext+$L1*0.5-($Rext+$Lext+0.15)*0.33
PARAMETER       L30     $Lext+$L1*0.5-($Rext+$Lext+0.15)*0.33
PARAMETER       L31     2*$tf+$liv
PARAMETER       L32     $L1*0.3
PARAMETER       L33     $L2*0.5
PARAMETER       L34     $L2+$tf*0.5

BODY BLOCK NAME=1 OPTION=CENTERED POSITION=VECTOR
ORIENTAT=SYSTEM,
     CX1=0 CX2=0 CX3=0,
     SYSTEM=0 DX1=$L1 DX2=$L2 DX3=$tf

BODY BLOCK NAME=2 OPTION=CENTERED POSITION=VECTOR
ORIENTAT=SYSTEM,
     CX1=0 CX2=0 CX3=$L3,
     SYSTEM=0 DX1=$L1 DX2=$tw1 DX3=$hliv

BODY BLOCK NAME=3 OPTION=CENTERED POSITION=VECTOR
ORIENTAT=SYSTEM,
     CX1=0 CX2=-$L5 CX3=$L3,
     SYSTEM=0 DX1=$tw2 DX2=$L4 DX3=$hliv

BODY BLOCK NAME=4 OPTION=CENTERED POSITION=VECTOR
ORIENTAT=SYSTEM,
     CX1=0 CX2=$L5 CX3=$L3,
     SYSTEM=0 DX1=$tw2 DX2=$L4 DX3=$hliv

BODY BLOCK NAME=5 OPTION=CENTERED POSITION=VECTOR
ORIENTAT=SYSTEM,
     CX1=0 CX2=-$L7 CX3=$L8,
     SYSTEM=0 DX1=$tw2 DX2=$L6 DX3=$L6

BODY BLOCK NAME=6 OPTION=CENTERED POSITION=VECTOR
ORIENTAT=SYSTEM,
     CX1=0 CX2=$L7 CX3=$L8,
     SYSTEM=0 DX1=$tw2 DX2=$L6 DX3=$L6

BODY SUBTRACT NAME=4 KEEP-TOO=NO KEEP-IMP=NO
@CLEAR
6
@

BODY SUBTRACT NAME=3 KEEP-TOO=NO KEEP-IMP=NO
@CLEAR
5
```

```
@

BODY BLEND NAME=4 OPTION=CONSTANT R1=$rat
@CLEAR
15
@

BODY BLEND NAME=3 OPTION=CONSTANT R1=$rat
@CLEAR
13
@

BODY MERGE NAME=1 KEEP-TOO=NO MERGE-IM=YES
@CLEAR
2
3
4
@

BODY CHAMFER NAME=1 R1=$L9 R2=$L9 OPTION=EDGE
15 0
@
BODY CHAMFER NAME=1 R1=$L9 R2=$L9 OPTION=EDGE
46 0
@
BODY CHAMFER NAME=1 R1=$L9 R2=$L9 OPTION=EDGE
18 0
@
BODY CHAMFER NAME=1 R1=$L9 R2=$L9 OPTION=EDGE
33 0
@
BODY CHAMFER NAME=1 R1=$L9 R2=$L9 OPTION=EDGE
40 0
@
BODY CHAMFER NAME=1 R1=$L9 R2=$L9 OPTION=EDGE
15 0
@
BODY CHAMFER NAME=1 R1=$L9 R2=$L9 OPTION=EDGE
15 0
@
BODY CHAMFER NAME=1 R1=$L9 R2=$L9 OPTION=EDGE
41 0
@
BODY CHAMFER NAME=1 R1=$L9 R2=$L9 OPTION=EDGE
33 0
@
BODY CHAMFER NAME=1 R1=$L9 R2=$L9 OPTION=EDGE
35 0
@
BODY CHAMFER NAME=1 R1=$L9 R2=$L9 OPTION=EDGE
35 0
@
BODY CHAMFER NAME=1 R1=$L9 R2=$L9 OPTION=EDGE
25 0
@
BODY CHAMFER NAME=1 R1=$L9 R2=$L9 OPTION=EDGE
20 0
@
```

```
BODY CHAMFER NAME=1 R1=$L9 R2=$L9 OPTION=EDGE
21 0
@
BODY CHAMFER NAME=1 R1=$L9 R2=$L9 OPTION=EDGE
18 0
@
BODY CHAMFER NAME=1 R1=$L9 R2=$L9 OPTION=EDGE
23 0
@
BODY CHAMFER NAME=1 R1=$L9 R2=$L9 OPTION=EDGE
30 0
@


BODY BLOCK NAME=2 OPTION=CENTERED POSITION=VECTOR
ORIENTAT=SYSTEM,
     CX1=0 CX2=-$L11 CX3=$L12,
     SYSTEM=0 DX1=$tw1 DX2=$L13 DX3=$L10

BODY BLOCK NAME=3 OPTION=CENTERED POSITION=VECTOR
ORIENTAT=SYSTEM,
     CX1=0 CX2=$L11 CX3=$L12,
     SYSTEM=0 DX1=$tw1 DX2=$L13 DX3=$L10


BODY SUBTRACT NAME=1 KEEP-TOO=NO KEEP-IMP=NO
@CLEAR
2
3
@

BODY BLEND NAME=1 OPTION=CONSTANT R1=$r
@CLEAR
116
124
122
118
110
112
106
104
@

BODY BLOCK NAME=2 OPTION=CENTERED POSITION=VECTOR
ORIENTAT=SYSTEM,
     CX1=0 CX2=-$L14 CX3=$L15,
     SYSTEM=0 DX1=$tw1 DX2=$L10 DX3=$L16

BODY BLOCK NAME=3 OPTION=CENTERED POSITION=VECTOR
ORIENTAT=SYSTEM,
     CX1=0 CX2=$L14 CX3=$L15,
     SYSTEM=0 DX1=$tw1 DX2=$L10 DX3=$L16

BODY SUBTRACT NAME=1 KEEP-TOO=NO KEEP-IMP=NO
@CLEAR
2
3
@
```

```
BODY BLEND NAME=1 OPTION=CONSTANT R1=$r
@CLEAR
139
149
151
161
142
145
154
157
@

BODY BLEND NAME=1 OPTION=CONSTANT R1=$r
@CLEAR
66
@
BODY BLEND NAME=1 OPTION=CONSTANT R1=$r
@CLEAR
65
@
BODY BLEND NAME=1 OPTION=CONSTANT R1=$r
@CLEAR
66
@
BODY BLEND NAME=1 OPTION=CONSTANT R1=$r
@CLEAR
65
@
BODY BLEND NAME=1 OPTION=CONSTANT R1=$r
@CLEAR
66
@
BODY BLEND NAME=1 OPTION=CONSTANT R1=$r
@CLEAR
65
@
BODY BLEND NAME=1 OPTION=CONSTANT R1=$r
@CLEAR
64
@
BODY BLEND NAME=1 OPTION=CONSTANT R1=$r
@CLEAR
63
@

BODY BLEND NAME=1 OPTION=CONSTANT R1=$r
@CLEAR
66
@
BODY BLEND NAME=1 OPTION=CONSTANT R1=$r
@CLEAR
65
@
BODY BLEND NAME=1 OPTION=CONSTANT R1=$r
@CLEAR
65
@
```

```
BODY BLEND NAME=1 OPTION=CONSTANT R1=$r
@CLEAR
63
@
BODY BLEND NAME=1 OPTION=CONSTANT R1=$r
@CLEAR
65
@
BODY BLEND NAME=1 OPTION=CONSTANT R1=$r
@CLEAR
65
@
BODY BLEND NAME=1 OPTION=CONSTANT R1=$r
@CLEAR
63
@
BODY BLEND NAME=1 OPTION=CONSTANT R1=$r
@CLEAR
63
@
BODY BLEND NAME=1 OPTION=CONSTANT R1=$r
@CLEAR
33
@
BODY BLEND NAME=1 OPTION=CONSTANT R1=$r
@CLEAR
32
@
BODY BLEND NAME=1 OPTION=CONSTANT R1=$r
@CLEAR
43
@
BODY BLEND NAME=1 OPTION=CONSTANT R1=$r
@CLEAR
42
@
BODY BLEND NAME=1 OPTION=CONSTANT R1=$r
@CLEAR
38
@
BODY BLEND NAME=1 OPTION=CONSTANT R1=$r
@CLEAR
37
@
BODY BLEND NAME=1 OPTION=CONSTANT R1=$r
@CLEAR
34
@
BODY BLEND NAME=1 OPTION=CONSTANT R1=$r
@CLEAR
33
@
BODY BLEND NAME=1 OPTION=CONSTANT R1=$r
@CLEAR
48
@
BODY BLEND NAME=1 OPTION=CONSTANT R1=$r
@CLEAR
```

```
47
@
BODY BLEND NAME=1 OPTION=CONSTANT R1=$r
@CLEAR
46
@
BODY BLEND NAME=1 OPTION=CONSTANT R1=$r
@CLEAR
45
@

TRANSFORMATI REFLECTION NAME=1 MODE=POINTS P1=253 P2=259 P3=241

BODY TRANSFORMED NAME=2 OPTION=COPY PARENT=1 TRANSFOR=1 NCOPY=1,
     MESH=NO EGROUP=0 NCOINCID=NO NTOLERAN=1E-05

MATERIAL ELASTIC NAME=1 E=210E+9 NU=0.3 DENSITY=7800

BODY MERGE NAME=1 KEEP-TOO=NO MERGE-IM=YES
@CLEAR
1
2
@

BODY SWEEP NAME=2 FACE=0 OPTION=VECTOR DX=$Lext,
     DY=0 DZ=0 SYSTEM=0 BODY=0 MESH=NO,
     NODES=0 SUBSTRUC=0 3D-EGROU=0 NDIV=1 NCOINCID=BOUNDARIES,
     NCTOLERA=1E-05 DELETE-F=ALL,
     TWIST-AN=0 MERGE=YES
@CLEAR
7 1
@

BODY SWEEP NAME=2 FACE=0 OPTION=VECTOR DX=-$Rext,
     DY=0 DZ=0 SYSTEM=0 BODY=0 MESH=NO,
     NODES=0 SUBSTRUC=0 3D-EGROU=0 NDIV=1 NCOINCID=BOUNDARIES,
     NCTOLERA=1E-05 DELETE-F=ALL,
     TWIST-AN=0 MERGE=YES
@CLEAR
4 1
@

BODY BLOCK NAME=2 OPTION=CENTERED POSITION=VECTOR
ORIENTAT=SYSTEM,
     CX1=-$L27 CX2=0 CX3=-$tf,
     SYSTEM=0 DX1=$L26 DX2=$L2 DX3=$tf

BODY BLOCK NAME=3 OPTION=CENTERED POSITION=VECTOR
ORIENTAT=SYSTEM,
     CX1=$L28 CX2=0 CX3=-$tf,
     SYSTEM=0 DX1=$L26 DX2=$L2 DX3=$tf

BODY BLOCK NAME=4 OPTION=CENTERED POSITION=VECTOR
ORIENTAT=SYSTEM,
     CX1=-$L29 CX2=0 CX3=$L31,
     SYSTEM=0 DX1=$L26 DX2=$L2 DX3=$tf
```

```
BODY BLOCK NAME=5 OPTION=CENTERED POSITION=VECTOR
ORIENTAT=SYSTEM,
     CX1=$L30 CX2=0 CX3=$L31,
     SYSTEM=0 DX1=$L26 DX2=$L2 DX3=$tf

BODY MERGE NAME=1 KEEP-TOO=NO MERGE-IM=YES
@CLEAR
1
2
3
4
5
@

SHEET PLANE NAME=1 OPTION=POINT-NORMAL POSITION=VECTOR,
     X=0 Y=0 Z=0,
     NX=0 NY=1 NZ=0,
     SYSTEM=0

BODY SECTION NAME=1 KEEP-SHE=NO KEEP-IMP=NO OPTION=SHEET
@CLEAR
1 0
@

DELETE BODY FIRST=2 LAST=2

SHEET PLANE NAME=1 OPTION=POINT-NORMAL POSITION=VECTOR,
     X=0 Y=0 Z=0,
     NX=1 NY=0 NZ=0,
     SYSTEM=0

BODY SECTION NAME=1 KEEP-SHE=NO KEEP-IMP=NO OPTION=SHEET
@CLEAR
1 0
@

DELETE BODY FIRST=2 LAST=2

FIXITY NAME=YX
 'Y-TRANSLATION'
 'X-TRANSLATION'
 'OVALIZATION'
@

FIXITY NAME=Z
 'Z-TRANSLATION'
 'OVALIZATION'
@

FIXITY NAME=Y
 'Y-TRANSLATION'
 'OVALIZATION'
@

FIXITY NAME=X
 'X-TRANSLATION'
 'OVALIZATION'
@
```

```
FIXBOUNDARY TWO-D FIXITY=Z
91 1  'Z'
@

FIXBOUNDARY THREE-D FIXITY=Y
39 1  'Y'
@

FIXBOUNDARY THREE-D FIXITY=X
7 1  'X'
@

LOAD PRESSURE NAME=1 MAGNITUD=-1000000 BETA=0.0 LINE=0 SYSTEM=0

APPLY-LOAD BODY=1
@CLEAR
1  'PRESSURE' 1  'FACE' 31 0 1 0.0 13 -1 0 1 0  'NO',
     0.0 0.0 1 0  'MID'
@

SUBDIVIDE MODEL MODE=LENGTH SIZE=$cmesh NDIV=1,
     PROGRESS=GEOMETRIC MINCUR=1

EGROUP THREEDSOLID NAME=1 DISPLACE=DEFAULT STRAINS=DEFAULT
MATERIAL=1,
     RSINT=DEFAULT TINT=DEFAULT RESULTS=STRESSES DEGEN=DEFAUL,
     FORMULAT=DEFAULT STRESSRE=GLOBAL INITIALS=NONE FRACTUR=NO,
     CMASS=DEFAULT STRAIN-F=0 UL-FORMU=DEFAULT LVUS1=0 LVUS2=0
SED=NO,
     RUPTURE=ADINA INCOMPAT=DEFAULT TIME-OFF=0.0,
     POROUS=NO WTMC=1.0 OPTION=NONE DESCRIPT='NONE',
     PRINT=DEFAULT SAVE=DEFAULT TBIRTH=0.0,
     TDEATH=0.00000000000000 TMC-MATE=1 RUPTURE-=0 EM=NO
JOULE=NO,
     BOLT-NUM=0 BOLT-PLA=0 BOLT-LOA=0.0,
     BOLT-TOL=0.0 TETINT=DEFAULT

SIZE-FUNCTIO BOUNDS NAME=3 XMIN=-$L32 YMIN=-$L33 ZMIN=-$L12,
     XMAX=$L32 YMAX=$L33 ZMAX=$L31,
     SIZE1=$fmesh,
     SIZE2=$fmesh SIZE3=$fmesh,
     SIZE4=$fmesh SIZE5=$fmesh,
     SIZE6=$fmesh SIZE7=$fmesh,
     SIZE8=$fmesh

SIZE-FUNCTIO BOUNDS NAME=1 XMIN=$L35 YMIN=$L18 ZMIN=$L20,
     XMAX=$L17 YMAX=$L19 ZMAX=$L21,
     SIZE1=$nmesh,
     SIZE2=$nmesh SIZE3=$nmesh,
     SIZE4=$nmesh SIZE5=$nmesh,
     SIZE6=$nmesh SIZE7=$nmesh,
     SIZE8=$nmesh


SIZE-FUNCTIO COMBINED NAME=4
1
3
```

```
@

GBODY NODES=10 NCOINCID=NO NCTOLERA=1.0E-05,
     SUBSTRUC=0 GROUP=1 PREFSHAP=AUTOMATIC COLLAPSE=NO SIZE-
FUN=4,
     DELETE-S=NO ANGLE-MI=5.0 MIDNODES=CURVED,
     METHOD=DELAUNAY PATTERN=0 MESHING=FREE-FORM DEGENERA=YES,
     BOUNDARY=DELAUNAY DEG-EDGE=0 GEO-ERRO=0.0,
     SAMPLING=20 MIN-SIZE=$cmesh NLAYER=1 NLTABL=0,
     AUTO-GRA=YES SIMULATE=NO PYRAMIDS=NO DANGMAXB=80.0,
     DANGMAXC=80.0 DANGMAXD=80.0 HEXALAYE=NO,
     AUTO-REF=YES EVEN=SUM DENSITY=2 MIDFACEN=QUAD,
     REFINE=EDGE-MIDDLE GRID=YES BREFINE=EDGE-MIDDLE BLTABL=0,
     PREFSHA2=QUADRILATERAL NOPTI=1
1 0
@

MASTER ANALYSIS=STATIC MODEX=EXECUTE TSTART=0.00
IDOF=000111 OVALIZAT=NONE FLUIDPOT=NO CYCLICPA=1
IPOSIT=STOP REACTION=YES INITIALS=NO FSINTERA=NO IRINT=DEFAULT
CMASS=NO SHELLNDO=AUTOMATIC AUTOMATI=OFF SOLVER=3D-ITERATIVE
CONTACT-=CONSTRAINT-FUNCTION TRELEASE=0.0
RESTART-=NO FRACTURE=NO LOAD-CAS=NO LOAD-PEN=NO SINGULAR=YES
STIFFNES=0.0001 MAP-OUTP=NONE MAP-FORM=NO
NODAL-DE='' POROUS-C=NO ADAPTIVE=0 ZOOM-LAB=1 AXIS-CYC=0
PERIODIC=NO VECTOR-S=GEOMETRY EPSI-FIR=NO STABILIZ=NO
STABFACT=1.00E-10 RESULTS=PORTHOLE FEFCORR=NO
BOLTSTEP=1 EXTEND-S=YES CONVERT-=NO DEGEN=YES TMC-MODE=NO
ENSIGHT-=NO IRSTEPS=1 INITIALT=NO TEMP-INT=NO ESINTERA=NO
OP2GEOM=NO INSITU-D=NO OP2ERCS=ELEMENT 2DPL-AX=YZ-Z

ADINA          OPTIMIZE=SOLVER    FILE='3Dsymmetry1.dat'
               FIXBOUND=YES MID=NO      OVERWRIT=YES
```

B3 Linux script

```
mkdir modell_1
sleep 0.5
adina9.1 modell_1.dat
sleep 0.5
mv modell_1.por \modell_1
mv modell_1.mds \modell_1
mv modell_1.msg \modell_1
mv modell_1.out \modell_1
mv modell_1.res \modell_1
sleep 0.5
cp run_modell_1.plo \modell_1
cp resultat.plo \modell_1
sleep 0.5
cd modell_1
mkdir rse
aui9.1 -m 3000mb  -s run_modell_1.plo -cmd
sleep 0.5
cd ..
```

B4 .plo-files

Run_model_1.plo

```
DATABASE   NEW   SAVE=UNKNOWN     PROMPT=NO
*
LOADPORTHOLE     OPERATIO=CREATE  FILE='modell_1.por'
*
READ  FILE='resultat.plo'
*
end   s=no  pr=n  i=y
```

resultat.plo

```
FILESESSION NO
CONTROL UNDO=-1 AUTOMREBUILD=NO SESSIONSTORAGE=NO
FILEECHO OPTION=FILE F=post.ut
FILELOG OPTION=FILE F=post.ut

FILELIST FILE F='rse/EG1_effective_stress.txt'

ZONEMAX ZONENAME=EG1 TYPE=ABSMAX NUMBER=1 RESULTGR=DEFAULT,
     SMOOTHIN=AVERAGED RESULTCO=DEFAULT RESPOPTI=RESPRANGE,
     RESPONSE=DEFAULT RESPRANG=DEFAULT VARIABLE=SIGMA-P1
```

Appendix C

All the FE-results for one- and double-sided transverse stiffener in 2D as well as the 3D results are presented in this appendix.

C1 2D FE-results, one-sided model

Number	Folder	File	Position	Principal stress [Pa]	t_f [m]	t_w [m]	a [m]	L [m]	K_t [-]	$\Delta\sigma_{e,NS}$ [MPa]
1	modell_1	EG1_effective_stress.txt	E5	2110650	0.0200	0.0060	0.0030	0.0145	2.11	106.6022
2	modell_2	EG1_effective_stress.txt	E6	2189890	0.0200	0.0060	0.0036	0.0162	2.19	102.7449
3	modell_3	EG1_effective_stress.txt	E7	2248790	0.0200	0.0060	0.0042	0.0179	2.25	100.0538
4	modell_4	EG1_effective_stress.txt	E8	2293100	0.0200	0.0060	0.0048	0.0196	2.29	98.1204
5	modell_5	EG1_effective_stress.txt	E9	2326430	0.0200	0.0060	0.0054	0.0213	2.33	96.7147
6	modell_6	EG1_effective_stress.txt	E10	2191780	0.0200	0.0080	0.0032	0.0171	2.19	102.6563
7	modell_7	EG1_effective_stress.txt	E11	2271000	0.0200	0.0080	0.0040	0.0193	2.27	99.0753
8	modell_8	EG1_effective_stress.txt	E12	2323860	0.0200	0.0080	0.0048	0.0216	2.32	96.8217
9	modell_9	EG1_effective_stress.txt	E13	2359090	0.0200	0.0080	0.0056	0.0238	2.36	95.3758
10	modell_10	EG1_effective_stress.txt	E14	2382240	0.0200	0.0080	0.0064	0.0261	2.38	94.4489
11	modell_11	EG1_effective_stress.txt	E15	2260460	0.0200	0.0100	0.0034	0.0196	2.26	99.5373
12	modell_12	EG1_effective_stress.txt	E16	2332310	0.0200	0.0100	0.0044	0.0224	2.33	96.4709
13	modell_13	EG1_effective_stress.txt	E17	2374370	0.0200	0.0100	0.0054	0.0253	2.37	94.7620
14	modell_14	EG1_effective_stress.txt	E18	2398190	0.0200	0.0100	0.0064	0.0281	2.40	93.8208
15	modell_15	EG1_effective_stress.txt	E19	2410690	0.0200	0.0100	0.0074	0.0309	2.41	93.3343
16	modell_16	EG1_effective_stress.txt	E20	2317980	0.0200	0.0120	0.0036	0.0222	2.32	97.0673
17	modell_17	EG1_effective_stress.txt	E21	2377720	0.0200	0.0120	0.0048	0.0256	2.38	94.6285
18	modell_18	EG1_effective_stress.txt	E22	2406990	0.0200	0.0120	0.0060	0.0290	2.41	93.4777
19	modell_19	EG1_effective_stress.txt	E23	2419480	0.0200	0.0120	0.0072	0.0324	2.42	92.9952
20	modell_20	EG1_effective_stress.txt	E24	2422900	0.0200	0.0120	0.0084	0.0358	2.42	92.8639
21	modell_21	EG1_effective_stress.txt	E25	2365670	0.0200	0.0140	0.0038	0.0247	2.37	95.1105
22	modell_22	EG1_effective_stress.txt	E26	2410530	0.0200	0.0140	0.0052	0.0287	2.41	93.3405
23	modell_23	EG1_effective_stress.txt	E27	2426830	0.0200	0.0140	0.0066	0.0327	2.43	92.7135
24	modell_24	EG1_effective_stress.txt	E28	2429370	0.0200	0.0140	0.0080	0.0366	2.43	92.6166
25	modell_25	EG1_effective_stress.txt	E29	2425890	0.0200	0.0140	0.0094	0.0406	2.43	92.7495
26	modell_26	EG1_effective_stress.txt	E30	2404850	0.0200	0.0160	0.0040	0.0273	2.40	93.5609
27	modell_27	EG1_effective_stress.txt	E31	2433480	0.0200	0.0160	0.0056	0.0318	2.43	92.4602
28	modell_28	EG1_effective_stress.txt	E32	2437650	0.0200	0.0160	0.0072	0.0364	2.44	92.3020
29	modell_29	EG1_effective_stress.txt	E33	2432150	0.0200	0.0160	0.0088	0.0409	2.43	92.5107
30	modell_30	EG1_effective_stress.txt	E34	2424050	0.0200	0.0160	0.0104	0.0454	2.42	92.8199
31	modell_31	EG1_effective_stress.txt	E35	2439480	0.0200	0.0180	0.0042	0.0299	2.44	92.2328
32	modell_32	EG1_effective_stress.txt	E36	2448810	0.0200	0.0180	0.0060	0.0350	2.45	91.8814
33	modell_33	EG1_effective_stress.txt	E37	2442230	0.0200	0.0180	0.0078	0.0401	2.44	92.1289
34	modell_34	EG1_effective_stress.txt	E38	2430740	0.0200	0.0180	0.0096	0.0452	2.43	92.5644
35	modell_35	EG1_effective_stress.txt	E39	2420020	0.0200	0.0180	0.0114	0.0502	2.42	92.9744
36	modell_36	EG1_effective_stress.txt	E40	2467360	0.0200	0.0200	0.0044	0.0324	2.47	91.1906
37	modell_37	EG1_effective_stress.txt	E41	2458230	0.0200	0.0200	0.0064	0.0381	2.46	91.5293
38	modell_38	EG1_effective_stress.txt	E42	2442610	0.0200	0.0200	0.0084	0.0438	2.44	92.1146
39	modell_39	EG1_effective_stress.txt	E43	2427040	0.0200	0.0200	0.0104	0.0494	2.43	92.7055
40	modell_40	EG1_effective_stress.txt	E44	2415340	0.0200	0.0200	0.0124	0.0551	2.42	93.1546
41	modell_41	EG1_effective_stress.txt	E45	2283550	0.0300	0.0090	0.0033	0.0183	2.28	98.5308
42	modell_42	EG1_effective_stress.txt	E46	2395750	0.0300	0.0090	0.0042	0.0209	2.40	93.9163
43	modell_43	EG1_effective_stress.txt	E47	2478950	0.0300	0.0090	0.0051	0.0234	2.48	90.7642
44	modell_44	EG1_effective_stress.txt	E48	2541940	0.0300	0.0090	0.0060	0.0260	2.54	88.5151
45	modell_45	EG1_effective_stress.txt	E49	2590050	0.0300	0.0090	0.0069	0.0285	2.59	86.8709
46	modell_46	EG1_effective_stress.txt	E50	2402220	0.0300	0.0120	0.0036	0.0222	2.40	93.6634
47	modell_47	EG1_effective_stress.txt	E51	2512020	0.0300	0.0120	0.0048	0.0256	2.51	89.5694
48	modell_48	EG1_effective_stress.txt	E52	2586350	0.0300	0.0120	0.0060	0.0290	2.59	86.9952
49	modell_49	EG1_effective_stress.txt	E53	2638450	0.0300	0.0120	0.0072	0.0324	2.64	85.2773
50	modell_50	EG1_effective_stress.txt	E54	2675490	0.0300	0.0120	0.0084	0.0358	2.68	84.0967
51	modell_51	EG1_effective_stress.txt	E55	2506110	0.0300	0.0150	0.0039	0.0260	2.51	89.7806
52	modell_52	EG1_effective_stress.txt	E56	2602730	0.0300	0.0150	0.0054	0.0303	2.60	86.4477
53	modell_53	EG1_effective_stress.txt	E57	2663910	0.0300	0.0150	0.0069	0.0345	2.66	84.4623
54	modell_54	EG1_effective_stress.txt	E58	2701300	0.0300	0.0150	0.0084	0.0388	2.70	83.2932
55	modell_55	EG1_effective_stress.txt	E59	2722680	0.0300	0.0150	0.0099	0.0430	2.72	82.6392
56	modell_56	EG1_effective_stress.txt	E60	2595550	0.0300	0.0180	0.0042	0.0299	2.60	86.6868
57	modell_57	EG1_effective_stress.txt	E61	2672530	0.0300	0.0180	0.0060	0.0350	2.67	84.1899
58	modell_58	EG1_effective_stress.txt	E62	2715350	0.0300	0.0180	0.0078	0.0401	2.72	82.8622
59	modell_59	EG1_effective_stress.txt	E63	2736300	0.0300	0.0180	0.0096	0.0452	2.74	82.2278
60	modell_60	EG1_effective_stress.txt	E64	2744210	0.0300	0.0180	0.0114	0.0502	2.74	81.9908
61	modell_61	EG1_effective_stress.txt	E65	2668880	0.0300	0.0210	0.0045	0.0337	2.67	84.3050
62	modell_62	EG1_effective_stress.txt	E66	2722900	0.0300	0.0210	0.0066	0.0397	2.72	82.6325
63	modell_63	EG1_effective_stress.txt	E67	2747050	0.0300	0.0210	0.0087	0.0456	2.75	81.9060
64	modell_64	EG1_effective_stress.txt	E68	2753440	0.0300	0.0210	0.0108	0.0515	2.75	81.7160
65	modell_65	EG1_effective_stress.txt	E69	2750930	0.0300	0.0210	0.0129	0.0575	2.75	81.7905
66	modell_66	EG1_effective_stress.txt	E70	2728380	0.0300	0.0240	0.0048	0.0376	2.73	82.4665
67	modell_67	EG1_effective_stress.txt	E71	2758080	0.0300	0.0240	0.0072	0.0444	2.76	81.5785
68	modell_68	EG1_effective_stress.txt	E72	2764900	0.0300	0.0240	0.0096	0.0512	2.76	81.3773
69	modell_69	EG1_effective_stress.txt	E73	2759400	0.0300	0.0240	0.0120	0.0579	2.76	81.5395
70	modell_70	EG1_effective_stress.txt	E74	2749760	0.0300	0.0240	0.0144	0.0647	2.75	81.8253
71	modell_71	EG1_effective_stress.txt	E75	2776140	0.0300	0.0270	0.0051	0.0414	2.78	81.0478
72	modell_72	EG1_effective_stress.txt	E76	2781780	0.0300	0.0270	0.0078	0.0491	2.78	80.8835
73	modell_73	EG1_effective_stress.txt	E77	2773140	0.0300	0.0270	0.0105	0.0567	2.77	81.1355
74	modell_74	EG1_effective_stress.txt	E78	2758630	0.0300	0.0270	0.0132	0.0643	2.76	81.5622
75	modell_75	EG1_effective_stress.txt	E79	2744710	0.0300	0.0270	0.0159	0.0720	2.74	81.9759
76	modell_76	EG1_effective_stress.txt	E80	2814360	0.0300	0.0300	0.0054	0.0453	2.81	79.9471
77	modell_77	EG1_effective_stress.txt	E81	2796560	0.0300	0.0300	0.0084	0.0538	2.80	80.4560
78	modell_78	EG1_effective_stress.txt	E82	2774850	0.0300	0.0300	0.0114	0.0622	2.77	81.0855
79	modell_79	EG1_effective_stress.txt	E83	2754150	0.0300	0.0300	0.0144	0.0707	2.75	81.6949
80	modell_80	EG1_effective_stress.txt	E84	2738350	0.0300	0.0300	0.0174	0.0792	2.74	82.1663

81	modell_81	EG1_effective_stress.txt	E85	2435590	0.0400	0.0120	0.0036	0.0222	2.44	92.3801
82	modell_82	EG1_effective_stress.txt	E86	2569640	0.0400	0.0120	0.0048	0.0256	2.57	87.5609
83	modell_83	EG1_effective_stress.txt	E87	2671060	0.0400	0.0120	0.0060	0.0290	2.67	84.2362
84	modell_84	EG1_effective_stress.txt	E88	2751410	0.0400	0.0120	0.0072	0.0324	2.75	81.7763
85	modell_85	EG1_effective_stress.txt	E89	2814080	0.0400	0.0120	0.0084	0.0358	2.81	79.9551
86	modell_86	EG1_effective_stress.txt	E90	2594140	0.0400	0.0160	0.0040	0.0273	2.59	86.7339
87	modell_87	EG1_effective_stress.txt	E91	2722260	0.0400	0.0160	0.0056	0.0318	2.72	82.6519
88	modell_88	EG1_effective_stress.txt	E92	2814040	0.0400	0.0160	0.0072	0.0364	2.81	79.9562
89	modell_89	EG1_effective_stress.txt	E93	2879160	0.0400	0.0160	0.0088	0.0409	2.88	78.1478
90	modell_90	EG1_effective_stress.txt	E94	2924710	0.0400	0.0160	0.0104	0.0454	2.92	76.9307
91	modell_91	EG1_effective_stress.txt	E95	2726730	0.0400	0.0200	0.0044	0.0324	2.73	82.5164
92	modell_92	EG1_effective_stress.txt	E96	2837050	0.0400	0.0200	0.0064	0.0381	2.84	79.3077
93	modell_93	EG1_effective_stress.txt	E97	2910070	0.0400	0.0200	0.0084	0.0438	2.91	77.3177
94	modell_94	EG1_effective_stress.txt	E98	2955950	0.0400	0.0200	0.0104	0.0494	2.96	76.1177
95	modell_95	EG1_effective_stress.txt	E99	2983310	0.0400	0.0200	0.0124	0.0551	2.98	75.4196
96	modell_96	EG1_effective_stress.txt	E100	2834950	0.0400	0.0240	0.0048	0.0376	2.83	79.3665
97	modell_97	EG1_effective_stress.txt	E101	2920920	0.0400	0.0240	0.0072	0.0444	2.92	77.0305
98	modell_98	EG1_effective_stress.txt	E102	2972470	0.0400	0.0240	0.0096	0.0512	2.97	75.6946
99	modell_99	EG1_effective_stress.txt	E103	2999250	0.0400	0.0240	0.0120	0.0579	3.00	75.0188
100	modell_100	EG1_effective_stress.txt	E104	3010700	0.0400	0.0240	0.0144	0.0647	3.01	74.7335
101	modell_101	EG1_effective_stress.txt	E105	2922570	0.0400	0.0280	0.0052	0.0427	2.92	76.9870
102	modell_102	EG1_effective_stress.txt	E106	2981330	0.0400	0.0280	0.0080	0.0506	2.98	75.4697
103	modell_103	EG1_effective_stress.txt	E107	3011210	0.0400	0.0280	0.0108	0.0585	3.01	74.7208
104	modell_104	EG1_effective_stress.txt	E108	3021040	0.0400	0.0280	0.0136	0.0665	3.02	74.4777
105	modell_105	EG1_effective_stress.txt	E109	3020090	0.0400	0.0280	0.0164	0.0744	3.02	74.5011
106	modell_106	EG1_effective_stress.txt	E110	2993200	0.0400	0.0320	0.0056	0.0478	2.99	75.1704
107	modell_107	EG1_effective_stress.txt	E111	3023630	0.0400	0.0320	0.0088	0.0569	3.02	74.4139
108	modell_108	EG1_effective_stress.txt	E112	3033410	0.0400	0.0320	0.0120	0.0659	3.03	74.1739
109	modell_109	EG1_effective_stress.txt	E113	3029330	0.0400	0.0320	0.0152	0.0750	3.03	74.2738
110	modell_110	EG1_effective_stress.txt	E114	3019800	0.0400	0.0320	0.0184	0.0840	3.02	74.5082
111	modell_111	EG1_effective_stress.txt	E115	3049880	0.0400	0.0360	0.0060	0.0530	3.05	73.7734
112	modell_112	EG1_effective_stress.txt	E116	3052240	0.0400	0.0360	0.0096	0.0632	3.05	73.7164
113	modell_113	EG1_effective_stress.txt	E117	3044140	0.0400	0.0360	0.0132	0.0733	3.04	73.9125
114	modell_114	EG1_effective_stress.txt	E118	3029430	0.0400	0.0360	0.0168	0.0835	3.03	74.2714
115	modell_115	EG1_effective_stress.txt	E119	3014710	0.0400	0.0360	0.0204	0.0937	3.01	74.6340
116	modell_116	EG1_effective_stress.txt	E120	3094860	0.0400	0.0400	0.0064	0.0581	3.09	72.7012
117	modell_117	EG1_effective_stress.txt	E121	3070230	0.0400	0.0400	0.0104	0.0694	3.07	73.2844
118	modell_118	EG1_effective_stress.txt	E122	3047100	0.0400	0.0400	0.0144	0.0807	3.05	73.8407
119	modell_119	EG1_effective_stress.txt	E123	3024910	0.0400	0.0400	0.0184	0.0920	3.02	74.3824
120	modell_120	EG1_effective_stress.txt	E124	3007780	0.0400	0.0400	0.0224	0.1034	3.01	74.8060
121	modell_121	EG1_effective_stress.txt	E125	2581220	0.0500	0.0150	0.0039	0.0260	2.58	87.1681
122	modell_122	EG1_effective_stress.txt	E126	2731500	0.0500	0.0150	0.0054	0.0303	2.73	82.3723
123	modell_123	EG1_effective_stress.txt	E127	2847550	0.0500	0.0150	0.0069	0.0345	2.85	79.0153
124	modell_124	EG1_effective_stress.txt	E128	2938240	0.0500	0.0150	0.0084	0.0388	2.94	76.5765
125	modell_125	EG1_effective_stress.txt	E129	3009210	0.0500	0.0150	0.0099	0.0430	3.01	74.7705
126	modell_126	EG1_effective_stress.txt	E130	2768430	0.0500	0.0200	0.0044	0.0324	2.77	81.2735
127	modell_127	EG1_effective_stress.txt	E131	2907980	0.0500	0.0200	0.0064	0.0381	2.91	77.3733
128	modell_128	EG1_effective_stress.txt	E132	3010330	0.0500	0.0200	0.0084	0.0438	3.01	74.7426
129	modell_129	EG1_effective_stress.txt	E133	3083900	0.0500	0.0200	0.0104	0.0494	3.08	72.9596
130	modell_130	EG1_effective_stress.txt	E134	3136050	0.0500	0.0200	0.0124	0.0551	3.14	71.7463
131	modell_131	EG1_effective_stress.txt	E135	2919910	0.0500	0.0250	0.0049	0.0389	2.92	77.0572
132	modell_132	EG1_effective_stress.txt	E136	3037900	0.0500	0.0250	0.0074	0.0459	3.04	74.0643
133	modell_133	EG1_effective_stress.txt	E137	3119300	0.0500	0.0250	0.0099	0.0530	3.12	72.1316
134	modell_134	EG1_effective_stress.txt	E138	3171720	0.0500	0.0250	0.0124	0.0601	3.17	70.9394
135	modell_135	EG1_effective_stress.txt	E139	3203580	0.0500	0.0250	0.0149	0.0671	3.20	70.2339
136	modell_136	EG1_effective_stress.txt	E140	3042440	0.0500	0.0300	0.0054	0.0453	3.04	73.9538
137	modell_137	EG1_effective_stress.txt	E141	3132760	0.0500	0.0300	0.0084	0.0538	3.13	71.8217
138	modell_138	EG1_effective_stress.txt	E142	3190350	0.0500	0.0300	0.0114	0.0622	3.19	70.5252
139	modell_139	EG1_effective_stress.txt	E143	3221530	0.0500	0.0300	0.0144	0.0707	3.22	69.8426
140	modell_140	EG1_effective_stress.txt	E144	3235560	0.0500	0.0300	0.0174	0.0792	3.24	69.5397
141	modell_141	EG1_effective_stress.txt	E145	3141050	0.0500	0.0350	0.0059	0.0517	3.14	71.6321
142	modell_142	EG1_effective_stress.txt	E146	3200790	0.0500	0.0350	0.0094	0.0616	3.20	70.2951
143	modell_143	EG1_effective_stress.txt	E147	3234570	0.0500	0.0350	0.0129	0.0715	3.23	69.5610
144	modell_144	EG1_effective_stress.txt	E148	3246870	0.0500	0.0350	0.0164	0.0814	3.25	69.2975
145	modell_145	EG1_effective_stress.txt	E149	3247080	0.0500	0.0350	0.0199	0.0913	3.25	69.2930
146	modell_146	EG1_effective_stress.txt	E150	3220220	0.0500	0.0400	0.0064	0.0581	3.22	69.8710
147	modell_147	EG1_effective_stress.txt	E151	3248510	0.0500	0.0400	0.0104	0.0694	3.25	69.2625
148	modell_148	EG1_effective_stress.txt	E152	3260170	0.0500	0.0400	0.0144	0.0807	3.26	69.0148
149	modell_149	EG1_effective_stress.txt	E153	3256930	0.0500	0.0400	0.0184	0.0920	3.26	69.0835
150	modell_150	EG1_effective_stress.txt	E154	3247380	0.0500	0.0400	0.0224	0.1034	3.25	69.2866
151	modell_151	EG1_effective_stress.txt	E155	3283340	0.0500	0.0450	0.0069	0.0645	3.28	68.5278
152	modell_152	EG1_effective_stress.txt	E156	3280840	0.0500	0.0450	0.0114	0.0772	3.28	68.5800
153	modell_153	EG1_effective_stress.txt	E157	3272770	0.0500	0.0450	0.0159	0.0900	3.27	68.7491
154	modell_154	EG1_effective_stress.txt	E158	3257690	0.0500	0.0450	0.0204	0.1027	3.26	69.0673
155	modell_155	EG1_effective_stress.txt	E159	3242190	0.0500	0.0450	0.0249	0.1154	3.24	69.3975
156	modell_156	EG1_effective_stress.txt	E160	3333230	0.0500	0.0500	0.0074	0.0709	3.33	67.5021
157	modell_157	EG1_effective_stress.txt	E161	3301300	0.0500	0.0500	0.0124	0.0851	3.30	68.1550
158	modell_158	EG1_effective_stress.txt	E162	3276580	0.0500	0.0500	0.0174	0.0992	3.28	68.6692
159	modell_159	EG1_effective_stress.txt	E163	3253070	0.0500	0.0500	0.0224	0.1134	3.25	69.1654
160	modell_160	EG1_effective_stress.txt	E164	3234840	0.0500	0.0500	0.0274	0.1275	3.23	69.5552
161	modell_161	EG1_effective_stress.txt	E165	2717630	0.0600	0.0180	0.0042	0.0299	2.72	82.7927
162	modell_162	EG1_effective_stress.txt	E166	2878340	0.0600	0.0180	0.0060	0.0350	2.88	78.1701
163	modell_163	EG1_effective_stress.txt	E167	3004190	0.0600	0.0180	0.0078	0.0401	3.00	74.8954
164	modell_164	EG1_effective_stress.txt	E168	3103110	0.0600	0.0180	0.0096	0.0452	3.10	72.5079
165	modell_165	EG1_effective_stress.txt	E169	3181030	0.0600	0.0180	0.0114	0.0502	3.18	70.7318
166	modell_166	EG1_effective_stress.txt	E170	2925870	0.0600	0.0240	0.0048	0.0376	2.93	76.9002
167	modell_167	EG1_effective_stress.txt	E171	3072610	0.0600	0.0240	0.0072	0.0444	3.07	73.2276
168	modell_168	EG1_effective_stress.txt	E172	3183240	0.0600	0.0240	0.0096	0.0512	3.18	70.6827
169	modell_169	EG1_effective_stress.txt	E173	3263710	0.0600	0.0240	0.0120	0.0579	3.26	68.9399
170	modell_170	EG1_effective_stress.txt	E174	3321260	0.0600	0.0240	0.0144	0.0647	3.32	67.7454

171	modell_171	EG1_effective_stress.txt	E175	3092690	0.0600	0.0300	0.0054	0.0453	3.09	72.7522
172	modell_172	EG1_effective_stress.txt	E176	3215160	0.0600	0.0300	0.0084	0.0538	3.22	69.9810
173	modell_173	EG1_effective_stress.txt	E177	3303070	0.0600	0.0300	0.0114	0.0622	3.30	68.1184
174	modell_174	EG1_effective_stress.txt	E178	3360670	0.0600	0.0300	0.0144	0.0707	3.36	66.9509
175	modell_175	EG1_effective_stress.txt	E179	3396190	0.0600	0.0300	0.0174	0.0792	3.40	66.2507
176	modell_176	EG1_effective_stress.txt	E180	3226560	0.0600	0.0360	0.0060	0.0530	3.23	69.7337
177	modell_177	EG1_effective_stress.txt	E181	3318800	0.0600	0.0360	0.0096	0.0632	3.32	67.7956
178	modell_178	EG1_effective_stress.txt	E182	3381100	0.0600	0.0360	0.0132	0.0733	3.38	66.5464
179	modell_179	EG1_effective_stress.txt	E183	3415800	0.0600	0.0360	0.0168	0.0835	3.42	65.8704
180	modell_180	EG1_effective_stress.txt	E184	3431990	0.0600	0.0360	0.0204	0.0937	3.43	65.5596
181	modell_181	EG1_effective_stress.txt	E185	3334080	0.0600	0.0420	0.0066	0.0607	3.33	67.4849
182	modell_182	EG1_effective_stress.txt	E186	3393130	0.0600	0.0420	0.0108	0.0725	3.39	66.3105
183	modell_183	EG1_effective_stress.txt	E187	3429880	0.0600	0.0420	0.0150	0.0844	3.43	65.6000
184	modell_184	EG1_effective_stress.txt	E188	3444160	0.0600	0.0420	0.0192	0.0963	3.44	65.3280
185	modell_185	EG1_effective_stress.txt	E189	3445190	0.0600	0.0420	0.0234	0.1082	3.45	65.3084
186	modell_186	EG1_effective_stress.txt	E190	3419900	0.0600	0.0480	0.0072	0.0684	3.42	65.7914
187	modell_187	EG1_effective_stress.txt	E191	3445270	0.0600	0.0480	0.0120	0.0819	3.45	65.3069
188	modell_188	EG1_effective_stress.txt	E192	3458200	0.0600	0.0480	0.0168	0.0955	3.46	65.0627
189	modell_189	EG1_effective_stress.txt	E193	3455640	0.0600	0.0480	0.0216	0.1091	3.46	65.1109
190	modell_190	EG1_effective_stress.txt	E194	3446040	0.0600	0.0480	0.0264	0.1227	3.45	65.2923
191	modell_191	EG1_effective_stress.txt	E195	3488220	0.0600	0.0540	0.0078	0.0761	3.49	64.5028
192	modell_192	EG1_effective_stress.txt	E196	3480560	0.0600	0.0540	0.0132	0.0913	3.48	64.6448
193	modell_193	EG1_effective_stress.txt	E197	3472390	0.0600	0.0540	0.0186	0.1066	3.47	64.7969
194	modell_194	EG1_effective_stress.txt	E198	3456850	0.0600	0.0540	0.0240	0.1219	3.46	65.0882
195	modell_195	EG1_effective_stress.txt	E199	3440730	0.0600	0.0540	0.0294	0.1372	3.44	65.3931
196	modell_196	EG1_effective_stress.txt	E200	3541970	0.0600	0.0600	0.0084	0.0838	3.54	63.5240
197	modell_197	EG1_effective_stress.txt	E201	3503060	0.0600	0.0600	0.0144	0.1007	3.50	64.2296
198	modell_198	EG1_effective_stress.txt	E202	3476890	0.0600	0.0600	0.0204	0.1177	3.48	64.7130
199	modell_199	EG1_effective_stress.txt	E203	3452220	0.0600	0.0600	0.0264	0.1347	3.45	65.1755
200	modell_200	EG1_effective_stress.txt	E204	3432970	0.0600	0.0600	0.0324	0.1516	3.43	65.5409

One-sided stiffener, t_f varies					
Nr	**t_f [m]**	**t_w [m]**	**a [m]**	**L [m]**	**K_t [-]**
1	0.006	0.006	0.006	0.0230	1.716
2	0.008	0.006	0.006	0.0230	1.868
3	0.01	0.006	0.006	0.0230	1.996
4	0.02	0.006	0.006	0.0230	2.371
5	0.03	0.006	0.006	0.0230	2.511
6	0.04	0.006	0.006	0.0230	2.572
7	0.05	0.006	0.006	0.0230	2.601
8	0.06	0.006	0.006	0.0230	2.617
9	0.006	0.009	0.009	0.0345	1.712
10	0.008	0.009	0.009	0.0345	1.856
11	0.01	0.009	0.009	0.0345	1.981
12	0.02	0.009	0.009	0.0345	2.433
13	0.03	0.009	0.009	0.0345	2.682
14	0.04	0.009	0.009	0.0345	2.813
15	0.05	0.009	0.009	0.0345	2.885
16	0.06	0.009	0.009	0.0345	2.928

One-sided stiffener, t_w varies					
Nr	**t_f [m]**	**t_w [m]**	**a [m]**	**L [m]**	**K_t [-]**
17	0.02	0.006	0.006	0.0230	2.371
18	0.02	0.012	0.006	0.0290	2.426
19	0.02	0.018	0.006	0.0350	2.467
20	0.02	0.024	0.006	0.0410	2.499
21	0.02	0.03	0.006	0.0470	2.525
22	0.02	0.036	0.006	0.0530	2.546
23	0.02	0.042	0.006	0.0590	2.562
24	0.02	0.048	0.006	0.0650	2.575

One-sided stiffener, a varies					
Nr	**t_f [m]**	**t_w [m]**	**a [m]**	**L [m]**	**K_t [-]**
25	0.06	0.036	0.003	0.0445	3.189
26	0.06	0.036	0.006	0.0530	3.226
27	0.06	0.036	0.012	0.0699	3.364
28	0.06	0.036	0.018	0.0869	3.423
29	0.06	0.036	0.024	0.1039	3.437
30	0.06	0.036	0.03	0.1209	3.434
31	0.06	0.036	0.036	0.1378	3.426
32	0.06	0.036	0.042	0.1548	3.419
33	0.06	0.036	0.048	0.1718	3.415
34	0.06	0.036	0.054	0.1887	3.414

C2 2D FE-results, double-sided model

Number	Folder	File	Position	Principal stress [Pa]	t_f [m]	t_w [m]	a [m]	L [m]	K_t [-]	$\Delta\sigma_{c,NS}$ [MPa]
1	modell_1	EG1_effective_stress.txt	E5	2179970	0.0200	0.0060	0.0030	0.0145	2.180	103.212
2	modell_2	EG1_effective_stress.txt	E6	2299970	0.0200	0.0060	0.0036	0.0162	2.300	97.827
3	modell_3	EG1_effective_stress.txt	E7	2400410	0.0200	0.0060	0.0042	0.0179	2.400	93.734
4	modell_4	EG1_effective_stress.txt	E8	2486080	0.0200	0.0060	0.0048	0.0196	2.486	90.504
5	modell_5	EG1_effective_stress.txt	E9	2559890	0.0200	0.0060	0.0054	0.0213	2.560	87.894
6	modell_6	EG1_effective_stress.txt	E10	2288930	0.0200	0.0080	0.0032	0.0171	2.289	98.299
7	modell_7	EG1_effective_stress.txt	E11	2426650	0.0200	0.0080	0.0040	0.0193	2.427	92.720
8	modell_8	EG1_effective_stress.txt	E12	2537030	0.0200	0.0080	0.0048	0.0216	2.537	88.686
9	modell_9	EG1_effective_stress.txt	E13	2628750	0.0200	0.0080	0.0056	0.0238	2.629	85.592
10	modell_10	EG1_effective_stress.txt	E14	2710600	0.0200	0.0080	0.0064	0.0261	2.711	83.007
11	modell_11	EG1_effective_stress.txt	E15	2389060	0.0200	0.0100	0.0034	0.0196	2.389	94.179
12	modell_12	EG1_effective_stress.txt	E16	2536790	0.0200	0.0100	0.0044	0.0224	2.537	88.695
13	modell_13	EG1_effective_stress.txt	E17	2657090	0.0200	0.0100	0.0054	0.0253	2.657	84.679
14	modell_14	EG1_effective_stress.txt	E18	2754140	0.0200	0.0100	0.0064	0.0281	2.754	81.695
15	modell_15	EG1_effective_stress.txt	E19	2832080	0.0200	0.0100	0.0074	0.0309	2.832	79.447
16	modell_16	EG1_effective_stress.txt	E20	2483750	0.0200	0.0120	0.0036	0.0222	2.484	90.589
17	modell_17	EG1_effective_stress.txt	E21	2641530	0.0200	0.0120	0.0048	0.0256	2.642	85.178
18	modell_18	EG1_effective_stress.txt	E22	2761890	0.0200	0.0120	0.0060	0.0290	2.762	81.466
19	modell_19	EG1_effective_stress.txt	E23	2854370	0.0200	0.0120	0.0072	0.0324	2.854	78.827
20	modell_20	EG1_effective_stress.txt	E24	2925510	0.0200	0.0120	0.0084	0.0358	2.926	76.910
21	modell_21	EG1_effective_stress.txt	E25	2576270	0.0200	0.0140	0.0038	0.0247	2.576	87.336
22	modell_22	EG1_effective_stress.txt	E26	2733570	0.0200	0.0140	0.0052	0.0287	2.734	82.310
23	modell_23	EG1_effective_stress.txt	E27	2849570	0.0200	0.0140	0.0066	0.0327	2.850	78.959
24	modell_24	EG1_effective_stress.txt	E28	2934840	0.0200	0.0140	0.0080	0.0366	2.935	76.665
25	modell_25	EG1_effective_stress.txt	E29	2997180	0.0200	0.0140	0.0094	0.0406	2.997	75.071
26	modell_26	EG1_effective_stress.txt	E30	2660510	0.0200	0.0160	0.0040	0.0273	2.661	84.570
27	modell_27	EG1_effective_stress.txt	E31	2813750	0.0200	0.0160	0.0056	0.0318	2.814	79.964
28	modell_28	EG1_effective_stress.txt	E32	2922830	0.0200	0.0160	0.0072	0.0364	2.923	76.980
29	modell_29	EG1_effective_stress.txt	E33	2999220	0.0200	0.0160	0.0088	0.0409	2.999	75.020
30	modell_30	EG1_effective_stress.txt	E34	3051970	0.0200	0.0160	0.0104	0.0454	3.052	73.723
31	modell_31	EG1_effective_stress.txt	E35	2737150	0.0200	0.0180	0.0042	0.0299	2.737	82.202
32	modell_32	EG1_effective_stress.txt	E36	2883880	0.0200	0.0180	0.0060	0.0350	2.884	78.020
33	modell_33	EG1_effective_stress.txt	E37	2984210	0.0200	0.0180	0.0078	0.0401	2.984	75.397
34	modell_34	EG1_effective_stress.txt	E38	3050660	0.0200	0.0180	0.0096	0.0452	3.051	73.755
35	modell_35	EG1_effective_stress.txt	E39	3093580	0.0200	0.0180	0.0114	0.0502	3.094	72.731
36	modell_36	EG1_effective_stress.txt	E40	2807200	0.0200	0.0200	0.0044	0.0324	2.807	80.151
37	modell_37	EG1_effective_stress.txt	E41	2945160	0.0200	0.0200	0.0064	0.0381	2.945	76.397
38	modell_38	EG1_effective_stress.txt	E42	3035420	0.0200	0.0200	0.0084	0.0438	3.035	74.125
39	modell_39	EG1_effective_stress.txt	E43	3091360	0.0200	0.0200	0.0104	0.0494	3.091	72.783
40	modell_40	EG1_effective_stress.txt	E44	3124740	0.0200	0.0200	0.0124	0.0551	3.125	72.006
41	modell_41	EG1_effective_stress.txt	E45	2341750	0.0300	0.0090	0.0033	0.0183	2.342	96.082
42	modell_42	EG1_effective_stress.txt	E46	2495270	0.0300	0.0090	0.0042	0.0209	2.495	90.171
43	modell_43	EG1_effective_stress.txt	E47	2622100	0.0300	0.0090	0.0051	0.0234	2.622	85.809
44	modell_44	EG1_effective_stress.txt	E48	2732040	0.0300	0.0090	0.0060	0.0260	2.732	82.356
45	modell_45	EG1_effective_stress.txt	E49	2832030	0.0300	0.0090	0.0069	0.0285	2.832	79.448
46	modell_46	EG1_effective_stress.txt	E50	2491630	0.0300	0.0120	0.0036	0.0222	2.492	90.302
47	modell_47	EG1_effective_stress.txt	E51	2667190	0.0300	0.0120	0.0048	0.0256	2.667	84.358
48	modell_48	EG1_effective_stress.txt	E52	2811420	0.0300	0.0120	0.0060	0.0290	2.811	80.031
49	modell_49	EG1_effective_stress.txt	E53	2931750	0.0300	0.0120	0.0072	0.0324	2.932	76.746
50	modell_50	EG1_effective_stress.txt	E54	3033020	0.0300	0.0120	0.0084	0.0358	3.033	74.183
51	modell_51	EG1_effective_stress.txt	E55	2638800	0.0300	0.0150	0.0039	0.0260	2.639	85.266
52	modell_52	EG1_effective_stress.txt	E56	2822880	0.0300	0.0150	0.0054	0.0303	2.823	79.706
53	modell_53	EG1_effective_stress.txt	E57	2970130	0.0300	0.0150	0.0069	0.0345	2.970	75.754
54	modell_54	EG1_effective_stress.txt	E58	3089010	0.0300	0.0150	0.0084	0.0388	3.089	72.839
55	modell_55	EG1_effective_stress.txt	E59	3185160	0.0300	0.0150	0.0099	0.0430	3.185	70.640
56	modell_56	EG1_effective_stress.txt	E60	2770340	0.0300	0.0180	0.0042	0.0299	2.770	81.217
57	modell_57	EG1_effective_stress.txt	E61	2955730	0.0300	0.0180	0.0060	0.0350	2.956	76.123
58	modell_58	EG1_effective_stress.txt	E62	3100610	0.0300	0.0180	0.0078	0.0401	3.101	72.566
59	modell_59	EG1_effective_stress.txt	E63	3213490	0.0300	0.0180	0.0096	0.0452	3.213	70.017
60	modell_60	EG1_effective_stress.txt	E64	3301320	0.0300	0.0180	0.0114	0.0502	3.301	68.155
61	modell_61	EG1_effective_stress.txt	E65	2888250	0.0300	0.0210	0.0045	0.0337	2.888	77.902
62	modell_62	EG1_effective_stress.txt	E66	3069870	0.0300	0.0210	0.0066	0.0397	3.070	73.293
63	modell_63	EG1_effective_stress.txt	E67	3208590	0.0300	0.0210	0.0087	0.0456	3.209	70.124
64	modell_64	EG1_effective_stress.txt	E68	3312780	0.0300	0.0210	0.0108	0.0515	3.313	67.919
65	modell_65	EG1_effective_stress.txt	E69	3390360	0.0300	0.0210	0.0129	0.0575	3.390	66.365
66	modell_66	EG1_effective_stress.txt	E70	2994010	0.0300	0.0240	0.0048	0.0376	2.994	75.150
67	modell_67	EG1_effective_stress.txt	E71	3168270	0.0300	0.0240	0.0072	0.0444	3.168	71.017
68	modell_68	EG1_effective_stress.txt	E72	3298510	0.0300	0.0240	0.0096	0.0512	3.299	68.213
69	modell_69	EG1_effective_stress.txt	E73	3392310	0.0300	0.0240	0.0120	0.0579	3.392	66.326
70	modell_70	EG1_effective_stress.txt	E74	3458780	0.0300	0.0240	0.0144	0.0647	3.459	65.052
71	modell_71	EG1_effective_stress.txt	E75	3089060	0.0300	0.0270	0.0051	0.0414	3.089	72.838
72	modell_72	EG1_effective_stress.txt	E76	3253750	0.0300	0.0270	0.0078	0.0491	3.254	69.151
73	modell_73	EG1_effective_stress.txt	E77	3373630	0.0300	0.0270	0.0105	0.0567	3.374	66.694
74	modell_74	EG1_effective_stress.txt	E78	3456000	0.0300	0.0270	0.0132	0.0643	3.456	65.104
75	modell_75	EG1_effective_stress.txt	E79	3511010	0.0300	0.0270	0.0159	0.0720	3.511	64.084
76	modell_76	EG1_effective_stress.txt	E80	3175140	0.0300	0.0300	0.0054	0.0453	3.175	70.863
77	modell_77	EG1_effective_stress.txt	E81	3328140	0.0300	0.0300	0.0084	0.0538	3.328	67.605
78	modell_78	EG1_effective_stress.txt	E82	3436420	0.0300	0.0300	0.0114	0.0622	3.436	65.475
79	modell_79	EG1_effective_stress.txt	E83	3506870	0.0300	0.0300	0.0144	0.0707	3.507	64.160
80	modell_80	EG1_effective_stress.txt	E84	3550650	0.0300	0.0300	0.0174	0.0792	3.551	63.369

81	modell_81	EG1_effective_stress.txt	E85	2490900	0.0400	0.0120	0.0036	0.0222	2.491	90.329
82	modell_82	EG1_effective_stress.txt	E86	2668780	0.0400	0.0120	0.0048	0.0256	2.669	84.308
83	modell_83	EG1_effective_stress.txt	E87	2820190	0.0400	0.0120	0.0060	0.0290	2.820	79.782
84	modell_84	EG1_effective_stress.txt	E88	2950820	0.0400	0.0120	0.0072	0.0324	2.951	76.250
85	modell_85	EG1_effective_stress.txt	E89	3064970	0.0400	0.0120	0.0084	0.0358	3.065	73.410
86	modell_86	EG1_effective_stress.txt	E90	2687730	0.0400	0.0160	0.0040	0.0273	2.688	83.714
87	modell_87	EG1_effective_stress.txt	E91	2883470	0.0400	0.0160	0.0056	0.0318	2.883	78.031
88	modell_88	EG1_effective_stress.txt	E92	3045970	0.0400	0.0160	0.0072	0.0364	3.046	73.868
89	modell_89	EG1_effective_stress.txt	E93	3182260	0.0400	0.0160	0.0088	0.0409	3.182	70.704
90	modell_90	EG1_effective_stress.txt	E94	3297320	0.0400	0.0160	0.0104	0.0454	3.297	68.237
91	modell_91	EG1_effective_stress.txt	E95	2862330	0.0400	0.0200	0.0044	0.0324	2.862	78.607
92	modell_92	EG1_effective_stress.txt	E96	3064260	0.0400	0.0200	0.0064	0.0381	3.064	73.427
93	modell_93	EG1_effective_stress.txt	E97	3229040	0.0400	0.0200	0.0084	0.0438	3.229	69.680
94	modell_94	EG1_effective_stress.txt	E98	3363050	0.0400	0.0200	0.0104	0.0494	3.363	66.904
95	modell_95	EG1_effective_stress.txt	E99	3472300	0.0400	0.0200	0.0124	0.0551	3.472	64.799
96	modell_96	EG1_effective_stress.txt	E100	3016600	0.0400	0.0240	0.0048	0.0376	3.017	74.587
97	modell_97	EG1_effective_stress.txt	E101	3217040	0.0400	0.0240	0.0072	0.0444	3.217	69.940
98	modell_98	EG1_effective_stress.txt	E102	3378320	0.0400	0.0240	0.0096	0.0512	3.378	66.601
99	modell_99	EG1_effective_stress.txt	E103	3505410	0.0400	0.0240	0.0120	0.0579	3.505	64.187
100	modell_100	EG1_effective_stress.txt	E104	3605190	0.0400	0.0240	0.0144	0.0647	3.605	62.410
101	modell_101	EG1_effective_stress.txt	E105	3152970	0.0400	0.0280	0.0052	0.0427	3.153	71.361
102	modell_102	EG1_effective_stress.txt	E106	3347250	0.0400	0.0280	0.0080	0.0506	3.347	67.219
103	modell_103	EG1_effective_stress.txt	E107	3501160	0.0400	0.0280	0.0108	0.0585	3.501	64.264
104	modell_104	EG1_effective_stress.txt	E108	3618560	0.0400	0.0280	0.0136	0.0665	3.619	62.179
105	modell_105	EG1_effective_stress.txt	E109	3706900	0.0400	0.0280	0.0164	0.0744	3.707	60.698
106	modell_106	EG1_effective_stress.txt	E110	3274130	0.0400	0.0320	0.0056	0.0478	3.274	68.721
107	modell_107	EG1_effective_stress.txt	E111	3458850	0.0400	0.0320	0.0088	0.0569	3.459	65.051
108	modell_108	EG1_effective_stress.txt	E112	3603080	0.0400	0.0320	0.0120	0.0659	3.603	62.447
109	modell_109	EG1_effective_stress.txt	E113	3709070	0.0400	0.0320	0.0152	0.0750	3.709	60.662
110	modell_110	EG1_effective_stress.txt	E114	3785120	0.0400	0.0320	0.0184	0.0840	3.785	59.443
111	modell_111	EG1_effective_stress.txt	E115	3382490	0.0400	0.0360	0.0060	0.0530	3.382	66.519
112	modell_112	EG1_effective_stress.txt	E116	3555340	0.0400	0.0360	0.0096	0.0632	3.555	63.285
113	modell_113	EG1_effective_stress.txt	E117	3688120	0.0400	0.0360	0.0132	0.0733	3.688	61.007
114	modell_114	EG1_effective_stress.txt	E118	3781620	0.0400	0.0360	0.0168	0.0835	3.782	59.498
115	modell_115	EG1_effective_stress.txt	E119	3845090	0.0400	0.0360	0.0204	0.0937	3.845	58.516
116	modell_116	EG1_effective_stress.txt	E120	3479780	0.0400	0.0400	0.0064	0.0581	3.480	64.659
117	modell_117	EG1_effective_stress.txt	E121	3639000	0.0400	0.0400	0.0104	0.0694	3.639	61.830
118	modell_118	EG1_effective_stress.txt	E122	3759300	0.0400	0.0400	0.0144	0.0807	3.759	59.852
119	modell_119	EG1_effective_stress.txt	E123	3839670	0.0400	0.0400	0.0184	0.0920	3.840	58.599
120	modell_120	EG1_effective_stress.txt	E124	3890730	0.0400	0.0400	0.0224	0.1034	3.891	57.830
121	modell_121	EG1_effective_stress.txt	E125	2638130	0.0500	0.0150	0.0039	0.0260	2.638	85.288
122	modell_122	EG1_effective_stress.txt	E126	2832990	0.0500	0.0150	0.0054	0.0303	2.833	79.421
123	modell_123	EG1_effective_stress.txt	E127	2998250	0.0500	0.0150	0.0069	0.0345	2.998	75.044
124	modell_124	EG1_effective_stress.txt	E128	3141300	0.0500	0.0150	0.0084	0.0388	3.141	71.626
125	modell_125	EG1_effective_stress.txt	E129	3266380	0.0500	0.0150	0.0099	0.0430	3.266	68.884
126	modell_126	EG1_effective_stress.txt	E130	2863870	0.0500	0.0200	0.0044	0.0324	2.864	78.565
127	modell_127	EG1_effective_stress.txt	E131	3073170	0.0500	0.0200	0.0064	0.0381	3.073	73.214
128	modell_128	EG1_effective_stress.txt	E132	3249400	0.0500	0.0200	0.0084	0.0438	3.249	69.244
129	modell_129	EG1_effective_stress.txt	E133	3398070	0.0500	0.0200	0.0104	0.0494	3.398	66.214
130	modell_130	EG1_effective_stress.txt	E134	3524170	0.0500	0.0200	0.0124	0.0551	3.524	63.845
131	modell_131	EG1_effective_stress.txt	E135	3060400	0.0500	0.0250	0.0049	0.0389	3.060	73.520
132	modell_132	EG1_effective_stress.txt	E136	3273730	0.0500	0.0250	0.0074	0.0459	3.274	68.729
133	modell_133	EG1_effective_stress.txt	E137	3451770	0.0500	0.0250	0.0099	0.0530	3.452	65.184
134	modell_134	EG1_effective_stress.txt	E138	3597910	0.0500	0.0250	0.0124	0.0601	3.598	62.536
135	modell_135	EG1_effective_stress.txt	E139	3717500	0.0500	0.0250	0.0149	0.0671	3.718	60.525
136	modell_136	EG1_effective_stress.txt	E140	3232410	0.0500	0.0300	0.0054	0.0453	3.232	69.608
137	modell_137	EG1_effective_stress.txt	E141	3442500	0.0500	0.0300	0.0084	0.0538	3.443	65.359
138	modell_138	EG1_effective_stress.txt	E142	3616260	0.0500	0.0300	0.0114	0.0622	3.616	62.219
139	modell_139	EG1_effective_stress.txt	E143	3754690	0.0500	0.0300	0.0144	0.0707	3.755	59.925
140	modell_140	EG1_effective_stress.txt	E144	3863890	0.0500	0.0300	0.0174	0.0792	3.864	58.231
141	modell_141	EG1_effective_stress.txt	E145	3383400	0.0500	0.0350	0.0059	0.0517	3.383	66.501
142	modell_142	EG1_effective_stress.txt	E146	3585410	0.0500	0.0350	0.0094	0.0616	3.585	62.754
143	modell_143	EG1_effective_stress.txt	E147	3751060	0.0500	0.0350	0.0129	0.0715	3.751	59.983
144	modell_144	EG1_effective_stress.txt	E148	3878900	0.0500	0.0350	0.0164	0.0814	3.879	58.006
145	modell_145	EG1_effective_stress.txt	E149	3975830	0.0500	0.0350	0.0199	0.0913	3.976	56.592
146	modell_146	EG1_effective_stress.txt	E150	3516810	0.0500	0.0400	0.0064	0.0581	3.517	63.978
147	modell_147	EG1_effective_stress.txt	E151	3707530	0.0500	0.0400	0.0104	0.0694	3.708	60.687
148	modell_148	EG1_effective_stress.txt	E152	3862700	0.0500	0.0400	0.0144	0.0807	3.863	58.249
149	modell_149	EG1_effective_stress.txt	E153	3978220	0.0500	0.0400	0.0184	0.0920	3.978	56.558
150	modell_150	EG1_effective_stress.txt	E154	4061830	0.0500	0.0400	0.0224	0.1034	4.062	55.394
151	modell_151	EG1_effective_stress.txt	E155	3635340	0.0500	0.0450	0.0069	0.0645	3.635	61.892
152	modell_152	EG1_effective_stress.txt	E156	3812780	0.0500	0.0450	0.0114	0.0772	3.813	59.012
153	modell_153	EG1_effective_stress.txt	E157	3955660	0.0500	0.0450	0.0159	0.0900	3.956	56.881
154	modell_154	EG1_effective_stress.txt	E158	4057870	0.0500	0.0450	0.0204	0.1027	4.058	55.448
155	modell_155	EG1_effective_stress.txt	E159	4127940	0.0500	0.0450	0.0249	0.1154	4.128	54.507
156	modell_156	EG1_effective_stress.txt	E160	3741260	0.0500	0.0500	0.0074	0.0709	3.741	60.140
157	modell_157	EG1_effective_stress.txt	E161	3903920	0.0500	0.0500	0.0124	0.0851	3.904	57.634
158	modell_158	EG1_effective_stress.txt	E162	4033450	0.0500	0.0500	0.0174	0.0992	4.033	55.784
159	modell_159	EG1_effective_stress.txt	E163	4121630	0.0500	0.0500	0.0224	0.1134	4.122	54.590
160	modell_160	EG1_effective_stress.txt	E164	4178440	0.0500	0.0500	0.0274	0.1275	4.178	53.848
161	modell_161	EG1_effective_stress.txt	E165	2775150	0.0600	0.0180	0.0042	0.0299	2.775	81.077
162	modell_162	EG1_effective_stress.txt	E166	2981220	0.0600	0.0180	0.0060	0.0350	2.981	75.472
163	modell_163	EG1_effective_stress.txt	E167	3157680	0.0600	0.0180	0.0078	0.0401	3.158	71.255
164	modell_164	EG1_effective_stress.txt	E168	3310880	0.0600	0.0180	0.0096	0.0452	3.311	67.958
165	modell_165	EG1_effective_stress.txt	E169	3445290	0.0600	0.0180	0.0114	0.0502	3.445	65.307
166	modell_166	EG1_effective_stress.txt	E170	3024060	0.0600	0.0240	0.0048	0.0376	3.024	74.403
167	modell_167	EG1_effective_stress.txt	E171	3242600	0.0600	0.0240	0.0072	0.0444	3.243	69.389
168	modell_168	EG1_effective_stress.txt	E172	3429990	0.0600	0.0240	0.0096	0.0512	3.430	65.598
169	modell_169	EG1_effective_stress.txt	E173	3589070	0.0600	0.0240	0.0120	0.0579	3.589	62.690
170	modell_170	EG1_effective_stress.txt	E174	3724460	0.0600	0.0240	0.0144	0.0647	3.724	60.411

171	modell_171	EG1_effective_stress.txt	E175	3238660	0.0600	0.0300	0.0054	0.0453	3.239	69.473
172	modell_172	EG1_effective_stress.txt	E176	3459890	0.0600	0.0300	0.0084	0.0538	3.460	65.031
173	modell_173	EG1_effective_stress.txt	E177	3648800	0.0600	0.0300	0.0114	0.0622	3.649	61.664
174	modell_174	EG1_effective_stress.txt	E178	3805030	0.0600	0.0300	0.0144	0.0707	3.805	59.132
175	modell_175	EG1_effective_stress.txt	E179	3933360	0.0600	0.0300	0.0174	0.0792	3.933	57.203
176	modell_176	EG1_effective_stress.txt	E180	3425050	0.0600	0.0360	0.0060	0.0530	3.425	65.692
177	modell_177	EG1_effective_stress.txt	E181	3641830	0.0600	0.0360	0.0096	0.0632	3.642	61.782
178	modell_178	EG1_effective_stress.txt	E182	3825980	0.0600	0.0360	0.0132	0.0733	3.826	58.808
179	modell_179	EG1_effective_stress.txt	E183	3973970	0.0600	0.0360	0.0168	0.0835	3.974	56.618
180	modell_180	EG1_effective_stress.txt	E184	4091220	0.0600	0.0360	0.0204	0.0937	4.091	54.996
181	modell_181	EG1_effective_stress.txt	E185	3588160	0.0600	0.0420	0.0066	0.0607	3.588	62.706
182	modell_182	EG1_effective_stress.txt	E186	3795510	0.0600	0.0420	0.0108	0.0725	3.796	59.281
183	modell_183	EG1_effective_stress.txt	E187	3970980	0.0600	0.0420	0.0150	0.0844	3.971	56.661
184	modell_184	EG1_effective_stress.txt	E188	4107700	0.0600	0.0420	0.0192	0.0963	4.108	54.775
185	modell_185	EG1_effective_stress.txt	E189	4211770	0.0600	0.0420	0.0234	0.1082	4.212	53.422
186	modell_186	EG1_effective_stress.txt	E190	3731480	0.0600	0.0480	0.0072	0.0684	3.731	60.298
187	modell_187	EG1_effective_stress.txt	E191	3926490	0.0600	0.0480	0.0120	0.0819	3.926	57.303
188	modell_188	EG1_effective_stress.txt	E192	4090780	0.0600	0.0480	0.0168	0.0955	4.091	55.002
189	modell_189	EG1_effective_stress.txt	E193	4214430	0.0600	0.0480	0.0216	0.1091	4.214	53.388
190	modell_190	EG1_effective_stress.txt	E194	4304450	0.0600	0.0480	0.0264	0.1227	4.304	52.271
191	modell_191	EG1_effective_stress.txt	E195	3858470	0.0600	0.0540	0.0078	0.0761	3.858	58.313
192	modell_192	EG1_effective_stress.txt	E196	4039070	0.0600	0.0540	0.0132	0.0913	4.039	55.706
193	modell_193	EG1_effective_stress.txt	E197	4190540	0.0600	0.0540	0.0186	0.1066	4.191	53.692
194	modell_194	EG1_effective_stress.txt	E198	4300020	0.0600	0.0540	0.0240	0.1219	4.300	52.325
195	modell_195	EG1_effective_stress.txt	E199	4375720	0.0600	0.0540	0.0294	0.1372	4.376	51.420
196	modell_196	EG1_effective_stress.txt	E200	3971490	0.0600	0.0600	0.0084	0.0838	3.971	56.654
197	modell_197	EG1_effective_stress.txt	E201	4136550	0.0600	0.0600	0.0144	0.1007	4.137	54.393
198	modell_198	EG1_effective_stress.txt	E202	4273930	0.0600	0.0600	0.0204	0.1177	4.274	52.645
199	modell_199	EG1_effective_stress.txt	E203	4368710	0.0600	0.0600	0.0264	0.1347	4.369	51.503
200	modell_200	EG1_effective_stress.txt	E204	4430280	0.0600	0.0600	0.0324	0.1516	4.430	50.787

Double-sided stiffener, t_f varies					
Nr	**t_f [m]**	**t_w [m]**	**a [m]**	**L [m]**	**K_t [-]**
1	0.006	0.006	0.006	0.023	2.152
2	0.008	0.006	0.006	0.023	2.327
3	0.010	0.006	0.006	0.023	2.441
4	0.020	0.006	0.006	0.023	2.643
5	0.030	0.006	0.006	0.023	2.674
6	0.040	0.006	0.006	0.023	2.674
7	0.050	0.006	0.006	0.023	2.671
8	0.060	0.006	0.006	0.023	2.667
9	0.006	0.009	0.009	0.034	2.141
10	0.008	0.009	0.009	0.034	2.357
11	0.010	0.009	0.009	0.034	2.522
12	0.020	0.009	0.009	0.034	2.912
13	0.030	0.009	0.009	0.034	3.021
14	0.040	0.009	0.009	0.034	3.05
15	0.050	0.009	0.009	0.034	3.058
16	0.060	0.009	0.009	0.034	3.057

Double-sided stiffener, t_w varies					
Nr	**t_f [m]**	**t_w [m]**	**a [m]**	**L [m]**	**K_t [-]**
17	0.020	0.006	0.006	0.023	2.643
18	0.020	0.012	0.006	0.029	2.762
19	0.020	0.018	0.006	0.035	2.883
20	0.020	0.024	0.006	0.041	2.994
21	0.020	0.030	0.006	0.047	3.094
22	0.020	0.036	0.006	0.053	3.187
23	0.020	0.042	0.006	0.059	3.273
24	0.020	0.048	0.006	0.065	3.353

Double-sided stiffener, a varies					
Nr	**t_f [m]**	**t_w [m]**	**a [m]**	**L [m]**	**K_t [-]**
25	0.060	0.036	0.003	0.044	3.283
26	0.060	0.036	0.006	0.053	3.425
27	0.060	0.036	0.012	0.070	3.768
28	0.060	0.036	0.018	0.087	4.016
29	0.060	0.036	0.024	0.104	4.183
30	0.060	0.036	0.030	0.121	4.295
31	0.060	0.036	0.036	0.138	4.369
32	0.060	0.036	0.042	0.155	4.419
33	0.060	0.036	0.048	0.172	4.451
34	0.060	0.036	0.054	0.189	4.516

C3 3D FE-results

Here are the indata for the 3D FE-analyses listed. Instead of extracting the nominal stress in the post-processing, the nominal stress is calculated analytically and used to calculate the stress concentration factor K_t.

Indata					
Nr	Lit.ref	Flange thickn., tf [m]	Web thickn., tw1 [m]	weld throat, a [m]	Web height, hw [m]
1	SCB	0.010	0.007	0.005	0.332
2	B+SB	0.025	0.005	0.005	0.254
3	BT	0.014	0.009	0.008	0.150
4	A,B,C,D	0.019	0.019	0.006	0.610
5	SGB/SGC/SBB	0.013	0.006	0.005	0.940
6	TEST 1	0.030	0.010	0.010	0.332
7	TEST 2	0.030	0.010	0.010	0.332
8	TEST 3	0.030	0.010	0.010	0.332
9	TEST 4	0.030	0.010	0.010	0.332

E [Pa]	σ [Pa]
2.10E+11	1000000

Indata				
Nr	h,tot [m]	Half span-0,075 m, Lext/Rext [m]	Span in model [m]	Flange width, L2 [m]
1	0.351	1.525	2.900	0.172
2	0.305	1.220	2.290	0.127
3	0.178	0.941	1.732	0.178
4	0.648	1.868	3.586	0.305
5	0.965	2.973	5.796	0.197
6	0.392	1.525	2.900	0.300
7	0.392	1.525	2.900	0.300
8	0.392	1.525	2.900	0.300
9	0.392	1.525	2.900	0.300

Deflection						
Nr	**z,c [m]**	**I [m^4]**	**a [m]**	**F [N]**	**delta,1 [m]**	**delta,tot [m]**
1	0.175	0.0001172	0.906	17200	0.0002895	0.0005790
2	0.152	0.0001328	0.705	12700	0.0000919	0.0001839
3	0.089	0.0000360	0.521	17800	0.0002021	0.0004041
4	0.324	0.0015075	1.132	30500	0.0000760	0.0001520
5	0.483	0.0015750	1.862	19700	0.0002008	0.0004016
6	0.196	0.0006215	0.906	30000	0.0000953	0.0001905
7	0.196	0.0006215	0.906	30000	0.0000953	0.0001905
8	0.196	0.0006215	0.906	30000	0.0000953	0.0001905
9	0.196	0.0006215	0.906	30000	0.0000953	0.0001905

Nominal stress				**Effective notch stress**	
Nr	**M.max [Nm]**	**W [m^3]**	**Nominal stress [MPa]**	**ENS [MPa]**	**K_t [-]**
1	15585.5	0.0007067	22.053	50.980	2.312
2	8949.7	0.0010453	8.562	21.810	2.547
3	9266.0	0.0004802	19.297	52.680	2.730
4	34537.6	0.0049468	6.982	18.280	2.618
5	36675.1	0.0033510	10.944	25.320	2.314
6	27184.0	0.0037442	7.260	24.280	3.344
7	27184.0	0.0037442	7.260	23.200	3.195
8	27184.0	0.0037442	7.260	24.940	3.435
9	27184.0	0.0037442	7.260	25.820	3.556

3D analyses					
Nr	**t_w [m]**	**a [m]**	**L [m]**	**K_t [-]**	**$\Delta\sigma_C$ [MPa]**
1	0.0071	0.00476	0.0206	2.312	97.33
2	0.0064	0.00476	0.0198	2.547	88.32
3	0.0127	0.00794	0.0352	2.730	82.42
4	0.0079	0.00635	0.0259	2.618	85.94
5	0.0064	0.00476	0.0198	2.314	97.25
6	0.0320	0.01000	0.0603	3.344	67.28
7	0.0220	0.01000	0.0503	3.195	70.41
8	0.0420	0.01000	0.0703	3.435	65.50
9	0.0520	0.01000	0.0803	3.556	63.27

Appendix D

This appendix presents the data, which is used to derive the equations presented in Section 5.3.5 for both one- and double-sided transverse stiffener.

D1 One-sided equation

Curve-fitting factors for K_t-L-curve									
$t_f = 0.02$ m		$t_f = 0.03$ m		$t_f = 0.04$ m		$t_f = 0.05$ m		$t_f = 0.06$ m	
K_t = A*L^2+B*L+C		K_t = A*L^2+B*L+C		K_t = A*L^2+B*L+C		K_t = A*L^2+B*L+C		K_t = A*L^2+B*L+C	
A	-735.197	A	-539.004	A	-399.804	A	-291.831	A	-203.611
B	52.624	B	51.789	B	49.106	B	44.573	B	38.191
C	1.531	C	1.528	C	1.568	C	1.651	C	1.778
L	**K_t**	**L**	**K_t**	**L**	**K_t**	**L**	**K_t**	**L**	**K_t**
0.005	1.776	0.005	1.773	0.005	1.803	0.005	1.867	0.005	1.964
0.010	1.984	0.010	1.992	0.010	2.019	0.010	2.068	0.010	2.140
0.015	2.155	0.015	2.183	0.015	2.215	0.015	2.254	0.015	2.305
0.020	2.290	0.020	2.348	0.020	2.390	0.020	2.426	0.020	2.461
0.025	2.387	0.025	2.486	0.025	2.546	0.025	2.583	0.025	2.606
0.030	2.448	0.030	2.596	0.030	2.681	0.030	2.726	0.030	2.741
0.035	2.472	0.035	2.680	0.035	2.797	0.035	2.854	0.035	2.865
0.040	2.472	0.040	2.737	0.040	2.892	0.040	2.967	0.040	2.980
0.045	2.472	0.045	2.767	0.045	2.968	0.045	3.066	0.045	3.084
0.050	2.472	0.050	2.770	0.050	3.024	0.050	3.150	0.050	3.179
0.055	2.472	0.055	2.770	0.055	3.059	0.055	3.220	0.055	3.263
0.060	2.472	0.060	2.770	0.060	3.075	0.060	3.275	0.060	3.337
0.065	2.472	0.065	2.770	0.065	3.075	0.065	3.316	0.065	3.400
0.070	2.472	0.070	2.770	0.070	3.075	0.070	3.341	0.070	3.454
0.075	2.472	0.075	2.770	0.075	3.075	0.075	3.353	0.075	3.497
0.080	2.472	0.080	2.770	0.080	3.075	0.080	3.353	0.080	3.530
0.085	2.472	0.085	2.770	0.085	3.075	0.085	3.353	0.085	3.553
0.090	2.472	0.090	2.770	0.090	3.075	0.090	3.353	0.090	3.566
0.095	2.472	0.095	2.770	0.095	3.075	0.095	3.353	0.095	3.566
0.100	2.472	0.100	2.770	0.100	3.075	0.100	3.353	0.100	3.566
0.105	2.472	0.105	2.770	0.105	3.075	0.105	3.353	0.105	3.566
0.110	2.472	0.110	2.770	0.110	3.075	0.110	3.353	0.110	3.566
0.115	2.472	0.115	2.770	0.115	3.075	0.115	3.353	0.115	3.566
0.120	2.472	0.120	2.770	0.120	3.075	0.120	3.353	0.120	3.566
0.125	2.472	0.125	2.770	0.125	3.075	0.125	3.353	0.125	3.566
0.130	2.472	0.130	2.770	0.130	3.075	0.130	3.353	0.130	3.566
0.135	2.472	0.135	2.770	0.135	3.075	0.135	3.353	0.135	3.566
0.140	2.472	0.140	2.770	0.140	3.075	0.140	3.353	0.140	3.566

Curve-fitting factors for the factors from K_t-L-curve					
A		**B**		**C**	
A = A1*ln(tf)+A2		B = B1*L^2+B2*L+B3		C = C1*L^2+C2*L+C3	
A1	483.870	B1	-92.457	C1	2.168
A2	43.562	B2	37.882	C2	-1.117
		B3	48.746	C3	1.668
A	**t_f**	**B**	**t_f**	**C**	**t_f**
-735.197	0.2	52.624	0.2	1.531	0.2
-539.004	0.3	51.789	0.3	1.528	0.3
-399.804	0.4	49.106	0.4	1.568	0.4
-291.831	0.5	44.573	0.5	1.651	0.5
-203.611	0.6	38.191	0.6	1.778	0.6

Points where the equations reaches their maximum value	
t_f	**L**
0.02	0.035
0.03	0.05
0.04	0.06
0.05	0.075
0.06	0.09
Curve-fitting for L_{max}	
$L_{max} = L_{max}1*t_f+L_{max}2$	
$L_{max}1$	1.35
$L_{max}2$	0.008
t_f	**L**
0.02	0.035
0.03	0.0485
0.04	0.062
0.05	0.0755
0.06	0.089

Equation for one-sided stiffener
$L \le 1.35*t_f+0.008$
$K_t = A*L^2+B*L+C$
$A = 483.87*\ln(t_f)+43.562$ $B = -92.457*t_f^2+37.882*t_f+48.476$ $C = 2.168*t_f^2-1.117*t_f+1.668$
$L > 1.35*t1+0.008$
$K_t = A*L_{max}^2+B*L_{max}+C$ $L_{max} = 1.35*t_f+0.008$

D2 Double-sided equation

Curve-fitting factors for K_t-L-curve									
t_f = 0.02 m		**t_f = 0.03 m**		**t_f = 0.04 m**		**t_f = 0.05 m**		**t_f = 0.06 m**	
K_t = A*L^2+B*L+C		K_t = A*L^2+B*L+C		K_t = A*L^2+B*L+C		K_t = A*L^2+B*L+C		K_t = A*L^2+B*L+C	
A	-559.110	A	-336.150	A	-225.260	A	-158.800	A	-119.290
B	60.574	B	50.911	B	43.516	B	37.945	B	33.775
C	1.530	C	1.600	C	1.730	C	1.910	C	1.990
L	**K_t**	**L**	**K_t**	**L**	**K_t**	**L**	**K_t**	**L**	**K_t**
0.005	1.819	0.005	1.846	0.005	1.942	0.005	2.096	0.005	2.156
0.010	2.080	0.010	2.075	0.010	2.143	0.010	2.274	0.010	2.316
0.015	2.313	0.015	2.288	0.015	2.332	0.015	2.443	0.015	2.470
0.020	2.518	0.020	2.484	0.020	2.510	0.020	2.605	0.020	2.618
0.025	2.695	0.025	2.663	0.025	2.677	0.025	2.759	0.025	2.760
0.030	2.844	0.030	2.825	0.030	2.833	0.030	2.905	0.030	2.896
0.035	2.965	0.035	2.970	0.035	2.977	0.035	3.044	0.035	3.026
0.040	3.058	0.040	3.099	0.040	3.110	0.040	3.174	0.040	3.150
0.045	3.124	0.045	3.210	0.045	3.232	0.045	3.296	0.045	3.268
0.050	3.161	0.050	3.305	0.050	3.343	0.050	3.410	0.050	3.381
0.055	3.170	0.055	3.383	0.055	3.442	0.055	3.517	0.055	3.487
0.060	3.170	0.060	3.445	0.060	3.530	0.060	3.615	0.060	3.587
0.065	3.170	0.065	3.489	0.065	3.607	0.065	3.705	0.065	3.681
0.070	3.170	0.070	3.517	0.070	3.672	0.070	3.788	0.070	3.770
0.075	3.170	0.075	3.527	0.075	3.727	0.075	3.863	0.075	3.852
0.080	3.170	0.080	3.527	0.080	3.770	0.080	3.929	0.080	3.929
0.085	3.170	0.085	3.527	0.085	3.801	0.085	3.988	0.085	3.999
0.090	3.170	0.090	3.527	0.090	3.822	0.090	4.039	0.090	4.064
0.095	3.170	0.095	3.527	0.095	3.831	0.095	4.082	0.095	4.122
0.100	3.170	0.100	3.527	0.100	3.831	0.100	4.117	0.100	4.175
0.105	3.170	0.105	3.527	0.105	3.831	0.105	4.143	0.105	4.221
0.110	3.170	0.110	3.527	0.110	3.831	0.110	4.162	0.110	4.262
0.115	3.170	0.115	3.527	0.115	3.831	0.115	4.174	0.115	4.297
0.120	3.170	0.120	3.527	0.120	3.831	0.120	4.177	0.120	4.325
0.125	3.170	0.125	3.527	0.125	3.831	0.125	4.177	0.125	4.348
0.130	3.170	0.130	3.527	0.130	3.831	0.130	4.177	0.130	4.365
0.135	3.170	0.135	3.527	0.135	3.831	0.135	4.177	0.135	4.376
0.140	3.170	0.140	3.527	0.140	3.831	0.140	4.177	0.140	4.380
0.145	3.170	0.145	3.527	0.145	3.831	0.145	4.177	0.145	4.380
0.150	3.170	0.150	3.527	0.150	3.831	0.150	4.177	0.150	4.380

Curve-fitting factors for the factors from K_t-L-curve					
A		**B**		**C**	
A = A1*L^3+A2*L^2+A3*L+A4		B = B1*ln(tf)+B2		C = C1*L^3+C2*L^2+C3*L+C4	
A1	7093	B1	-24.6	C1	-13.33
A2	-11450	B2	21.1	C2	16.50
A3	6571			C3	-5.12
A4	-1471			C4	2
A	**t_f**	**B**	**t_f**	**C**	**t_f**
-558.034	0.2	60.692	0.2	1.529	0.2
-338.651	0.3	50.718	0.3	1.589	0.3
-220.589	0.4	43.641	0.4	1.739	0.4
-161.288	0.5	38.151	0.5	1.899	0.5
-118.187	0.6	33.666	0.6	1.989	0.6

Points where the equations reaches their maximum value	
t_f	**L**
0.02	0.055
0.03	0.075
0.04	0.095
0.05	0.120
0.06	0.140
Curve-fitting for L_{max}	
$L_{max} = L_{max}1 * t_f + L_{max}2$	
$L_{max}1$	2.15
$L_{max}2$	0.011
t_f	**L**
0.02	0.054
0.03	0.0755
0.04	0.097
0.05	0.1185
0.06	0.14

Equation for double-sided stiffener
$L <= 2.15 * t_f + 0.011$
K_t = A*L^2+B*L+C
A = 7093*L^3-11450*L^2+6571*L-1471.4 B = -24.6*ln(tf)+21.1 C = -13.33*L^3+16.5*L^2-5.12*L+2
L > 2.15*t1+0.011
$K_t = A*L_{max}$^2+B*L_{max}+C $L_{max} = 2.15*t_f+0.011$

Curve-fitting factors for K_t-L-curve	
Factor 1	1
Factor 2	6.45
K_t = Factor 1*ln(L)+Factor 2	
L	**K_t**
0.005	1.1517
0.01	1.8448
0.015	2.2503
0.02	2.5380
0.025	2.7611
0.03	2.9434
0.035	3.0976
0.04	3.2311
0.045	3.3489
0.05	3.4543
0.055	3.5496
0.06	3.6366
0.065	3.7166
0.07	3.7907
0.075	3.8597
0.08	3.9243
0.085	3.9849
0.09	4.0421
0.095	4.0961
0.1	4.1474
0.105	4.1962
0.11	4.2427
0.115	4.2872
0.12	4.3297
0.125	4.3706
0.13	4.4098
0.135	4.4475
0.14	4.4839